THE UNIVERSITY *of* EDINBURGH

THE UNIVERSITY
of EDINBURGH

Developing a Click Chemistry Imaging Platform Using Aromatic Ynamines

Emma Alexander

Thesis submitted to the University of Edinburgh in fulfilment of the requirements for the degree of Doctor of Philosophy

July 2024

Academic Supervisor: Prof. Glenn. A. Burley

Contents

Acknowledgements

I would like to thank Prof. Glenn Burley for the opportunity to undertake a PhD in his research group and for his guidance throughout the years that I spent in the group. I would also like to thank the OPTIMA CDT for offering a unique PhD opportunity, I am continuing to draw on the experience that I gained through the business school classes and workshops over the years.

I would like to thank all the members of the Burley group, past and present, at The University of Strathclyde: Iain, Jack and Emma1 for being there from when I started and helping me settle into the group, and Otto, Helena and Admir for making my final years fun and this would not have been possible without Andrea, Fergus and Fred for keeping the group supplied with chemicals and working HPLCs, amongst a whole lot more. And to Charlotte, for keeping me sane through the OPTIMA courses and beyond.

I would also specifically like to thank the members of Team Ynamine: Andrea, Fred and Roderick, for the years spent sharing the ynamine joy. And to Andrea and Fred for their proofreading and advice whilst unravelling the ynamine mystery.

Additionally, I would like to thank Domainex for hosting me for a placement as part of the PhD. A break from the world of ynamines allowed me to fully appreciate them on my return.

Finally, I would like to thank Sean for his support and patience, especially over the past year (and help with last minute formatting issues), and my parents for their support over the years.

Abstract

The copper-catalysed azide alkyne cycloaddition (CuAAC) is a widely used bio-orthogonal reaction. However, drawbacks include oxidative damage of biomolecules leading to cytotoxicity which limits the *in vivo* applications of the CuAAC reaction. Strategies to temper oxidative damage include the use of ligands and chelating azides, yet there has been little development on the alkyne design. Aromatic ynamines are alkyne analogues displaying an enhanced reactivity relative to conventional terminal alkynes. This enhanced reactivity provides rapid kinetics for the CuAAC reaction, enabling low copper loadings without using ligand or additives. However, the aromatic ynamine core – the benzimidazole heterocycle – has yet to be systematically investigated. This work aims to investigate how the structure of the ynamine influences the CuAAC reaction and solvent on reactivity. These findings will then be applied to construct a probe for calcium imaging, in an attempt to utilise the unique reactivity of the ynamine for addition of a fluorophore or an organelle targeting moiety.

A palette of benzimidazole and imidazole ynamine substrates containing various electron-donating and electron-withdrawing groups were synthesised. First, hydrogen deuterium exchange (HDE) was utilised to probe how substituents affect the alkyne proton lability. It was found that the substituent changes on benzimidazole influenced the HDE, with EDGs increasing the rate of HDE and EWGs reducing the rate. Imidazole substituents were slower to exchange than the benzimidazole equivalents, and a larger difference was observed between substituents. Then HPLC analysis was used to investigate the influence of the modification on the CuAAC reaction. The experiments showed how reaction kinetics are strongly affected by varying the heterocycle and the substituents in the aromatic moiety, with a 5,6-dimethoxy benzimidazole displaying fast reaction kinetics in MeCN with 5,6-difluoro benzimidazole significantly slower. When these groups were substituted on imidazole ynamine scaffolds, the fluorine substituent gave faster reaction rates. Additionally, reaction rates and side product formation are highly dependent on solvents and copper-catalyst loading, with the catalyst percentage able to be lowered to 0.15 mol% for a benzimidazole ynamine containing two methoxy groups on the scaffold. The changes in reaction rates in solvents are substrate dependent, however, it was consistently observed that using HFIP/water resulted in no side product formation, but solubility issues were common.

In addition, these results uncovered fundamental differences between imidazole and benzimidazole ynamines. This points to potential changes in rate determining step of the imidazole ynamine CuAAC.

The use of the ynamine in bioconjugation applications was explored through the use of calcium probes. Synthesis of calcium probes containing varying functional groups was attempted, with the aim of conjugation an ynamine, to allow for modular click modification with fluorophores. Research initially began with the conjugation of fluorophore to ynamine to determine precedent, and research on the BAPTA focused on the synthesis of probes with a range of linkers.

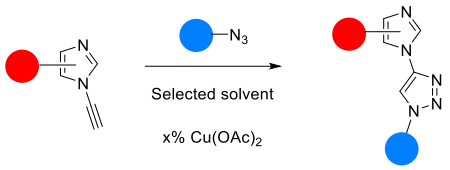

Scheme. Reaction of an aromatic ynamine with an azide to form a triazole.

The findings in this thesis underpin the potential of aromatic ynamines for bioconjugation. Specifically, future ynamine probes should utilise benzimidazole substituents to avoid solubility issues and use a 5,6 methoxy group in MeCN to maximise reactivity, however, all factors need to be taken into consideration before deciding on a system. Additionally, the lack of dependence on the copper concentration of imidazoles highlights their potential for bioconjugation/imaging which has not been explored yet.

Lay Summary

The copper-catalysed azide alkyne cycloaddition (CuAAC) is a chemical reaction that joins two different parts of a reaction (an azide and an alkyne) together. These parts of the reaction join easily together, like two jigsaw pieces fitting into each other. The CuAAC is a widely used reaction as it can be performed inside cells without causing any damage, and does not react with any other parts of the cell. However, the reaction requires copper, a metal that can react with components of a cell and cause damage. The aromatic ynamine, an alkyne puzzle piece, is extremely reactive in the CuAAC reaction and requires less copper than other alkynes to make the reaction work. This work investigates how changes to the structure of the aromatic ynamine can affect the much copper is required for the reaction to proceed, and also, how fast the reaction can go.

The first part of this work involved the chemical synthesis of the different aromatic ynamines. Then, to assess the impact of the changes to the structure, the CuAAC was performed with each of the new ynamines with the same azide, and the reaction was monitored by High-Performance Liquid-Chromatography (HPLC). HPLC is an analytical technique that is used to separate out mixtures, and to measure how much of a component is in the mixture. Analysis found that the changes made to the aromatic ynamines affected the reaction rate. The liquid that the reaction was performed in was also investigated, with this also having an impact on the speed of the reaction. During these investigations, the level of copper required in the reactions was tested, and it was found that some ynamines required very low levels of the metal, which is important for development in a cellular environment.

A potential use of the aromatic ynamines in calcium probes was investigated. Calcium probes measure the levels of calcium inside cells. Calcium is important in cells as it is involved, in signalling and cell communication, and any issues with the amount of calcium in a cell can cause diseases including heart conditions and cancer. Calcium probes with different structures were synthesised, and these were attempted to be connected to the aromatic ynamines, to allow for future CuAAC reactions.

The results of this thesis show that aromatic ynamines have potential for further use in biological applications, and that several factors must be taken into consideration, including structure and reaction liquid prior to design of a system.

Abbreviations

AM	Acetomethoxy Ester
BAPTA	1,2-Bis(o-aminophenoxy)ethane-N,N,N′,N′-tetraacetic acid
BCN	Bicyclononyne
BTTAA	2-(4-((Bis((1-(*tert*-butyl)-1*H*-1,2,3-triazol-4-yl)methyl)amino)methyl)-1*H*-1,2,3-triazol-1-yl)acetic acid
BTTES	3-(4-((Bis((1-(*tert*-butyl)-1*H*-1,2,3-triazol-4-yl)methyl)amino)methyl)-1*H*-1,2,3-triazol-1-yl)propane-1-sulfonic acid
BINAP	2,2′-Bis(diphenylphosphino)-1,1′-binaphthyl)
COMU	(1-Cyano-2-ethoxy-2-oxoethylidenaminooxy)dimethylamino-morpholino-carbenium hexafluorophosphate
$CDCl_3$	Deuterated chloroform
COSY	Correlation Spectroscopy
$Cu(OAc)_2$	Copper acetate
CuAAC	Copper Catalysed Azide-Alkyne Cycloaddition
DBCO	Dibenzocyclootyne
DCM	Dichloromethane
DFT	Density Functional Theory
DIC	*N,N*-Diisopropylcarbodiimide
DIPEA	*N,N*-Diisopropylethylamine
DMSO	Dimethylsulfoxide
EDC	1-Ethyl-3-(3-dimethylaminopropyl)carbodiimide
EDG	Electron Donating Group
EDTA	Ethylenediaminetetraacetic acid
EGTA	Ethylene glycol-bis(β-aminoethyl ether)-N,N,N′,N′-tetraacetic acid
ER	Endoplasmic Reticulum
EPR	Electron Paramagnetic Resonance
equiv	Equivalent
EtOAc	Ethyl acetate
EtOH	Ethanol
EWG	Electron Withdrawing Group
FE	Fluorescence Enhancement

GECI	Genetically Encoded Calcium Indicators
GSH	Glutathione
H_2O	Water
HATU	Hexafluorophosphate Azabenzotriazole Tetramethyl Uronium
HDE	Hydrogen-Deuterium Exchange
HFIP	Hexafluoroisopropyl alcohol
HMBC	Heteronuclear Multiple-Bond Correlation Spectroscopy
HOAt	1-Hydroxy-7-azabenzotriazole
HOBt	1-Hydroxybenzotriazole
HOMO	Highest Occupied Molecular Orbital
HPLC	High Performance Liquid Chromatography
HRMS	High Resolution Mass Spectrometry
HSQC	Heteronuclear Single Quantum Coherence
IEDDA	Inverse Electron Demand Diels-Alder
IPA	Isopropanol
IR	Infrared
LC-MS	Liquid Chromatography Mass Spectrometry
LUMO	Lowest Occupied Molecular Orbital
MeCN	Acetonitrile
MeOH	Methanol
NaAsc	Sodium ascorbate
NaOH	Sodium hydroxide
NBS	*N*-Bromo-succimide
NIR	Near-infra Red
NMR	Nuclear Magnetic Resonance
NOSEY	Nuclear Overhauser Effect Spectroscopy
PEG	Polyethylene Glycol
PeT	Photoinduced Electron Transfer
RDS	Rate Determining Step
ROS	Reactive Oxygen Species
RT	Retention Time
rt	Room temperature
SPAAC	Strain-Promoted Azide-Alkyne Cycloaddition

TBAF	Tetra-*n*-butylammonium fluoride
TBTA	Tris((1-benzyl-4-triazolyl)methyl)amine
*t*BuOH	tert-Butanol
TCO	*Trans* cyclooctyne
TFE	Trifluoroethanol
THF	Tetrahydrofuran
THPTA	Tris(benzyltriazolylmethyl)amine
TIPS	Triisopropylsilane
TLC	Thin-Layer Chromatography

Chapter 1

Introduction

1.1 Bioorthogonal Reactions

Understanding cellular processes is vital to deepen our understanding of biology and accelerate pharmaceutical drug development. Key to this understanding is the ability to label, track and visualise biomolecules inside their native environment.[1,2] The advent of bioorthogonal reactions accelerated this process immensely. These reactions are characterised by their high reactivity, metabolic stability, and specificity.[2] They include, but are not limited to, the Staudinger ligation, the copper catalysed azide-alkyne cycloaddition (CuAAC), the strain promoted azide-alkyne cycloaddition (SPAAC) and the inverse electron demand Diels-alder reaction (IEDDA).[3–6] The Staudinger ligation was the first developed, however, its slow kinetics allowed it to be leapfrogged in popularity by the others. The development of these reactions in bioorthogonal chemistry led to the development of the field and an explosion in research (Figure 1.1).

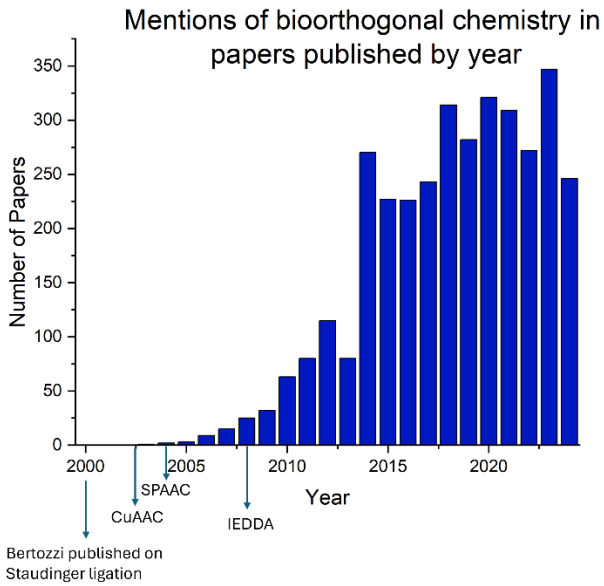

Figure 1.1. Papers published by year containing the term "bioorthogonal chemistry". Data obtained from Web of Science.

Alongside the extensive application of these reactions to different fields, such as biomedical imaging, medicinal chemistry, polymer science and materials and surface science, a large amount of research focused on the optimisation of these reactions.[7,8] Many factors, including the solvent, reaction partners, and in the case of the CuAAC, the ligands used, have been investigated.[9] During the optimisation of bioorthogonal reactions, the stability in physiological conditions, selectivity and reaction kinetics are important, and to achieve the ideal

bioorthogonal reaction, each attribute must be carefully balanced and appropriate to the application. This has allowed for reactions to take place at a high reaction rate and in varying reaction conditions, allowing increased utility in various biological settings, including drug discovery and imaging.[10]

1.1.1 The Staudinger Ligation

1.1.1.1 First Demonstration *In Vivo*

Herman Staudinger first described the reaction of an azide with a phosphine to produce an iminophosphorane in 1919.[11,12] The phosphine and the azide react to form an azaylide, which, in the presence of water, hydrolyses to form the desired primary amide and the phosphine oxide as a side product.[12] Neither azides or phosphines are present in biological organisms and, therefore, the Staudinger ligation was poised for potential bioorthogonal use. In 2000, Saxon *et al.* exploited the unique reactivity to use the Staudinger reaction for bio-orthogonal tagging (Scheme 1.1).[13]

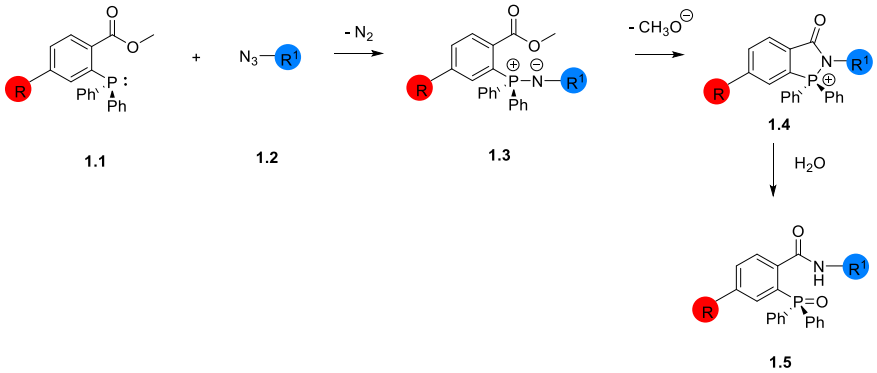

Scheme 1.1. First use of the Staudinger ligation.[13]

The key modification was the addition of a proximal methyl ester to the phosphine reagent **1.1**, which, after iminophosphorane (**1.3**) formation, acts as an electrophilic trap to form the nucleophilic aza-ylide (**1.4**) by an intramolecular cyclisation. After hydrolysis, the desired amide bond (**1.5**) is formed creating a stable linkage between the starting materials. To demonstrate the potential biological use of this reaction, azidoglycans on the surface of Jurkat cells were tagged with a biotin modified phosphine.[13] This was the first report of its kind, paving the way for the development of bio-orthogonal chemistry. Despite the success of the

reaction, disadvantages included the extremely slow reaction kinetics (with a rate typically between 1.9 x 10^{-3} $M^{-1}s^{-1}$ and 2.5 x 10^{-3} $M^{-1}s^{-1}$) and that the phosphine is prone to oxidation.[14]

1.1.1.2 Effect of Substrate

Further research attempted to optimise the Staudinger ligation by increasing the substrate scope.[14] It was found that the reaction tolerated a wide scope, however, the substituents influence the rate.[15] Modifications that were tested are given Figure 1.2A. The ester leaving group was found to not play an important role in the reaction rate, however, if bulky groups were added to **1.6** (*e.g. t*-Bu), there was significant amounts of aza-ylide hydrolysis, giving the phosphine oxide and amine, instead of the desired ligated product. Various para-substituted phenol esters (**1.7**) were tested, and no large changes in the rate constant was observed. However, adding substituents to the phenyl group attached to the phosphine (**1.8**) led to changes in the reaction rate.[15] The results showed that electron donating substituents led to an increase in reaction rate.

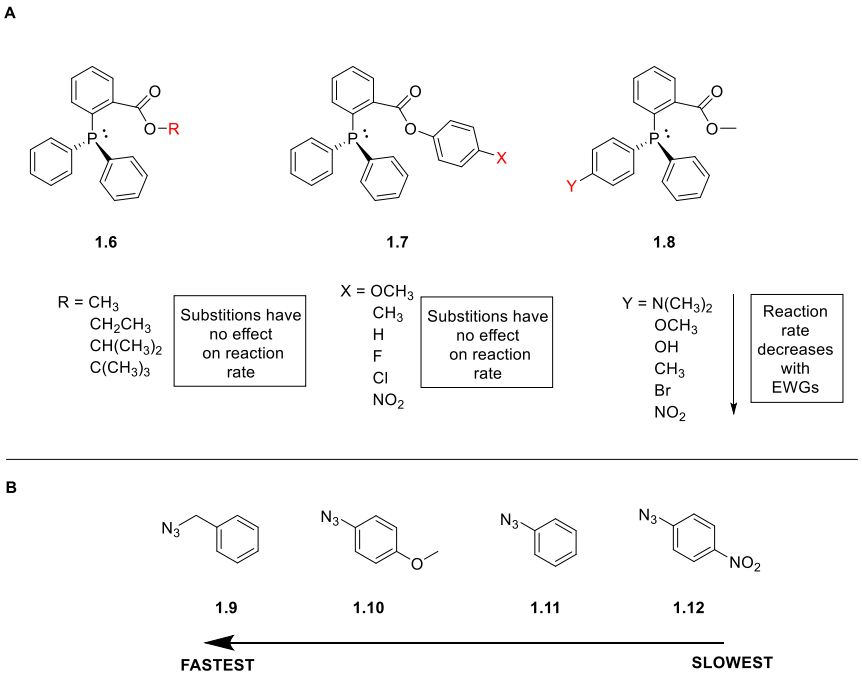

Figure 1.2. Changes made to the substrates in the Staudinger ligation to investigate substrate effect on reaction rate. **A)** Changes to the phosphine reactant; **B)** Changes to the azide reactant.[15]

The use of aryl azides was also investigated, and phosphine **1.6** bearing a methyl group was used (Figure 1.2B). Phenyl azide (**1.11**) gave a stable intermediate quickly, however, the conversion of the intermediate to the ligation product was slow (>24 h for complete

conversion) compared to benzyl azide (**1.9**) (35 min for complete conversion). 1-Azido-4-methoxybenzene (**1.10**) gave complete conversion within 8 h, however, *p*-nitrophenyl azide (**1.12**) took more than 48 h. All three phenyl substituted azides produced an aza-ylide intermediate rapidly before conversion to the desired product that is not formed with benzyl azide, suggesting that there is a change in the rate determining step (RDS) due to enhanced aza-ylide stability due to resonance stabilisation.[15]

1.1.1.3 Effect of Solvent on Bioorthogonal Reactivity

The effect of the solvent on the reaction rate has also been investigated, with more polar solvents and aqueous systems having superior reactivity.[15,16] These results indicated that the rate-limiting step of the reaction involves a polar transition state which is stabilised by polar solvents. Further differences observed between solvents with similar dielectric constants, such as CD_3OD and CD_3CN, suggest that the transition state may be stabilised through hydrogen bonding or other similar interactions. The reaction's ability to proceed at a fast rate in an aqueous environment is advantageous for biological systems.[17]

1.1.1.4 "Traceless" Staudinger Ligation

A modification to the Staudinger ligation, the "traceless" Staudinger ligation was simultaneously reported by the groups of Bertozzi and Raines (Scheme 1.2A).[3,18] In the "traceless" reaction, the desired product (**1.15**) does not contain phosphine oxide, it is released during hydrolysis. The proposed mechanism (Scheme 1.2B) was determined by monitoring the reaction using isotopically labelled water. ^{18}O was incorporated into phosphine oxide **1.20** which indicated that the reaction occurs through the formation of the amidophosphonium salt (**1.19**) and then hydrolysis.[19]

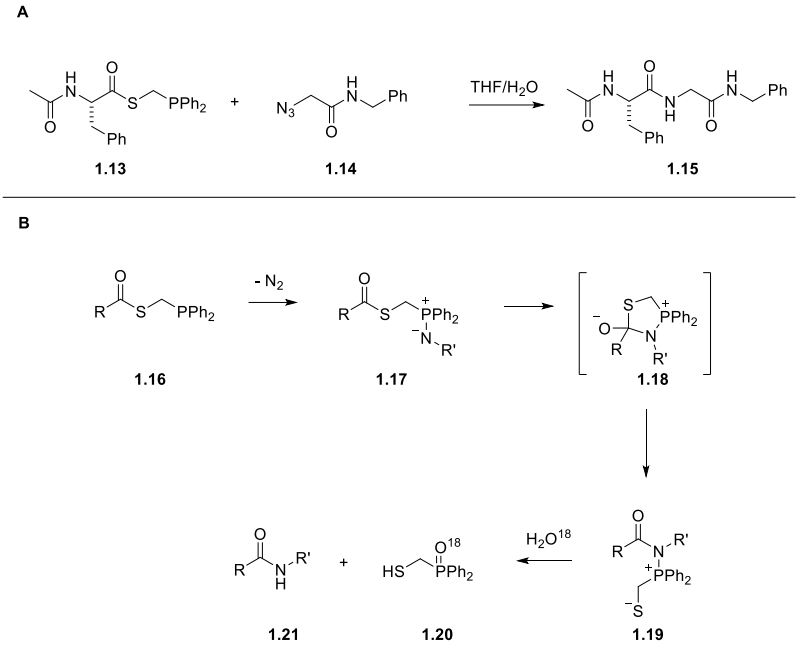

Scheme 1.2. A) Formation of an amide bond through a "traceless Staudinger"; **B)** The proposed mechanism of the traceless Staudinger reaction.[19]

When developed, the traceless Staudinger led the way for cellular applications and to date there have been many examples, including the ligation of biomolecules, imaging and radiolabelling.[14,20–22] The main advantage of the Staudinger ligation was the use of the azide which is not present in biomolecules, leading to selectivity and few side reactions in biological uses. However, the Staudinger ligation does have disadvantages. The reaction rate is slow, and the phosphine is liable to oxidation, both in air and by metabolic enzymes, limiting use *in vivo*.[7] In addition, due to the slow kinetics, higher concentrations of reagent are required to achieve suitable reaction rates, which increases the likelihood of toxicity. Other bioorthogonal reactions are therefore more used, including the SPAAC and the CuAAC.[7]

1.1.2 The Copper Catalysed Azide-Alkyne Cycloaddition

1.1.2.1 Discovery

Huisgen in 1963 first describes the 1,3-dipolar cycloaddition of an alkyne (**1.22**) and an azide (**1.23**).[23] This reaction was slow at room temperature; however, heating increased the yield and gave both the 1,4 (**1.24**) and 1,5 (**1.25**) substituted triazoles (Scheme 1.3).

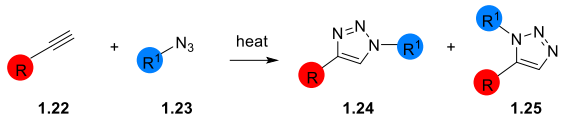

Scheme 1.3. The thermal Huisgen-Cycloaddition forming two regioisomers.[23]

In 2002, the groups of Sharpless and Meldal independently discovered that the reaction could be catalysed by copper salts.[4,24] The addition of copper as a catalyst significantly increased the reaction rate and formed exclusively the 1,4-substituted triazole (**1.17**) (Scheme 1.4).

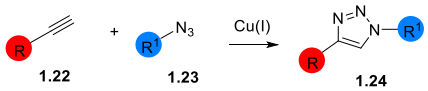

Scheme 1.4. The CuAAC reaction between an azide and an alkyne forming one desired product.

1.1.2.2 The Mechanism of the CuAAC

Sharpless first proposed a basic mechanism for the CuAAC in 2002,[4] however, research that followed has given the currently accepted mechanism of the CuAAC (Figure 1.3).[25–29]

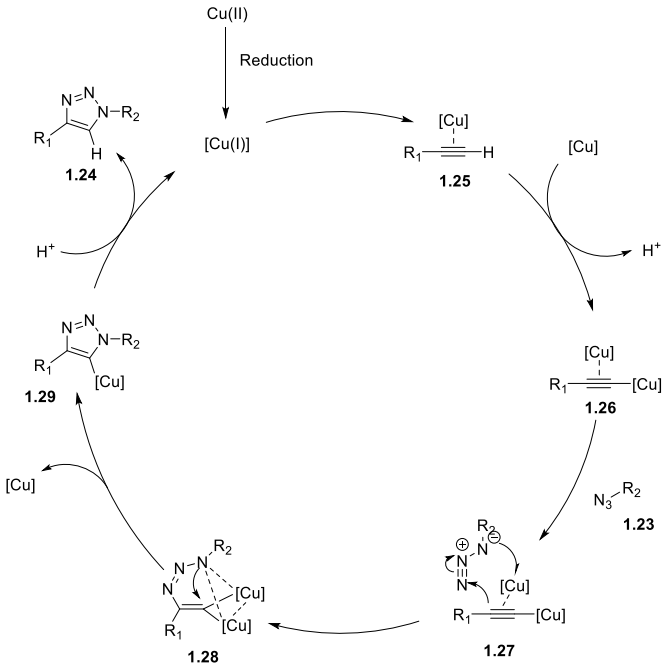

Figure 1.3. Mechanism of the CuAAC.

The initiation step is the co-ordination of Cu(I) to the alkyne triple bond to form a copper-acetylide species (**1.25**). The pK_a of the acetylide is then lowered which facilitates the formation of **1.26**.[30,31] The azide (**1.23**) then coordinates to the dinuclear complex **1.27** to form

intermediate **1.28**.[25,26,28] This intermediate then forms the mononuclear copper triazole **1.29**.[29] The final step is proto-demetallation to give the triazole product **1.24**. Cu(I) then re-enters the catalytic cycle. The RDS is the formation of **1.26**, the bis-acetylide complex.[25]

Key advantages of the CuAAC include fast reaction rates; regioselectivity with the 1,4-triazole exclusively produced; the reaction can be carried out in mild conditions (*e.g.,* room temperature and in water). As a result of these advantages, the CuAAC has been used in a variety of fields, such as organic synthesis, polymer chemistry and bioorthogonal applications, for an extensive range of uses.[31–35] The CuAAC also meets the criteria for a click reaction (modular, high yielding, stereospecific, large substrate scope and generating minimal side products).[36] The development of the CuAAC had a large impact on the field of bio-orthogonal chemistry, with its multiple advantages lending itself well to cellular applications. However, the reaction requires copper, which is cytotoxic.[37] This limits the use of this reaction *in vivo* and research has been ongoing to mitigate this effect.

1.1.2.3 Development of Cu-Stabilising Ligands for the CuAAC reaction

One of the main developments in the CuAAC has been in the ligands used for the transformation (Figure 1.4).[38]

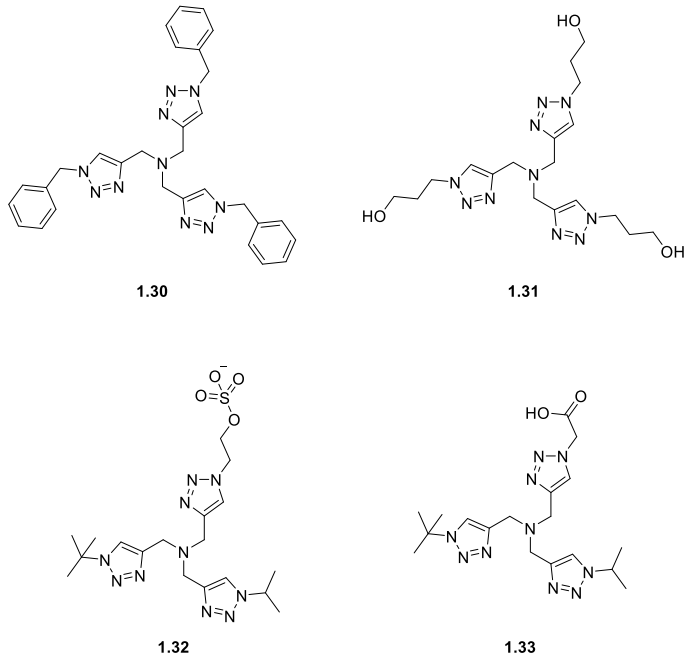

Figure 1.4. Common ligands used in the CuAAC reaction.

TBTA (**1.30**) was the first ligand shown to increase the reaction rate of the CuAAC.[39] It was believed to stabilise the Cu(I) by the chelation of the tetradentate centre to the Cu, forming a complex and to break any poly-copper complexes that were formed. However, TBTA was limited by its aqueous solubility, therefore THPTA (**1.31**) was developed.[9] Further developments led to the use of BTTAA (**1.32**) and BTTES (**1.33**) ligands, which enabled low copper loading leading to reduced Cu toxicity.[40] BTTAA and BTTES have also emerged as superior ligands for the CuAAC due to being tolerated in cellular conditions and increased water solublity.[41] In a demonstrative reaction, the reaction between azido sialic acid and biotin-alkyne was carried out in Jurkat cells. BTTAA- and BTTES-Cu(I) catalysts did not hinder cell proliferation and BTTAA-Cu(I) gave a significant rate improvement over THPTA. This lower toxicity is believed to originate from increased ability to stabilise the Cu(I).

1.1.2.4 Influence of Azide and Alkyne Substrates on the CuAAC Reaction

Another important development for the CuAAC reaction was chelating azides which were first used by Zhu in 2009 (Scheme 1.5).[42] It was found that the use of picolyl azide (**1.34**) resulted in an increase in the reaction rate of the CuAAC, without the use of a reductant.

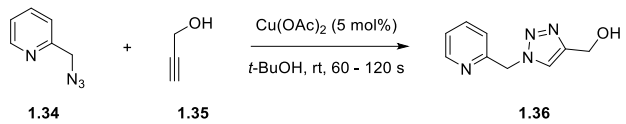

1.34 **1.35** **1.36**

Scheme 1.5. Formation of **1.36** without the use of a reductant.

Three copper salts were tested during the development of the reaction: $CuCl_2$, $CuSO_4$ and $Cu(OAc)_2$. Using 5 mol% $CuCl_2$, the reaction only proceeded in *i*-PrOH, EtOH and MeOH; there was no product observed in *t*-BuOH. This led to the theory that the Cu(I) species was generated by reduction of $CuCl_2$. The difference in counterion was then tested, and $Cu(OAc)_2$ gave product in *t*-BuOH, unlike others. The reaction was then carried out with $CuCl_2$ in *t*-BuOH with a reducing agent, NaAsc, producing the triazole in 88% conversion. This led to the speculation that Cu(I) could be formed from a Cu(II) catalysed Glaser reaction to form a diyne (Scheme 1.6A), or alcohol oxidation (Scheme 1.6B).

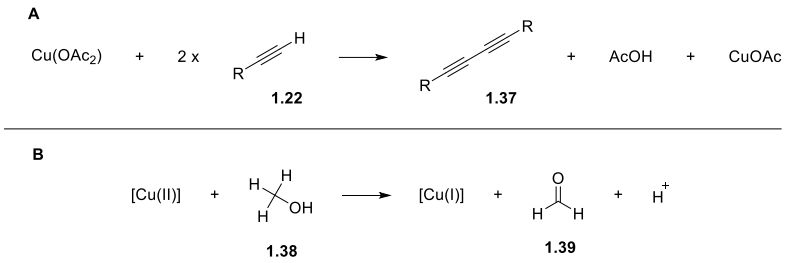

Scheme 1.6. Two potential methods for Cu(I) formation. **A) B)** Formation of glaser from alkyne; **B)** Formation of Cu(I) from alcohol oxidation.

Further work by Zhu to investigate the mechanism using the copper-chelating azides found that the increased reactivity of chelating azides contributed to the copper-azido interaction pre Cu(I) acetylide formation.[43] The copper complex is then reduced to give the Glaser product, giving increased precedence to the Cu(I) originating from Glaser formation.

A study by Kislukhin *et al.* investigated the reactivity of alkynes (Figure 1.5).[44] A variety of alkynes were tested and propargyl alkynes (such as propargyl ethers and *N*-propargylamide) gave a good combination of reactivity, ease of reaction and cost of substrate. Propiolamide **1.40**, was the most reactive, however, did have an increased tendency for Michael addition. Propargyl ethers **1.41** and **1.42** were the next fastest, however, aromatic and aliphatic alkynes **1.44** and **1.45** were the slowest. Tertiary propargyl esters and carbamates were found to not be suitable for the CuAAC. The leaving groups are lost upon formation of the Cu-acetylide to give Cu-stabilised propargyl cations which can trap nucleophiles. If this occurs in alcoholic solvents, propargylic alcohols are formed.[45]

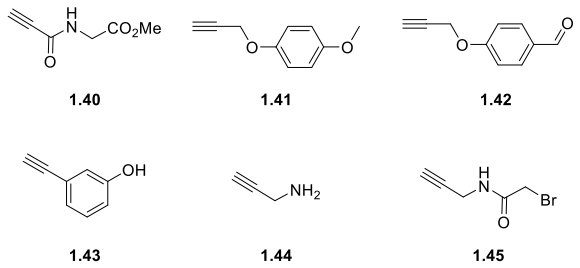

Figure 1.5. A selection of the alkynes tested by Kislukhin et *al.* [44]

1.1.2.5 Effect of Solvent

A main advantage of the CuAAC is its' versatility in different solvents, with the reaction able to proceed in organic solvents, water or ionic liquids.[46] During the ligand accelerated CuAAC,

the solvent chosen can play a large role.[30,47,48] There is competition for the accessible coordination sites of the Cu between the azide, the ligand and the solvent molecules. The azide tends to have a weak donor strength, but the tuning of the ligand and the solvent can impact their ability to concentrate. When weak donor ligands are in combination with water the rate of the reaction is accelerated but when in a strong donor solvent environment, *e.g.* DMSO, this is perturbed. This demonstrates that the solvent chosen can have change the mechanism of the reaction.

1.1.2.6 Limitations of CuAAC

The major limitation of the CuAAC reaction for use in live cells and *in vivo* is the use of copper in the reaction due to its cytotoxicity. Whilst copper is found in cells, the actual concentration depends on the cell type and there is almost no measurable level of unbound copper present in cells that would be capable of catalysing the CuAAC.[49] This is because free copper is cytotoxic due the formation of reactive oxygen species. The Cu(I) will react with dissolved molecular oxygen to form superoxide which can be converted to hydroxy radicals.[50] These hydroxy radicals can damage the cells in a number of ways, including damaging the DNA backbone through the cleavage of nucleic acids.[51,52] In addition to DNA, amino acids such as histidine and cysteine can be oxidsied.[53] Furthermore, ROS are involved in many critical roles of the cell and any dysregulation can cause problems.[54]

Whilst the addition of a ligand can reduce the copper loading necessary for the CuAAC reaction, copper free click reactions have largely superseded the CuAAC reaction in *in vivo* applications.

1.1.3 Strain-Promoted Azide-Alkyne Cycloaddition (SPAAC)

1.1.3.1 Development

In 2004, Agard *et al.* reported the first 1,3-dipolar cycloaddition between an azide and a cyclooctyne for bioconjugation.[5] This was named the strain-promoted alkyne-azide cycloaddition (SPAAC). SPAAC allowed the labelling of biomolecules without the need for cytotoxic copper and relies on the decreased activation energy of the strained cyclooctanes. The first *in vivo* use involved the labelling of the surface of azide-modified Jurkat (**1.46**) cells using a cyclooctyne (**1.45**) (Figure 1.6).

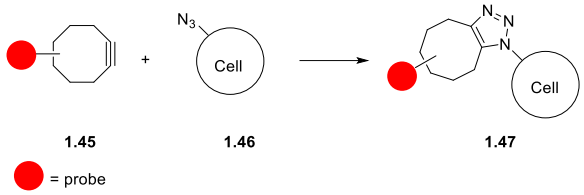

Figure 1.6. The SPAAC reaction between cyclooctyne **1.45** and azide **1.46.**

A limitation of the SPAAC was the slow reaction rate. In initial studies, the Staudinger ligation was the better performing bio-orthogonal method. However, subsequent modifications to the cyclooctyne aimed to increase the reaction kinetics.

1.1.3.2 Effect of Substrate

Initial modifications included the removal of the phenyl group (**1.49**) from **1.48** and incorporation of fluorine atoms (**1.50** and **1.51,** Figure 1.7).[55,56] The removal of the phenyl ring reduced the potential of a steric clash while the addition of a fluorine in **1.50** increased the rate constant by lowering the LUMO of the alkyne, thus reducing the gap between the HOMO of the azide. The addition of two fluorine groups to give **1.51** resulted in a large increase in the reaction rate.

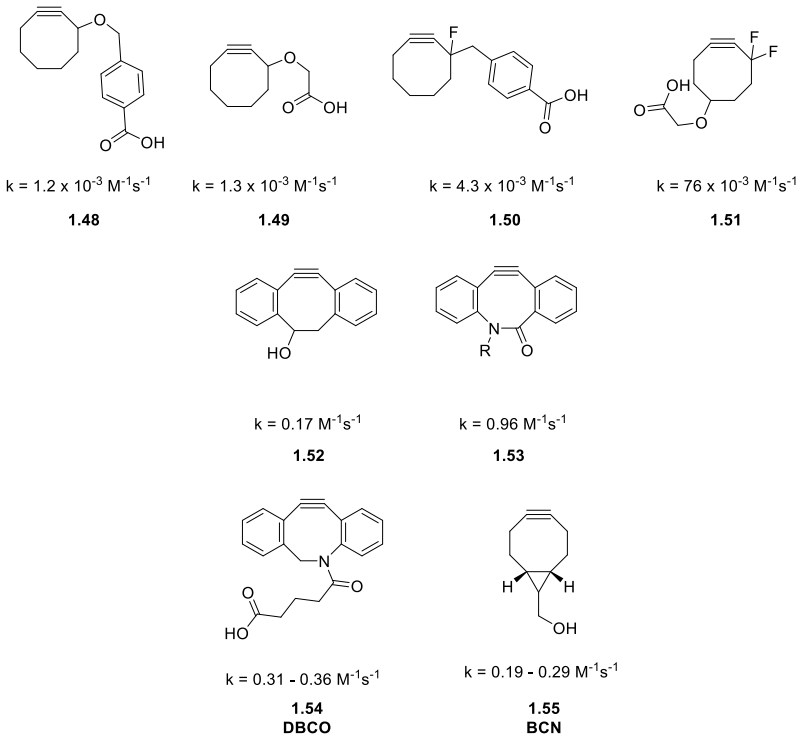

Figure 1.7. Cyclooctyne derivatives and their rate constants.

The addition of aryl rings to the cyclooctyne to increase ring strain was also investigated (**1.52**). Ning *et al.* had hypothesised that the increased ring strain coupled with ortho hydrogens potentially preventing nucleophilic attack through a steric clash would substantially increase reaction rate.[56,57] The reaction rate increased compared to **1.48** and **1.51**, however, in the biological systems tested, the solubility was low (100 μM). Debts *et al.* then attempted to increase the reaction rate, and the solubility, through the addition of a nitrogen into the ring (**1.53**).[58] Jewett *et al.* then further developed the system to give **1.54**.[59] The addition of an additional sp^2 carbon centre to the ring further increased the ring strain and largely increased the reaction rate. However, the stability of the substrate was decreased, with a 24 h half-life in the presence of an excess of GSH. Dommerholt *et al.* attempted to solve solubility and stability issues by developing bicyclo[6.1.0]nonyne (BCN) (**1.55**), which could be synthesised in only three steps to form two diastereomers. Both isomers have fast reaction rates and are stable in GSH for 48 h.[60]

1.1.3.3 Effect of Solvent

Further ways to improve the SPAAC reaction have also been investigated, including the solvent used. In a study by the Heemstra group, the effect of solvents and buffers was investigated on the reaction between a hydrophilic DBCO reagent and a hydrophilic azide.[61] It was found that the type of buffer and the pH did not affect the reaction rate significantly. However, when testing co-solvents it was observed that the rate decreased when a larger amount of co-solvent was present. For example, with MeCN as the co-solvent, a 50% decrease in the rate constant was observed for a change from 10 to 70% MeCN, resulting in a decrease in the water content of the reaction. The reasoning behind this was given as being a result of the loss of stabilising hydrogen bonding from water during the transition state.

1.1.3.4 Limitations of SPAAC

Despite the research into the rates and stability of reagents used in SPAAC, there remain limitations. The rate constants are still slow compared to other bioorthogonal reactions, and an increase in the reactivity often comes paired with a decrease in the stability.[62] The large size and hydrophobicity of the cyclooctynes also lead to decreased cell permeability and limited intracellular distribution. The synthesis to reach the desired cyclooctyne is also typically lengthy and the SPAAC reaction itself forms 2 regioisomers, which can be perceived as a limitation in some applications.[63,64] BCN and DBCO are the most commonly used SPAAC agents in current literature, owing to their favourable characteristics and commercial availability.[64,65]

1.1.4 Inverse Electron Demand Diels Alder

The currently fastest bioorthogonal reaction developed is the inverse-electron demand Diels-Alder (IEDDA) reaction (Scheme 1.7) which utilises a *trans*-cyclooctene (TCO, **1.56**) and a tetrazine (i.e. **1.57**). Since the first use in a biological application in 2008 by Blackman *et al.*, there has been significant developments in the field.[6] The initial reaction tested in a biological context gave a rate constant of 1140 M^{-1} s^{-1}, and an improvement to 2000 M^{-1} s^{-1} when used in a MeOH/H_2O (9:1) solvent system (Scheme 1.7). Alongside organic solvents, the reaction was successful in water, cell media and cell lysate while being Cu-free and only producing N_2 as a by-product. These reaction rates established a new standard for bioconjugation chemistry.

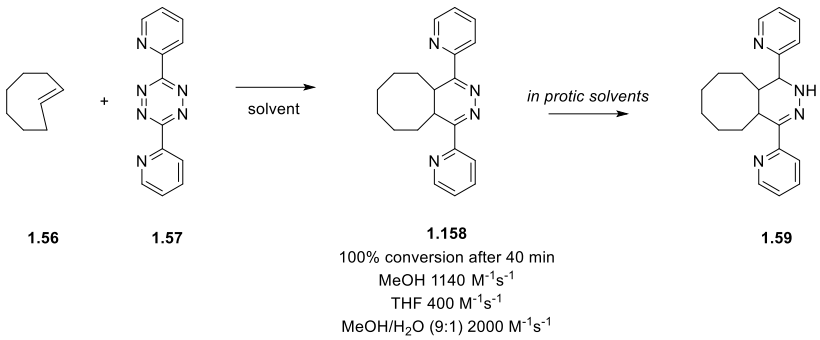

Scheme 1.7. The first use of the IEDDA in a biological context.[6]

In 2008, in parallel to the initial publication by Blackman *et al.*, Deveraj *et al.* had been working on the IEDDA using norborene (Scheme 1.8).[66] In this study, the reaction of tetrazine **1.61** with norbornene **1.60** gave a second order rate constant of 1.9 M^{-1} s^{-1} in aqueous buffer and in FBS a value of 1.6 M^{-1} s^{-1}. This was applied to a biological use with the reaction being used to tag SKBR3 cells with a tetrazine and subsequent reaction with a fluorophore modified with a norbornene group. Whilst this research indicated the feasibility for biological applications, the reaction rates are slow and need improvement.

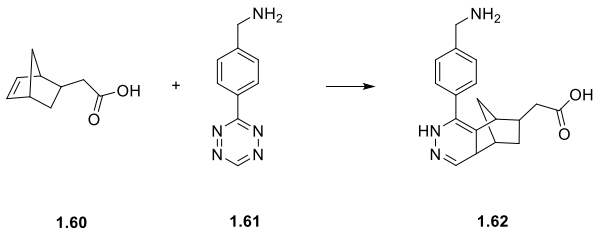

Scheme 1.8. First use of norbornene in a biological context.[66]

1.1.4.1 Mechanism

The reaction proceeds *via* a (4+2) cycloaddition between the diene (typically a tetrazine) and the dienophile (alkene or alkyne) to form a six-membered ring in a π4s + π2s fashion (Scheme 1.9). The diene and dienophile form a highly strained bicyclic adduct (**1.65**) which, through the release of nitrogen, is converted into a 4,5-dihydropyridazine (**1.67**). This then isomerises to the 1,4-dihydroisomers (**1.68** and **1.69**) and undergoes oxidation to the pyridazine product (**1.70**).

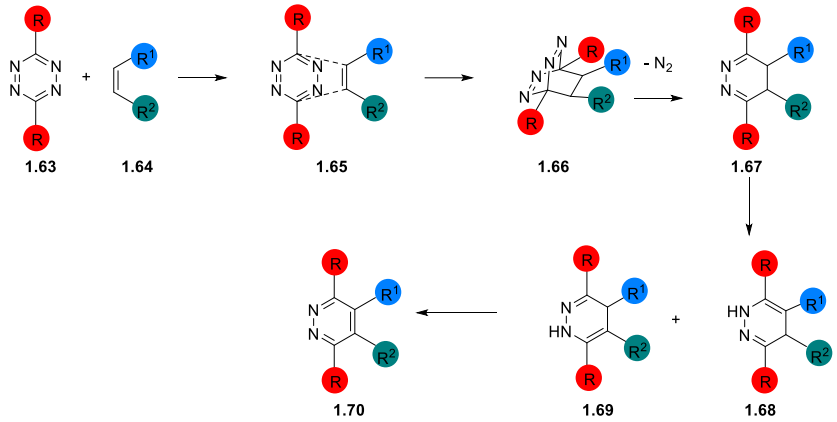

Scheme 1.9. Mechanism of the IEDDA reaction.

The reactivity of the IEDDA can be explained by molecular orbital theory, with the reaction rate determined by the gap between the $HOMO_{dienoiphile}$ and the $LUMO_{diene}$.[67] Pairs of reactants with a smaller energy difference will have a quicker reaction rate. By adapting the tetrazine and the dienophile the rate can be increased.

1.1.4.2 Substrate Effects - Dienophiles

Early work by Sauer found that dienophiles with electron-rich substituents tend to react faster.[68] The strain effect on the dienophile is also important. The addition of ring strain raises the $HOMO_{dienophile}$ as the conformation is distorted towards the transition state. Cyclopropene is therefore more reactive than cyclooctene. However, when TCO (**1.56**) was tested, it gave the fastest reaction rates, due to the crown conformation that it typically sits in (Figure 1.8). A stereochemistry effect is also present, with the axial isomer of a functionalised TCO (**1.73**) more reactive than the equatorial isomer **(1.72**) by around a factor of 4.

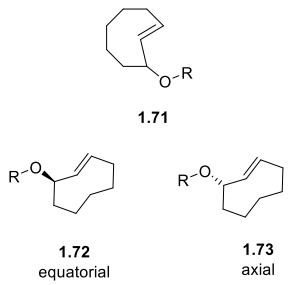

Figure 1.8. Stereochemical considerations of TCO analogues. [68]

1.1.4.3 Substrate Effects - Diene

The reactivity of the tetrazine used is influenced by the substitutions on the ring.[69] It was found that tetrazines attached to carboxylate groups (EWG) had faster kinetics than methoxy groups (EDG) due to lowering the LUMO energy. Mono-substituted groups tend to be more reactive than the di-substituted equivalents due to a reduction in steric clash. However, with increased reactivity of the tetrazine comes a loss of stability (Figure 1.9).[70]

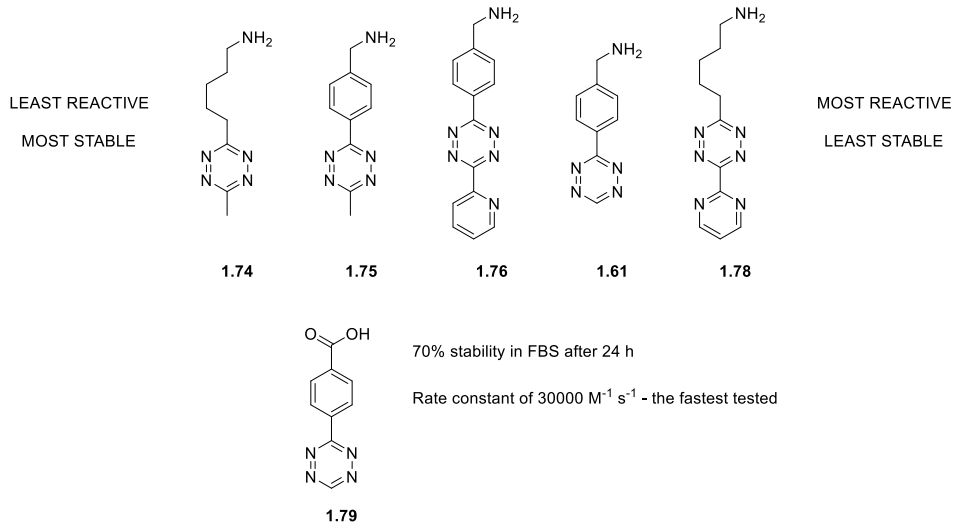

Figure 1.9. Tetrazine stability *vs.* reactivity. One outlier **1.79** was observed with relative stability and the best reaction rates.

One of the most commonly used tetrazines classes, due to fast reaction kinetics and the ability to be used at low concentrations, are tetrazines containing electron-deficient heteroaryl substituents such as pyridyl or pyrimidyl substrates (Figure 1.10).[71] It was previously assumed that the enhanced reactivity of these were due to the electron withdrawing effect of the heteroaryl group.[72] However, computational investigation has since shown that this is due to the tetrazine being distorted by repulsive N-N intramolecular forces.[73]

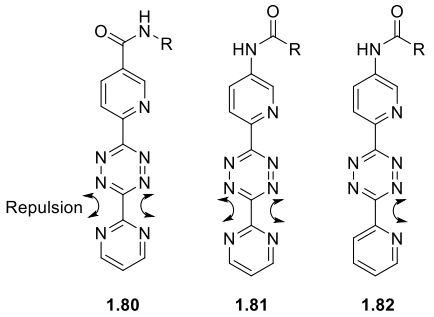

Figure 1.10. Tetrazines containing electron-deficient heteroaryl groups.

When designing a system for IEDDA, a balance of the properties of the tetrazines and the dienes needs to be taken into account in order to provide the best reaction rates and stability.

1.1.4.4 Click-to-Release Strategies

Whilst the IEDDA has been used in many biological and non-biological applications, one of the largest areas of research has been the click to release reaction. In 2013, Versteegen *et al.* reported a click-to-release as a new use for the IEDDA.[74] This involves the selective release of a functional group as a result of the IEDDA reaction. The first reported application involved the release of an Doxorubicon-amine (**1.87**) from a modified TCO (**1.83**).[74] The proof-of-principle study resulted in the formation of **1.87** in a 79% conversion using tetrazine **1.84**. It was found in the study that the bulkier tetrazines such as **1.57** gave poorer cleavage yields. This led to further investigations into click-to-release by Chen and Weissleder.[75,76] A follow up study by Chen then investigated a range of tetrazines to study what affected the release.[76] Various symmetrical and unsymmetrical tetrazines were tested (Figure 1.11B) with a fluorogenic TCO-conjugated coumarin reporter. The differences in reaction rate between tetrazines **1.84** and **1.90** confirmed that sterics played a part, with the less sterically hindered tetrazine giving the faster release. Electron rich and electron deficient tetrazines (**1.91** and **1.92**) were then tested, with the results showing poor efficiency in the reaction. The phenyl tetrazine showed higher reactivity than its EWG and EDG group counterparts. It was hypothesised that, since the decaging takes place in two steps, a cycloaddition followed by an elimination, that unsymmetrical molecules may be needed to have a functional group to facilitate both steps. All unsymmetric tetrazines tested were faster than their symmetric matched pairs.

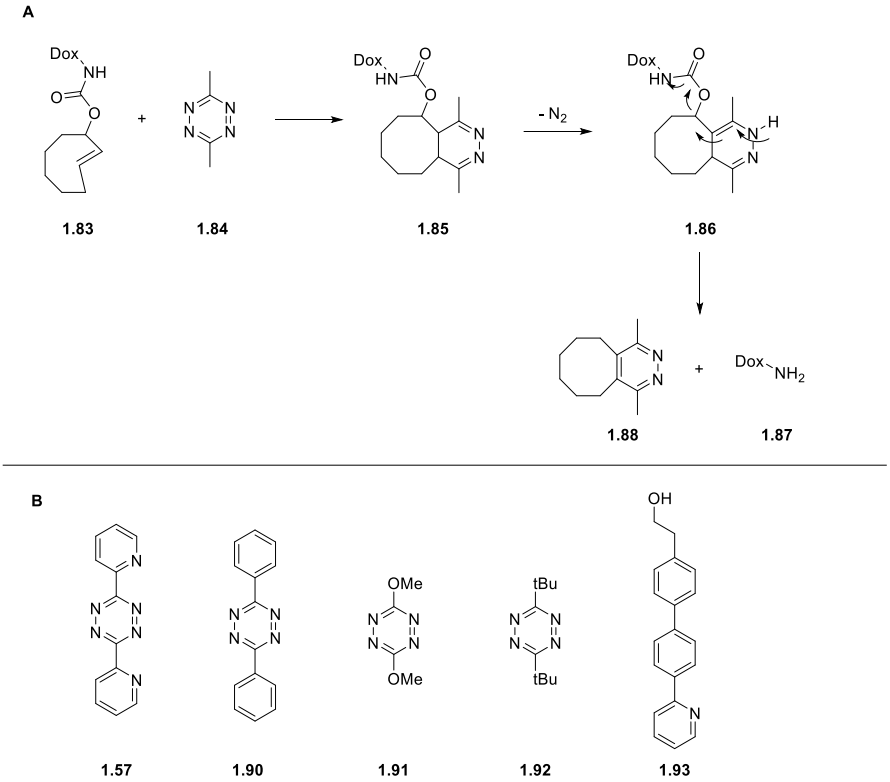

Figure 1.11. A) Click-to-release of Doxorubicin (Dox), **B)** Other tetrazines tested.

Carlson *et al*. then investigated the click-to-release reaction under biologically relevant conditions in 2018.[75] It was found that the release rate and the percentage of release obtained are environmentally specific. At a high pH, the release rate was found to be slow, however, at a mildly acidic pH (pH 5 or 6), the release rate is fast. During this study, the formation of a cyclised product (**1.94**) at high pH was observed, causing the low release yields (Figure 1.12). At a low pH, **1.95** tautomerized to **1.96** and **1.97** with only isomer **1.96** leading to successful release while **1.97** formed a dead end after oxidation.

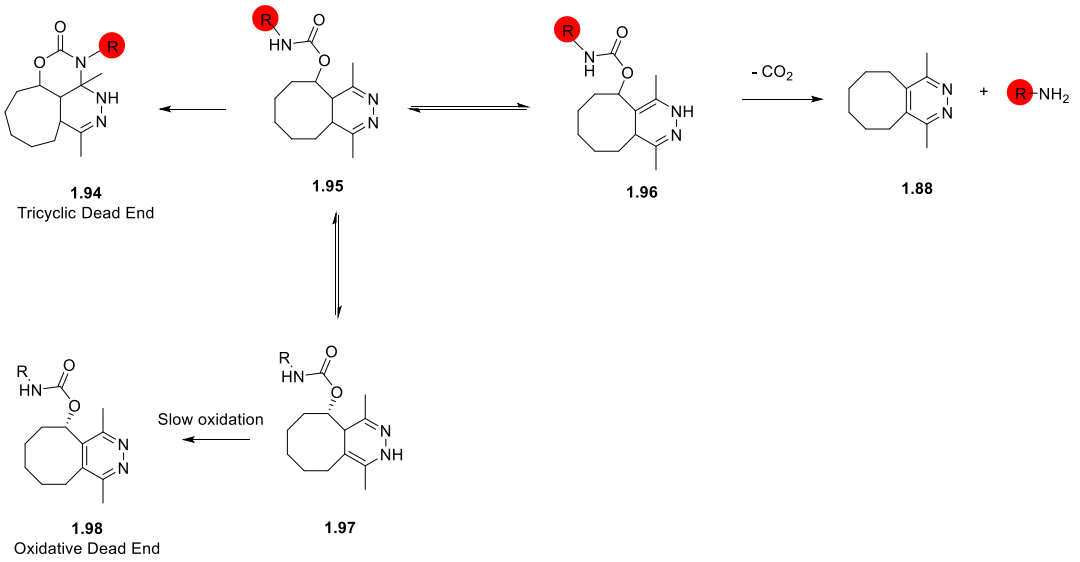

Figure 1.12. Routes to non-formation of desired product.[75]

1.1.4.5 Limitations of the IEDDA

The reaction rates of the IEDDA are unparalleled for bioorthogonal chemistry which results in reactions being able to be carried out at low concentrations. However, a balance needs to be obtained between reaction speed and stability. TCO is prone to *trans-cis* isomerisation by intracellular thiols, deactivating the strained system reducing the reactivity, and is also sensitive to acids and copper ions.[77]

1.1.5 Ynamine Structure and Reactivity

The conventional ynamine is an alkyne derivative where the nitrogen is in conjugation with the alkyne (**1.98**). The triple bond becomes polarised due to the nitrogen donating an electron pair into the triple bond, resulting in activation for protonation and the subsequent attack of water. However, this results in ynamines being unstable *via* hydrolysis (Scheme 1.10).[78]

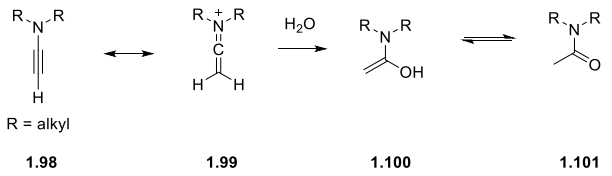

Scheme 1.10. Hydrolysis of an ynamine.

In contrast, Burley *et al.* have demonstrated that aromatic ynamines (**1.103**) are not prone to hydrolysis and also have a high reactivity in the CuAAC reaction.[79] The ability of the nitrogen

to donate electron density into the triple bond is reduced by the delocalisation of the lone pair in the aromatic ring (Scheme 1.11).[80]

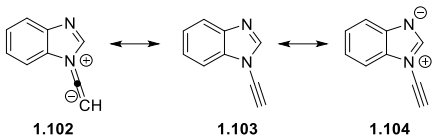

Scheme 1.11. Resonance forms of the aromatic ynamine.

1.1.5.1 Ynamine Reactivity in the CuAAC

The role of the ynamine in the CuAAC was investigated by Hatit *et al.*[81] This research showed that the ynamine exhibits reactivity with a wide variety of azides without a reducing agent. The alkyne used as a control in this study, *N*-phenylhept-6-ynamide (**1.105**) did not react in MeCN and in MeOH reached a lower conversion than with the ynamine (Scheme 1.12).

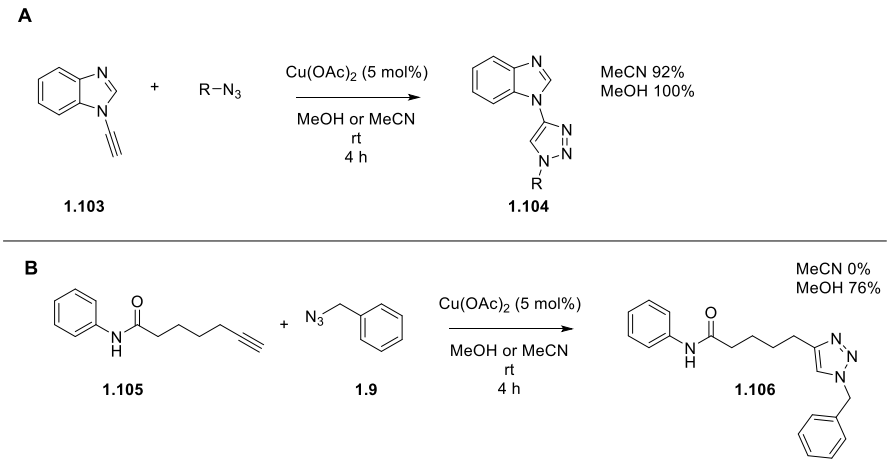

Scheme 1.12. A) Click reaction of the aromatic ynamine. R indicates a large azide scope; **B)** Click reaction of a conventional alkyne.

The addition of a reducing agent (NaAsc) and a ligand (TBTA) gave an increase in the conversion for the conventional alkyne **1.105**, something that is not required for the ynamine **1.103**. Competition experiments between the ynamine and conventional alkyne showed that the ynamine triazole (**1.104**) is the only product in a reaction with cyclohexyl azide in MeCN and MeOH and benzyl azide in MeCN. With benzyl azide **1.9** in MeOH, 90% of the triazole product was formed and only 10% of the conventional alkyne triazole.

This difference in reactivity was further probed by using a bifunctional system (**1.105**) with an ynamine and an aliphatic alkyne present (Scheme 1.13). The aromatic ynamine moiety

reacts first, followed by the aliphatic alkyne moiety reacting with a second azide in the presence of NaAsc and a ligand, to form either **1.107** or **1.106** – depending on the order of azide addition.

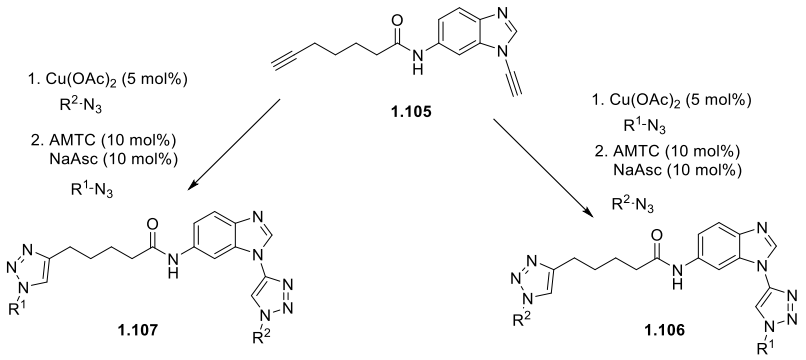

Scheme 1.13. Reaction of alkyne **1.95** with azide in MeOH/H_2O.[81]

The selectivity of azides for the ynamine over conventional alkynes was explored in a 2017 paper.[82] It was found that azide selectivity could be controlled by the use of a chelating azide such as picolyl azide **1.54**, with which alkynes are favoured over benzyl azide **1.9**. This allowed the selective reaction of the ynamine (**1.107**) and the alkyne (**1.108**) with the two azides (**1.9** and **1.54**) in a four-component reaction to form either **1.109** and **1.111** or **1.110** and **1.112** (Scheme 1.14).

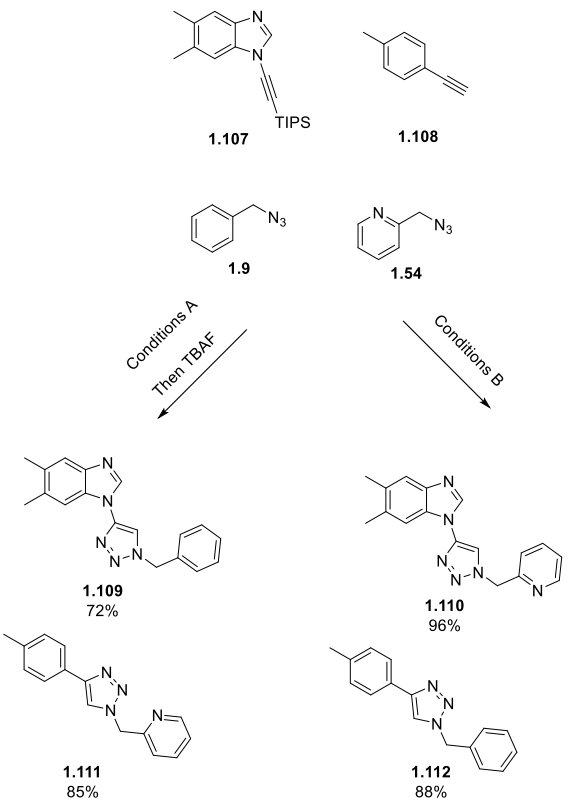

Scheme 1.14. Selective reaction of alkyne/azides. Conditions A: $Cu(OAc)_2$ (5 mol%), NaAsc (10 mol%), AMTC (10 mol%), DMSO/H_2O (1:1), r.t. Conditions B: $Cu(OAc)_2$, TBAF (1.1 equiv), MeCN, r.t.

A further study by Peschke *et al.*, investigated the influence of glutathione (GSH) on the ynamine-azide CuAAC (Scheme 1.15A).[83] GSH is present in millimolar concentrations in the cellular environment, and it can act as a chelating agent for Cu(II) as well as a reducing agent to form GSH-Cu(I) complexes. This results in GSH inhibiting the CuAAC reaction by sequestering copper. The stability of the ynamine to GSH was first tested, and in the presence of 5 mM of GSH, 10% of the ynamine was converted to GSH adducts.

The ynamine (**1.113**) and other alkynes (**1.114 – 1.116**) were then tested with benzyl azide (**1.9)** as the reactant partner, in the presence of GSH (Scheme 1.15B). The dimethyl ynamine (**1.13**) was found to react faster in the presence of GSH than other alkynes - which also required additional NaAsc to react, and this was true of the reaction with other azides (Scheme 1.15C), such as azido-ethanol (**1.117**) and picolyl azide (**1.54**).

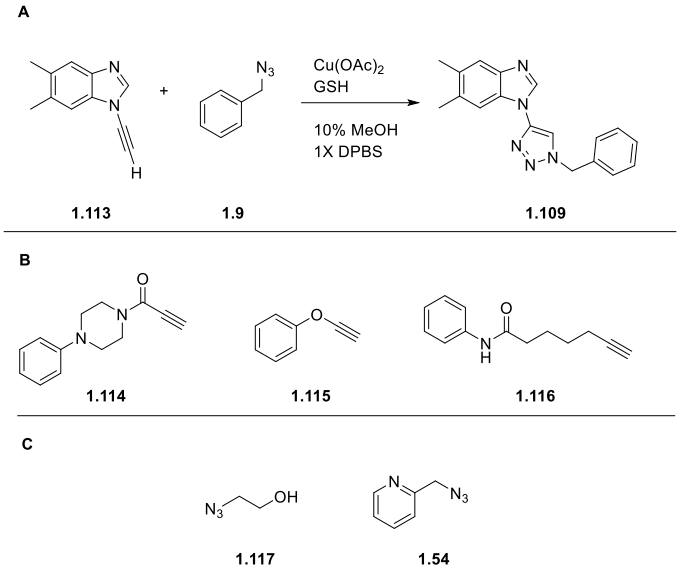

Scheme 1.15. A) CuAAC reaction of ynamine and benzyl azide in the presence of GSH; **B)** Alkynes also tested; **C)** Other azides tested.

Design of experiments was used then used to explore the influence of the Cu:GSH ratio on the reaction. It was discovered that ratios <2:1 accelerated the reaction while higher ratios (>3:1) inhibited reactivity. The optimum conditions were obtained as a GSH:Cu(II) ratio of 1:1 at 100 μM Cu. Additionally, the co-solvent of the reaction also influenced reaction kinetics with fluorinated solvents such as HFIP or TFE (both 10%) accelerating the reaction compared to MeCN as the solvent.

The use of GSH as an ynamine reactivity modulator was then explored with these optimised conditions (Scheme 1.16). Previous work has shown that Cu(I) can act as a protecting group for the internal alkyne of DBCO.[84,85] When a Cu chelator is then added, there is decomplexation and the alkyne is reactive again. By using the GSH, the Cu(II) can be reduced to Cu(I), allowing transient protection of the DBCO. This hypothesis was tested in the selective labelling of dual azide-tagged cell-penetrating peptide **1.118**.

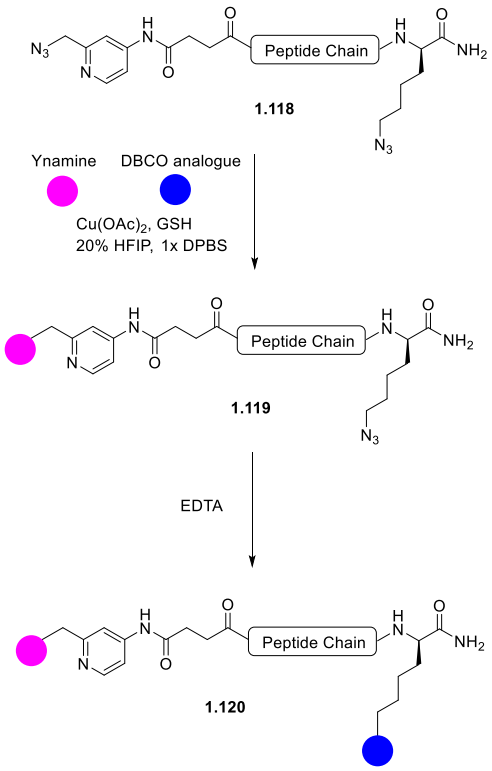

Scheme 1.16. Synthesis of a peptide containing an ynamine triazole and a SPAAC adduct.[83]

In the presence of $Cu(OAc)_2$, the ynamine reacts preferentially with the picolyl azide to form **1.119**, while the DBCO is protected by the reduced Cu(I). When EDTA is added to chelate the copper, the SPAAC reaction occurs to form **1.120**. This opens the possibility of using conditional reactivity for selective labelling of biomolecules.

1.1.5.2 Mechanistic Investigations of the Ynamine in the CuAAC

As has been shown, the ynamine exhibits a unique chemoselectivity and reactivity over conventional alkynes. To investigate the origin of this, NMR was used.[86] Competition experiments were carried out between the ynamine (**1.113**) and a series of representative alkynes (**1.121-1.125**) (Figure 1.13).

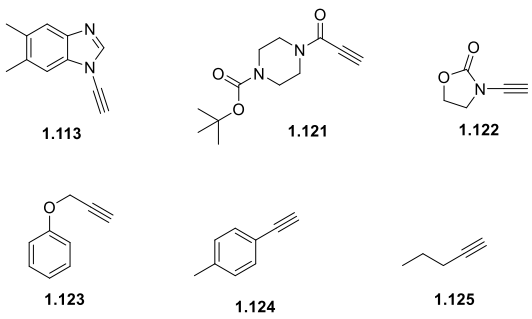

Figure 1.13. Alkyne substrate scope.

In the competition experiments, the ynamine (**1.113**) was the fastest alkyne tested, and almost always the exclusive product. When the reactions were conducted on individual alkynes, only **1.121** outperformed the ynamine **1.113**.

NMR experiments showed that in the CuAAC reaction, the reaction rate of the ynamine was independent of the concentration of alkyne (zero order), however, was second order dependent on concentration of azide. This contrasts from the conditions for conventional alkynes where there is a small negative dependency on the azide concentration. This suggests that there is a change in the azide RDS of the CuAAC when ynamines are the alkyne substrate. Further data also suggested that the rate of formation of copper acetylide was fast when compared to other alkynes and it was postulated that this was a result of the co-ordination of copper to the N3 in the benzimidazole ring. Further experiments confirmed this with the use of indole-ynamine, which performed worse than the ynamine **1.113** in competition experiments with **1.121**, with almost no chemoselectivity observed. Additionally, no changes in NMR shift upon addition of copper were observed with the TIPS protected indole **1.127** whereas complex formation was observed with the TIPS protected ynamine **1.126** (Figure 1.14A). Whilst it was not possible to monitor copper co-ordination with deprotected ynamine **1.113** due to rapid C-H insertion, other Lewis acids, such as scandium triflate could be used (Figure 1.14B). These experiments showed an increase in the alkyne C-H acidity – the pK_a of the alkyne proton is lowered (demonstrated by a shift in the ^1H NMR signal of the alkyne proton). The pK_a of the ynamine alkyne proton in the absence of binding to N3 is 27.9, compared to a typical alkyne pK_a of 25.[86]

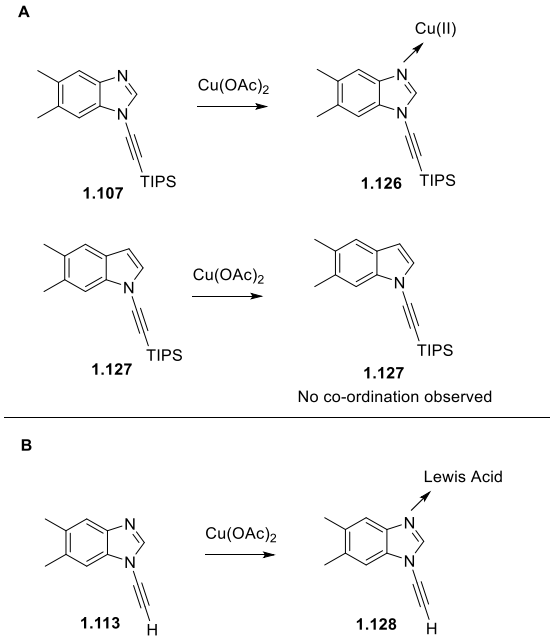

Figure 1.14. A) Chelating of Cu(II) to the benzimidazole N3; **B**) Chelating of a Lewis acid to the benzimidazole N3.

From this information the RDS for the ynamine CuAAC was postulated as shown in Figure 1.15. The Cu(II) coordination to the benzimidazole (**1.130**) results in an increase in the alkyne C-H acidity which gives a faster Cu acetylide insertion (**1.131**). The azide ligation/insertion (**1.132**) is then slower, and so the RDS for the ynamine is now this step. Further work is necessary to investigate the azide ligation/insertion step of this reaction to fully understand the parts of all the reactants in the mechanism.

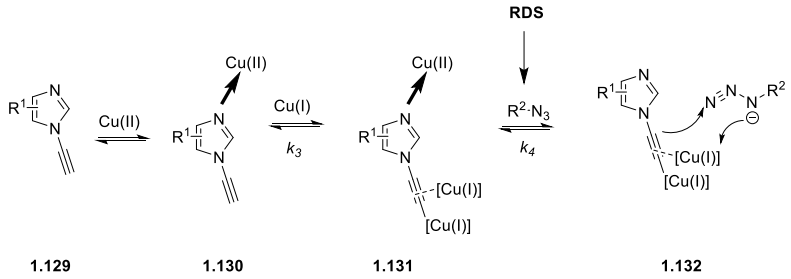

Figure 1.15. The RDS of the aromatic ynamine-CuAAC reaction.

1.2 Bioorthogonal Reactions in Imaging

The biggest use of bioorthogonal chemistry between 2010 and 2020 was for imaging, and it has been utilised for many biological targets due to its versatility.[7] Typically, in an imaging reaction involving click chemistry, a non-fluorescent molecule reacts with a coupling partner to give a fluorescent molecule. Dependent on the type of reaction required, a certain biorthogonal reagent may be more suited to a type of reaction than others.

1.2.1 Staudinger Ligation

Following on from the discovery of the Staudinger ligation, it became a powerful tool for imaging. The Staudinger ligation can be used in fluorophore labelling by forming a fluorescent turn-on probe (Scheme 1.17).[87] The coupling of a 7-amino coumarin-phosphine dye (**1.133**) to an azido target molecule (**1.134**) allows the formation of the phosphine oxide (**1.135**) which produces fluorescence.[88] This led to uses in the site-specific labelling of DNA and the tagging and subsequent imaging of cell-surface glycans.[89–91]

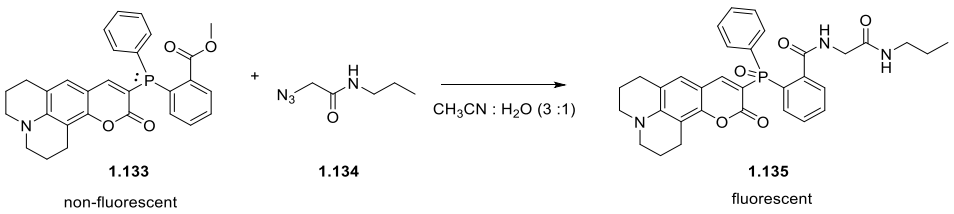

Scheme 1.17. Use of a fluorescence turn on probe.

However, as previously mentioned, the Staudinger ligation is no longer as commonplace due to its slow reaction rates, and much of the imaging that takes place using bioorthogonal tools uses reactions with faster reaction rates and more accessible coupling partners.

1.2.2 CuAAC

Since 2003 when Wang *et al.* reported the first biological application of the CuAAC, the reaction has been used in many forms of biological applications.[92] In 2012, fluorogenic azidofluoresceins were reported for no-wash imaging of cells upon the CuAAC.[93] This study established that rational design combined with DFT calculations could produce tailored probes for biological imaging. Following this rational, Shieh *et al.* developed a probe (**1.136**) which had a higher signal-to-noise ratio than probes previously reported (Scheme 1.18A).[94] This probe was used to label alkyne-tagged proteins *in vitro* to produce a fluorescent molecule **1.137**

and to then visualise the localisation of the alkyne-tagged glycoconjugates in cells at low concentrations.

A screening platform utilising CuAAC was instrumental in the reporting of the first examples of identification of a Fe^{II}/αKC-dependent pathway in the conversion of radical hydroxylases to halogenases (Scheme 1.18B).[95] The alkyne modified amino acid **1.138** was incorporated into the protein and a fluorogenic azide **1.139** was used, and upon the formation of the triazole **1.140**, fluorescence could be monitored. This fluorescence would only occur if the target had an alkyne, indicating hits.

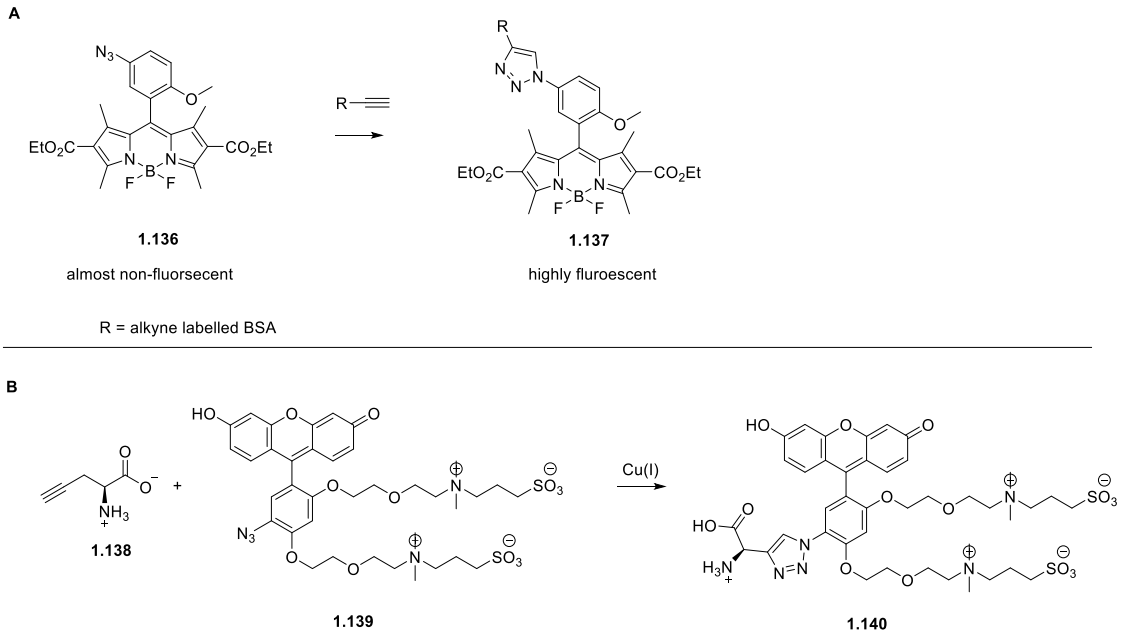

Scheme 1.18. Use of the CuAAC in fluorescence imaging. **A)** The labelling of alkyne tagged proteins; **B)** A screening platform using Cal-Fluor 488 (**1.139**)

1.2.3 SPAAC

The advantages of the SPAAC reaction for imaging include fast reaction rates and the use of azides and alkynes without the use of copper. It has been used in bioorthogonal glycan imaging.[96] The Kasper group used a TAMRA labelled DBCO **1.142** to fluorescently label commensal bacteria tagged with an azidoacetyl galactosamine derivative (**1.141**) (Figure 1.16A). In this study, both SPAAC and CuAAC were tested, and despite the copper promoted reaction giving higher fluorescence increase, the SPAAC technique was chosen due to its lack of the toxic copper.

Kleiner utilised SPAAC for the metabolic labelling of cellular RNA.[97] 2'-azidocytidine was used, in addition to a strained cyclooctyne imaging partner, and no degradation of the RNA

was observed, and the localisation of RNA was able to be imaged. SPAAC was also used in imaging by Teng *et al.* CAR-T cells were modified on the surface with tetraacetylated *N*-azidoacetyl-mannosamine (**1.144**) and following reaction with DBCO-Naph (**1.143**) formed a fluorescent molecule (**1.145**) (Figure 1.16B). This fluorescent molecule allowed the real-time fluorescent imaging of the cell to enable *in vivo* studies into cancer diagnosis.[98]

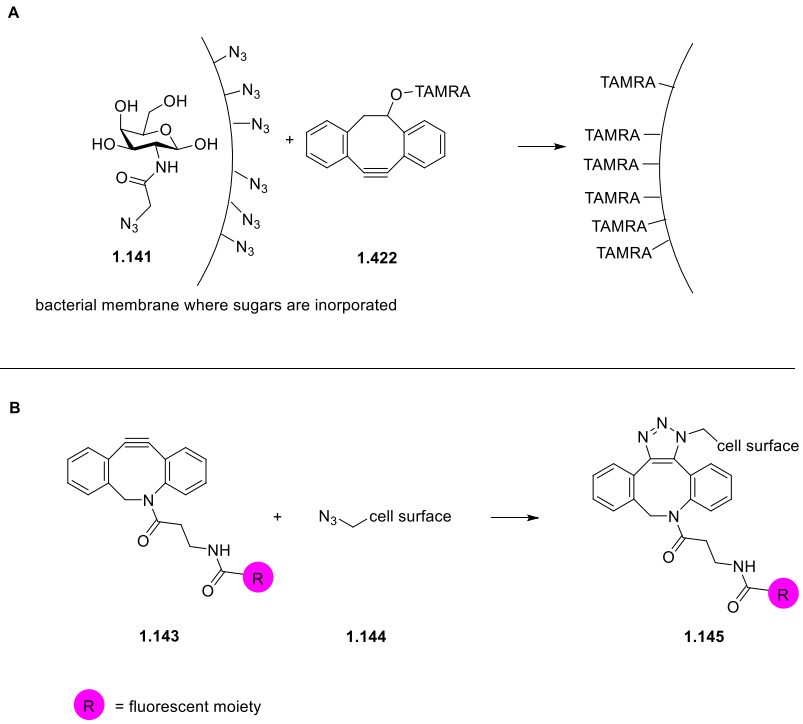

Figure 1.16. Imaging uses of IEDDA. **A)** Fluorescent labelling of commensal bacteria tagged with an azidoacetyl galactosamine derivative; **B)** The metabolic labelling of cellular RNA.

1.2.4 IEDDA

Since the publications in 2008, into the use of the IEDDA as bioorthogonal markers to modify proteins, the reaction has been exploited for a wide range of targets and purposes.[6,66] The tetrazine has been shown to be one of the most common moieties to attach a fluorophore to due to its ability to quench fluorescence prior to the IEDDA.[99]

The IEDDA has been used largely on unnatural amino acids which were then installed into a protein.[71,100] These unnatural amino acids typically contain strained alkenes such as norbornene, cyclopropane or TCO and react with tetrazine-fluorophore conjugates. These reactions are fast, can easily be performed in cells and, due to the fluorophore linker, can be easily imaged.

It has been shown that DNA and RNA can be modified with strained alkenes by introducing them during in-cell synthesis. This allows labelling to be carried out using tetrazine-fluorophore conjugates. The Luedtke group incorporated 5-vinyl-*2*'-deoxyuridine into the DNA of HeLa cells imaged it by reaction with a tetrazine-fluorophore.[101]

This chemistry can also be applied to biomedical imaging markers. Due to the short half-lives of radioisotopes fast reaction rates are important for the connection of the probe to the target, and despite CuAAC chemistry and SPAAC leading initial research in the field, they had their limitations.[102] Rossin *et al.* led the field with the reporting of IEDDA in radiolabelling with a paper describing the use of an ^{111}In-DOTA tetrazine derivative (**1.147**) to label *in vivo* an antibody (**1.146**) (Scheme 1.17).[103] This has then led to the development of many ^{18}F and ^{11}C based probes.

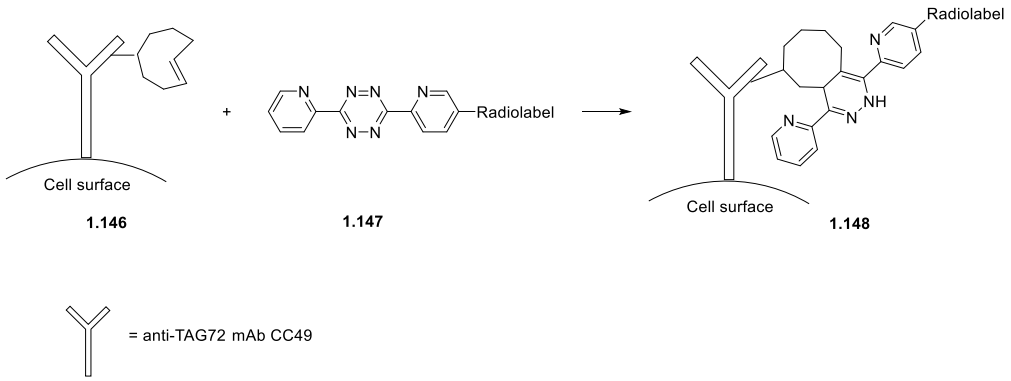

Figure 1.17. Use of the IEDDA in the radiolabelling of cell surfaces

1.2.5 Potential Future Uses

Despite the many applications of bioorthogonal chemistry in imaging, it has not yet been extensively applied to measuring cation concentration such as Ca^{2+} or K^{+}, although the CuAAC has been used to measure copper and zinc concentrations.[104,105] Measuring cation concentration can be challenging due to the fluxes in concentration, compartmentalisation, and low concentrations. The Ca^{2+} ion is an example of a cation that has had a large amount of research and development into probe synthesis and use.

1.3 Calcium Imaging

Calcium, a cellular second messenger, is a key component of cellular function. Ca^{2+} ions play a large role in communication and any dysregulation can plays a large role in key functions within the cell including muscle contraction, exocytosis, apoptosis, and cellular excitability.[106]

Due to its importance, the disruption of intracellular calcium is associated with neurodegenerative disorders, cardiovascular diseases, and cancer.[107]

The intracellular and extracellular concentration of Ca^{2+} is typically not in equilibrium and is fluid.[106] Intracellular concentration is typically around 100 nM, whereas extracellular is typically in the mM range (Figure 1.18).[106] Ca^{2+} transporting ATPases, Na^{+}/Ca^{2+} exchangers and Ca^{2+} binding proteins facilitate this gradient. This is different to the other divalent metal cation found in the cellular environment, Mg^{2+}, whose concentration does not vary as dramatically across the membrane (mM range).[108] The concentration of Ca^{2+} also varies in a particular cell depending on location, *e.g.* the cytosol, the endoplasmic reticulum, or the mitochondria (Figure 1.18). Under resting conditions within the cytosol, the concentration of Ca^{2+} is typically 100 nM, and can increase to <1 μM when activated.[109] However, this is lower than in the extracellular matrix, where the concentration of Ca^{2+} is as high as 1 mM. The mitochondria are involved in the release and take up of Ca^{2+} from the cytosol, regulating the concentration. Due to this active regulation, the concentration of Ca^{2+} can vary, typically from 100 nM to 10 μM.[110] Calcium stores, such as the endoplasmic reticulum (ER), typically have a Ca^{2+} concentration that can vary between 100 μM and 100 nM.[107] The levels of calcium within the cytoplasm are carefully controlled as an unregulated change will result in damage or death to the cell.[111]

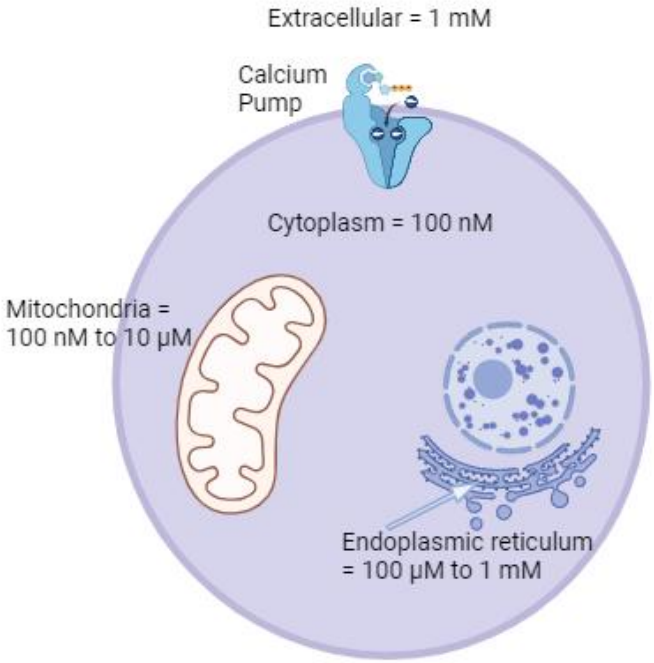

Figure 1.18. Illustrative calcium concentrations within the cell.[108–110]

The discovery of methods to measure Ca^{2+} concentration across the cell started a revolution in biology allowing to correlate Ca^{2+} flux oscillations with function and signalling processes. Nowadays, even physiological changes in the membrane potential and consequently changes in physiological Ca^{2+} currents can be measure by fluorescence-based optical techniques, in living cells, in their native environment. The main challenge that the field faces is how to assess to what extent the indicators attenuate the Ca^{2+} signal. At low concentration of the indicators, it is more likely that an unattenuated Ca^{2+} signal is being measured, whereas at high concentration of the indicators, it is more likely that Ca^{2+} flux is being measured.

1.3.1 Development of Calcium Probes

Calcium probes can be separated into two categories: chemical probes and genetically encoded Ca^{2+} indicators (GECIs).[112] GECIs can be used for imaging in both cellular models and living organisms. They were developed following the discovery of green fluorescent protein (GFP), the synthesis of different colour GFPs and the research into Ca^{2+} binding with calmodulin and M13. GECIs are useful in certain situations, such as neuroscience, and offer advantages that chemical Ca^{2+} indicators do not, including the precision of their targeted imaging and the ability to monitor Ca^{2+} over a long period of time.[113] However, chemical Ca^{2+} probes are more

accessible and commonly used. They have the advantages in that there is a large variety of probes already commercially available and the ease of use due to not needing to transfect cells. A disadvantage of the probes, however, is the lack of specificity, but ongoing research is attempting to tackle this.[114] This section will focus on chemical calcium probes.

1.3.1.1 History of Chemical Calcium Probes

The chemical Ca^{2+} indicators started with the development of quin-2 (**1.149,** Figure 1.19) by Tsien *et al.* in the late 1970s, which triggered a large amount of research. [115] Upon Ca^{2+} binding, the molecule rotates to cage the Ca^{2+} ion in a sphere. The Ca^{2+} ion can accommodate 4-12 oxygen atoms, with 6-8 being the most common. The K_d of quin-2 was ~ 100 nM, and was used extensively in biological studies, however, there were drawbacks associated with the probe.[107] The excitation wavelength is 339 nm, which posed issues with autofluorescence from cells and caused unwanted biological effects. The extinction coefficient (<5000) and fluorescence quantum yield (0.03 to 0.14) were low. This resulted in a large loading of dye being required, biasing the concentration measurement. The excitation and emission wavelength also did not increase upon the binding of the Ca^{2+}, only a fluorescence increase. This resulted in issues as the fluorescent intensity can differ on many other factors, such as dye concentration and cell thickness in the beam.

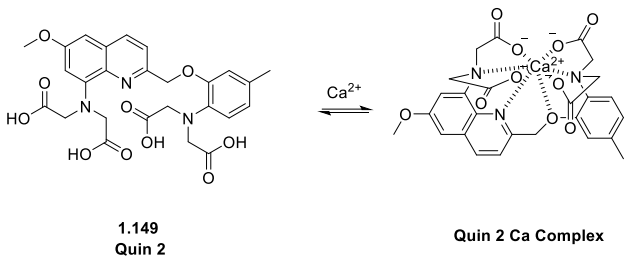

Figure 1.19. Structure of quin-2 (**1.149**) and a depiction of the confirmational change upon Ca^{2+} binding.

Following on from the quin-2 work, the discovery of the calcium chelating agent BAPTA (**1.150**) (Figure 1.20) led to its utilisation in many probes.[115] BAPTA improved binding for Ca^{2+} due to the 4 oxygen and 2 nitrogen groups present to facilitate the coordination. The unique motif preferentially binds Ca^{2+} over the smaller Mg^{2+} ion as the larger radius allows for an ideal size of chelate to form. It is still today the most prominent feature in calcium probes. BAPTA chelators were found to have advantages over the previously reported EDTA (**1.151**) and EGTA (**1.152**) in that it was less sensitive to intracellular pH changes, released the Ca^{2+} more quickly after binding and allowed for modification.[116]

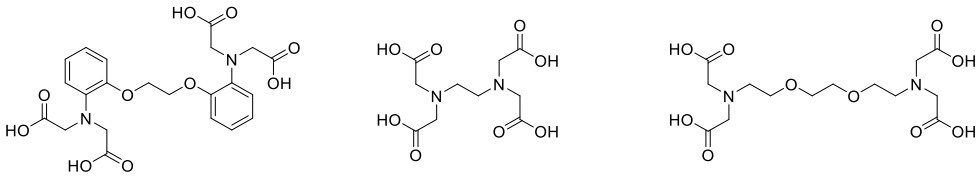

1.150 **1.151** **1.152**

Figure 1.20. Structure of BAPTA **1.150,** EDTA (**1.151**) and EGTA (**1.152**)

1.3.2 Design of BAPTA Calcium Probes

Current probes tend to combine the BAPTA moiety with a fluorophore and/or a targeting moiety. This allows the probe to be suitable to optical imaging of the Ca^{2+} within a cellular environment, and also allows targeting of a probe to a specific area. When designing a Ca^{2+} probe, it is not as simple as combining BAPTA with a fluorescent moiety. There are three main features that need to be considered: The dissociation constant, K_d; the spectral properties of the probe; and the behaviour of the probe in cells.[114]

1.3.2.1 Affinity

The dissociation constant, K_d, is the concentration of Ca^{2+} at which half the probe molecules are bound to Ca^{2+} at equilibrium. This is used to describe how tightly the Ca^{2+} ion is bound to the probe. Generally, probes should be chosen to measure a calcium concentration that is between 0.1 and 10 times their K_d as this is the region where fluorescence changes that are a result of Ca^{2+} ions are largest. It is therefore important that the K_d of a Ca^{2+} probe is in the range of the $[Ca^{2+}]$ in the target location. There are currently a wide range of calcium probes available that have K_d's ranging from 50 nM to greater than 50 μM. The K_d of a probe is dependent on many factors, including, but not limited to, the pH, temperature, and the presence of other competitive ions, such as Mg^{2+}. As a result of this, the probe may have a different K_d *in vivo* and *in vitro* within each cellular compartment.

The K_d of the probe needs to be suitable for the type of free Ca^{2+} ions being monitored. For example, the ideal K_d of a probe for measuring the Ca^{2+} concentration in the ER is between 22 μM and 250 μM as the ER concentration in cells is 100 μM to 1000 μM.

It is possible however to attempt to control the K_d of the probe. The nitrogen atoms in BAPTA act as Lewis bases for the Ca^{2+} and the basicity of these can be controlled by the groups on the BAPTA ring. By introducing EWGs, such as halogens or nitro groups, the K_d can be increased, and upon the introduction of EDGs, *e.g.* methyl, the basicity of the Lewis acid can be increased (Figure 1.21).[117]

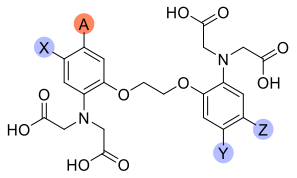

Figure 1.21. Structure of BAPTA with the opportunities for adding groups highlighted by X, Y and Z. A is for the linker to the fluorophore part of the probe.

1.3.2.2 Selectivity

Due to the similarities between calcium and other physiological ions, especially magnesium, some calcium probes are not specific for Ca^{2+}. Some of these probes, including Mag-Fura-2 (**1.153,** Figure 1.22) are indicators that can be used to image both Ca^{2+} and Mg^{2+}, albeit they are more selective for one over the other.[118,119] Generally, probes that bind Mg^{2+} bind Ca^{2+} at a 4-fold higher affinity. It is important to determine with probes whether Mg^{2+} binding has an impact on the fluorescence properties that could be interpreted as Ca^{2+} binding, or whether the magnesium, or other ions, have a discrete effect on the probe.

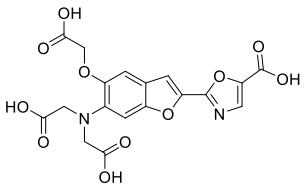

Figure 1.22. Structure of Mag-Fura-2 (**1.153**).

1.3.2.3 Spectral Properties

Probes can be classified as single wavelength or ratiometric. Single wavelength probes (Figure 1.23A) have a Ca^{2+} dependent change in their fluorescent intensity without exhibiting a change in the emission or absorption wavelength upon Ca^{2+} binding. Ratiometric indicators (Figure 1.23B) give a change in the absorption or emission wavelength upon Ca^{2+} binding. Because of this, the ratiometric probes are unaffected by any variances in concentration of the dye, changes in cell loading and photobleaching, allowing for a greater accuracy.[120]

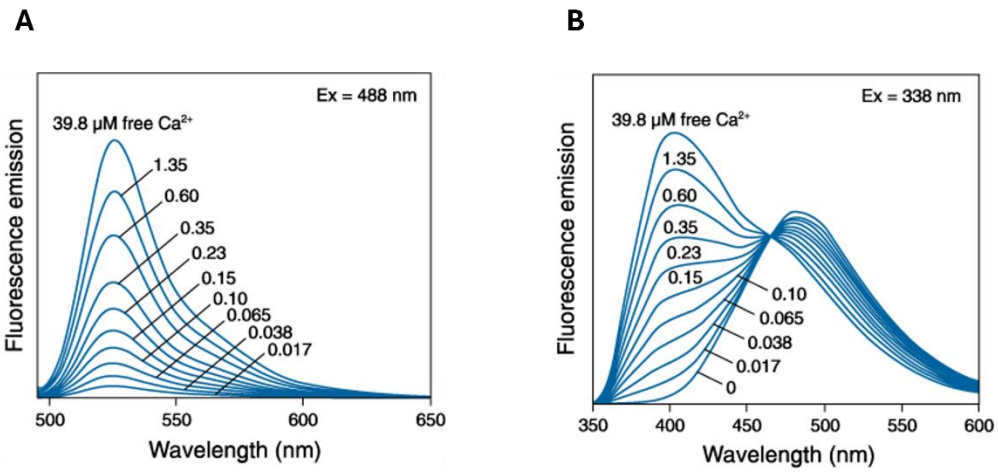

Figure 1.23. Example of a fluorescence emission spectra for: **A)** A single wavelength probe; **B)** A ratiometric probe.[121,122]

1.3.2.4 Entry Into Cells

The chemical form of calcium chelators is important as this determines the cell-permeating ability of the probe. Typically, calcium probes are found in three main forms: salts (**1.154**), dextran conjugates (**1.154-dextran**) and more typically for cellular activities, acetomethoxy esters (**1.154-AM**) (Figure 1.24).

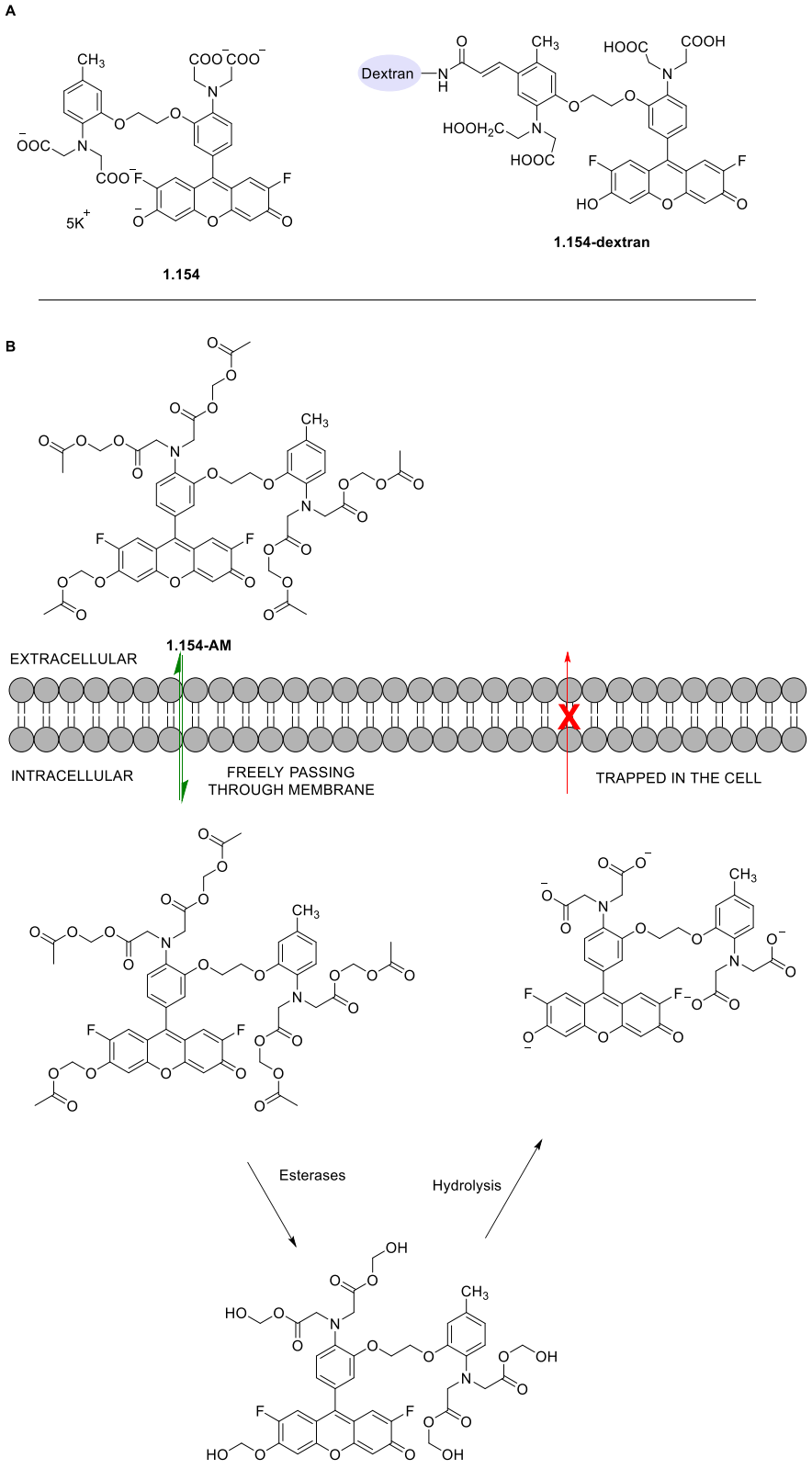

Figure 1.24. Different forms of probe for entering cells. **A)** The salt from and dextran conjugate of **1.152**; **B)** Depicts the AM ester of **1.152** entering the cell through the cell membrane and the cleavage of the esters

The simplest form that a probe can be found in is a salt (**1.154**). However, because of the hydrophilic nature of the salts, they do not pass through the cell membrane and prove difficult to be introduced to the cell. When probes are in the salt form, they equilibrate quickly and can only be used for short term calcium imaging. Calcium dyes in their salt form tend to compartmentalise into the membrane bound vacuoles which can diminish the Ca^{2+} cytosol measurements.[114] To attempt to resolve this issue, dextran conjugates (**1.154-dextran**) were synthesised which have many advantageous properties in addition to their lack of compartmentalisation, such as low levels of toxicity and high aqueous solubility. This results in the imaging of calcium being possible for an extended time. Like the salt forms, dextran conjugated probes can only be introduced to cells in an invasive manner due to their inability to permeate the membrane. Acetoxymethyl (AM) esters (**1.154-AM**) were added to the probe to increase cell permeability and were first developed by Tsien.[123] Most current probes can be found in the AM form. The AM ester increases the hydrophobicity of the probe, allowing it to pass through the cell membrane. When inside the cell, intracellular esterase's cleave the AM group and a hydrolysis occurs, leaving the probe charged and unable to leave the cell (Figure 1.24B). Due to their ability to get into cells, AM derived probes do not require invasive loading, instead, they can be added to the extracellular medium and will then pass into cells and are by far the most common form for cellular imaging.

1.3.2.5 The Design of the BAPTA Scaffold

An investigation into whether the BAPTA structure, with the aromatic rings and 2-carbon chain length between oxygen atoms, is as necessary as previous research suggests has been carried out. Cosmos *et al.* synthesised three known and four novel scaffolds containing a fluorophore and a Ca^{2+} sensing unit (Figure 1.25).[124] These changes included removing the second aromatic ring (**1.156**), adding an additional CH_2 linker (**1.157**), removing the second oxygen (**1.158** and **1.159**) and changing the chain length (**1.160** and **1.161**). The fluorescence intensity (FI) was determined for each of the compounds synthesised. As expected, the BAPTA analogue (**1.155**) performed the best (432 FI), however, **1.156** and **1.161** had high values (273 and 281 FI respectively). Ca^{2+} titrations were also performed, and compounds **1.156** and **1.161** gave favourable results. Computational studies carried out in this research showed that BAPTA has an optimal chain length between the aromatic rings, and exact cavity volume for Ca^{2+} binding.

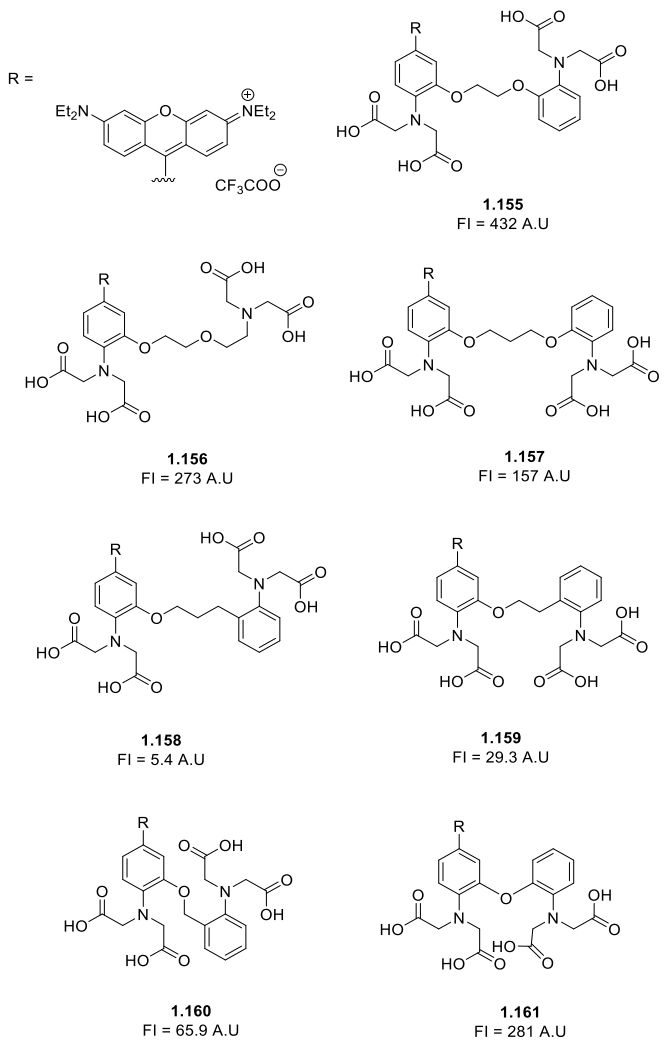

Figure 1.25. BAPTA scaffolds synthesised in the research and their corresponding fluorescence intensity (FI). [124]

This work has clarified that the BAPTA moiety is the best option for Ca^{2+} indicators, and that small changes, such as altering linker chain length, can affect the binding due to the need for optimal binding to the cation.

When designing a probe, the relative location of the fluorophore moiety to the BAPTA chelator is important. For example, in a rhodamine dye, incorporating the BAPTA into the pendant phenyl results in the largest of fluorescence increases. However, this is synthetically challenging and these indicators can lack in the quantum yield and calcium affinity.[117,125] For probes that rely on photoinduced electron transfer (PeT), the relative positions are key and the efficiency of quenching can depend on the distance between the electron donor and acceptor.[126] The closer the BAPTA is to the fluorophore, the more the fluorescence in the unbound state is quenched and therefore the fluorescence intensity upon Ca^{2+} binding will be higher. This is

illustrated for Oregon-Green (**1.162,** Figure 1.26A).[127] When the BAPTA chelates Ca^{2+}, the PeT is no longer quenched, and the molecule is fluorescent. The BAPTA group is not limited to attachments from the pendent phenyl rings, as shown by the probe (**1.163**) developed by Deo *et al.* (Figure 1.26B).[127] Here, the probe is attached to the xanthene core, and the PeT process is still in action.

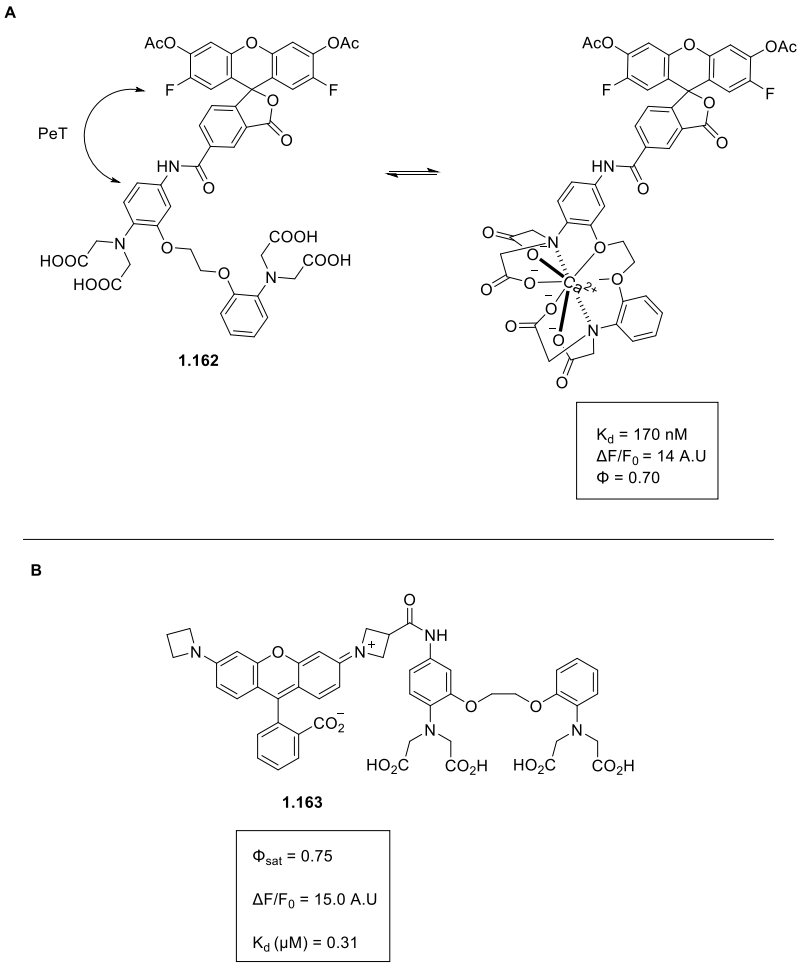

Figure 1.26. A) Demonstration of the PeT required in some BAPTA probes; **B)** BAPTA attached to the xanthene core.

1.3.3 Commonly Used Calcium Probes

Calcium probes currently in literature are a mixture of probes that were developed and commercialised in previous decades, and, ongoing research into new developments. Research in the chemistry field focuses on the development of new probes, and of also updating existing probes to address current challenges. However, probes that are typically used in biology research, are probes that have been well used over the years and are as standard for the purpose required. The structures and properties of some of these probes are given in Figure 1.27.[114]

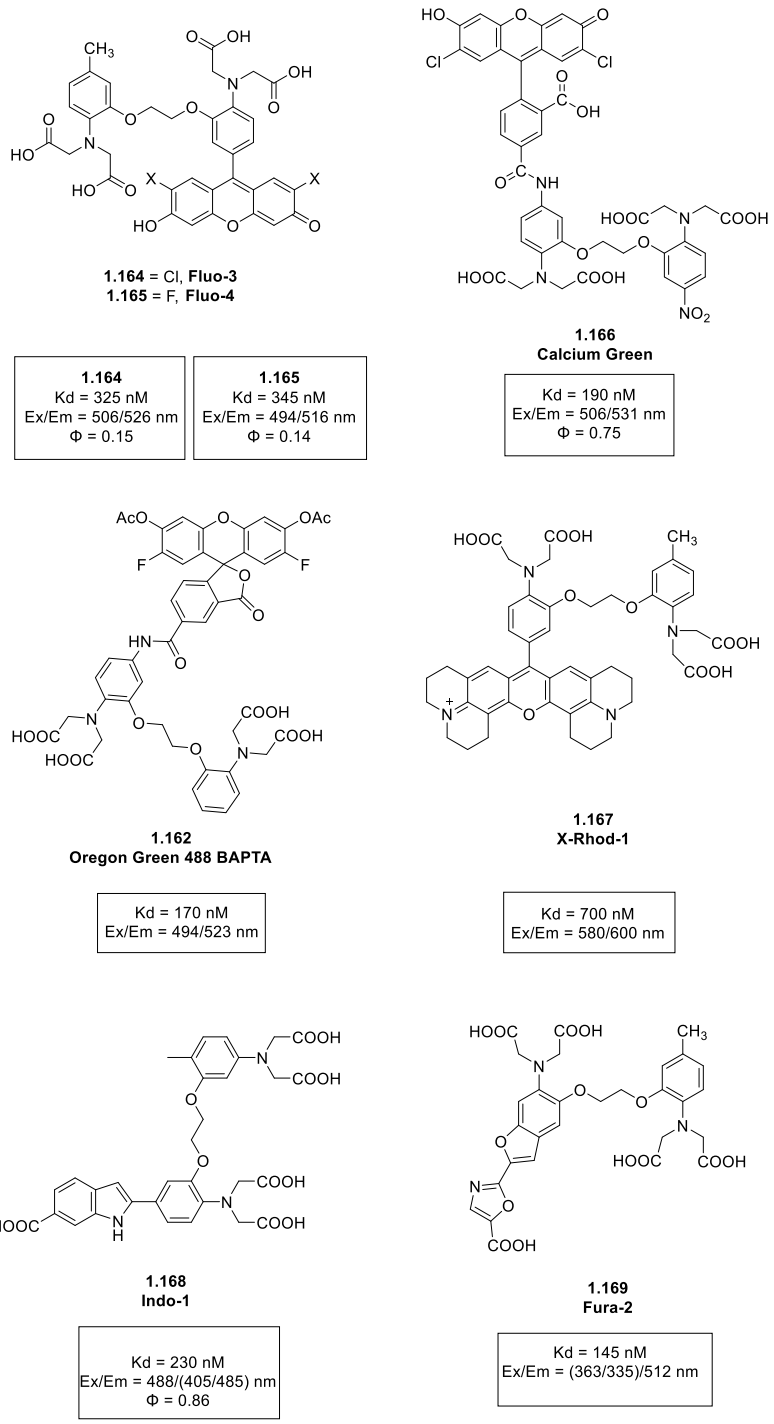

Figure 1.27 Commonly used calcium probes and their spectral properties.

The spectral properties can dictate the use of the probe. Fluo-3 (**1.164**) and Fluo-4 (**1.165**), derivatives of each other, have very similar spectral properties. Both are visible light-excitable single wavelength probes.[128] However, the small difference in excitation between the two

brings Fluo-4 closer to the wavelength of an argon 488 laser resulting in a probe that is brighter with increased photostability.[129]

Calcium Green (**1.166**) has a high quantum yield and favourable excitation and emission wavelengths that are suitable for almost all fluorescent microscopes. It is bright, with the fluorescence emission increasing 100-fold upon Ca^{2+} addition, allowing for it to be used at low concentrations.[130]

The Oregon-Green 488 BAPTA (**1.162**) is a member of a bright calcium probes that have similar characteristics to Calcium Green. However, the shorter wavelength (10 nm shorter) improves the excitation efficiency at the 488 nm argon laser line. The probe experiences a 14-fold increase in brightness upon Ca^{2+} binding and has a high quantum yield. This, and its small dissociation constant allow the use of the probe at lower dye concentrations.[131]

X-Rhod-1 (**1.167**) is based on a tetramethylrhodamine, with a shift towards the red zone for the wavelength properties. However, the K_d value is low, and this is suitable to measure Ca^{2+} concentration in mitochondria, which, due to the net positive charge of the AM ester, the X-rhod dyes tend to sequester.[114]

Indo-1 (**1.168**) and Fura-2 (**1.169**) are ratiometric dyes and have been used in a large number of applications, having been developed by Tsien.[132,133] Fura-2 has dual excitation at 340/380 nm and the fluorescence occurs at 500 nm. The ratiometric ability of Fura-2 is an advantage because it can give measurements of the Ca^{2+} ion concentration and the effects of photobleaching and dye leakage are largely mitigated. Indo-1 has advantages over Fura-2 in that the emission shifts from about 485 nm to about 400 nm when bound to Ca^{2+} and has a single emission, suiting it well to use in flow cytometry.

1.3.4 Recent Research into Calcium Probes

Recent research into calcium probes as focused on the issues that are common with probes, including the difficulties in organelle targeting and developing long wavelength probes. The NIR zone is particularly appealing for biological applications due to higher tissue penetration and lower phototoxicity. However, combining the visible light excitation with a high spectral shift to emitting in the NIR is difficult, without the added complications of the requirements of a high quantum yield and a resistance to photobleaching, and this has resulted in a lack of probes in this area.[117] However, several of these probes have been developed through recent research.

1.3.4.1 Development of Red Emitting (Long wavelength) Probes

Collot *et al.* reported Ca-NIR (**1.170**), the first ratiometric probe to emit in the NIR region (Figure 1.28).[134] It incorporates the BAPTA moiety fused to a fluorophore that emits in the NIR region. When the Ca^{2+} is bound, the electronic properties of the whole molecule shift, changing the spectral properties. Ca-NIR has two distinct emission bands, at 684 and 733 nm, that are dependent on the Ca^{2+} concentration, allowing ideal conditions for ratiometric imaging and it typically tends to localise in the nuclear envelope. However, the alkyne side chain is not exploited, and no further work has developed on this functionality.

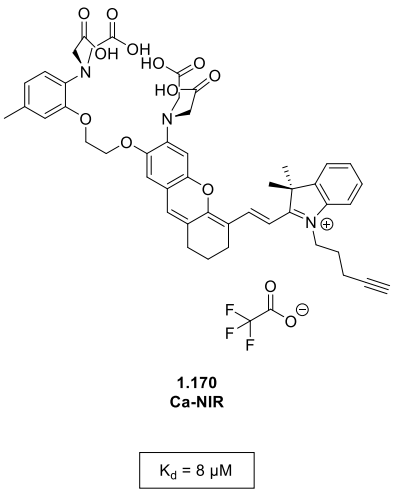

Figure 1.28. Structure of Ca-NIR (**1.168**).

Collet *et al.* have also developed a probe that is in the NIR region and deviates from the standard BAPTA based chelating model (**1.171**).[135] The pro-sensor is an alkyne (**1.172**) that can undergo a click reaction to form a 1,4-triazole (**1.173**) before base cleaves the ester to give **1.174** (Scheme 1.19).

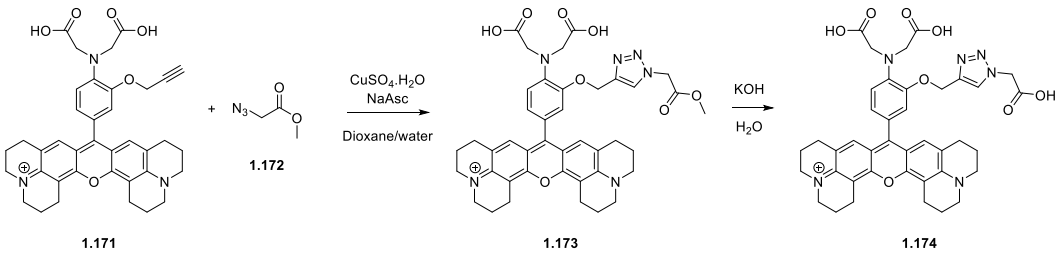

Scheme 1.19. Scheme depicting the formation of the 1,4-triazole from the alkyne pro-sensor.

It was found that probe **1.174** can chelate Ca^{2+} (49-fold increase in FE), in addition to Cd^{2+} (52 fold) and Zn^{2+}. The dissociation constant for the probe was then measured with both Ca^{2+} and Zn^{2+} ions. A similar affinity was obtained for both (K_d Ca^{2+} = 5.84 ± 0.21, K_d Zn^{2+} = 5.68 ± 0.14). However, the concentration of Zn^{2+} in cells is in the nanomolar region, which is below the dissociation constant obtained, and so the probe can still be categorised as a calcium sensor. This probe has a quantum yield of 0.78, a fluorescence enhancement of 65-fold and an emission wavelength of 604 nm. Dextran conjugates of this probe were also synthesised to aid in the hydrophilicity of the probe. Probe **1.174** is an efficient, low affinity Ca^{2+} sensor in the red region that is Mg^{2+} insensitive.

1.3.4.2 Probes with Handles for Functionalisation

The calcium rubies were developed to be red-emitting calcium probes that could be functionalised.[136,137] Ca-Ruby-Cl (**1.175**) (Figure 1.29) was the first to be synthesised and reported. It features a BAPTA moiety added to a rhodamine fluorophore with an azide side chain attached to the ethylene glycol bridge. The azide was added for potential uses in click chemistry or reduction to the amine group for amide couplings. The side chain was placed in this position to avoid interference with the BAPTA moiety.[138] Substitution on the BAPTA (Cl, F and CH_3) allows for the optimisation of the K_d and the synthesis of **1.176** and **1.177** followed (Figure 1.29).

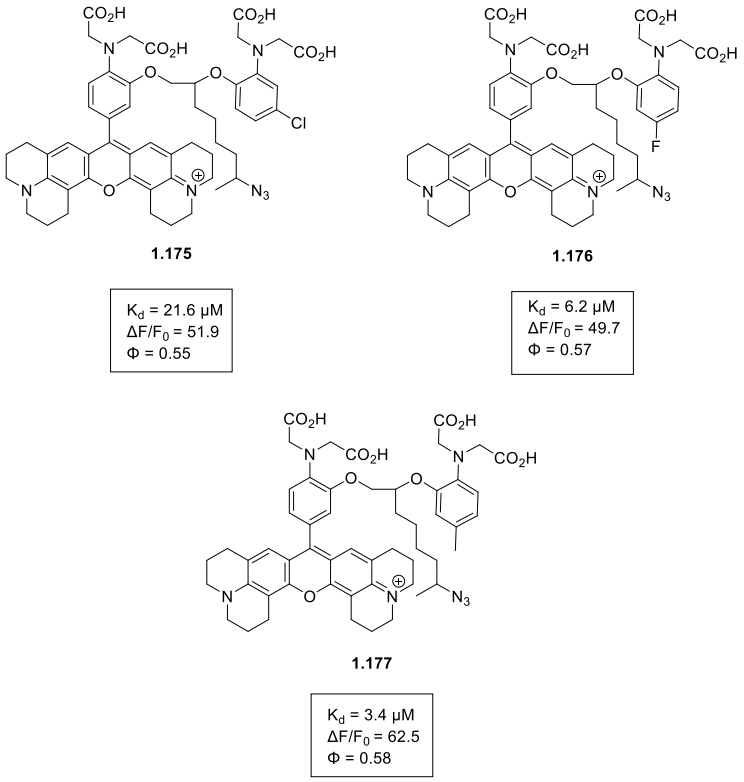

Figure 1.29. Structures of calcium rubies (**1.175 – 1.176**).

The three probes synthesised had similar absorbance and fluorescence peaks (~ 586 and 604 nm respectively) and fluorescence quantum yields in the area of 0.55 upon Ca^{2+} binding. The affinity for calcium varies for each probe, giving three probes whose K_d cover the range that is typically observed in probes, giving a toolbox of probes.[117] Due to their long wavelengths, the calcium rubies are good for use in challenging imaging experiments that rely on several excitation or emission bands.

1.3.5 Limitations of Existing Calcium Probe Designs

As well as the attempts to improve spectral properties and Ca^{2+} affinity mentioned, research has been ongoing into improving selectivity for organelles through creating hybrid chemical probes in combination with HaloTags.[127,139]

Despite extensive research, many of the probes have not had follow up research published from their original findings. This has led to many of the potential uses, *e.g.* the alkynes for further functionalisation of **1.161** and the azides of the calcium rubies, not being fully utilised. However, uptake on probes that have had a complete literature published on further projects is also limited due to a lack of commercial availability. There is scope for the development of

calcium probes with functionalisation for fluorophores or organelle targeting moieties to be developed and published in complete.

Due to the introduction of azides and alkynes into the molecules, an option for utilising these would be click chemistry. Click chemistry was previously used in research published in 2013 by Takei *et al.* to produce a probe that prolonged cytosolic retention (Scheme 1.20).[140] This utilised SPAAC chemistry (DBCO **1.178**) and a calcium probe **1.179** based on fura-2 to give **1.180.** DBCO modified with BSA was used to increase cytosolic targeting.

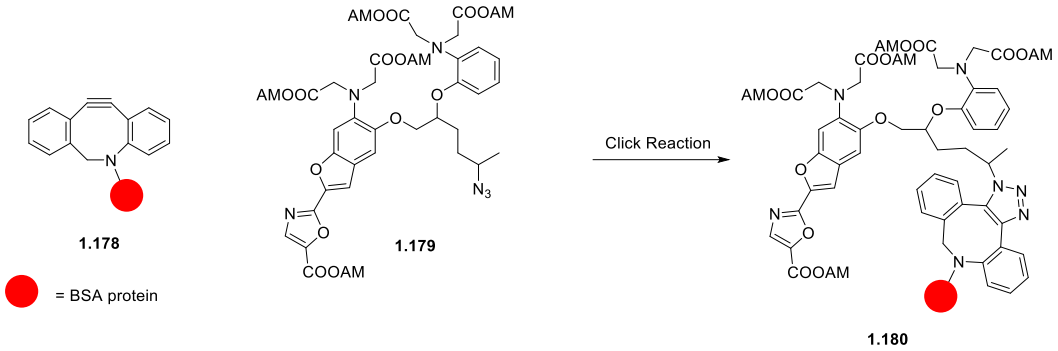

Scheme 1.20. SPAAC reaction between a BSA-labelled DBCO **1.178** and calcium chelator **1.179** to give probe **1.180.**

In this example, SPAAC was chosen as it did not utilise copper, however, if alkynes were used then the overall synthesis could be simplified. The alkyne moiety is smaller, typically has an simpler synthesis, the regioisomer formed can be controlled and will potentially have a higher cellular uptake. A potential issue for the use of copper in the reactions is that BAPTA may chelate the ion, despite its high affinity for Ca^{2+} over the copper ion.[141] Click reactions that utilised lower copper loadings could therefore have potential in calcium imaging.

1.4 Hypothesis

Despite large advances in the CuAAC reaction, little research has been made on the development of alkynes as a way to modulate the reaction rate and solvent use. Limitations of the CuAAC also remain, including the key drawback of copper toxicity. The aromatic ynamine is an alkyne surrogate which has demonstrated increased reactivity compared to more traditional alkynes. The main hypothesis to be tested in this thesis is that substituent changes on the aromatic ynamine will alter the reaction kinetics of the CuAAC reaction (Figure 1.30). It is also hypothesised that the rate of CuAAC of these new ynamines will also be affected by the reaction conditions, *e.g.* change of solvent and lowering of copper catalyst loading.

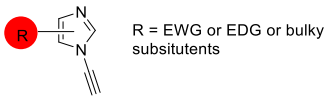

Figure 1.30. Substituent changes on the aromatic ynamine have potential to alter the reaction kinetics.

Additionally, ynamines with a biological application have not been investigated extensively. It is hypothesised that the development of ynamines would substantially improve the ease of synthesis or *in vivo* functionality of biological probes *via* an efficient click reaction. This theory will be explored on the example of calcium chelator probes.

1.5 Thesis Aims

The specific aims of this thesis are to:

i) Expand the scope of ynamines synthesised.

ii) Explore how the change of substituents can influence the mechanism of the CuAAC.

iii) Investigate the use of the ynamine for an imaging purpose, specifically calcium imaging.

Chapter 2

Expanding the Repertoire of Ynamine Substrates: Synthesis and Characterisation

2.1 Introduction

2.1.1 Cross Coupling Bond Forming Reactions

Cross coupling reactions are used to form C-C and C-N bonds and are typically metal catalysed. They are an important class of reaction in chemistry and are utilised in many different fields since their discovery.[142,143] The use of metal catalysts in these reactions allows for bond formations and transformations that would not be possible otherwise and the impact of these reactions is widespread.

2.1.1.1 Buchwald-Hartwig Amination

One of the most popular methods for the synthesis of C-N bonds is the Buchwald-Hartwig amination. In the 1980s, Stephen Buchwald and John Hartwig simultaneously established the Buchwald-Hartwig amination.[144,145] Their method proceeds *via* a coupling of an aryl halide as the electrophile and an amine in the presence of a Pd catalyst **(**Scheme 2.1). A Pd^{II} pre-catalyst is initially used which is reduced to Pd^0 *in situ*. This is followed by the oxidative addition of the aryl halide (II) to give intermediate III. This returns the Pd to a Pd^{II} state where the aromatic group is on the complex and a ligand then transferred out. The halide of III is then exchanged for the base (IV) which is then swapped for an amine (V). Reductive elimination then occurs to form the desired product (VI).

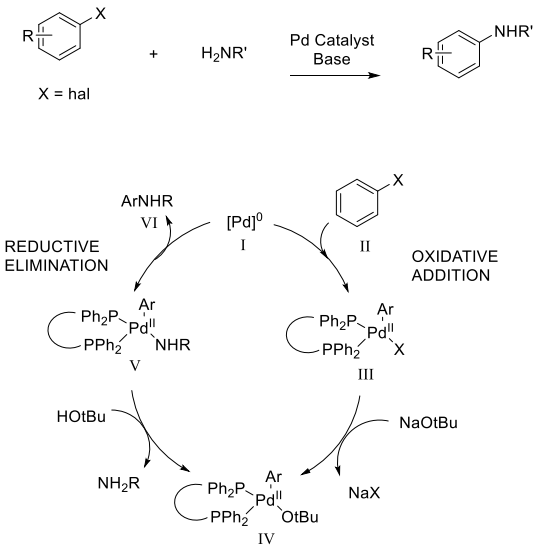

Scheme 2.1. General scheme and catalytic cycle for the Buchwald-Hartwig amination.

The main areas of development of the Buchwald reaction are the Pd catalyst and the ligand development (Figure 2.1). The synthesis of Pd^{II} pre-catalysts that undergo conversion to the Pd^0 species *in situ* have been reported (**2.1**).[146] These have the dual effect of increasing the synthetic ease and giving a better atom economy due to removing the requirement for a phosphine ligand. Two of the main areas of focus for ligand design are bidentate phosphine ligands (**2.2** – **2.4**) and sterically hindered ligands (**2.5** – **2.8**).

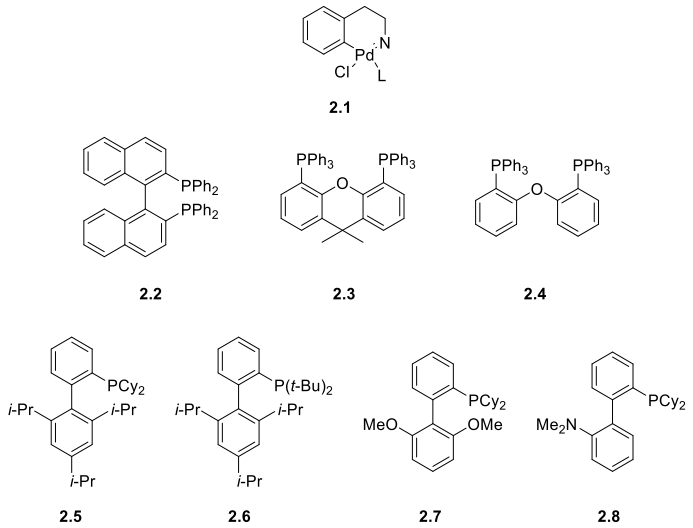

Figure 2.1. Pre-catalyst (**2.1**) and various phosphine ligands (**2.2 – 2.8**).

The use of BINAP (**2.2**) led to an increase in the scope of the reaction, existing yields, and reaction times. Phosphine ligands have been found to be efficient and robust in the reaction. Sterically hindered ligands (**2.5** – **2.8**) have been found to increase the rate the key steps of the catalytic cycle: the oxidative addition and the reductive elimination.[147–149] Many other factors such as the base, the solvent and the substrate scope can have effects on the Buchwald-Hartwig amination.

Although research is continuing, the high cost of Pd, associated ligands and troublesome catalyst removal remains a concern for large-scale applications.[150] This has resulted in more research being diverted to the Ullmann reaction.

2.1.1.2 Ullmann Reaction

The formation of a C-C bond mediated by copper was first reported by Ullmann and Goldberg in 1903 and is referred to as the Ullmann reaction.[151] This involved the copper-mediated reaction between two aryl halides (**2.9,** Scheme 2.2A). The initial reaction developed required

harsh conditions, high temperatures (>150 °C), strong bases and the use of stoichiometric copper. The later adapted Ullmann condensation involves the copper-mediated reaction between an aryl halide (**2.9**) and an amine, phenol or thiophenol (**2.11**) (Scheme 2.2B).[152]

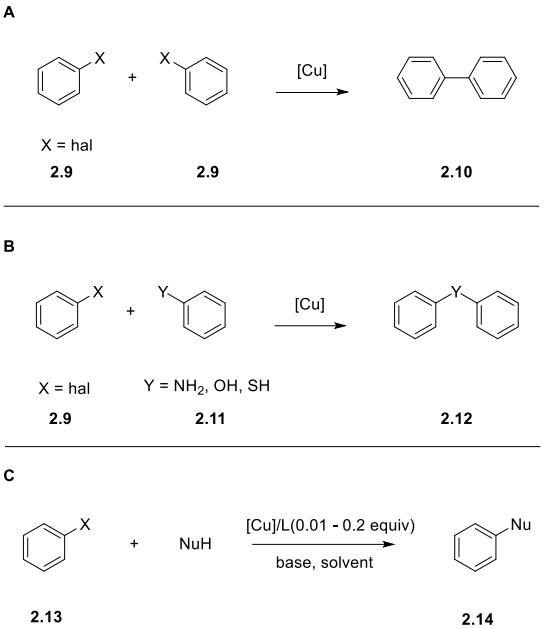

Scheme 2.2. A) The first discovery of the Ullmann reaction; **B)** the Ullmann condensation reaction; **C)** the modified Ullmann typical seen in modern research.

Following the traditional Ullmann couplings, a new method, termed the 'modified Ullmann coupling' was developed (Scheme 2.2C). The main difference of the modified Ullmann was the addition of a ligand which initially was introduced to improve the solubility of the Cu catalyst precursor.[153] The introduction of ligands made the use of much milder conditions possible, resulting in lower reaction temperatures (80-100 °C), reduced amount of copper (5-20%), shorter reaction times and in increased scope.

The use of ligands and additives was first suggested by Buchwald in the late 1990s, however, the role the addition of these played in the Ullmann was not obvious.[154] Since the early 2000s a significant effort has been made in investigating the function of the ligands in these couplings, with particular emphasis on discerning whether the increased solubility of copper species was the only factor. It soon become apparent that the choice of ligands can significantly impact the efficiency, selectivity, and scope of the coupling reaction. Bidentate ligands were discovered to be better than monodentate, and it was hypothesised that this was because they were blocking two adjacent sites, bringing the aryl ring and the nucleophile closer together.[155–160]

A desirable motif for ligands is the presence of a N or N-O copper coordinating motif.[161] This stabilises the Cu catalyst preventing unwanted side reactions and improving the catalytic efficiency. Ligands **2.15** and **2.16** were introduced by Ma *et al.* (Figure 2.2) who demonstrated that amino acids could be used as ligands, an advantage due to their low cost and the ready availability.[162] Cyclic β-ketone **2.17** has also allowed the reaction to proceed at room temperature in 2 – 4 h.[163] In the same study, it was found that **2.17** offered selectivity of the C-N bond formation over C-O formation. Ligand **2.18** gave the reverse results, favouring C-O formation. This shows that the choice of ligand is crucial in the selectivity of the reaction and can enable the coupling of a broader range of aryl halides and other substrates.

Aromatic imine groups bound to a pyridine group, such as ligand **2.19** have been found to enhance the yield.[164] It was hypothesised that the electron-rich pyridine could transfer electrons to the Cu, increasing its propensity for oxidative addition, and that the imine makes the Cu more electrophilic, increasing its likelihood of undergoing reductive eliminations. Ligand **2.20** is specific for C-C bond formations.[165]

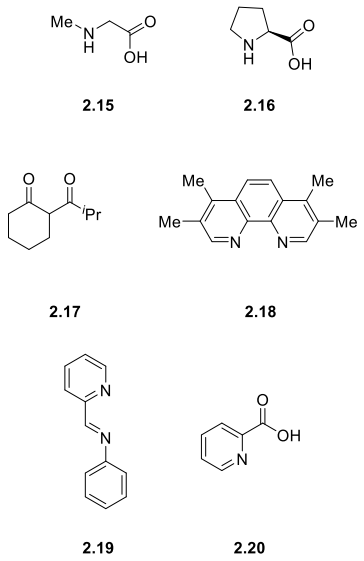

Figure 2.2. Various bidentate ligands used in the modified Ullmann.

The mechanism of the Ullmann reaction is still elusive, and there are two possible routes as depicted in Figure 2.3, however, the generally accepted mechanism involves the oxidative addition-reductive elimination cycle after the nucleophile has coordinated (Route 2).[166] However, the exact mechanism depends on many reaction factors, including the substrate, the ligands and whether the reaction is done under an inert atmosphere.[167]

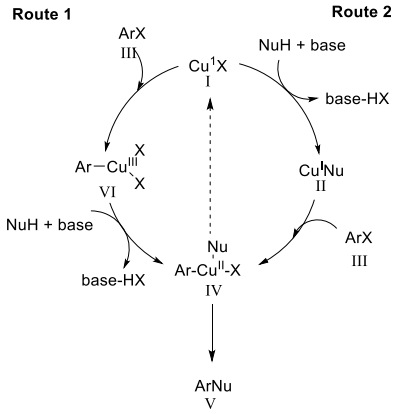

Figure 2.3. Two possible routes for the oxidative addition/reductive elimination pathways to form ArNu (V).

Research is still ongoing in the development of the Ullmann and the mechanistic aspects.[168] There are also ongoing attempts to bring the Ullmann in line with more green chemistry techniques, including solvent free reactions, microwave irradiation and easy to recover catalysts.[169]

Two methods of the formatting of C-N bonds have been discussed (Buchwald-Hartwig amination and the Ullmann coupling). The work described in this chapter involves the synthesis of aromatic ynamines, including a C-N bond formation by an Ullmann-like reaction.

2.2 Aims of Chapter 2

The aims of this chapter are to:

(i) Synthesise a palette of aromatic benzimidazole and imidazole ynamines (Scheme 2.3) using an Ullmann-like reaction followed by protecting group deprotection.

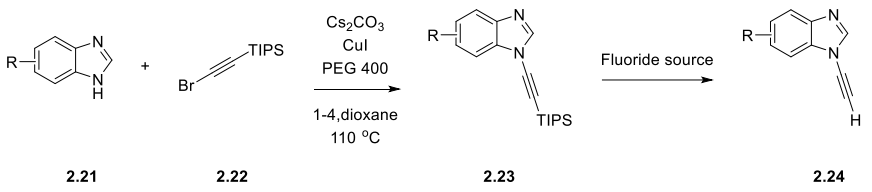

Scheme 2.3. General scheme for the synthesis of aromatic ynamines.

(ii) Develop a modular synthetic strategy to allow easy functionalisation of ynamines.

(iii) Investigate the broader application of ynamine substrates on representative CuAAC reactions.

2.3 Results & Discussion

2.3.1 Synthesis of Aromatic Ynamines

The preparation of ynamines involves an Ullmann-type coupling between a benzimidazole and a bromo-alkyne (BrTIPS, **2.22**). The bromo-alkyne (**2.22)** was synthesised *via* a silver-catalysed bromination of the TIPS-alkyne (**2.25**) using NBS (**2.26**). This reaction was high yielding (96%).

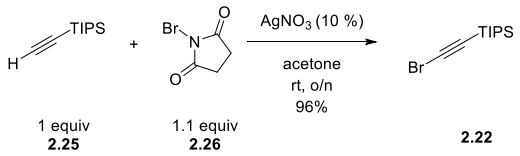

Scheme 2.4. Synthesis of **2.22**.

Previous work within the group has focused on the optimisation of Ullmann-type synthesis, with the optimised conditions using microwave irradiation given in Scheme 2.5.[86] To obtain the conditions in Scheme 2.5, various bases, solvents and heating conditions had been tested, however, microwave irradiation with caesium carbonate, copper(I) iodide and PEG 400 in 1,4-dioxane gave the best results.

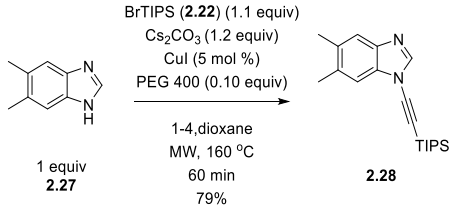

Scheme 2.5. Optimised synthesis of **2.28**.

However, a disadvantage of microwave synthesis is the small reaction scales (up to 15 mL volume of reaction) that can be used. Due to the large amount of material required for the future testing, and therefore large reaction volume, conventional heating was used for the majority of the ynamine reactions in this study. A disadvantage of this procedure is the poor to moderate yields (44 *vs*. 79%) despite heating for 2 to 3 days. This gives the desired TIPS-protected dimethyl ynamine (**2.12**) in a 44% yield (Scheme 2.6).

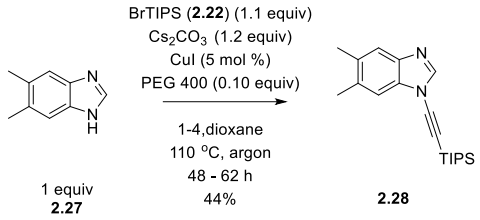

Scheme 2.6. Synthesis of **2.28**.

Following on from the synthesis of the dimethyl ynamine **2.28**, a small selection of other ynamines have been synthesised within the group for other uses, including isomers **2.29** and **2.30** and **2.31** and **2.32** (Figure 2.4).

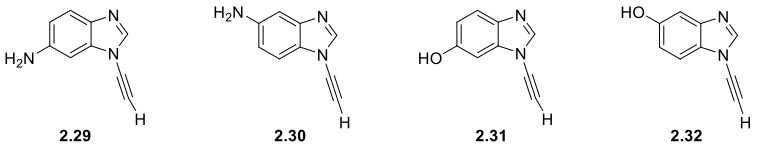

Figure 2.4. Aromatic ynamines previously synthesised within the group.

2.3.2 Synthesis of a Scope Benzimidazole Ynamines

The initial expansion of the ynamine palette focused on benzimidazoles, with a mixture of ynamines with different EWGs and EDGs added, and the expansion of the ring system (Figure 2.5).

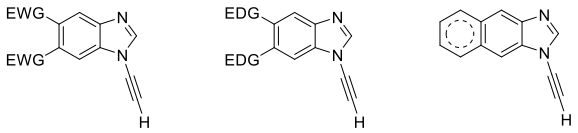

Figure 2.5. Areas of modification to the benzimidazoles.

The majority of the starting benzimidazoles were available commercially, however, the expanded ring systems had to be synthesised.

The napthobenzimidazole **2.35** was formed by the condensation of naphthalene-2,3-diamine **2.33** in formic acid at reflux to form the benzimidazole **2.35** in a 63% yield (Scheme 2.7).[170] The reaction was heated overnight; however, an increased reaction time may have led to an increased yield compared to the moderate 63% yield achieved.

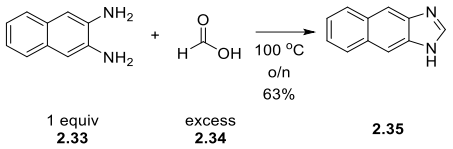

Scheme 2.7. Synthesis of **2.35**.

6,7-Dihydro-1H-[1,4]dioxino[2',3':4,5]benzo[1,2-d]imidazole (**2.42**) was synthesised using a longer multi-step route before the final condensation (Figure 2.4).[171] The synthesis began with the acetate protection of the aniline 6-amino-3,4-benzodioxane **2.36** followed by nitration at the ortho position to give **2.39**. The acetate group was then removed using sulphuric acid (**2.40**) and the nitro group reduced under a hydrogen atmosphere using Pd/C to produce **2.41**. The final benzimidazole **2.42** was obtained *via* condensation of 6,7-diamino-2,3-dihydro-1,4-benzodioxane **2.41** in formic acid at 100 °C in 66% yield.

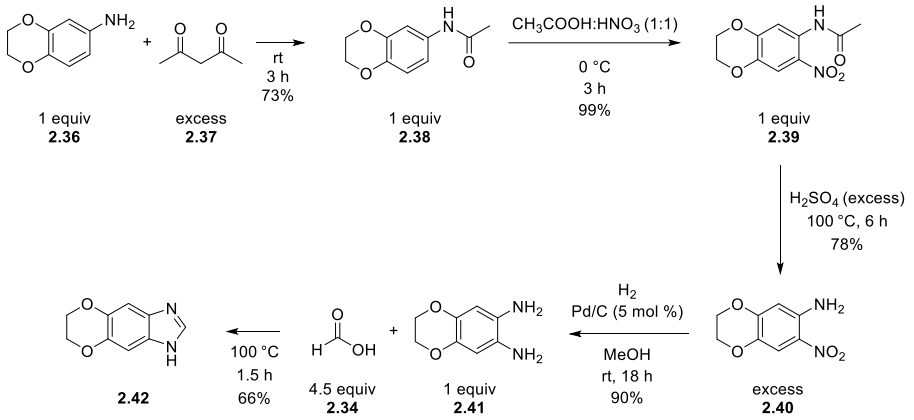

Scheme 2.8. Multi-step synthesis of **2.42.**

With all the benzimidazoles in hand the next step was performing the Ullmann reaction between the bromo alkyne **2.22** and the benzimidazole to obtain the benzimidazole ynamines **2.43 – 2.50**. The previously optimised reaction conditions (Section 2.3.1) used for the ynamine **2.28** were applied (Scheme 2.9).

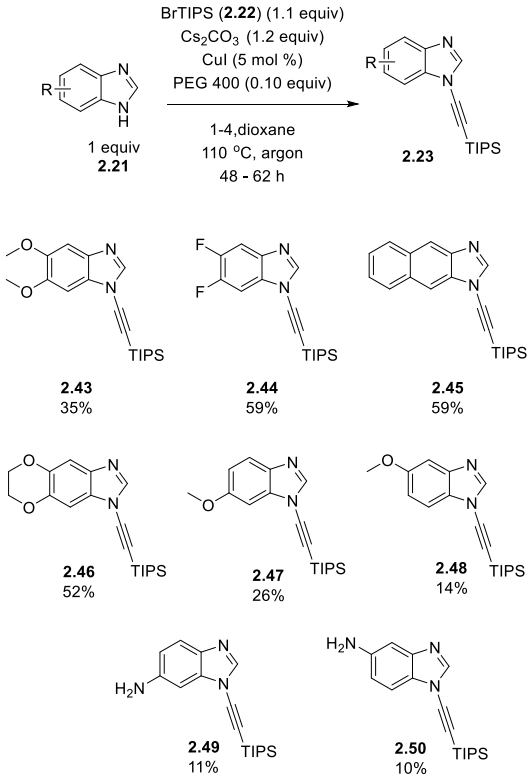

Scheme 2.9. Synthesis of benzimidazole ynamines.

The Ullmann proceeded with a wide range of yields dependent on the substrate. No issues during purification were observed for the ynamine synthesis: during the work-up the ynamine favoured the organic layer and no instability or column dragging was observed on purification. The electron donating -OMe groups (**2.43**, **2.47** and **2.48**) tended to give lower yields than the EWG of the fluorine (**2.44**). However, as previously discussed, the ynamine **2.28** containing electron donating methyl groups gives high yields of above 50%, and higher when microwave conditions are used. The aniline ynamines **2.49** and **2.50** also contain the electron-donating amine group, and the yields for these are low.

The unsymmetrical benzimidazoles produced two regioisomers. As a general trend, substitution on 7- position (regioisomer A) gives consistently slightly higher yields for the methoxy (**2.47**) and for the aniline (**2.49**) ynamine, although this effect is more pronounced for the -OMe group than the $-NH_2$ where the difference between the yields for the isomer is lower. This could be due to multiple reasons including sterics and electronics.

Due to the large amounts of material required, multiple batches of TIPS-ynamine were often synthesised and this revealed variation in the yields obtained for the same ynamine. It was initially thought that this may be linked to the scale of the reaction or the concentration, however, analysis of the yields ruled this out (Table 2.1).

Table 2.1. Yields obtained for the synthesis of various ynamines.

Ynamine	Yield (%)	Scale (mmol)	Conc (mM)
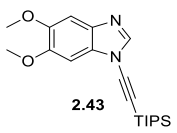 **2.43**	59	0.672	306
	29	4.61	115
	35	27.9	269
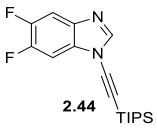 **2.44**	59	5.84	269
	45	0.672	306
	18	0.714	297
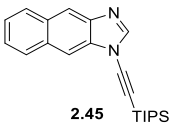 **2.45**	59	7.73	269
	59	0.595	270
	13	1.62	311
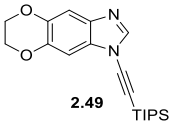 **2.49**	7.6	7.6	269
	52	4.45	226

As is shown in Table 2.1, the variability in the yields did not follow a particular pattern, with ynamine **2.43** having a large variation. A further consideration that could be causing the disparity in the yields is the solubility of the reagents in the reaction mixture. After the initial mixing, most of the reactants are in solution, however, a suspension forms as the reaction proceeds, and the PEG 400 has previously been indicated as a phase transfer agent in the reaction. It is hypothesised that the precipitation and occasional build-up of a brown residue on the inside of the reaction flask could be caused by poor mixing and solubility of the heterocyclic substrate. This could also sequester the catalyst resulting in it not being available for the reaction. The ynamine synthesis required degassing and the use of anhydrous solvents, however, the extent of these may affect the reaction.

2.3.2.1 Optimisation of the Removal of the TIPS Protecting Group

Two different methods of removing the TIPS protecting group to give the free alkyne (**2.24**) were trialled: fluoride on polymer in MeCN (Scheme 2.10A) and TBAF in THF (Scheme 2.10B). Fluoride on polymer was chosen due to the relatively mild reaction conditions required and the simplicity of the purification. Fluoride on polymer contains an aminiun ion and Amberlyst® polymer. Deprotection using fluoride on polymer was initially used due to previous success within the group at achieving high yields.[83] However, when expanding the ynamine scope the yields started to become inconsistent. Although the reaction profile on TLC was clean, with starting material having been consumed and only a product spot formed, the yields were lower than expected. It was hypothesised that adsorption onto the polymer was occurring. Despite washing the polymer with solvents including MeOH and EtOAc, no product was able to be removed from the polymer.

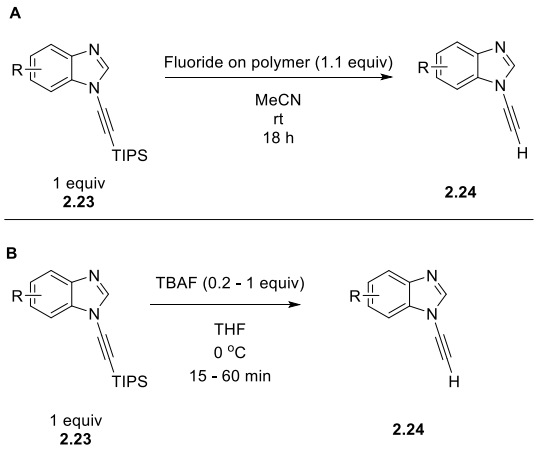

Scheme 2.10. The two methods tested for TIPS protecting group removal. **A**) deprotection using fluoride on polymer; **B**) deprotection using TBAF.

TBAF in THF was then trialled as an alternative deprotection method. When tested, the TBAF method tended to give higher yields, as well as achieving full conversion to the product within 15 mins to one hour. The disadvantage of TBAF, however, was the formation of another spot that could be seen *via* potassium permanganate stain on TLC analysis. This spot was isolated, and attempts were made to identify the structure, however, the NMR was inconclusive. The TBAF deprotection had to be optimised as it was observed that addition of stoichiometric equivalents of TBAF to the TIPS-ynamine in solution would lead to the reaction turning black and the yield decreasing due to potential decomposition. This procedure was unexpected due

to the small amounts of equivalents sometimes necessary for a full deprotection observed *via* TLC.

After further optimisation, a procedure for deprotection was therefore established in which the TBAF was added at 0 °C and in small equivalents at a time (0.1 – 0.2 equiv) with consistent TLC monitoring. This procedure was used going forward with the deprotection of the benzimidazole scope (Scheme 2.11).

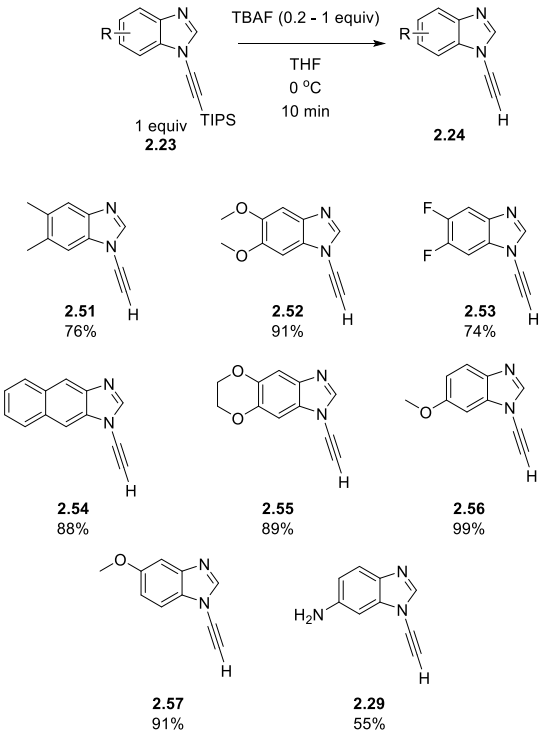

Scheme 2.11. Deprotection of benzimidazole ynamines using the TBAF method.

The successful deprotection gave a scope of benzimidazole ynamines (**2.52 – 2.57** and **2.29 – 2.30**) to be used in further studies.

2.3.3 Synthesis of a Scope of Imidazole Ynamines

Following the successful synthesis of benzimidazole ynamines, accessing a palette of imidazole ynamines with aromatic substituents was a promising avenue for exploring the unique ynamine reactivities and expanding the ynamine toolkit. Most of the imidazoles were available, apart from imidazole **2.60**. Imidazole **2.60** was prepared by a Suzuki-Miyaura coupling between 5-iodo-1H-imidazole (**2.58**) and (4-methoxyphenyl)boronic acid (**2.59**), as has previously been reported in literature.[172] The product was obtained in a yield of 69%, slightly lower than the literature yield of 81% (Scheme 2.12).

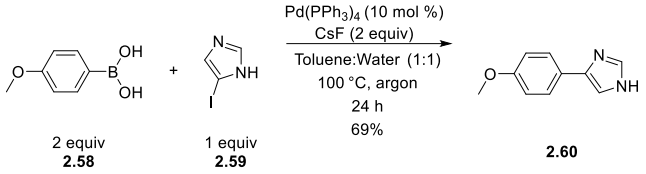

Scheme 2.12. Synthesis of imidazole **2.60**.

Using the same Ullmann conditions as given for the benzimidazole ynamines, imidazole ynamines were synthesised (Scheme 2.13), giving two regioisomers.

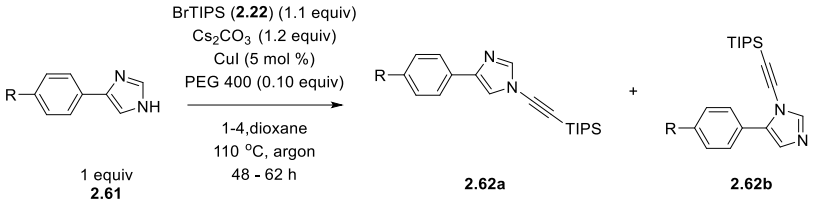

R Group	Yield (%)	
	Regioisomer A	Regiosisomer B
H (2.63)	65	5
Me (2.64)	57	6
OMe (2.65)	23	trace
F (2.66)	71	6
Br (2.67)	60	trace
NO_2 (2.68)	42	trace
CF_3 (2.69)	58	4
NH_2 (2.70)	10	-

Scheme 2.13. Synthesis of imidazole ynamines.

Due to the unsymmetrical nature of the imidazoles used as starting materials, the Ullmann reaction formed two regioisomers (**2.62a** and **2.62b)**. However, one symmetric imidazole was synthesised, the biphenyl imidazole **2.72**.

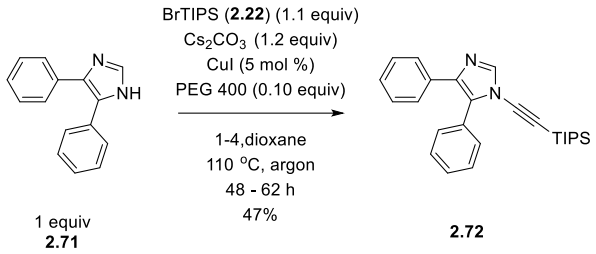

Scheme 2.14. Synthesis of **2.72**.

The relative yields of these regioisomers depended on the nature of the substituents on the aromatic ring. However, regioisomer A typically formed in greater yield, therefore, it was used for all following experiments. Isomer characterisation and designation will be discussed in Section 2.3.5. Due to the low yields in the synthesis of imidazole **2.70,** alongside benzimidazoles **2.49** and **2.50,** it was hypothesised that the -NH_2 group could be chelating the Cu in the Ullmann reaction. The aniline imidazole ynamine **2.70** gave a low yield and was not continued with.

Similar to the benzimidazole ynamines, the imidazole ynamines also exhibit variation in their yields over multiple synthesis attempts (Table 2.2). These low yields could be a result of the same factors given in Section 2.4.2.1.

Table 2.2. Yields obtained alongside the mmol scale of the starting imidazole and the concentration of the reaction.

Ynamine	Yield (%)	Scale (mmol)	Conc (mM)
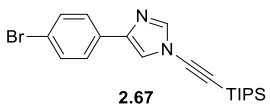 **2.67**	60	11.2	160
	42	0.672	306
	62	6.72	311
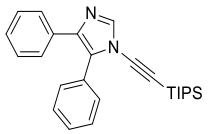 **2.72**	24	9.08	160
	9.4	6.63	260
	47	0.684	311
	17	0.427	297
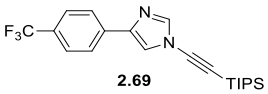 **2.69**	29	4.62	230
	58	4.62	230
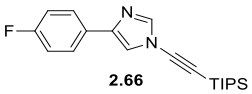 **2.66**	71	0.684	311
	43	5.25	309
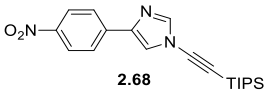 **2.68**	11	5.17	230
	42	12.7	269

Deprotection of the TIPS protected ynamines, using the previous method of TBAF, gave the terminal ynamine in moderate to excellent yields (Scheme 2.15). Following the successful deprotection to give **2.74** to **2.81**, a scope of ynamines was available for the next steps.

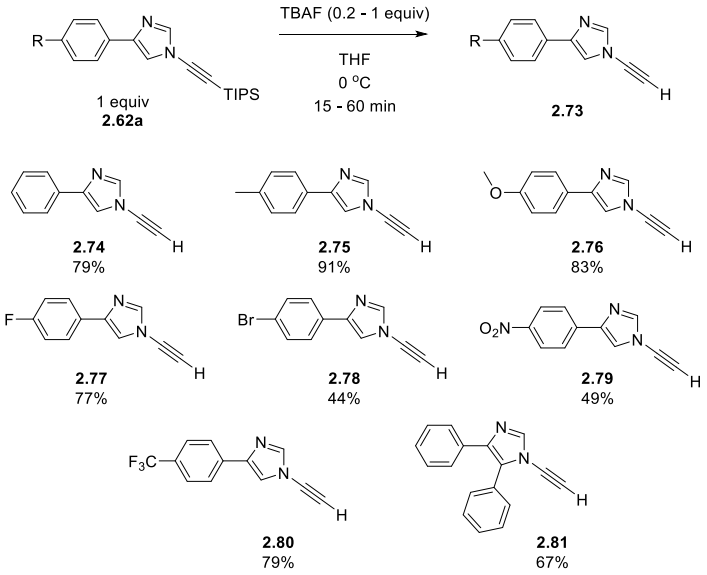

Scheme 2.15. Deprotection of the imidazole TIPS protected ynamine.

2.3.4 Unsuccessful Substrates for Ynamine Synthesis

Whilst ynamine synthesis for the majority of the benzimidazole and imidazole substrates tested was successful, some substrates were not reactive in the Ullmann (Figure 2.6). These included the triazoles 5,6-dimethyl-2H-benzo[d][1,2,3]triazole (**2.82**) and 6,7-dihydro-1H-[1,4]dioxino[2',3':4,5]benzo[1,2-d][1,2,3]triazole (**2.83)** alongside adenine (**2.84**) and 6-chloro-7H-purine (**2.85**) and a pyrimidine (**2.86**).

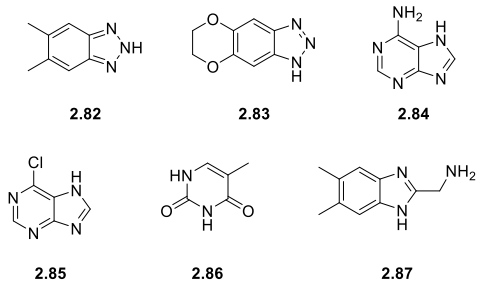

Figure 2.6. Unsuccessful substrates.

Compound **2.82** gave starting material and another unidentified peak. The two purines **2.84** and **2.85** did not show any product formed upon LC-MS analysis, only starting materials. Substrate **2.87** showed product formation *via* LC-MS analysis and the suspected product was isolated using column chromatography. However, upon characterisation of the isolated product it appeared that degradation had taken place.

There were also attempts to synthesise a symmetric ynamine with a functional handle to circumvent the issue of regioisomer formation during the ynamine synthesis. The first attempt at this involved the addition of an alcohol chain. This began with the oxidation of the methyl groups of the dimethyl benzimidazole **2.27** using potassium permanganate. This gave the dicarboxylic acid benzimidazole **2.88** in an 18% yield (Scheme 2.16).

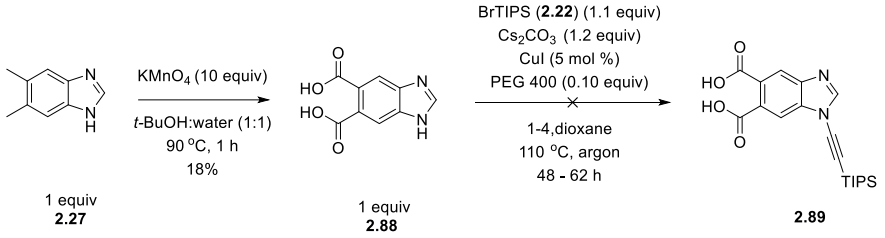

Scheme 2.16. Synthesis of **2.88** and the failed synthesis of the ynamine **2.89**.

The ynamine synthesis was attempted on the benzimidazole (**2.88**). However, this was unsuccessful with TLC showing starting material remaining. It was assumed that the acid groups caused low yields due to catalyst chelation, as was observed previously.

Following this, an alternative approach was taken (Scheme 2.17). Ring closure via amide coupling prior to ynamine synthesis was envisioned to improve the yield by removing the free acid group. A condensation reaction was carried out to add 3-aminopropan-1-ol (**2.75**) into 1H-benzo[d]imidazole-5,6-dicarboxylic acid (**2.88**).

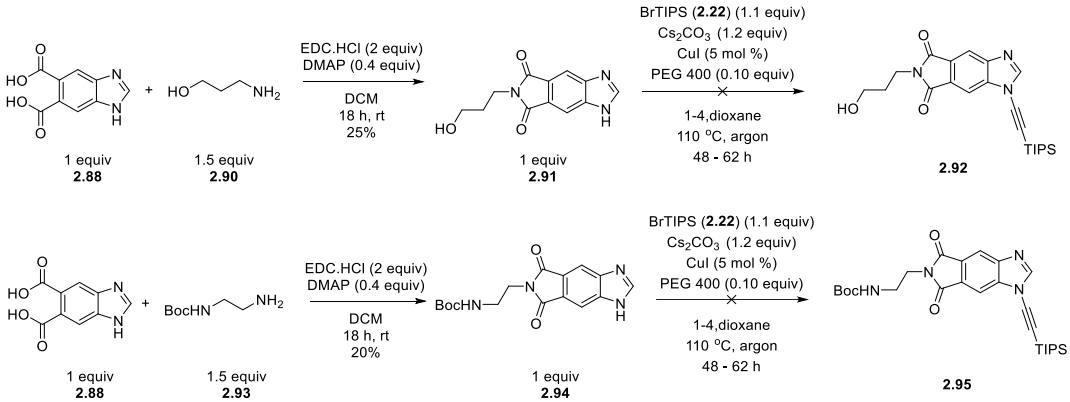

Scheme 2.17. Attempted synthesis of ynamines **2.99** and **2.102** with a functional handle through the formation of intermediates **2.98** and **2.101**.

Initially, the unprotected amino alcohol **2.90** was used to form the benzimidazole **2.91** that was then taken through to the ynamine formation. However, synthesis of **2.92** was not

successful with starting material remaining. The amide formation of **2.94** was then performed with the protected diamine (**2.93**). However, the Ullmann to form **2.95** was also unsuccessful and starting material remained *via* TLC. This route was abandoned, and no further optimisation was carried out.

2.3.5 Triazole Formation

Following on from the synthesis of the ynamine, the azide-alkyne (3+2) cycloaddition was performed with benzyl azide to obtain triazoles. Initial reactions were carried out in MeOH, however, other work ongoing concurrently in the group showed that a HFIP/water solvent system had a cleaner reaction profile. This will be discussed in detail in Chapter 3. Further triazole formations were then performed using HFIP/water, resulting in two different conditions used for the synthesis (Scheme 2.18).

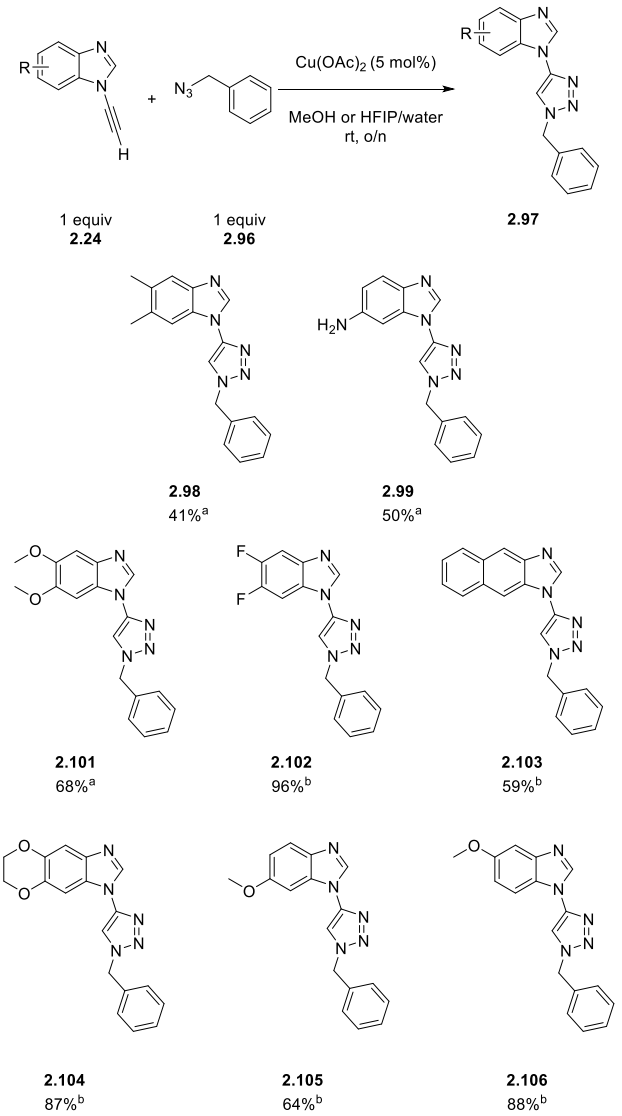

Scheme 2.18. Synthesis of triazoles. [a] denotes synthesis using MeOH, [b] denotes synthesis using HFIP/H_2O (40:60%).

As shown in Scheme 2.18, the yields for the synthesis of the triazoles of the benzimidazole ynamines varied. The reaction was shown to proceed cleanly *via* analysis on TLC and LC-MS and it is therefore assumed that there were issues in the purification of the substrates, which involved a separation into ethyl acetate following a wash with EDTA - to chelate the copper used in the reaction - and silica column chromatography.

Then, triazoles of the imidazole ynamines were formed (Scheme 2.19). As can be seen, some of the yields are similar to what was achieved for the benzimidazole ynamines. This can also be a result of purification issues as TLC always showed that the reaction had gone to completion.

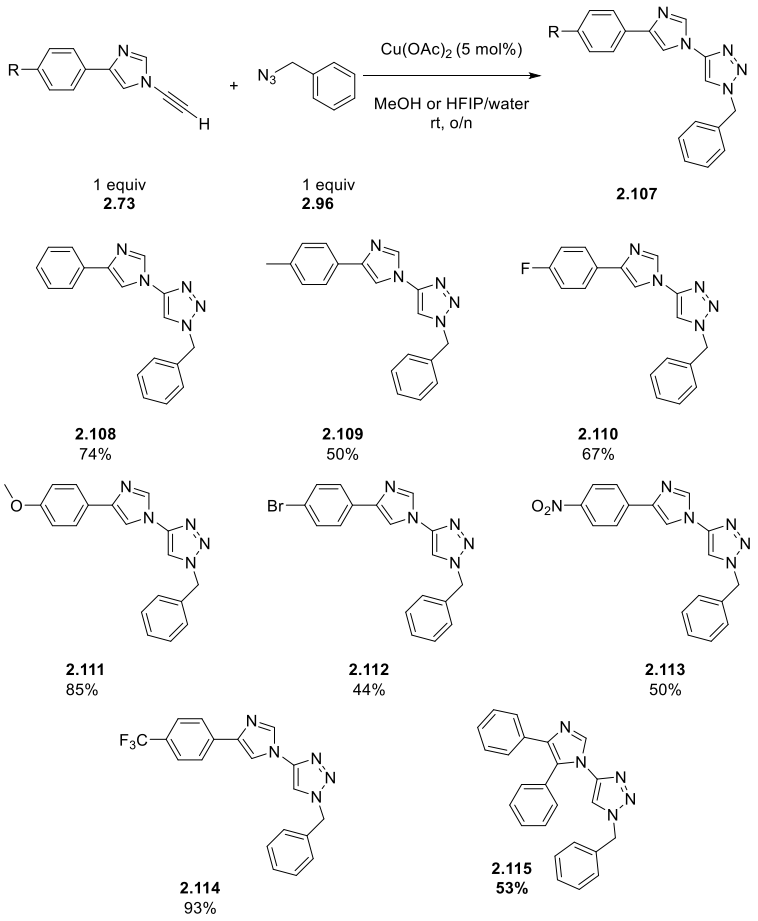

Scheme 2.19. Synthesis of imidazole triazoles. [a] denotes synthesis using MeCN, [b] denotes synthesis using HFIP/H_2O (40:60%).

2.3.6 Isomer Characterisation by NMR and Crystal Structure

As previously discussed, the imidazole forms two isomers during the Ullmann reaction and the orientation of each had to be determined. Literature suggests that the preferential addition is to the N1 due to sterics, with the complex formed during the Ullmann-like coupling clashing with the aromatic substitution on the 4-position.[173]

Proton NMR showed that the imidazole protons gave different chemical shifts depending on the isomer (addition to the N1 is shown in red, addition to the N3 is shown in teal), and that the aromatic protons were also affected (Figure 2.7).

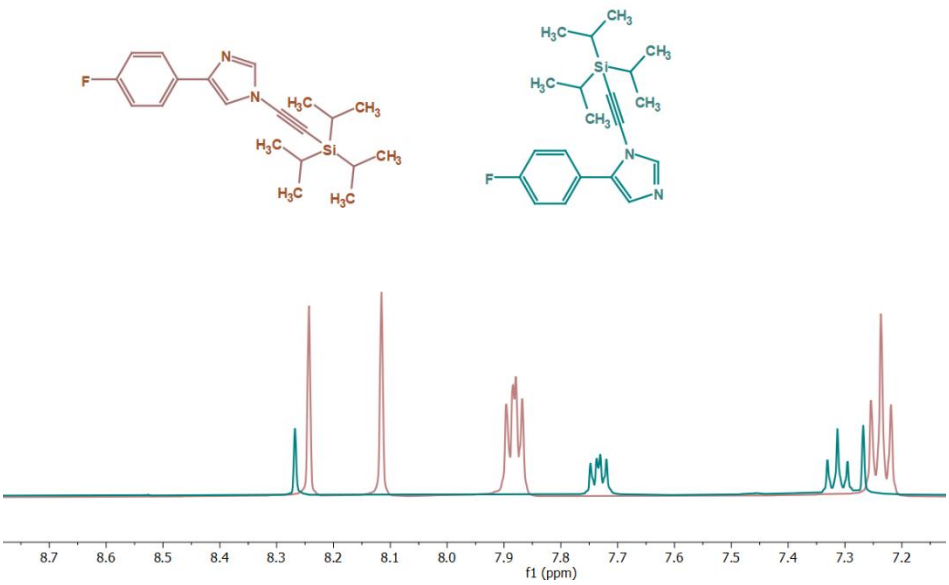

Figure 2.7. Stacked NMR spectra showing the aromatic region of the spectra for the two isomers of **2.66**: isomer A in the maroon and isomer B in the teal.

It was not possible to assign the isomers from these spectra. Analysis by 2D NMR was initially attempted, however, no diagnostic correlation between the N3/N1 proton and the aromatic protons on isomer A were observed *via* NOESY for any compound.

However, crystal structures for certain TIPS-ynamines could be obtained. The crystal structures in Figure 2.8 were crystalised from EtOAc/hexane. As can be seen, the TIPS-protected alkyne is on N1. This led to the allocation of Isomer A for compounds **2.64**, **2.65** and **2.66**. For the TIPS-protected ynamines where crystal structures could not be obtained, it was assumed that the formation of A as the major isomer was standard for all imidazole ynamine synthesised. No crystal structures of the minor isomer B were obtained.

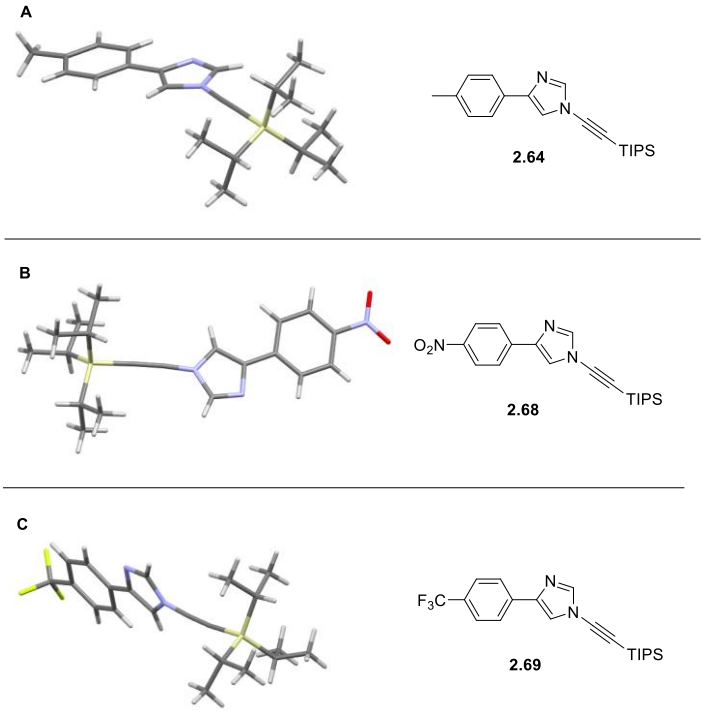

Figure 2.8. Crystal Structures for TIPS-protected ynamines **2.64**, **2.68** and **2.69**.

Further crystal structure of several imidazole ynamines were obtained, including ynamines for which the crystallisation of the TIPS-protected ynamine had failed. The crystal structures of the imidazole ynamines are given below, and these were obtained from EtOAc/hexane (Figure 2.9).

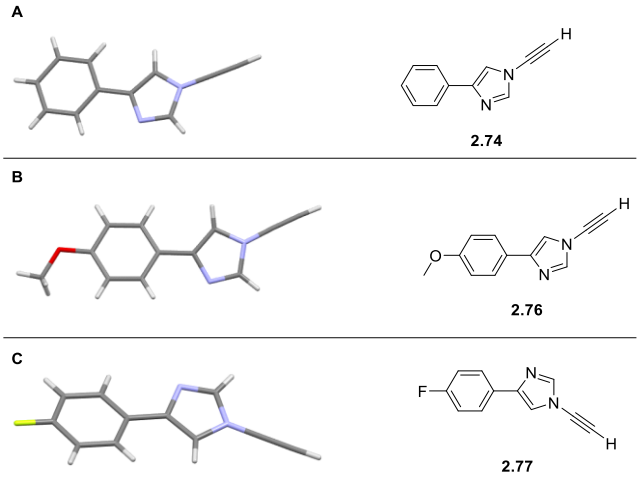

Figure 2.9. Crystal structures and the corresponding ynamine structure.

As can be seen in Figure 2.9, the obtained crystal structures further confirmed the main product in the reaction as isomer A. Some of the imidazole ynamine crystal structures obtained also

showed more than one unique molecule per unit cell. This polymorphism is observed for crystal structures of TIPS protected ynamines and the free alkyne ynamines (Figure 2.10).

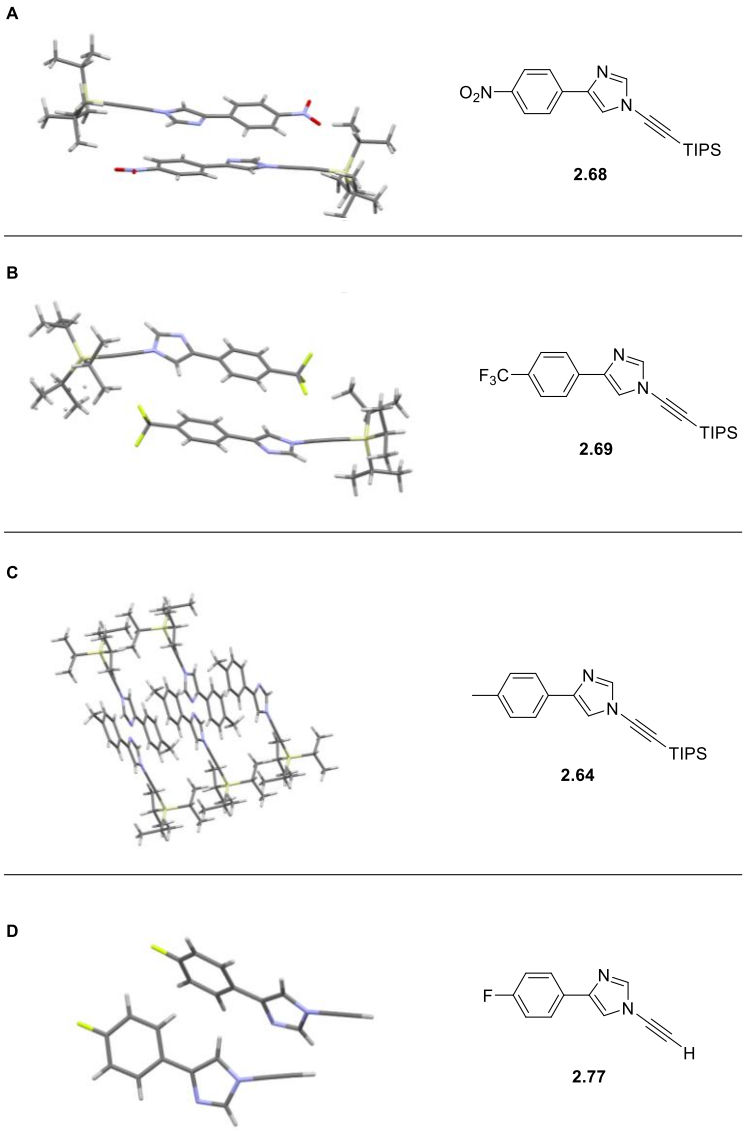

Figure 2.10. The crystal structures obtained for ynamines exhibiting more than one unique molecule per unit cell.

As shown, three of the ynamines have two unique molecules per unit cell. However, **2.64**, methyl imidazole, has five unique molecules per unit cell. This polymorphism was only observed for a selection of the imidazole ynamines and not for the benzimidazole ynamines.

2.3.7 Investigation of a Copper-Free Azide-Alkyne Cycloaddition

Previous exploratory work within the group showed that the CuAAC reaction between an ynamine and an azide can be catalysed using salts, such as calcium carbonate and sodium

chloride instead of copper. Initially it was planned to carry out a high-throughput fluorescent plate-based assay using ynamine **2.51** and coumarin azide **2.116** (Scheme 2.20A), but these plans were abandoned due the extremely poor solubility of triazole **2.117**. Instead, an initial investigation using the dimethyl ynamine **2.13** and benzyl azide **2.103** was carried out (Scheme 2.20B).

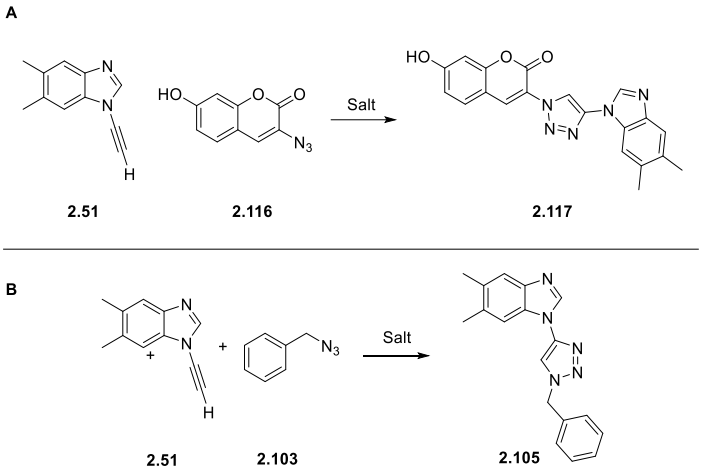

Scheme 2.20. A) Azide-alkyne cycloaddition between **2.51** and **2.116** to form fluorescent triazole **2.117** using a salt. **B)** Azide-alkyne cycloaddition between **2.51** and **2.103** to form **2.105** using a salt.

The initial screening used a range of calcium, sodium and potassium salts, selected due to their previous positive results within the group and vital roles in biological systems.[174] One of the main disadvantages about the use of the CuAAC compared to other methods of bioorthogonal chemistry is the use of copper, which is cytotoxic at around 50 – 75 μM copper concentration.[41] The advancement of the azide-alkyne cycloaddition to be performed without copper would lead to large developments in bioorthogonal chemistry. Despite the development of other bioorthogonal reactions that are copper-free (such as SPAAC and IEDDA), these typically utilise large, hydrophobic groups and give regioisomers as products, all attributes that are not desired.[2,175] Additionally, it was hoped that on successful development of a Cu-free azide-alkyne cycloaddition that the process could be used in biological systems for ion imaging.

HPLC analysis was initially used to follow the formation of the triazole formed. When preparing the experiments, new spatulas, stirrer bars and vials were used, alongside salts that were extra pure wherever possible to avoid any potential copper contamination. The testing used equimolar amounts of alkyne and azide in a methanol : water (1 : 1) solvent system. The reactions were carried out in triplicate and the results for the HPLC analysis are given in Figure 2.11. No internal standard (IS) was used, the conversions given are based on the peak areas of

the ynamine starting material **2.51** and the triazole product **2.105**. If an IS was used, this would give a more accurate representation of the percentage conversion.

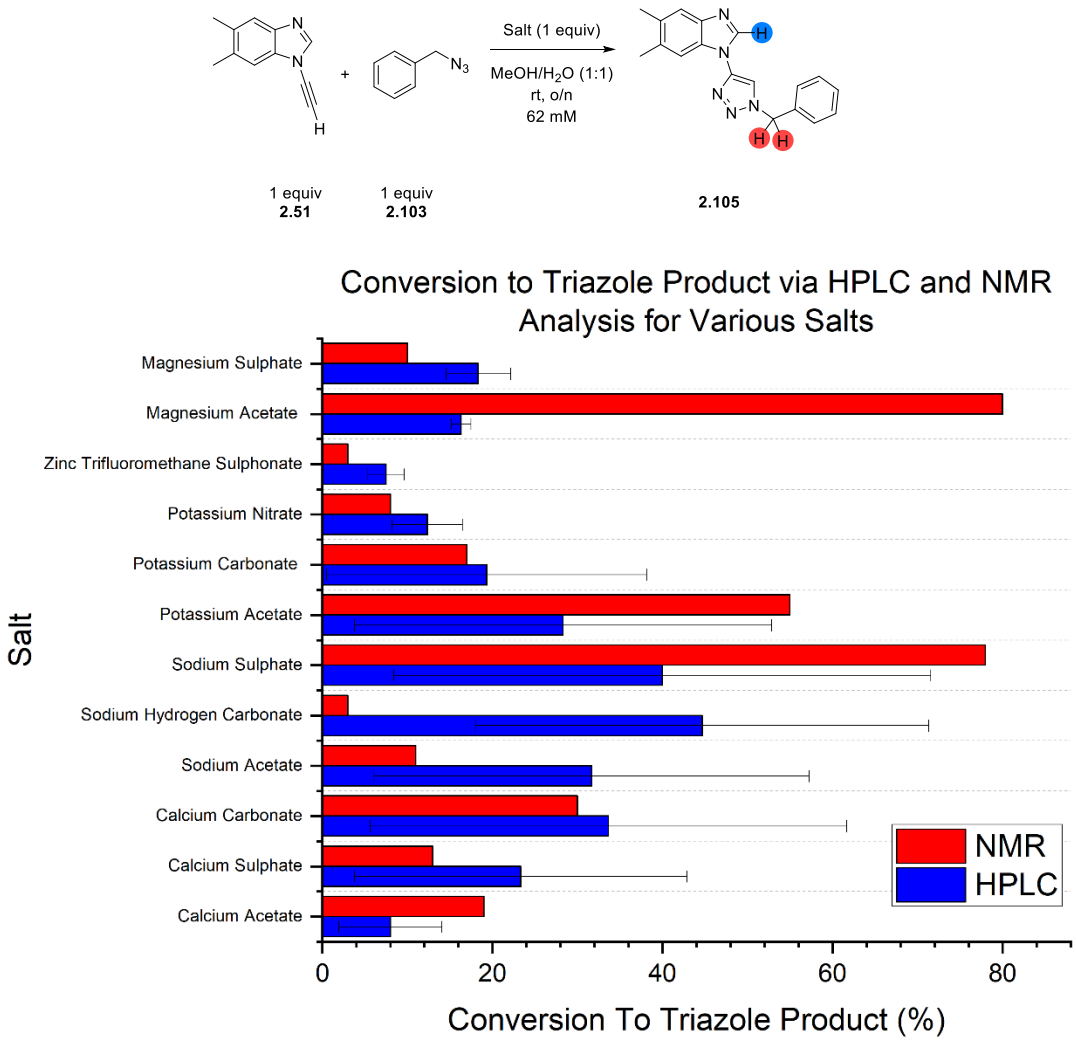

Figure 2.11. Graph showing the conversion to triazole for the salts tested for HPLC and NMR. The HPLC error bars are representative of N=3, with the exception of zinc trifluoromethane sulphonate which had an N=2. Only one reaction for each salt was tested by NMR analysis. No IS used.

As can be seen in Figure 2.11, triazole formation was observed *via* HPLC analysis, however the results were extremely inconsistent. One potential source of error was the sampling protocol and analysis by HPLC, as these reactions generally presented as a suspension, therefore, further tests were then carried out by NMR analysis. The reactions were set up as before, and after the overnight stirring, DCM was added to the reaction vial to attempt a mini work-up for each of the reactions. The DCM layer was extracted using a pipette and the solvent

removed *in vacuo*. The crude obtained was dissolved in the NMR solvent (C_2D_6OS) and analysed using proton NMR which allowed a percentage of product formed to be obtained (Figure 2.11). No IS was used. To obtain the percentage conversions, the integration of the two benzylic protons (highlighted in red in **2.105** (Figure 2.11)) was compared to the integration of the benzimidazole proton (highlighted in blue in **2.105** (Figure 2.11)) As can be seen in the graph above, NMR analysis confirms that product is being formed during the reaction, however, the conversion varies compared to the HPLC data.

Attempts to confirm the accuracy of the product formation were tested by comparing results of HPLC analysis to NMR results. This experiment was attempted using three salts, calcium carbonate, sodium chloride and sodium sulphate. This analysis showed that NMR gave a higher estimate of the triazole formed than the HPLC. For example, samples of reactions using sodium chloride and calcium carbonate gave respectively a product : starting material ratio of 59:41 and 51:49, however, both HPLC samples gave conversions of approx. 30%. This could be due to sampling issues with the HPLC, as many of the samples were not homogenous and accurate sampling may not have been obtained. NMR analysis could lead to more accurate results as a work-up is taking place prior to sampling, ensuring all material is in the sample submitted for analysis.

One possible explanation for the observed product formation could be that the metal ions play a role as Lewis acids. To investigate this theory, reactions were repeated with the addition of a crown ether to the reaction mix. It was hoped that these crown ethers would chelate their respective salt and no triazole product would be obtained. However, conversions were still obtained for the majority of salts tested, although conversions were lower than previously obtained.

Table 2.3. Conversion to triazole **2.105** from **2.51** and **2.103** using various salts and a respective crown ether. Reaction performed in MeOH/H_2O (1:1), rt, on, 62 mM. N=1. Conversions obtained by HPLC.

Salt	Conversion (%)
$Ca(OAc)_2$	11
$CaSO_4$	10
$CaCO_3$	11
NaOAc	19
$NaHCO_3$	12
Na_2SO_4	23
KOAc	11
K_2CO_3	8
K_2NO_3	11
$Zn(OTf)_2$	3
$Mg(OAc)_2$	12
$MgSO_4$	12

While it is possible that the crown ethers had failed to chelate the metal ion of the salt and that pre-stirring between the salt and chelating agent would be necessary, these results indicate that the metal ions are not solely responsible for the observed reaction. A variable that had not been tested yet was carrying out the reaction without a salt. Unexpectedly, a small conversion (up to 6%), was achieved when the reaction was carried out without a salt present. This could be a result of Cu contaminated equipment or reagents, however, attempts to mitigate this were taken as mentioned above.

Another hypothesis is the "on-water" effect, which has been observed for cycloadditions in the literature.[176,177] This is where the aggregation of hydrophobic molecules in aqueous environments increases the effective local concentration, and this results in an increase in the rate of reaction. Sharpless *et al.* investigated this effect and found that the cycloaddition between quadrucyclane and dimethyl azodicarboxylate gave the desired product quicker than in organic solvents, with a MeOH:H_2O (1:1) being the optimum conditions.[178] This is "on water" effect holds for other substrates tested. The possibility of conducting a reaction "on water" is of great interest due to the mildness of the conditions and the environmental implications of less solvent used.[179] To test whether the on water is responsible for the conversion to triazole **2.105**, the reaction could be repeated with a water-soluble azide such as azido-ethanol instead of benzyl azide.

In conclusion, the preliminary observations that the ynamine click reaction could proceed in the absence of copper catalyst were confirmed. However, the results were highly variable, and no clear trends could be established. The fact that the reaction proceeded in the presence of metal chelating crown ethers as well as in pure water points to the "on water" effect for a possible explanation of this phenomenon.[178] Factors that have not been investigated include water soluble azides, pH, concentration, and ionic strength and could potentially also play a role. However, the obtained results did not provide enough confidence that this type of reaction could be translated into an *in vivo* system or any other useful application. Therefore, further development on this part of the project was therefore abandoned and efforts were concentrated on elucidating the effects of substituents on the ynamine CuAAC reaction.

2.4 Summary and Future Work

In this chapter, the scope of the ynamine synthesis was explored. A range of substituted benzimidazole and imidazole ynamines bearing electron donating and electron withdrawing substituents were synthesised. The obtained yields were inconsistent for each substrate as well as varying between substrates, with no influence from reaction scale or concentration, as demonstrated in Table 2.1 and Table 2.2. This suggests that there are other factors impacting the reaction, such as the stirring or the degassing of the reaction.

These substrates have demonstrated the scope of the ynamine synthesis and also the unsuitability of some substrates, such as purine (**2.92**) and triazoles (**2.90** and **2.91**). The consistent low yields for the synthesis of substrates containing an amine motif (**2.49, 2.50** and **2.70**) suggest that the amine is interfering with the reaction, potentially chelating the copper catalyst.

The optimum method for the TIPS deprotection of the substrates has also been explored, with the fluoride on polymer method giving lower yields then TLC analysis suggests. The TBAF method was optimised after initial low yields and apparent degradation observed.

In future, the scope of the ynamines could be expanded further (Figure 2.12). The addition of further electronic groups into the benzimidazole substrates could be tested, including other halogens (**2.118**, **2.119** and **2.125**). The conjugation of a pyrimidine to the imidazole to form azabenzmidazoles could be explored to investigate further the effects that additional nitrogen's have on the synthesis (**2.120**). In the current work, only substitutions at the 6- and 7- positions have been explored and so 5,8 substituted ynamines could be synthesised (**2.121, 2.122** and **2.123**). An interesting imidazole that was not further explored was the diphenyl imidazole (**2.89**), and the substitution on the ring could be investigated (**2.124**).

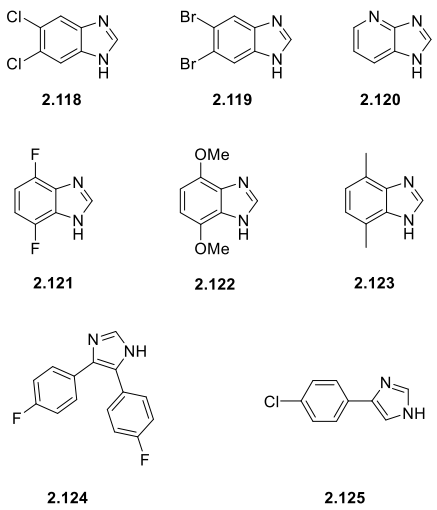

Figure 2.12. Potential substrates that could be used to expand the ynamine palette.

The proposed Cu-free azide-alkyne cycloaddition was investigated using various salts with ynamine **2.51** and azide **2.103**. However, inconsistent results were obtained despite attempts to develop the reaction. After an initial screen showed that the reaction appeared to be possible, the sampling method was tested, with NMR and HPLC giving inconsistent results, hypothesised to be a result of sampling issues for the HPLC analysis. An IS could be used to confirm if sampling is an issue and standardise the results. If this were to be performed again, the product would be isolated to confirm yields. One possible reason for the triazole formation could be the "on-water" effect causing the azide and alkyne to react due to high concentration and proximity. Contamination of the equipment remains a possibility, despite various precautions taken. If the reaction was to be investigated in future, there are several avenues to explore including the trying different ynamine substrates, such as the ones that have been synthesised in this chapter, and different azides. An alkyne could also be tested, such as phenylacetylene (**2.124**), to investigate whether this is a phenomenon unique to ynamine reactivity. Water-soluble azides, such as **2.126**, and chelating azides (**2.125**) alongside fluorescent azides and biotin-tagged azides could be used (Figure 2.13).[43,180] Other reaction variables could also be tested, such as the pH; differing the concentrations of the reactants or adding a surfactant to help with solubility issues.

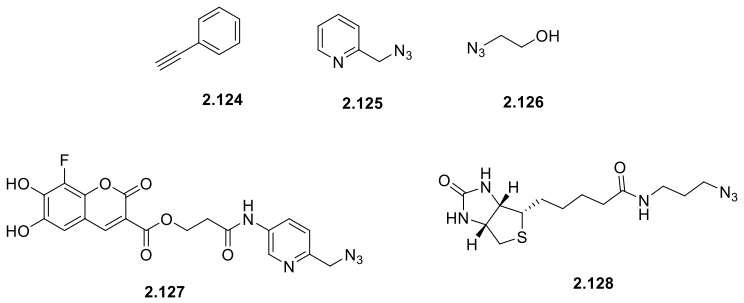

Figure 2.13. Potential substrates for Cu-free click.

2.5 Experimental

2.5.1 General Experimental Techniques and Procedures

2.5.1.1 Reagents and Solvents

All reagents and solvents were used as supplied from commercial sources and used without further purification unless otherwise stated.

2.5.1.2 Column Chromatography

Thin layer chromatography (TLC) was carried out using Merck silica plates coated with fluorescent indicator UV254. TLC plates were analysed under 254 nm UV light or developed using potassium permanganate solution. Normal-phase flash chromatography was carried out using ZEOprep 60 HYD 40-63 μm silica gel. Automatic purification was carried out on an Interchim PuriFLASH XS52Plus system, using Silicycle 230-400 mesh 40-63 μm silica columns of various sizes.

2.5.1.3 NMR Spectroscopy

NMR spectroscopy was carried out using either a Bruker 400 UltraShield™ B-ACS 60 spectrometer, Bruker AV500 spectrometer at 500 MHz (^{1}H) and 126 Hz (^{13}C) or Bruker AV600 spectrometer at 156 Hz (^{13}C). All chemical shifts (δ) in $CDCl_3$ were referenced at 7.26 (^{1}H) and 77.06 ppm (^{13}C), in C_2D_6OS at 2.50 (^{1}H) and 39.52 (^{13}C), in D_2O at 4.79 ppm (^{1}H) and in CD_3CN at 1.94 (^{1}H) and 118.26 ppm (^{13}C) and reported in parts per million (ppm). Coupling constants are quoted in hertz (Hz). Abbreviations for splitting patterns are s (singlet), br. s (broad singlet), d (doublet), dd (doublet of doublets), ddd (doublet of doublets of doublets), t (triplet), td (triplet of doublets), app. t (apparent triplet), q (quartet) and m (multiplet). All NMR data was processed using Mestrenova 11.0 software. Proton and carbon chemical shifts were assigned using proton (^{1}H), carbon (^{13}C), Heteronuclear Single Quantum Coherence (HSQC), Heteronuclear Multiple-Bond Correlation Spectroscopy (HMBC) and Correlation Spectroscopy (COSY) and Nuclear Overhauser Effect Spectroscopy (NOESY) whenever possible.

2.5.1.4 High Resolution Mass Spectrometry

High-resolution mass spectra were recorded on a ThermoScientific Exactive™ Plus Orbitrap Mass Spectrometer at the University of Strathclyde or a Bruker Micro TOF II at The University of Edinburgh.

2.5.1.5 IR Spectroscopy

IR data was collected on either an Agilent or Shimadzu FTIR spectrometer and the data processed using the proprietary software. Only major absorbances were reported.

2.5.2 Liquid Chromatography-Mass Spectrometry (LC-MS) and Ultra-Performance-Mass-Spectrometry (UPLC-MS)

LC-MS was carried out on an Agilent HPLC instrument in conjunction with an Agilent Quadrupole mass detector on an Agilent Poroshell 120 C18 column (75 mm × 4.6 mm, 2.7 μm). UPLC-MS was carried out on an AVANT UPLC with an Advion Expression CMS L attached for mass detection on a Phenomenex Kinetex C18 column (30 mm × 2.1 mm, 2.7 μm). Electrospray ionization (ESI) was used in all cases.

2.5.3 General Procedures

General Procedure A: Synthesis of aromatic ynamines

To a solution of the corresponding benzimidazole or imidazole (1 equiv), caesium carbonate (1.1 equiv), copper iodide (0.05 equiv), PEG 400 in anhydrous 1,4-dioxane (269 mM) was added (bromoethynyl)triisopropylsilane (1.1 equiv) under argon atmosphere. The mixture was heated to 110 °C and stirred for 48 h. After cooling the reaction mixture to rt it was then diluted with EtOAc. Then, the mixture was washed with saturated EDTA solution and brine. The organic layer was then dried over anhydrous Na_2SO_4, filtered and the solvent removed *in vacuo*. The crude residue was purified by flash column chromatography (silica gel) to afford the desired product.

General Procedure B: Deprotection of TIPS-protected aromatic ynamines

To a solution of the corresponding benzimidazole or imidazole protected ynamine (1 equiv) in THF (0.05 M) was added TBAF (0.1 to 1 equiv) dropwise at 0 °C under argon atmosphere. The reaction was monitored by TLC and upon full consumption of starting material the THF was evaporated under an air stream. The crude product was purified by flash column chromatography to afford the desired product.

General Procedure C: Conditions for the CuAAC reaction of aromatic ynamines in MeOH or MeCN

To a solution of ynamine (1 equiv) in MeOH (62 mM) was added benzyl azide (1 equiv) and copper(II) acetate monohydrate (0.05 equiv). The reaction was left to stir and monitored by

TLC. Upon completion, the reaction was quenched with EDTA, and the solution washed with ethyl acetate. The organic extracts were washed with brine, dried over anhydrous sodium acetate and filtered. The organic solvent was removed *in vacuo*. The crude residue was purified by column chromatography (silica gel) to give the desired product.

General Procedure D: Conditions for the CuAAC reaction of aromatic ynamines in HFIP/Water

To a solution of ynamine (1 equiv) in HFIP/water (40:60, 62 mM) was added benzyl azide (1 equiv) and copper(II) acetate monohydrate (0.05 equiv). The reaction was left to stir and monitored by TLC. Upon completion, the HFIP was removed *in vacuo* and the residue remaining was diluted with ethyl acetate and washed with EDTA. The organic extracts were combined andwashed with brine, dried over anhydrous sodium acetate and filtered. The organic solvent was removed *in vacuo*. The crude residue was purified by column chromatography (silica gel) to give the desired product.

2.5.4 Synthetic Procedures

*(Bromoethynyl)triisopropylsilane (**2.22**)*[181]

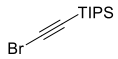

A solution of TIPS-acetylene (7.00 g, 38.0 mmol), *N*-bromosuccinimde (7.51 g, 43.0 mmol) and silver nitrate (653 mg, 3.80 mmol) in acetone (37 mL) was covered in foil and stirred for 16 h at rt. The mixture was filtered through a celite pad and concentrated *in vacuo.* The crude mixture was passed through a silica plug using petroleum ether to elute. The solvent was removed *in vacuo* and the desired product obtained as a colourless liquid (10.7 g, 40.8 mmol, 97%).

^{1}H NMR (500 MHz, $CDCl_3$) δ 0.97 – 0.93 (m, 21H).

^{13}C NMR (125 MHz, $CDCl_3$) δ 83.6, 61.8, 18.6, 11.6.

NMR spectra in accordance with literature values.[182]

*5,6-Dimethyl-1-((triisopropylsilyl)ethynyl)-1H-benzo[d]imidazole (**2.28**)*[183]

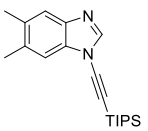

Prepared according to the General Procedure A using 5,6-dimethyl-1*H*-benzo[*d*]imidazole (3.54 g, 24.4 mmol), caesium carbonate (9.37 g, 28.8 mmol), copper iodide (220 mg, 1.55 mmol), PEG 400 (960 mg, 2.40 mmol) and (bromoethynyl)triisopropylsilane (7.46 mL, 28.5 mmol) in 1,4-dioxane (90 mL) The residue was purified by column chromatography (0 – 20% ethyl acetate in petroleum ether) to give the desired product as a colourless oil (3.48 g, 10.6 mmol, 44%).

^{1}H NMR (500 MHz, $CDCl_3$) δ 7.97 (s, 1H), 7.55 (s, 1H), 7.28 (s, 1H), 2.40 (s, 3H), 2.37 (s, 3H), 1.19 – 1.15 (m, 21H).

^{13}C NMR (126 MHz, $CDCl_3$) δ 143.1, 140.4, 134.2, 133.1, 133.0, 120.9, 111.2, 90.7, 72.4, 20.7, 20.3, 18.7, 18.7, 17.9, 12.5, 11.4.

IR ν_{max} (cm^{-1}) 2943 (C-H), 2807 (C-H), 2182 (C≡C), 1560 (C=C), 1467 (C=C).

NMR spectra in accordance with literature values.[183]

*1-Ethynyl-1H-benzo[d]imidazol-6-amine (**2.29**)*

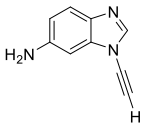

Prepared according to the general procedure B using 1-((triisopropylsilyl)ethynyl)-1H-benzo[d]imidazol-5-amine (463 mg, 1.48 mmol) and TBAF (280 μL, 1.02 mmol) in THF (5 mL). The crude was purified by column chromatography (50% ethyl acetate in hexane) to give the desired product as a light brown (128 mg, 81.5 mmol, 55%).

^{1}H NMR (400 MHz, DMSO) δ 8.22 (s, 1H), 7.38 (d, *J* = 8.6 Hz, 1H), 6.73 – 6.68 (m, 1H), 6.63 (dd, *J* = 8.6, 2.1 Hz, 1H), 5.34 (bs, 2H), 4.59 (s, 1H).

IR ν_{max} (cm^{-1}) 3321 (N-H), 2962 (C-H), 2878 (C-H), 2174 (C≡C).

NMR spectra in accordance with literature values.[83]

*1-Ethynyl-1H-benzo[d]imidazol-5-amine (**2.30**)*

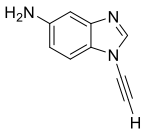

A mixture of 1-((triisopropylsilyl)ethynyl)-1H-benzo[d]imidazol-5-amine (870 mg, 2.78 mmol) and fluoride on polymer (925 mg, 2.78 mmol) in acetonitrile (9 mL) was stirred for 16 h at rt. The mixture was filtered, and the filtrate concentrated *in vacuo.* The residue was purified by column chromatography (20 – 80% ethyl acetate in hexane) to give the desired product as a light brown solid (200 mg, 1.27 mmol, 46%).

^{1}H NMR (400 MHz, DMSO) δ 8.38 (s, 1H), 7.26 (d, *J* = 8.6 Hz, 1H), 6.87 (d, *J* = 2.0 Hz, 1H), 6.74 (dd, *J* = 8.6, 2.1 Hz, 1H), 5.05 (bs, 2H), 4.58 (s, 1H).

^{13}C NMR (126 MHz, $CDCl_3$) δ 144.1, 143.9, 143.2, 128.0, 114.6, 111.4, 105.8, 61.7 (1 carbon not observed).

HR-MS (ESI) $C_9H_7N_3^+$ calc 158.0713 found 158.0712.

IR ν_{max} (cm^{-1}) 3325 (N-H), 3210 (N-H), 2947 (C-H), 2869 (C-H), 2184 (C≡C), 1485 (C=C).

*1H-Naphtho[2,3-d]imidazole (**2.35**)*[170]

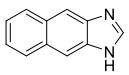

2,3-dihydrobenzo[*b*][1,4]dioxine-6,7-diamine (500 mg, 3.16 mmol) was dissolved in formic acid and the solution heated to reflux for 36 h. The reaction mixture was allowed to cool to rt. The reaction was basified with NaOH and then the aqueous layer was extracted with $CHCl_3$ to give the desired product as a red solid (0.424 g, 2.52 mmol, 75%).

^{1}H NMR (500 MHz, DMSO) δ 12.49 (s, 1H), 8.46 (s, 1H), 8.21 (s, 1H), 8.00 (d, *J* = 9.0 Hz, 3H), 7.37 (d, *J* = 7.2 Hz, 2H).

^{13}C NMR (101 MHz, DMSO) δ 146.98, 130.17, 128.26, 123.80, 115.98, 107.24.

IR ν_{max} (cm^{-1}) 2542 (C-H), 2408 (C-H), 1491 (C-H).

Proton count in accordance with literature values.[170]

*N-(2,3-dihydrobenzo[b][1,4]dioxin-6-yl)acetamide (**2.38**)*[171]

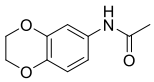

1,4-benzodioxan-6-amine (3.00 g, 19.8 mmol) was suspended in acetic anhydride (50 mL) and stirred at rt for 3 h. The solution was poured onto ice cold water and extracted with DCM. The combined organic layers were washed with brine, dried over anhydrous sodium sulphate, filtered and concentrated under reduced pressure to give the desired product as a brown solid (2.80 g, 14.5 mmol, 73%).

^{1}H NMR (500 MHz, DMSO) δ 9.72 (s, 1H), 7.21 (d, *J* = 2.4 Hz, 1H), 6.93 (dd, *J* = 8.7, 2.4 Hz, 1H), 6.75 (d, *J* = 8.6 Hz, 1H), 4.23 – 4.16 (m, 4H), 1.98 (s, 3H).

^{13}C NMR (126 MHz, DMSO) δ 167.7, 142.8, 139.1, 133.0, 116.6, 112.2, 108.1, 64.2, 63.9, 23.8.

*N-(7-nitro-2,3-dihydrobenzo[b][1,4]dioxin-6-yl)acetamide (**2.39**)*[171]

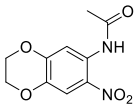

N-(2,3-dihydrobenzo[b][1,4]dioxin-6-yl)acetamide (3.00 g, 15.5 mmol) was dissolved in acetic acid (24 mL) and cooled to 0 °C. Nitric acid (24 mL) was added dropwise and the resulting mixture stirred for 1 h. The solution was added to ice water and the pH adjusted to pH 8 - 9 using NaOH solution. The aqueous solution was extracted into DCM (3 × 20 mL) and the organics combined, washed with brine, dried over anhydrous sodium sulphate and filtered. The solvent was removed *in vacuo* to give the desired product as an orange solid (3.70 g, 15.4 mmol, 99%).

^{1}H NMR (400 MHz, DMSO) δ 10.03 (s, 1H), 7.55 (s, 1H), 7.30 (s, 1H), 4.40 – 4.34 (m, 2H), 4.33 – 4.28 (m, 2H), 2.06 (s, 3H).

*7-Nitro-2,3-dihydrobenzo[b][1,4]dioxin-6-amine (**2.40**)*[171]

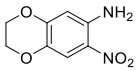

N-(7-nitro-2,3-dihydrobenzo[b][1,4]dioxin-6-yl)acetamide (3.55 g, 14.9 mmol) was dissolved in 2 M sulphuric acid (140 mL) and heated to 110 °C for 6 h. The reaction mixture was allowed to cool to rt and then cooled to 0 °C. The precipitate formed was filtered and washed with water to give the desired product as a dark orange solid (2.27 g, 11.6 mmol, 78%).

^{1}H NMR (400 MHz, DMSO) δ 7.40 (s, 1H), 7.12 (s, 2H), 6.43 (s, 1H), 4.37 – 4.30 (m, 2H), 4.24 – 4.17 (m, 2H).

^{13}C NMR (101 MHz, DMSO) δ 151.6, 143.3, 134.6, 124.2, 111.3, 103.4, 65.2, 63.7.

*2,3-Dihydrobenzo[b][1,4]dioxine-6,7-diamine (**2.41**)*[171]

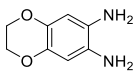

7-nitro-2,3-dihydrobenzo[b][1,4]dioxin-6-amine (2.25 g, 11.5 mmol) and Palladium on Carbon (10% wt.%) (122 mg, 1.15 mmol) was dissolved in MeOH (80 mL) and placed under an argon atmosphere. The reaction was placed under a hydrogen atmosphere and left to stir overnight. The reaction was filtered over celite and washed with MeOH. The filtrate was removed *in vacuo* to give the desired product (1.91 g, 11.5 mmol, 90%) as a dark orange solid.

^{1}H NMR (400 MHz, DMSO) δ 6.08 (s, 2H), 4.05 (s, 4H), 4.03 (s, 4H).

^{13}C NMR (101 MHz, DMSO) δ 134.7, 129.5, 103.7, 64.2.

IR ν_{max} (cm^{-1}) 3124 (N-H), 1595 (N-H), 1510 (N-H), 1342 (C-N), 728 (N-H).

*6,7-Dihydro-1H-[1,4]dioxino[2',3':4,5]benzo[1,2-d]imidazole (**2.42**)*

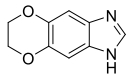

To 2,3-dihydrobenzo[b][1,4]dioxine-6,7-diamine (2.00 g, 12.0 mmol) was added formic acid (2.00 mL, 53.0 mmol). The solution was heated to 100 °C for 6 h. After cooling to rt, the solution was basified using NaOH and extracted into chloroform. The solvent was removed *in vacuo* to give the product as a brown solid (1.39 g, 7.90 mmol, 66%).

^{1}H NMR (400 MHz, DMSO) δ 12.04 (s, 1H), 8.31 (s, 1H), 8.00 (s, 1H), 7.00 (s, 1H), 4.22 (s, 4H).

^{13}C NMR (101 MHz, DMSO) δ 141.5, 140.2, 79.2 , 63.9 (2 quaternary carbons not observed).

HRMS (ESI) $C_9H_8N_2O_2^+$ calculated 177.0659, found 177.0655.

*5,6-Dimethoxy-1-((triisopropylsilyl)ethynyl)-1H-benzo[d]imidazole (**2.43**)*

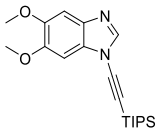

Prepared according to the general procedure A using 5,6-dimethoxy-1*H*-benzo[*d*]imidazole (4.98 g, 27.9 mmol), caesium carbonate (10.0 g, 30.7 mmol), copper iodide (266 mg, 1.40 mmol), PEG 400 (1.12 g, 2.79 mmol) and (bromoethynyl)triisopropylsilane (8.03 g, 30.7 mmol) in anhydrous 1,4-dioxane (104 mL). The crude residue was dry loaded and purified by automated flash column chromatography (0 – 20% ethyl acetate in hexane) to give the desired product as an off-white solid (3.53 g, 9.85 mmol, 35%).

^{1}H NMR (400 MHz, $CDCl_3$) δ 7.94 (s, 1H), 7.25 (s, 1H), 7.00 (s, 1H), 3.94 (s, 3H), 3.93 (s, 3H) 1.19-1.12 (m, 21H).

^{13}C NMR (101 MHz, $CDCl_3$) δ 148.8, 147.9, 142.1, 135.2, 128.6, 102.6, 93.6, 90.6, 72.8, 56.5, 56.3, 18.7, 11.3.

HRMS (ESI) $C_{20}H_{30}N_2O_2Si^+$ calculated 359.2149, found 359.2148.

IR ν_{max} (cm^{-1}) 3111 (C-H), 2945 (C-H), 2867 (C-H), 2174 (C≡C), 1474 (ar. C=C), 1223 (C-O), 1139 (C-O).

*5,6-Difluoro-1-((triisopropylsilyl)ethynyl)-1H-benzo[d]imidazole (**2.44**)*

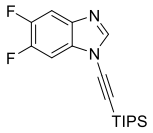

Prepared according to General Procedure A using 5,6-difluoro-1*H*-benzo[*d*]imidazole (900 mg, 5.84 mmol), (bromoethynyl)triisopropylsilane (1.68 g, 6.42 mmol), caesium carbonate (2.09 g, 6.42 mmol), copper iodide (55.6 mg, 292 μmol) and PEG 400 (25.8 mg, 584 μmol) in anhydrous 1,4-dioxane (22 mL). The crude residue was purified by column chromatography (0 – 30% ethyl acetate in hexane) to give the desired product as a white solid (1.15 g, 3.42 mmol, 59%).

^{1}H NMR (500 MHz, $CDCl_3$) δ 8.08 (s, 1H), 7.59 (dd, *J* = 10.0, 7.1 Hz, 1H), 7.32 (dd, *J* = 9.0, 6.7 Hz, 1H), 1.18 – 1.15 (m, 21H).

^{13}C NMR (126 MHz, $CDCl_3$) δ 150.5 (dd, *J* = 245 Hz, 15 Hz), 148.9 (dd, *J* = 243.8, 15 Hz), 145.2 (d, *J* = 3.8 Hz), 137.2 (d, *J* = 11.25 Hz), 130.2 (d, *J* = 11.25 Hz), 108.7 (d, *J* = 20 Hz), 99.5 (d, *J* = 23.7 Hz), 89.3, 74.1, 18.8, 17.6, 12.5, 11.3.

^{19}F NMR (471 MHz, $CDCl_3$) δ -138.16 – -138.26 (m), -140.92 – -141.02 (m).

HR-MS (ESI) $C_{18}H_{24}F_2N_2Si^+$ calculated 335.1749, found 335.1749.

IR ν_{max} (cm^{-1}) 2945 (C-H), 2869 (C-H), 2189 (C≡C), 1467 (C=C).

*1-((Triisopropylsilyl)ethynyl)-1H-naphtho[2,3-d]imidazole (**2.45**)*

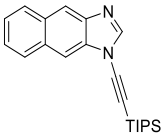

Prepared according to General Procedure A using 1*H*-naphtho[2,3-*d*]imidazole (1.30 g, 7.73 mmol), caesium carbonate (2.77 g, 8.50 mmol), copper iodide (73.6 mg, 387 μmol), PEG 400 (309 mg, 773 μmol) and (bromoethynyl)triisopropylsilane (2.02 g, 8.50 mmol) in anhydrous 1,4-dioxane (29 mL). The crude residue was cry-loaded onto silica gel and purified by flash column chromatography (0 – 5% ethyl acetate in hexane) to give the desired product as an off white solid (1.60 g, 4.59 mmol, 59%).

^{1}H NMR (500 MHz, DMSO) δ 8.86 (s, 1H), 8.38 (s, 1H), 8.12 (dd, *J* = 8.2, 4.0 Hz, 2H), 7.97 (s, 1H), 7.57 – 7.48 (m, 2H), 1.22 – 1.14 (m, 21H).

^{13}C NMR (126 MHz, DMSO) δ 148.6, 141.7, 134.4, 131.3, 131.1, 129.0, 128.2, 126.0, 125.0, 118.6, 107.1, 91.1, 72.8, 19.0, 11.2.

HR-MS (ESI) $C_{22}H_{28}N_2Si^+$ calculated 349.2095, found 349.2092.

IR ν_{max} (cm^{-1}) 2949 (C-H), 2867 (C-H), 2199 (C≡C), 1513 (ar. C=C).

1-((Triisopropylsilyl)ethynyl)-6,7-dihydro-1H-[1,4]dioxino[2',3':4,5]benzo[1,2-d]imidazole ***(2.46)***

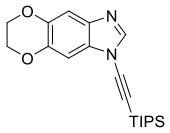

Prepared according to the General Procedure A using 6,7-dihydro-1*H*-[1,4]dioxino[2',3':4,5]benzo[1,2-*d*]imidazole (800 mg, 4.45 mmol), (bromoethynyl)triisopropylsilane (1.30 g, 4.99 mmol), caesium carbonate (1.63 mg, 5.00 mmol), copper(I) iodide (43.2 mg, 227 μmol) and PEG 400 (18.2 mg, 45.0 μmol) in 1,4-dioxane (20 mL). The crude obtained was purified by column chromatography (0 – 10% ethyl acetate in hexane) to give the desired product (0.845 g, 2.37 mmol, 52%).

^{1}H NMR (400 MHz, $CDCl_3$) δ 7.93 (s, 1H), 7.28 (s, 1H), 7.00 (s, 1H), 4.33 – 4.27 (m, 4H), 1.16-1.14 (m, 21H).

^{13}C NMR (101 MHz, $CDCl_3$) δ 143.5, 143.4, 142.8, 141.9, 136.3, 129.5, 108.1, 108.0, 98.7, 90.5, 72.7, 64.6, 64.3, 18.8, 11.4.

HR-MS (ESI) $C_{20}H_{28}O_2N_2Si^+$ calculated 357.1993, found 357.1990.

IR ν_{max} (cm^{-1}) 2943 (C-H), 2867 (C-H), 2180 (C≡C), 1465 (C=C), 1310 (C-O).

*6-Methoxy-1-((triisopropylsilyl)ethynyl)-1H-benzo[d]imidazole (**2.47**)*

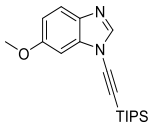

Prepared according to General Procedure A using (2.61 g, 17.6 mmol), caesium carbonate (6.31 g, 19.4 mmol), copper(I) iodide (168 mg, 881 μmol), PEG 400 (705 mg, 1.76 mmol) and (bromoethynyl)triisopropylsilane (5.06 g, 19.4 mmol) in anhydrous 1,4-dioxane (77 mL). The crude residue was dry loaded onto silica gel and purified by flash column chromatography (0 – 10% ethyl acetate in hexane) to give the desired product as a colourless oil (1.53 g, 4.65 mmol, 26%).

^{1}H NMR (400 MHz, $CDCl_3$) δ 7.92 (s, 1H), 7.58 (d, J = 8.8 Hz, 1H), 6.91 (d, J = 2.3 Hz, 1H), 6.86 (dd, J = 8.8, 2.4 Hz, 1H), 3.76 (s, 3H), 1.12-1.05 (m, 21H).

^{13}C NMR (101 MHz, $CDCl_3$) δ 157.9, 142.2, 135.9, 135.4, 121.0, 112.9, 94.2, 90.2, 72.7, 55.4, 18.4, 11.1.

HR-MS (ESI) $C_{19}H_{28}N_2OSi^+$ calculated 329.2044, found 329.2044.

*5-Methoxy-1-((triisopropylsilyl)ethynyl)-1H-benzo[d]imidazole (**2.48**)*

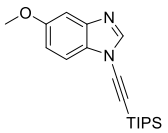

Prepared according to General Procedure A using (2.61 g, 17.6 mmol), caesium carbonate (6.31 g, 19.4 mmol), copper(I) iodide (168 mg, 881 μmol), PEG 400 (705 mg, 1.76 mmol) and (bromoethynyl)triisopropylsilane (5.06 g, 19.4 mmol) in anhydrous 1,4-dioxane (77 mL). The crude residue was purified by flash column chromatography (0 – 10% ethyl acetate in hexane) to give the desired product as a colourless solid (838 mg, 2.55 mmol, 14%).

^{1}H NMR (500 MHz, $CDCl_3$) δ 8.03 (s, 1H), 7.41 (d, *J* = 8.8 Hz, 1H), 7.28 (d, *J* = 2.3 Hz, 1H), 7.04 (dd, *J* = 8.7, 2.4 Hz, 1H), 3.87 (s, 3H), 1.19-1.13 (m, 21H).

^{13}C NMR (126 MHz, $CDCl_3$) δ 157.8, 144.5, 143.1, 129.3, 150.0, 111.7, 103.5, 90.7, 72.9, 56.3, 19.0, 11.6.

HR-MS (ESI) $C_{19}H_{28}N_2OSi^+$ calculated 329.2043, found 329.2038.

IR ν_{max} (cm^{-1}) 2945 (C-H), 2867 (C-H), 2191 (C≡C), 1484 (C=C), 1446 (C-O).

*1-((Triisopropylsilyl)ethynyl)-1H-benzo[d]imidazol-6-amine (**2.49**)*

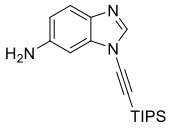

Prepared according to the General Procedure A using 5-aminobenzimidazole (2.00 g, 15.0 mmol), caesium carbonate (5.87 g, 18.0 mmol), copper(I) iodide (143 mg, 751.0 μmol), PEG 400 (600 mg, 150 μmol) and (bromoethynyl)triisopropylsilane (4.71 g, 18.0 mmol) in anhydrous 1,4-dioxane (90 mL). The crude residue was purified by flash column chromatography (50 – 70% ethyl acetate in hexane) to give the desired product as a dark orange solid (512 mg, 1.63 mmol, 11%).

^{1}H NMR (400 MHz, DMSO) δ 8.22 (s, 1H), 7.38 (d, *J* = 9.1 Hz, 1H), 6.63 (dt, *J* = 4.7, 2.2 Hz, 2H), 5.42 (s, 2H), 1.15 – 1.12 (m, 21H).

^{13}C NMR (101 MHz, DMSO) δ 147.3, 141.2, 135.5, 132.7, 120.5, 112.7, 93.3, 91.2, 70.9, 18.5, 10.7.

IR ν_{max} (cm^{-1}): 3366 (N-H), 3215 (N-H), 2945 (C-H), 2867 (C-H), 2189 (C≡C), 1500 (C=C).

NMR spectra in accordance with literature values.[83]

*1-((Triisopropylsilyl)ethynyl)-1H-benzo[d]imidazol-5-amine (**2.50**)*

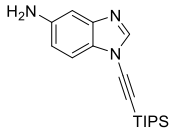

Prepared according to the General Procedure A using 5-aminobenzimidazole (2.00 g, 15.0 mmol), caesium carbonate (5.87 g, 18.0 mmol), copper iodide (143 mg, 751 μmol), PEG 400 (600 mg, 1.50 mmol) and (bromoethynyl)triisopropylsilane (4.71 g, 18.0 mmol) in anhydrous 1,4-dioxane (90 mL). The crude residue was purified by flash column chromatography (50 – 70% ethyl acetate in hexane) to give the desired product as a dark orange solid (450 mg, 1.43 mmol, 10%).

^{1}H NMR (400 MHz, DMSO) δ 8.39 (s, 1H), 7.16 (d, *J* = 8.6 Hz, 1H), 6.88 (d, *J* = 2.0 Hz, 1H), 6.76 (dd, *J* = 8.5, 2.1 Hz, 1H), 5.07 (s, 2H), 1.12 – 1.08 (m, 21H).

^{13}C NMR (101 MHz, DMSO) δ 146.0, 143.9, 142.6, 125.4, 113.4, 109.9, 103.1, 91.0, 70.6, 18.2, 10.4.

IR ν_{max} (cm^{-1}): 3327 (N-H), 3211 (N-H), 2947 (C-H), 2869 (C-H), 2184 (C≡C), 1485 (C=C), 1454 (C=C).

*1-Ethynyl-5,6-dimethyl-1H-benzo[d]imidazole (**2.51**)*[183]

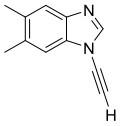

A mixture of 5,6-dimethyl-1-((triisopropylsilyl)ethynyl)-1*H*-benzo[*d*]imidazole (3.48 g, 10.7 mmol) and fluoride on polymer (3.56 g, 10.7 mmol) in acetonitrile (40 mL) was stirred for 16 h at rt. The mixture was filtered, and the filtrate concentrated *in vacuo.* The residue was purified by column chromatography (0 – 20% ethyl acetate in petroleum ether) to give the desired product as an off-white solid (1.27 g, 7.46 mmol, 70%).

^{1}H NMR (500 MHz, $CDCl_3$) δ 7.89 (s, 1H), 7.48 (s, 1H), 7.17 (s, 1H), 3.17 (s, 1H), 2.32 (s, 3H), 2.29 (s, 3H).

^{13}C NMR (125 MHz, $CDCl_3$) δ 142.8, 140.2, 134.2, 133.0, 132.7, 120.7, 110.9, 70.6, 61.5, 20.3, 20.1.

IR ν_{max} (cm^{-1}) 3202 (C-H), 3103 (C-H), 2152 (C≡C), 1454 (C=C), 1199 (C=C).

NMR spectra in accordance with literature values.[183]

*1-Ethynyl-5,6-dimethoxy-1H-benzo[d]imidazole (**2.52**)*

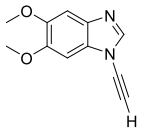

Prepared according to the general procedure B using 5,6-dimethoxy-1-((triisopropylsilyl)ethynyl)-1*H*-benzo[*d*]imidazole (2.00 g, 5.58 mmol) in THF (112 mL) and TBAF (900 µL, 3.28 mmol). The crude product was purified by column chromatography (0 – 20% ethyl acetate in hexane) to afford the desired product as an off-white solid (1.03 g, 5.09 mmol, 91%).

^{1}H NMR (400 MHz, $CDCl_3$) δ 7.93 (s, 1H), 7.25 (s, 1H), 7.00 (s, 1H), 3.95 (s, 3H), 3.92 (s, 3H), 3.27 (s, 1H).

^{13}C NMR (101 MHz, $CDCl_3$) δ 148.9, 148.0, 142.2, 135.2, 128.2, 102.7, 93.5, 70.7, 62.0, 56.5, 56.4.

HR-MS (ESI) $C_{11}H_{10}N_2O_2^+$ calculated 203.0815, found 203.0824.

IR ν_{max} (cm^{-1}) 3167 (C-H), 2148 (C≡C), 1485 (C-C), 1215 (C-O), 1143 (C-O).

*1-Ethynyl-5,6-difluoro-1H-benzo[d]imidazole (**2.53**)*

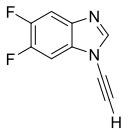

Prepared according to General Procedure B using 5,6-difluoro-1-((triisopropylsilyl)ethynyl)-1*H*-benzo[*d*]imidazole (507 mg, 1.52 mmol), TBAF (191 mg, 728 mmol) in THF (30 mL). The crude residue was purified by column chromatography to give the desired product as a pink solid (200 mg, 1.12 mmol, 74%).

^{1}H NMR (400 MHz, DMSO) δ 8.73 (s, 1H), 7.91 (dd, *J* = 10.7, 7.3 Hz, 1H), 7.79 (dd, *J* = 9.7, 7.1 Hz, 1H), 4.79 (s, 1H).

^{19}F NMR (376 MHz, DMSO) δ -139.61 (ddd, *J* = 21.4, 9.7, 7.3 Hz), -142.13 (ddd, *J* = 21.5, 10.7, 7.1 Hz).

^{13}C NMR (101 MHz, DMSO) δ 148.2 (dd, *J* = 244, 16 Hz), 147.9 (dd, *J* = 263, 15 Hz), 146.8 (d, *J* = 4 Hz) 136.8 (d, *J* = 11.0 Hz), 129.7 (d, *J* = 11.4 Hz), 108.3 (d, *J* = 20.3 Hz), 99.7 (d, *J* = 23.7 Hz), 69.4, 65.5.

HR-MS (ESI): $C_9H_4F_2N_2^+$ calculated 179.0425, found 179.0412.

IR ν_{max} (cm^{-1}): 3193 (C-H), 2161 (C≡C), 1471 (C-C), 1480 (ar. C-C), 1225 (C-F).

*1-Ethynyl-1H-naphtho[2,3-d]imidazole (**2.54**)*

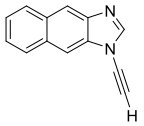

Prepared according to the General Procedure B using 1-((triisopropylsilyl)ethynyl)-1*H*-naphtho[2,3-*d*]imidazole (444 mg, 1.26 mmol), TBAF (572 mg, 2.18 mmol) in THF (25 mL). The crude residue was purified by column chromatography (0 – 20% ethyl acetate in hexane) to give the desired product as a pale brown solid (243 mg, 1.10 mmol, 87%)

^{1}H NMR (400 MHz, DMSO) δ 8.84 (s, 1H), 8.37 (s, 1H), 8.17 – 8.08 (m, 3H), 7.56 – 7.46 (m, 2H), 4.81 (s, 1H).

^{13}C NMR (101 MHz, DMSO) δ 148.2, 141.2, 133.8, 130.9, 130.5, 128.4, 127.7, 125.4, 124.5, 117.8, 107.0, 70.5, 65.3.

HR-MS (ESI) $C_{13}H_8N_2^+$ calculated 193.0760, found 193.0759.

IR ν_{max} (cm^{-1}) 3191 (C-H), 2148 (C≡C), 1508 (C-C), 1202 (C-C).

*1-Ethynyl-6,7-dihydro-1H-[1,4]dioxino[2',3':4,5]benzo[1,2-d]imidazole (**2.55**)*

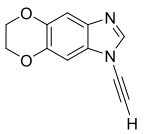

Prepared according to the General Procedure B using 1-((triisopropylsilyl)ethynyl)-6,7-dihydro-1*H*-[1,4]dioxino[2',3':4,5]benzo[1,2-*d*]imidazole (760 mg, 2.13 mmol) and TBAF (585 µL, 2.13 mmol) in THF (43 mL). The crude residue was purified by column chromatography (0 – 20% ethyl acetate in hexane) to give the desired product as a light brown solid (380 mg, 1.90 mmol, 89%).

^{1}H NMR (400 MHz, DMSO) δ 8.46 (s, 1H), 7.23 (s, 1H), 7.02 (s, 1H), 4.65 (s, 1H), 4.28 (m, 4H).

^{13}C NMR (101 MHz, DMSO) δ 144.3, 142.4, 141.5, 135.5, 128.5, 107.2, 97.8, 70.3, 64.5, 64.1, 63.7.

HR-MS (ESI) $C_{11}H_8O_2N_2^+$ calc 201.0659, found 201.0656.

IR ν_{max} (cm^{-1}) 3271 (C-H), 3083 (C-H), 2150 (C≡C), 1461 (C-C).

*1-Ethynyl-6-methoxy-1H-benzo[d]imidazole (**2.56**)*

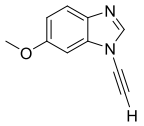

Prepared according to the general procedure B using 6-methoxy-1-((triisopropylsilyl)ethynyl)-1*H*-benzo[*d*]imidazole (1.00 g, 3.04 mmol) and TBAF (572 mg, 2.19 mmol) in THF (61 mL). The crude was purified by column chromatography (0 – 20% ethyl acetate in hexane) to give the desired product as an off-white solid (516 mg, 3.00 mmol, 99%).

^{1}H NMR (400 MHz, $CDCl_3$) δ 7.97 (s, 1H), 7.67 (dd, *J* = 8.8, 0.5 Hz, 1H), 7.03 (d, *J* = 2.4 Hz, 1H), 6.97 (dd, *J* = 8.8, 2.4 Hz, 1H), 3.89 (s, 3H), 3.29 (s, 1H).

^{13}C NMR (101 MHz, $CDCl_3$) δ 158.4 142.6, 136.2, 135.4, 121.5, 113.7, 94.4, 70.5, 62.3, 56.0.

HR-MS (ESI) $C_{10}H_8N_2O^+$ calc 173.0705 found 173.0705.

IR ν_{max} (cm^{-1}) 3118 (C-H), 2145 (C≡C), 1491 (C-H), 1219 (C-O), 811 (C-O).

*1-Ethynyl-5-methoxy-1H-benzo[d]imidazole (**2.57**)*

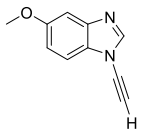

Prepared according to the general procedure B using 5-methoxy-1-((triisopropylsilyl)ethynyl)-1*H*-benzo[*d*]imidazole (713 mg, 2.17 mmol) and TBAF (400 µL, 1.46 mmol) in THF (43 mL). The crude was purified by column chromatography (0 – 20% ethyl acetate in hexane) to give the desired product as a white solid (374 mg, 2.0 mmol, 91%).

^{1}H NMR (400 MHz, $CDCl_3$) δ 8.04 (s, 1H), 7.44 (dd, *J* = 8.8, 0.5 Hz, 1H), 7.28 (d, *J* = 2.4 Hz, 1H), 7.03 (dd, *J* = 8.8, 2.4 Hz, 1H), 3.86 (s, 3H), 3.26 (s, 1H).

^{13}C NMR (101 MHz, $CDCl_3$) δ 157.6, 144.2, 142.8, 128.8, 114.9, 111.4, 103.3, 70.6, 61.9, 56.0.

HR-MS (ESI) $C_{10}H_8ON_2^+$ calculated 173.0709, found 173.0708.

IR ν_{max} (cm^{-1}) 3183 (C-H), 2150 (C≡C), 1487 (C-C), 1242 (C-C), 1145 (C-O).

*4-(4-Methoxyphenyl)-1H-imidazole (**2.60**)* [172]

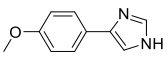

4-iodiimidazole (500 g, 2.58 mmol) was dissolved in toluene (10 mL) and water (3 mL). The mixture was placed under an argon atmosphere and 4-methoxyphenylboronic acid (784 mg, 516 µmol), tetrakis(triphenylphosphine)palladium(0) (300 mg, 28.0 µmol) and caesium fluoride (780 mg, 516 µmol) was added. The reaction was heated to 100 ˚C and stirred overnight. The aqueous layer was separated and extracted with ethyl acetate (3 × 20 mL). The organics were combined, washed with brine and dried over anhydrous sodium sulphate and solvent removed *in vacuo*. The crude product was purified by column chromatography (3% MeOH in DCM) to obtain the desired compound 4-(4-methoxyphenyl)-1*H*-imidazole (305 mg, 17 µmol, 69%) as an orange solid.

^{1}H NMR (400 MHz, DMSO) δ 7.76 – 7.65 (m, 3H), 7.45 (s, 1H), 6.93 (d, *J* = 8.8 Hz, 2H), 3.75 (s, 3H).

^{13}C NMR (101 MHz, DMSO) δ 157.9, 137.7, 135.9, 135.6, 126.6, 125.6, 114.2, 114.0, 113.0, 55.0.

NMR spectra in accordance with literature values[172]

*4-Phenyl-1-((triisopropylsilyl)ethynyl)-1H-imidazole (**2.63a**)*

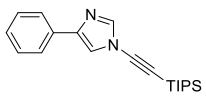

Prepared according to the General Procedure A using 5-phenyl-1*H*-imidazole (2.00 g, 13.8 mmol), caesium carbonate (5.39 g, 16.6 mmol), copper iodide (130 mg, 6.90 mmol), PEG 400 (640 mg, 1.60 mmol) and (bromoethynyl)triisopropylsilane (3.96 g, 15.2 mmol) in anhydrous 1,4-dioxane (85 mL). The crude residue was purified by flash column chromatography (0 – 10% ethyl acetate in hexane) to give the desired product as a dark orange/pink viscous oil (2.93 g, 9.03 mmol, 65%).

^{1}H NMR (500 MHz, $CDCl_3$) δ 7.78 (d, *J* = 8.1 Hz, 3H), 7.41 – 7.37 (m, 3H), 7.29 (t, *J* = 7.4 Hz, 1H), 1.16 – 1.12 (m, 21H).

^{13}C NMR (126 MHz, $CDCl_3$) δ 141.6, 140.3, 132.6, 128.6, 127.5, 125.2, 116.8, 91.6, 70.1, 18.5, 11.1.

HR-MS (ESI) $C_{20}H_{28}N_2Si^+$ calculated 325.2095, found 325.2092.

IR ν_{max} (cm^{-1}) 2945 (C-H), 2867 (C-H), 2197 (C≡C), 1495 (C=C).

5-Phenyl-1-((triisopropylsilyl)ethynyl)-1H-imidazole ***(2.63b***)

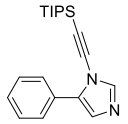

Prepared according to the General Procedure A using 5-phenyl-1*H*-imidazole (2.00 g, 13.8 mmol), caesium carbonate (5.39 g, 16.6 mmol), copper iodide (130 mg, 6.90 mmol), PEG 400 (640 mg, 1.60 mmol) and (bromoethynyl)triisopropylsilane (3.96 g, 15.2 mmol) in anhydrous 1,4-dioxane (85 mL). The crude residue was purified by flash column chromatography (0 – 10% ethyl acetate in hexane) to give the desired product as a dark orange/pink viscous oil (240 mg, 0.730 μmol, 5%).

^{1}H NMR (500 MHz, $CDCl_3$) δ 7.82 (s, 1H), 7.72 – 7.66 (m, 2H), 7.39 (m, 3H), 7.13 (s, 1H), 1.10 – 1.05 (m, 21H).

^{13}C NMR (126 MHz, $CDCl_3$) δ 141.7, 134.7, 128.7, 128.6, 128.1, 127.7, 126.3, 91.3, 73.2, 18.7, 17.9, 12.4, 11.4.

HR-MS (ESI) $C_{20}H_{28}N_2Si^+$ calculated 325.2094, actual 325.2096.

IR ν_{max} (cm^{-1}) 2943 (C-H), 2867 (C-H), 2199 (C≡C), 1472 (C=C).

*4-(P-tolyl)-1-((triisopropylsilyl)ethynyl)-1H-imidazole (**2.64a**)*

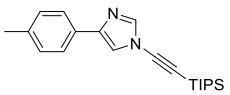

Prepared according to the General Procedure A using 4-(p-tolyl)-1*H*-imidazole (999 mg, 6.31 mmol), caesium carbonate (2.26 g, 6.95 mmol), copper iodide (60.1 mg, 316 μmol), PEG 400 (255 mg, 638 μmol) and (bromoethynyl)triisopropylsilane (1.81 g, 6.95 mmol) in anhydrous 1,4-dioxane (28 mL). The crude residue was purified by flash column chromatography (0 – 20% ethyl acetate in hexane) to give the desired product as a dark red viscous oil (1.22 g, 3.60 mmol, 57%)

^{1}H NMR (400 MHz, $CDCl_3$) δ 7.77 (d, J = 1.3 Hz, 1H), 7.69 – 7.65 (m, 2H), 7.34 (d, J = 1.3 Hz, 1H), 7.20 (d, J = 7.9 Hz, 2H), 2.37 (s, 3H), 1.15 – 1.12 (m, 21H).

^{13}C NMR (101 MHz, $CDCl_3$) δ 142.0, 140.5, 137.5, 130.1, 129.5, 125.3, 116.6, 92.0, 77.5, 21.4, 18.7, 11.4.

HR-MS (ESI) $C_{21}H_{30}N_2Si^+$ calculated 339.2251, found 339.2250.

IR ν_{max} (cm^{-1}) 3105 (C-H), 2945 (C-H), 2867 (C-H), 2197 (C≡C), 1465 (C=C), 1495 (C=C).

*5-(P-tolyl)-1-((triisopropylsilyl)ethynyl)-1H-imidazole (**2.64b**)*

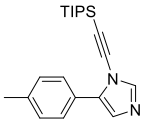

Prepared according to the General Procedure A using 4-(p-tolyl)-1*H*-imidazole (999 mg, 6.31 mmol), caesium carbonate (2.26 g, 6.95 mmol), copper iodide (60.1 mg, 316 µmol), PEG 400 (255 mg, 638 µmol) and (bromoethynyl)triisopropylsilane (1.81 g, 6.95 mmol) in anhydrous 1,4-dioxane (28 mL). The crude residue was purified by flash column chromatography (0 – 20% ethyl acetate in hexane) to give the desired product as a dark red viscous oil (120 mg, 354 µmol, 6%).

^{1}H NMR (400 MHz, $CDCl_3$) δ 7.78 (s, 1H), 7.62 – 7.55 (m, 2H), 7.20 (d, *J* = 7.9 Hz, 2H), 7.09 (s, 1H), 2.38 (s, 3H), 1.11 – 1.04 (m, 21H).

^{13}C NMR (101 MHz, $CDCl_3$) δ 141.5, 138.5, 134.6, 129.3, 127.5, 126.1, 125.4, 91.5, 73.0, 21.5, 18.7, 11.4.

HR-MS (ESI) $C_{21}H_{30}N_2Si^+$ calculated 339.2251, found 339.2251.

*4-(4-Methoxyphenyl)-1-((triisopropylsilyl)ethynyl)-1H-imidazole (**2.65**)*

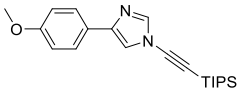

Prepared according to the General Procedure A using 4-(4-methoxyphenyl)-1*H*-imidazole (850 mg, 4.88 mmol), (bromoethynyl)triisopropylsilane (1.40 g, 5.37 mmol), caesium carbonate (1.75 g, 5.37 mmol), copper(I) iodide (46.5 mg, 244 µmol) and PEG 400 (195 mg, 488 µmol) in anhydrous 1,4-dioxane (18mL). The crude residue was purified by flash column chromatography (0 – 20% ethyl acetate in hexane) to give the desired product as a dark pink viscous oil (503 mg, 1.50 mmol, 31%).

^{1}H NMR (400 MHz, DMSO) δ 8.18 (d, *J* = 1.3 Hz, 1H), 7.97 (d, *J* = 1.3 Hz, 1H), 7.78 – 7.73 (m, 2H), 6.97 – 6.94 (m, 2H), 3.77 (s, 3H), 1.12 – 1.09 (m, 21H).

^{13}C NMR (101 MHz, DMSO) δ 158.7, 141.0, 140.7, 126. 2, 125.3, 116.5, 114.0, 92.4, 68.6, 55.1, 18.4, 17.8, 12.1, 10.7.

HR-MS (ESI) $C_{21}H_{30}N_2OSi^+$ calculated 355.2200, found 355.2200.

IR ν_{max} (cm^{-1}) 2945 (C-H), 2867 (C-H), 2197 (C≡C), 1508 (C=C), 1506 (C=C), 1251 (C-O).

*4-(4-Fluorophenyl)-1-((triisopropylsilyl)ethynyl)-1H-imidazole (**2.66**)*

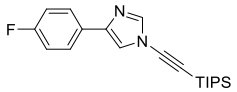

Prepared according to the General Procedure A using 4-(4-fluorophenyl)-1*H*-imidazole (110 mg, 678 µmol), (bromoethynyl)triisopropylsilane (211 mg, 814 µmol), caesium carbonate (267 mg, 814 µmol), copper(I) iodide (7.00 mg, 34.0 µmol) and PEG 400 (27.0 mg, 68.0 µmol) in anhydrous 1,4-dioxane (2 mL). The crude residue was purified by flash column chromatography (0 – 5% ethyl acetate in hexane) to give the desired as a red viscous oil (167 mg, 487 µmol, 71%).

^{1}H NMR (400 MHz, CD_3CN) δ 7.85 (d, *J* = 1.2 Hz, 1H), 7.83 – 7.78 (m, 2H), 7.59 (d, *J* = 1.2 Hz, 1H), 7.16 – 7.10 (m, 2H), 1.16 – 1.12 (m, 21H).

^{13}C NMR (101 MHz, CD_3CN) δ 163.2 (d, *J* = 244 Hz), 142.0, 141.4, 130.5, 128.0, 127.9, 118.3, 116.4 (d, *J* = 22 Hz), 92.9, 70.4, 18.9, 12.0.

^{19}F NMR (376 MHz, CD_3CN) δ -116.46 (s).

HR-MS (ESI) $C_{20}H_{27}FN_2Si^+$ calculated 343.2000, found 343.1996.

IR ν_{max} (cm^{-1}) 2945 (C-H), 2859 (C-H), 2197 (C≡C), 1504 (C=C), 1236 (C-F).

*5-(4-Fluorophenyl)-1-((triisopropylsilyl)ethynyl)-1H-imidazole (**2.66b**)*

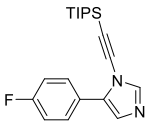

Prepared according to the General Procedure A using 4-(4-fluorophenyl)-1*H*-imidazole (110 mg, 678 µmol), (bromoethynyl)triisopropylsilane (211 mg, 814 µmol), caesium carbonate (267 mg, 814 µmol), copper(I) iodide (7.00 mg, 34.0 µmol) and PEG 400 (27.0 mg, 68.0 µmol) in anhydrous 1,4-dioxane (2 mL). The crude residue was purified by flash column chromatography (0 – 5% ethyl acetate in hexane) to give the desired product as a red viscous oil (14.4 mg, 42.0 µmol, 6%).

^{1}H NMR (500 MHz, DMSO) δ 8.25 (s, 1H), 7.72 (dd, *J* = 8.6, 5.5 Hz, 2H), 7.30 (t, *J* = 8.8 Hz, 2H), 7.25 (s, 1H), 1.06 – 0.98 (m, 21H).

^{19}F NMR (471 MHz, DMSO) δ -112.76 (s).

HR-MS (ESI) $C_{20}H_{27}FN_2Si^+$ calculated 343.20006, found 343.2000.

IR ν_{max} (cm^{-1}) 2945 (C-H), 2867 (C-H), 2195 (C≡C), 1696 (C=C), 1508 (C=C), 1238 (C-F).

*4-(4-Bromophenyl)-1-((triisopropylsilyl)ethynyl)-1H-imidazole (**2.67**)*

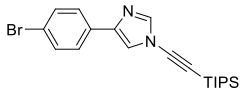

Prepared according to the General Procedure A using 4-(4-bromophenyl)-1*H*-imidazole (2.50 g, 11.2 mmol), (bromoethynyl)triisopropylsilane (3.51 g, 13.4 mmol), caesium carbonate (4.02 g, 12.3 mmol), copper(I) iodide (107 mg, 0.560 mmol) and PEG 400 (448 mg, 1.12 mmol) in 1,4-dioxane (70 mL). The crude residue was purified using flash column chromatography to give the desired product as a red oil (2.73 g, 6.78 mmol, 60%).

^{1}H NMR (500 MHz, DMSO) δ 8.23 (s, 1H), 8.16 (s, 1H), 7.79 (d, J = 8.5 Hz, 2H), 7.56 (d, J = 8.3 Hz, 2H), 1.10 – 1.05 (m, 21H).

^{13}C NMR (101 MHz, DMSO) δ 141.3, 139.6, 131.9, 131.5, 126.8, 120.2, 118.4, 92.0, 68.91, 18.3, 10.6.

HRMS (ESI) $C_{20}H_{27}BrN_2Si^+$ calculated 403.1120, found 403.1195.

4-(4-Nitrophenyl)-1-((triisopropylsilyl)ethynyl)-1H-imidazole (**2.68**)

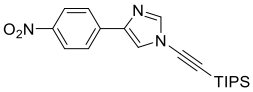

Prepared according to the General Procedure A using 4-(4-nitrophenyl)-1H-imidazole (2.41 g, 12.7 mmol), (bromoethynyl)triisopropylsilane (3.66 g, 14.0 mmol), caesium carbonate (4.57 g, 14.0 mmol), copper iodide (121 mg, 637 μmol) and PEG 400 (31.4 mg, 1.27 mmol) in 1,4-dioxane (47 mL). The crude residue was purified by column chromatography (0 – 20% ethyl acetate in hexane) to give the desired product as an orange solid (1.98 g, 5.38 mmol, 42%).

^{1}H NMR (400 MHz, $CDCl_3$) δ 8.27 – 8.22 (m, 2H), 7.95 – 7.90 (m, 2H), 7.82 (d, *J* = 1.1 Hz, 1H), 7.56 (d, *J* = 1.3 Hz, 1H), 1.16 – 1.10 (m, 21H).

^{13}C NMR (101 MHz, $CDCl_3$) δ 147.0, 141.2, 139.7, 139.2, 125.7, 124.4, 119.5, 91.1, 71.5, 18.7, 11.3.

HR-MS (ESI) $C_{20}H_{27}N_3O_2Si^+$ calculated 370.1945, found 370.1940.

IR ν_{max} (cm^{-1}) 2945 (C-H), 2867 (C-H), 2200 (C≡C), 1606 (C=C), 1521 (N-O), 1336 (N-O).

*4-(4-(Trifluoromethyl)phenyl)-1-((triisopropylsilyl)ethynyl)-1H-imidazole (**2.69**)*

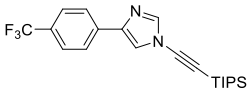

Prepared according to the General Procedure A using 4-(4-(trifluoromethyl)phenyl)-1*H*-imidazole (980 mg, 4.62 mmol), bromoethynyl)triisopropylsilane (1.33 g, 5.08 mmol,) caesium carbonate (1.66 g, 5.08 mmol), copper iodide (44.0 mg, 231 µmol) and PEG 400 (185 mg, 462 µmol) in 1,4-dioxane (20 mL). The crude residue was purified by column chromatography (0 - 100% ethyl acetate in hexane) to give the desired product as a light pink solid (1.05 g, 2.68 mmol, 58%).

^{1}H NMR (400 MHz, $CDCl_3$) δ 7.88 (d, *J* = 8.1 Hz, 2H), 7.80 (d, *J* = 1.2 Hz, 1H), 7.64 (d, *J* = 8.2 Hz, 2H), 7.50 – 7.45 (m, 1H), 1.14 (m, 21H).

^{19}F NMR (376 MHz, $CDCl_3$) δ -62.50 (s).

^{13}C NMR (101 MHz, $CDCl_3$) δ 140.6, 140.2, 136.0, 129.2 (q, *J* = 32.4 Hz), 125.5, 125.12, 124.0 (q, *J* = 274.7 Hz), 118.0, 91.1, 70.7, 18.4, 11.0.

HR-MS (ESI): $C_{21}H_{27}N_2F_3Si^+$ calculated 393.1968, found 393.1962.

IR ν_{max} (cm^{-1}) 3105 (C-H), 2947 (C-H), 2869 (C-H), 2202 (C≡C), 1498 (C-H), 1300 (C-CF_3), 1121 (C-F).

*5-(4-(Trifluoromethyl)phenyl)-1-((triisopropylsilyl)ethynyl)-1H-imidazole (**2.69b**)*

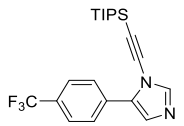

Prepared according to the General Procedure A using 4-(4-(trifluoromethyl)phenyl)-1*H*-imidazole (980 mg, 4.62 mmol), bromoethynyl)triisopropylsilane (1.33 g, 5.08 mmol,) caesium carbonate (1.66 g, 5.08 mmol), copper iodide (44.0 mg, 231 µmol) and PEG 400 (185 mg, 462 µmol) in 1,4-dioxane (20 mL). The crude residue was purified by column chromatography (0 - 100% ethyl acetate in hexane) to give the desired product as a light pink solid (9.00 mg, 22.9 µmol, 4%).

^{1}H NMR (400 MHz, DMSO) δ 8.35 (d, *J* = 0.9 Hz, 1H), 7.93 (d, *J* = 7.8 Hz, 2H), 7.80 (d, *J* = 8.1 Hz, 2H), 7.44 (d, *J* = 0.9 Hz, 1H), 1.08 – 0.99 (m, 21H).

^{19}F NMR (376 MHz, DMSO) δ -61.24 (s).

^{13}C NMR (101 MHz, DMSO) δ 143.0, 141.6, 132.2, 131.6, 128.6 (q, *J* = 32.3 Hz), 128.0, 127.8, 125.5 (q, *J* = 4.0 Hz), 125.3, 123.1 (q, *J* = 313.1 Hz), 91.1, 72.4, 18.3, 10.6.

LC-MS (ESI) $C_{21}H_{27}N_2F_3Si^+$ calculated 393.2, found 393.3, RT = 11.702 min.

*4-(1-((Triisopropylsilyl)ethynyl)-1H-imidazol-4-yl)aniline (**2.70**)*

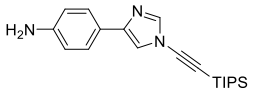

Prepared according to the General Procedure A using 4-(1*H*-imidazol-4-yl)aniline (100 mg, 628 μmol), (bromoethynyl)triisopropylsilane (0.181 mg, 691 μmol), caesium carbonate (225 mg, 391 μmol), copper iodide (5.98 mg, 31.4 μmol) and PEG 400 (25.1 mg, 62.8 μmol) in 1,4-dioxane (3 mL). The crude residue was purified using flash column chromatography (20 – 50% ethyl acetate in hexane) to give the desired product as a red oil (26.0 mg, 0.0763 mmol, 12%).

^{1}H NMR (500 MHz, $CDCl_3$) δ 7.73 (s, 1H), 7.57 (d, *J* = 8.5 Hz, 2H), 7.22 (s, 1H), 6.71 (d, *J* = 8.6 Hz, 2H), 3.72 (s, 2H), 1.16 – 1.10 (m, 21H).

^{13}C NMR (126 MHz, $CDCl_3$) δ 146.4, 142.4, 140.5, 129.2, 126.9, 123.9, 115.6, 115.5, 115.2, 92.4, 70.2, 19.0, 11.6.

HR-MS (ESI) $C_{20}H_{29}N_3Si^+$ calculated 340.2196, found 340.2196.

*4,5-Diphenyl-1-((triisopropylsilyl)ethynyl)-1H-imidazole (**2.72**)*

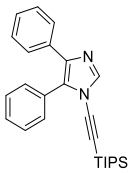

Prepared according to the General Procedure A using 4,5-diphenyl-1*H*-imidazole (2.00 g, 9.08 mmol), (bromoethynyl)triisopropylsilane (2.85 g, 10.1 mmol), caesium carbonate (3.25 g, 9.99 mmol), copper iodide (86.5 mg, 454 μmol) and PEG 400 (363 mg, 908 μmol) in 1,4-dioxane (57 mL). The crude residue was purified by column chromatography (0 – 5% ethyl acetate in hexane) to give the desired product as a yellow solid (0.88 g, 2.20 mmol, 24%).

^{1}H NMR (400 MHz, $CDCl_3$) δ 7.93 (s, 1H), 7.66 – 7.56 (m, 2H), 7.55 – 7.49 (m, 2H), 7.48 – 7.41 (m, 3H), 7.35 – 7.26 (m, 3H), 1.07 – 1.02 (m, 21H).

^{13}C NMR (126 MHz, DMSO) δ 140.5, 136.3, 133.3, 130.4, 129.7, 129.4, 128.9, 128.5, 128.5, 127.3, 126.6, 91.1, 72.0, 18.4, 10.7.

HR-MS (ESI) $C_{26}H_{32}N_2Si^+$ calculated 401.2408, found 401.2402.

IR ν_{max} (cm^{-1}) 2947 (C-H), 2855 (C-H), 2182 (C≡C), 1471 (C=C).

*1-Ethynyl-4-phenyl-1H-imidazole (**2.74**)*

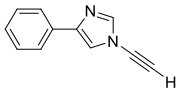

Prepared according to the General Procedure B using 4-phenyl-1-((triisopropylsilyl)ethynyl)-1*H*-imidazole (790 mg, 2.43 mmol) and TBAF (636 mg, 2.34 mmol) in THF (24 mL). The crude obtained was purified by flash column chromatography (0 – 20% ethyl acetate in hexane) to give the desired product as a light brown solid (323 mg, 2.43 mmol, 79%).

^{1}H NMR (400 MHz, $CDCl_3$) δ 7.83 – 7.74 (m, 3H), 7.43 – 7.35 (m, 3H), 7.32 – 7.27 (m, 1H), 3.06 (s, 1H).

^{13}C NMR (101 MHz, $CDCl_3$) δ 142.1, 140.5, 132.6, 128.8, 127.8, 125.4, 116.7, 71.7, 59.6.

HR-MS (ESI) $C_{11}H_8N_2^+$ calculated 169.0760, found 169.0753.

IR ν_{max} (cm^{-1}) 3148 (C-H), 2154 (C≡C), 1491 (C=C), 1195 (C=C).

*1-Ethynyl-4-(p-tolyl)-1H-imidazole (**2.75**)*

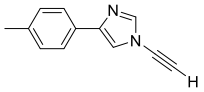

Prepared according to the General Procedure B using 4-(*p*-tolyl)-1-((triisopropylsilyl)ethynyl)-1*H*-imidazole (770 mg, 2.27 mmol) and TBAF (400 μL, 1.46 mmol) in THF (46 mL). The crude obtained was purified by flash column chromatography 0 – 10% ethyl acetate in hexane) to give the desired product as a light brown solid (376 mg, 2.07 mmol, 91%).

^{1}H NMR (400 MHz, $CDCl_3$) δ 7.79 (d, *J* = 1.3 Hz, 1H), 7.69 – 7.62 (m, 2H), 7.33 (d, *J* = 1.3 Hz, 1H), 7.20 (d, *J* = 7.9 Hz, 2H), 3.05 (s, 1H), 2.37 (s, 3H).

^{13}C NMR (101 MHz, $CDCl_3$) δ 142.1, 140.4, 137.6, 129.8, 129.5, 125.3, 116.2, 71.8, 59.5, 21.3.

HR-MS (ESI) $C_{12}H_{10}N_2^+$ calculated 183.0917, found 183.0920.

IR ν_{max} (cm^{-1}) 3206 (C-H), 2156 (C≡C), 1493 (C=C), 1221 (C=C), 1185 (C=C).

*1-Ethynyl-4-(4-methoxyphenyl)-1H-imidazole (**2.76**)*

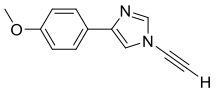

Prepared according to the General Procedure B using 4-(4-methoxyphenyl)-1-((triisopropylsilyl)ethynyl)-1*H*-imidazole (560 mg, 1.58 mmol), TBAF (334 mg, 1.28 mmol) in THF (32 mL). The crude was purified by flash column chromatography (0 – 20% ethyl acetate in hexane) to give the desired product (260 mg, 1.31 mmol, 83%).

^{1}H NMR (400 MHz, $CDCl_3$) δ 7.78 (s, 1H), 7.71 – 7.67 (m, 2H), 7.28 (s, 1H), 6.95 – 6.90 (m, 2H), 3.83 (s, 3H), 3.05 (s, 1H).

^{13}C NMR (101 MHz, $CDCl_3$) δ 158.8, 141.4, 139.8, 126.1, 124.9, 115.0, 113.7, 71.2, 58.8, 54.8.

HR-MS (ESI) $C_{12}H_{10}N_2O^+$ calculated 199.0866, found 199.0862.

IR ν_{max} (cm^{-1}) 3258 (C-H), 2158 (C≡C), 1504 (C=C).

*1-Ethynyl-4-(4-fluorophenyl)-1H-imidazole (**2.77**)*

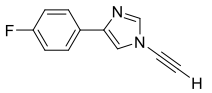

Prepared according to the General Procedure B using 4-(4-fluorophenyl)-1-((triisopropylsilyl)ethynyl)-1*H*-imidazole (525 mg, 1.55 mmol) and TBAF (525 mg, 2.01 mmol) in THF (31 mL). The crude was purified by flash column chromatography (0 – 10% ethyl acetate in hexane) to give the desired product as an off white solid (220 mg, 1.18 mmol, 77%).

^{1}H NMR (400 MHz, $CDCl_3$) δ 7.80 (d, J = 1.3 Hz, 1H), 7.76 – 7.70 (m, 2H), 7.33 (d, J = 1.2 Hz, 1H), 7.12 – 7.05 (m, 2H), 3.06 (s, 1H).

^{13}C NMR (101 MHz, $CDCl_3$) δ 162.3 (d, J = 247 Hz), 141.0, 140.3, 128.6 (d, J = 3 Hz), 126.8 (d, J = 8 Hz), 116.1, 115.5 (d, J = 21 Hz), 71.3, 59.4.

^{19}F NMR (471 MHz, $CDCl_3$) δ -114.26.

HR-MS (ESI) $C_{11}H_7FN_2^+$ calculated 187.0666, found 209.0480.

*4-(4-Bromophenyl)-1-ethynyl-1H-imidazole (**2.78**)*

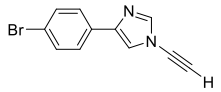

Prepared according to the General Procedure B using 4-(4-bromophenyl)-1-((triisopropylsilyl)ethynyl)-1*H*-imidazole (1.00 g, 2.48 mmol) and TBAF (200 µL, 729 µmol) in THF (50 mL). The crude residue was purified by column chromatography (2 – 10% ethyl acetate in hexane) to give the desired product as a light pink solid (0.268 g, 1.09 mmol, 44%).

^{1}H NMR (400 MHz, $CDCl_3$) δ 7.82 (d, *J* = 1.3 Hz, 1H), 7.69 – 7.62 (m, 2H), 7.57 – 7.50 (m, 2H), 7.40 (d, *J* = 1.3 Hz, 1H), 3.09 (s, 1H).

^{13}C NMR (101 MHz, $CDCl_3$) δ 140.5, 140.0, 131.3, 131.0, 126.3, 121.1, 116.4, 70.9, 59.2.

HR-MS (ESI) $C_{11}H_7N_2Br^+$ calculated 246.9865, found 246.9864.

IR ν_{max} (cm^{-1}) 3295 (C-H), 2161 (C≡C), 1465 (C=C), 1387 (C-H), 1197 (C=C).

*1-Ethynyl-4-(4-nitrophenyl)-1H-imidazole (**2.79**)*

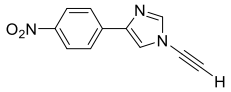

Prepared according to the General Procedure B using 4-(4-nitrophenyl)-1-((triisopropylsilyl)ethynyl)-1*H*-imidazole (260 mg, 704 µmol) and TBAF (150 µl, 547 µmol) in THF (14 mL). The crude residue was purified by column chromatography (0 – 20% ethyl acetate in hexane) to give the product as a dark yellow solid (74.1 mg, 347 µmol, 49%).

^{1}H NMR (400 MHz, DMSO) δ 8.39 (s, 1H), 8.33 (s, 1H), 8.26 (d, *J* = 8.9 Hz, 2H), 8.05 (d, *J* = 9.0 Hz, 2H), 4.58 (s, 1H).

^{13}C NMR (101 MHz, DMSO) δ 146.2, 142.0, 138.6, 125.5, 124.1, 120.8, 71.4, 62.6.

HR-MS (ESI) $C_{11}H_7N_3O_2^+$ calculated 214.0611, found 214.0609.

IR ν_{max} (cm^{-1}) 3262 (C-H), 2161 (C≡C), 1605 (N-O), 1508 (C=C), 1329 (C=C).

*1-Ethynyl-4-(4-(trifluoromethyl)phenyl)-1H-imidazole (**2.80**)*

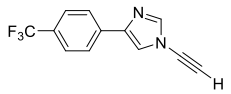

Prepared according to the General Procedure B using 4-(4-(trifluoromethyl)phenyl)-1-((triisopropylsilyl)ethynyl)-1*H*-imidazole (460 mg, 1.17 mmol) and TBAF (250 µl. 912 µmol) in THF (23 mL). The crude material was purified by column chromatography (0 – 20% ethyl acetate in hexane) to give the product as a pink solid (220 mg, 931 µmol, 79%).

^{1}H NMR (400 MHz, $CDCl_3$) δ 7.86 (d, *J* = 8.2 Hz, 2H), 7.82 (s, 1H), 7.64 (d, *J* = 8.4 Hz, 2H), 7.46 (d, *J* = 3.9 Hz, 1H), 3.08 (s, 1H).

^{19}F NMR (376 MHz, $CDCl_3$) δ -62.52 (s).

^{13}C NMR (101 MHz, $CDCl_3$) δ 140.9, 140.8, 136.1, 129.6 (q, *J* = 32.3 Hz), 127.1 (q, *J* = 3.0 Hz), 124.3 (q, *J* = 270.0 Hz) 125.5, 118.0, 71.3, 60.0.

HR-MS (ESI) $C_{12}H_7F_3N_2^+$, calculated 237.0644, found 237.0635.

IR ν_{max} (cm^{-1}) 3317 (C-H), 2169 (C≡C), 1623 (C-H), 1327 (C=C), 1106 (C-F).

*1-Ethynyl-4,5-diphenyl-1H-imidazole (**2.81**)*

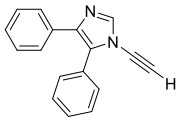

Prepared according to the General Procedure B using 4,5-diphenyl-1-((triisopropylsilyl)ethynyl)-1*H*-imidazole (250 mg, 624 μmol), TBAF (163 mg, 624 μmol) in THF (13 mL). The crude material was purified by flash column chromatography (0 – 20% in ethyl acetate) to give the desired product 1-ethynyl-4,5-diphenyl-1*H*-imidazole as a white solid (102 mg, 417 μmol, 67%).

^{1}H NMR (400 MHz, DMSO) δ 8.36 (s, 1H), 7.52 – 7.42 (m, 7H), 7.26 (m, 3H), 4.38 (s, 1H).

^{13}C NMR (101 MHz, DMSO) δ 140.7, 136.3, 133.1, 130.2, 129.3, 129.2, 128.9, 128.3, 128.2, 127.2, 126.5, 70.8, 64.6.

HR-MS (ESI) $C_{17}H_{12}N_2^+$ calculated 245.1073, found 245.1070.

IR ν_{max} (cm^{-1}) 3275 (C-H), 2150 (C≡C), 1495 (C=C), 1229 (C=C).

*1H-Benzo[d]imidazole-5,6-dicarboxylic acid (**2.88**)* [184]

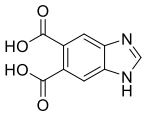

To a solution of benzimidazole (1.08 g, 9.00 mmol) in tert-butanol (35 mL) was added a solution of potassium permanganate (10.9 g, 69 mmol) in water (35 mL). The solution was heated to reflux for 1 h. Anhydrous sodium sulphite (3.00 g, 24.0 mmol) was added and the resulting cake filtered and washed with water. The filtrate was concentrated in vacuo until a small amount of solution remained. The remaining solution was acidified with aqueous acetic acid (2:1) and the resulting precipitate filtered and dried to give a white solid (330 mg, 1.60 mmol, 18%).

^{1}H NMR (500 MHz, DMSO) δ 12.86 (s, 2H), 8.45 (s, 1H), 7.88 (s, 2H).

^{13}C NMR (126 MHz, DMSO) δ 172.1, 169.2, 145.5, 138.8, 127.5, 116.2.

*6-(3-Hydroxypropyl)imidazo[4,5-f]isoindole-5,7(1H,6H)-dione (**2.91**)*

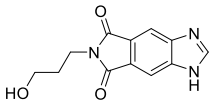

1*H*-benzo[*d*]imidazole-5,6-dicarboxylic acid (100 mg, 485 μmol), EDC.HCl (186 mg, 974 μmol) and DMAP (23.0 mg, 188 μmol) were dissolved in DCM (5 mL) and stirred for 15 mins. The 3-amino-1-propanol was then added (55.0 mg, 733 μmol) and the reaction left to stir for 18 h. The reaction mixture was washed with ethyl acetate and the aqueous layer concentrated *in vacuo*. The crude residue was purified by column chromatography (10% MeOH in DCM) to give a colourless solid (31.0 mg, 123 μmol, 25%).

^{1}H NMR (500 MHz, DMSO-d_6) δ 9.20 (s, 1H), 8.16 (s, 2H), 3.69 (t, 2H, *J* = 6.7 Hz), 3.46 (t, 2H, *J* = 6.2 Hz), 1.75 (quint, 2H, *J* = 6.7 Hz).

^{13}C NMR (126 MHz, DMSO) δ 168.1, 146.1, 125.7, 111.1, 58.6, 35.1, 31.4 (5 carbons not observed/coincident).

*1-(1-Benzyl-1H-1,2,3-triazol-4-yl)-5,6-dimethyl-1H-benzo[d]imidazole (**2.98**)*

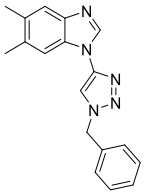

Prepared according to the General Procedure D using 1-ethynyl-5-6-dimethyl-1*H*-benzo[*d*]imidazole (200 mg, 1.75 mmol), benzyl azide (150 mg, 1.52 mmol) and copper(II) acetate monohydrate (42.0 mg, 210 μmol) in MeOH (40 mL). The crude product was purified by column chromatography (80% ethyl acetate in petroleum ether) to give the desired product as a white solid (220 mg, 724 μmol, 41%).

^{1}H NMR (500 MHz, $CDCl_3$) δ 8.83 (s, 1H), 7.99 (s, 1H), 7.65 (d, *J* = 6.9 Hz, 2H), 7.48 – 7.32 (m, 5H), 5.65 (s, 2H), 2.40 (d, *J* = 6.5 Hz, 6H).

^{13}C NMR (126 MHz, $CDCl_3$) δ 142.44, 135.40, 134.46, 133.80, 129.57, 129.46, 128.46, 118.80, 114.87, 112.59, 55.44, 20.76, 20.44.

IR ν_{max} (cm^{-1}) 3109 (C-H), 2993 (C-H), 1593 (C=C), 1504 (C=C), 1464 (C=C).

Values correspond to literature values.[183]

*1-(1-Benzyl-1H-1,2,3-triazol-4-yl)-1H-benzo[d]imidazol-6-amine (**2.99**)*

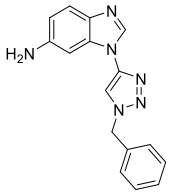

Prepared according to General Procedure C using 1-ethynyl-1*H*-benzo[*d*]imidazol-6-amine (50.0 mg, 318 µmol), benzyl azide (42.4 µL, 318 µmol) and copper(II) acetate monohydrate (3.18 mg, 15.9 µmol) in MeCN (6 mL). The crude product was purified by column chromatography (50 – 100% ethyl acetate in hexane) to give the desired product as a dark brown solid (50.0 mg, 172 µmol, 50%).

^{1}H NMR (400 MHz, $CDCl_3$) δ 8.22 (s, 1H), 7.68 (s, 1H), 7.58 (dd, *J* = 10.0, 7.1 Hz, 2H), 7.48 – 7.32 (m, 5H), 5.63 (s, 2H) (Exchangeable NH_2 protons not observed due to exchange in deuterated solvent).

*1-(1-Benzyl-1H-1,2,3-triazol-4-yl)-5,6-dimethoxy-1H-benzo[d]imidazole (**2.101**)*

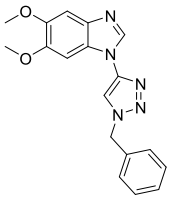

Prepared according to General Procedure C using 1-ethynyl-5,6-dimethoxy-1*H*-benzo[*d*]imidazole (80.0 mg, 396 µmol), benzyl azide (49.4 µL, 396 µmol) and copper(II) acetate monohydrate (3.59 mg, 19.8 µmol) in MeOH (6.4 mL). The crude product was purified by column chromatography (50 – 100% ethyl acetate in hexane) to give the desired product as a white solid (90.0 mg, 268 µmol, 68%).

^{1}H NMR (400 MHz, $CDCl_3$) δ 8.10 (s, 1H), 7.68 (s, 1H), 7.49 – 7.35 (m, 6H), 7.32 (s, 1H), 5.64 (s, 2H), 3.96 (d, *J* = 2.1 Hz, 6H).

^{13}C NMR (101 MHz, $CDCl_3$) δ 148.7, 147.8, 134.2, 129.8, 129.7, 128.7, 114.0, 102.5, 95.1, 56.9, 56.7, 55.6.

HRMS (ESI) $C_{18}H_{17}N_5O_2^+$ calculated 336.1455, found 336.1451.

IR ν_{max} (cm^{-1}) 3103 (C-H), 1692 (C=C), 1590 (C=C), 1482 (C=C), 1223 (C-O).

*1-(1-Benzyl-1H-1,2,3-triazol-4-yl)-5,6-difluoro-1H-benzo[d]imidazole) (**2.102**)*

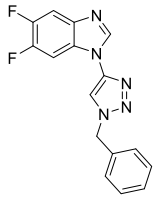

Prepared according to the General Procedure C using 1-ethynyl-5,6-difluoro-1*H*-benzo[*d*]imidazole (50.1 mg, 281 µmol), benzyl azide (35.1 µL, 281 µmol) and copper(II) acetate monohydrate (2.55 mg, 14.1 µmol) in HFIP/water (2 mL/3 mL). The crude was purified by column chromatography (80 – 20% ethyl acetate in hexane) to give the desired product as a white solid (84.0 mg, 269 µmol, 96%).

^{1}H NMR (400 MHz, $CDCl_3$) δ 8.23 (s, 1H), 7.66 (s, 1H), 7.60 (m, 2H), 7.47 – 7.35 (m, 5H), 5.64 (s, 2H).

^{13}C NMR (101 MHz, $CDCl_3$) δ 149.4 (dd, *J* = 66, 16 Hz), 147.0 (d, *J* = 147.0, 6, 16 Hz), 141.9, 141.8, 138.5, 138.4, 133.0, 128.9, 127.4 (d, *J* = 119.8 Hz), 113.1, 107.5 (d, *J* = 20.2 Hz), 99.4 (d, *J* = 24.2 Hz), 54.8.

^{19}F NMR (471 MHz, $CDCl_3$) δ -139.15, -139.18 (d, *J* = 7.7 Hz), -139.20 – -139.24 (m), -141.78 (ddd, *J* = 20.1, 10.0, 6.9 Hz).

HR-MS (ESI) $C_{16}H_{11}F_2N_5^+$ calc 312.10553, found 312.1052.

IR ν_{max} (cm^{-1}) 3124 (C-H), 3064 (C-H), 1588 (C=C), 1461 (C=C), 1134 (C-F).

*1-(1-Benzyl-1H-1,2,3-triazol-4-yl)-1H-naphtho[2,3-d]imidazole (**2.103**)*

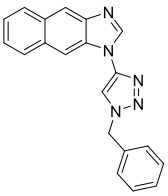

Prepared according to the General Procedure D using 1-ethynyl-1*H*-naphtho[2,3-*d*]imidazole (110 mg, 0.572 mmol), benzyl azide (76.1 mg, 0.572 mmol), copper(II) acetate monohydrate (5.30 mg, 28.6 µmol) in HFIP/water (4 mL /5 mL). The crude was purified using column chromatography (20% ethyl acetate in hexane) to give the desired product as a white solid (111 mg, 341 µmol, 60%).

^{1}H NMR (500 MHz, $CDCl_3$) δ 8.54 (s, 1H), 8.34 (s, 1H), 8.09 (s, 1H), 8.05 – 8.01 (m, 1H), 7.95 (d, *J* = 7.0 Hz, 1H), 7.79 (s, 1H), 7.50 – 7.38 (m, 6H), 5.69 (s, 2H).

^{13}C NMR (126 MHz, $CDCl_3$) δ 144.6, 143.5, 133.8, 131.2, 129.5, 129.3, 128.7, 128.3, 127.7, 125.2, 124.2, 118.1, 113.2, 107.3, 55.3.

HR-MS (ESI) $C_{20}H_{15}N_5^+$ calc 326.1400, found 326.1395.

IR ν_{max} (cm^{-1}) 3115 (C-H), 1597 (C=C), 1510 (C=C), 1210 (C-N).

*1-(1-Benzyl-1H-1,2,3-triazol-4-yl)-6,7-dihydro-1H-[1,4]dioxino[2',3':4,5]benzo[1,2-d]imidazole (**2.104**)*

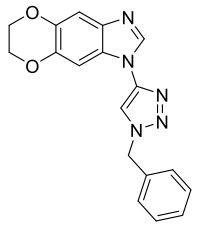

Prepared according to the General Procedure D using 1-ethynyl-6,7-dihydro-1*H*-[1,4]dioxino[2',3':4,5]benzo[1,2-*d*]imidazole (81.0 mg, 405 µmol), benzyl azide (53.9 mg, 405 µmol) and copper(II) acetate monohydrate (3.67 mg, 20.2 µmol) in HFIP/water (3 mL/4 mL). The reaction as purified using column chromatography (50 – 100% ethyl acetate in hexane) to give the desired product as an off-white solid (117 mg, 351 µmol, 87%).

^{1}H NMR (400 MHz, $CDCl_3$) δ 8.15 (s, 1H), 7.68 (s, 1H), 7.38 – 7.26 (m, 5H), 7.23 (s, 1H), 7.08 (s, 1H), 5.55 (s, 2H), 4.20 (s, 4H).

^{13}C NMR (101 MHz, $CDCl_3$) δ 143.1, 142.5, 141.5, 141.0, 138.4, 134.2, 129.6, 129.4, 128.5, 113.5, 113.5, 107.7, 98.9, 64.7, 64.4, 55.4.

HR-MS (ESI) Calc $C_{18}H_{15}N_5O_2^+$ calc 334.1298, found 334.1294.

IR ν_{max} (cm^{-1}) 3109 (C-H), 3124 (C-H), 1588 (C=C), 1202 (C-O).

*1-(1-Benzyl-1H-1,2,3-triazol-4-yl)-6-methoxy-1H-benzo[d]imidazole (**2.105**)*

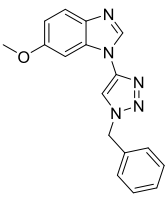

Prepared according to the General Procedure D using 1-ethynyl-6-methoxy-1*H*-benzo[*d*]imidazole (150 mg, 871 µmol), benzyl azide (116 mg, 0.871 mmol) and copper(II) acetate monohydrate (8.70 mg, 43.6 µmol) in HFIP/water (6 mL/ mL). The crude was purified using flash column chromatography (50 – 100% ethyl acetate/hexane to give the desired product as a pale yellow solid (170 mg, 556 µmol, 64%).

^{1}H NMR (400 MHz, $CDCl_3$) δ 8.18 (s, 1H), 7.76 – 7.59 (m, 2H), 7.47 – 7.30 (m, 5H), 7.23 (s, 1H), 6.95 (d, J = 5.9 Hz, 1H), 5.61 (s, 2H), 3.84 (s, 3H).

^{13}C NMR (101 MHz, $CDCl_3$) δ 157.8, 143.1, 133.9, 129.5, 129.4, 128.3, 121.1, 113.8, 112.5, 95.3, 56.1, 55.3.

HR-MS (ESI) $C_{17}H_{15}N_5O^+$ calc 306.1349 found 306.1345.

IR ν_{max} (cm^{-1}) 3126 (C-H), 1592 (C=C), 1500 (C=C), 1223 (C-O).

*1-(1-Benzyl-1H-1,2,3-triazol-4-yl)-5-methoxy-1H-benzo[d]imidazole (**2.106**)*

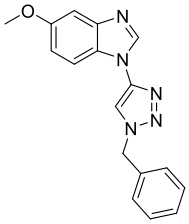

Prepared according to the General Procedure D using 1-ethynyl-5-methoxy-1*H*-benzo[*d*]imidazole (63.8 mg, 371 μmol), benzyl azide (49.3 mg, 371 μmol) and copper(II) acetate monohydrate (3.70 mg, 185 μmol) in HFIP/water (2 mL/3 mL). The crude was purified by flash column chromatography to give the desired product as a pale-yellow solid (100 mg, 371 μmol, 88%).

^{1}H NMR (400 MHz, DMSO) δ 8.80 (s, 1H), 8.63 (s, 1H), 7.79 (d, *J* = 8.9 Hz, 1H), 7.47 – 7.35 (m, 5H), 7.32 (d, *J* = 2.4 Hz, 1H), 7.02 (dd, *J* = 8.9, 2.3 Hz, 1H), 5.73 (s, 2H), 3.83 (s, 3H).

^{13}C NMR (101 MHz, DMSO) δ 156.1, 142.1, 135.5, 128.9, 128.4, 128.1, 115.7, 113.4, 112.2, 102.4, 55.5, 53.8.

HR-MS (ESI) $C_{17}H_{15}ON_5^+$ calculated 306.1349, found 306.1346.

IR ν_{max} (cm^{-1}) 3118 (C-H), 2940 (C-H), 2837 (C-H), 1584 (C=C), 1487 (C=C, 1448 (C=C), 1147 (C-O).

*1-Benzyl-4-(4-phenyl-1H-imidazol-1-yl)-1H-1,2,3-triazole (**2.108**)*

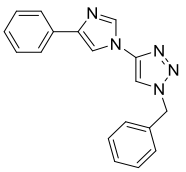

Prepared according to the General Procedure C using 1-ethynyl-4-phenyl-1*H*-imidazole (100 mg, 0.594 mmol), benzyl azide (79.1 mg, 594 μmol) and copper(II) acetate monohydrate (5.93 mg, 29.7 μmol) in MeOH (9.7 mL). The crude material was purified by flash column chromatography (20 – 50% ethyl acetate in hexane) to give the desired product as an off white solid (132 mg, 438 μmol, 74%).

^{1}H NMR (500 MHz, $CDCl_3$) δ 7.99 (d, *J* = 1.3 Hz, 1H), 7.83 – 7.78 (m, 2H), 7.64 (d, *J* = 1.3 Hz, 1H), 7.52 (s, 1H), 7.47 – 7.33 (m, 7H), 7.28 (d, *J* = 7.4 Hz, 1H), 5.58 (s, 2H).
^{13}C NMR (126 MHz, $CDCl_3$) δ 144.8, 143.6, 134.0, 131.4, 129.6, 129.5, 128.8, 128.4, 127.9, 125.3, 124.4, 118.3, 113.3, 107.5, 55.4.
HR-MS (ESI) $C_{18}H_{15}N_5^+$ calculated 302.1400, found 302.1398.
IR ν_{max} (cm^{-1}) 3103 (C-H), 3122 (C-H), 1597 (C=C).

*1-Benzyl-4-(4-(p-tolyl)-1H-imidazol-1-yl)-1H-1,2,3-triazole (**2.109**)*

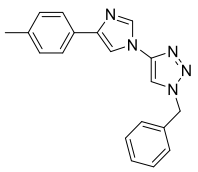

Prepared according to the General Procedure D using 1-ethynyl-4-(*p*-tolyl)-1*H*-imidazole (70.0 mg, 384 μmol), benzyl azide (51.1 mg, 384 μmol), copper(II) acetate monohydrate (3.49 mg, 19.2 μmol) in HFIP/water (2.5 mL/4 mL). The crude as purified using column chromatography (50-100% ethyl acetate in hexane to give the desired product as a white solid (60.0 mg, 190 μmol, 50%).
^{1}H NMR (400 MHz, $CDCl_3$) δ 7.97 (d, *J* = 1.3 Hz, 1H), 7.77 – 7.63 (m, 2H), 7.59 (d, *J* = 1.3 Hz, 1H), 7.51 (s, 1H), 7.45 – 7.28 (m, 5H), 7.19 (d, *J* = 7.8 Hz, 2H), 5.55 (s, 2H), 2.36 (s, 3H).
^{13}C NMR (101 MHz, $CDCl_3$) δ 143.8, 143.3, 137.2, 135.4, 133.8, 130.7, 129.5, 129.4, 128.4, 125.1, 112.7, 112.6, 55.2, 21.4.
HR-MS (ESI) $C_{19}H_{17}N_5^+$ calc 316.1557, found 316.1554.
IR ν_{max} (cm^{-1}) 3105 (C-H), 3120 (C-H), 1595 (C=C), 1497 (C=C).

*1-Benzyl-4-(4-(4-fluorophenyl)-1H-imidazol-1-yl)-1H-1,2,3-triazole (**2.110**)*

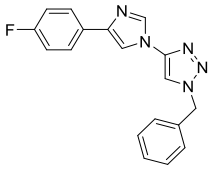

Prepared according to the General Procedure D using 1-ethynyl-4-(4-fluorophenyl)-1*H*-imidazole (40.0 mg, 215 μmol) benzyl azide (28.6 mg, 215 μmol), copper(II) acetate monohydrate (2.14 mg, 21.4 μmol) in HFIP/water (2 mL/1 mL). The crude was purified using flash column chromatography (50 - 100% ethyl acetate in hexane) to give the desired product as a white solid (60.0 mg, 187 μmol, 87%).

^{1}H NMR (400 MHz, DMSO) δ 8.58 (s, 1H), 8.22 (dd, *J* = 31.9, 1.3 Hz, 2H), 7.93 – 7.82 (m, 2H), 7.49 – 7.32 (m, 5H), 7.30 – 7.16 (m, 2H), 5.70 (s, 2H).

^{19}F NMR (376 MHz, DMSO) δ -115.54 (s).

^{13}C NMR (101 MHz, DMSO) δ 161.3 (d, *J* = 244 Hz), 142.73, 140.68, 136.0, 135.4, 130.2 (d, *J* = 4 Hz), 128.9, 128.4, 128.1, 126.4 (d, *J* = 8 Hz, 2 x CH), 115.4 (d, *J* = 16 Hz, 2 x CH), 115.1, 113.7, 53.8.

HR-MS (ESI) $C_{18}H_{14}FN_5^+$ calculated 320.1306, found 320.1300.

IR ν_{max} (cm^{-1}) 3111 (C-H), 1595 (C=C), 1500 (C=C), 1219 (C-F).

*1-Benzyl-4-(4-(4-methoxyphenyl)-1H-imidazol-1-yl)-1H-1,2,3-triazole (**2.111**)*

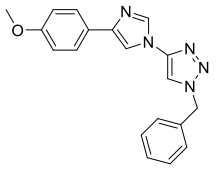

Prepared according to the General Procedure D using 1-ethynyl-4-(4-methoxyphenyl)-1H-imidazole (70.0 mg, 353 μmol) benzyl azide (47.0 mg, 353 μmol), copper(II) acetate monohydrate (3.53 mg, 17.7 μmol) in HFIP/water (1.5 mL/2 mL). The crude was purified using flash column chromatography (50 - 100% ethyl acetate in hexane) to give the desired product as a white solid (100 mg, 301 μmol, 85%).

^{1}H NMR (400 MHz, $CDCl_3$) δ 7.97 (d, *J* = 1.4 Hz, 1H), 7.76 – 7.68 (m, 2H), 7.53 (d, *J* = 1.4 Hz, 1H), 7.51 (s, 1H), 7.38 – 7.30 (m, 2H), 6.96 – 6.90 (m, 2H), 5.56 (s, 2H), 3.82 (s, 3H).

^{13}C NMR (101 MHz, $CDCl_3$) δ 159.2, 143.8, 143.1, 135.4, 133.9, 129.5, 129.4, 128.4, 126.5, 114.2, 112.7, 112.0, 55.4, 55.2.

HR-MS (ESI) $C_{19}H_{17}N_5O^+$ calc 332.1493, found 332.1501.

IR ν_{max} (cm^{-1}) 3124 (C-H), 1588 (C=C), 1502 (C=C), 1251 (C-O).

*1-Benzyl-4-(4-(4-bromophenyl)-1H-imidazol-1-yl)-1H-1,2,3-triazole (**2.112**)*

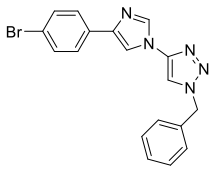

Prepared according to General Procedure C using 4-(4-bromophenyl)-1-((triisopropylsilyl)ethynyl)-1*H*-imidazole (65.0 mg, 260 μmol), benzyl azide (45.0 mg, 260 μmol), copper(II) acetate monohydrate (2.70 mg, 13.3 μmol) in MeOH (0.60 mL). The

crude was purified using column chromatography (50% ethyl acetate in petroleum ether) to give the desired product as an off white solid (57.2 mg, 0.15 mmol, 58%).

^{1}H NMR (500 MHz, $CDCl_3$) δ 7.98 (s, 1H), 7.71 – 7.64 (m, 3H), 7.65 (d, *J* = 1.2 Hz, 2H), 7.54 – 7.48 (m, 3H), 7.47 – 7.32 (m, 5H), 5.59 (s, 2H).

^{13}C NMR (126 MHz, $CDCl_3$) δ 143.5, 142.1, 135.6, 133.6, 132.3, 131.8, 129.4, 129.3, 128.3, 126.6, 121.1, 113.2, 112.6, 55.2.

HR-MS (ESI) $C_{18}H_{14}BrN_5^+$ calculated 380.0505, found 380.0508.

IR ν_{max} (cm^{-1}) 3107 (C-H), 1597 (C=C), 711 (C-Br).

*1-Benzyl-4-(4-(4-nitrophenyl)-1H-imidazol-1-yl)-1H-1,2,3-triazole (**2.113**)*

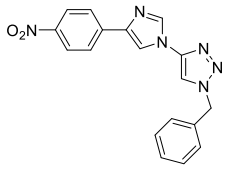

Prepared according to the general procedure D using 4-(4-nitrophenyl)-1-((triisopropylsilyl)ethynyl)-1*H*-imidazole (100 mg, 0.469 mmol), benzyl azide (62.5 mg, 469 μmol) and copper(II) acetate monohydrate (4.69 mg, 23.5 μmol) in a mixture of HFIP/water (1.5 mL/2 mL). The crude residue was purified using column chromatography (80 - 100% ethyl acetate in hexane) to give the desired product 1-benzyl-4-(4-(4-nitrophenyl)-1H-imidazol-1-yl)-1H-1,2,3-triazole as a light orange solid (82.0 mg, 236 μmol, 50%).

^{1}H NMR (400 MHz, DMSO) δ 8.62 (s, 1H), 8.52 (d, *J* = 1.2 Hz, 1H), 8.37 (d, *J* = 1.2 Hz, 1H), 8.29 – 8.24 (m, 2H), 8.13 – 8.08 (m, 2H), 7.46 – 7.34 (m, 5H), 5.72 (s, 2H).

^{13}C NMR (101 MHz, DMSO) δ 145.8, 142.4, 140.2, 139.5, 137.0, 135.3, 128.9, 128.4, 128.1, 125.2, 124.2, 117.1, 115.5, 53.8.

HR-MS (ESI) $C_{18}H_{14}N_6O_2^+$ calculated 347.1251, found 347.1248.

IR ν_{max} (cm^{-1}) 3124 (C-H), 1595 (N-O), 1510 (N-O), 1342 (C-N).

*1-Benzyl-4-(4-(4-(trifluoromethyl)phenyl)-1H-imidazol-1-yl)-1H-1,2,3-triazole (**2.114**)*

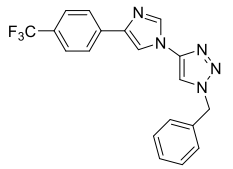

Prepared according to the General Procedure D using 1-ethynyl-4-(4-(trifluoromethyl)phenyl)-1*H*-imidazole (110 mg, 0.466 mmol, 1 equiv), benzyl azide (62.0 mg, 0.466 mmol, copper(II) acetate monohydrate (4.65 mg, 0.0233 mmol, 0.05 equiv) in

HFIP/water (4 mL/3 mL). The crude was purified by flash column chromatography (50 – 100% ethyl acetate in hexane) to give the desired product as a white solid (160 mg, 0.420 mmol, 93%).

^{1}H NMR (400 MHz, DMSO) δ 8.60 (s, 1H), 8.39 (d, *J* = 1.3 Hz, 1H), 8.32 (d, *J* = 1.3 Hz, 1H), 8.09 – 8.03 (m, 2H), 7.75 (d, *J* = 8.3 Hz, 2H), 7.47 – 7.34 (m, 5H), 5.71 (s, 2H).

^{19}F NMR (376 MHz, DMSO) δ -60.77.

^{13}C NMR (101 MHz, DMSO) δ 142.6, 140.1, 137.6, 136.6, 135.3, 128.9, 128.4, 128.1, 127.0 (q, *J* = 32.3 Hz),124 (q, *J* = 272.7 Hz) 125.6 (q, *J* = 4.0 Hz), 125.0, 115.7, 115.4, 53.8.

HR-MS (ESI) $C_{19}H_{14}F_3N_5^+$ calculated 370.1274, found 347.1267.

IR ν_{max} (cm^{-1}) 3175 (C-H), 1611 (C=C), 1114 (C-F).

*1-Benzyl-4-(4,5-diphenyl-1H-imidazol-1-yl)-1H-1,2,3-triazole (**2.115**)*

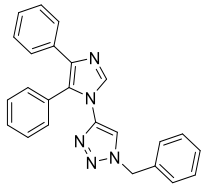

Prepared according to the General Procedure C using 1-ethynyl-4,5-diphenyl-1*H*-imidazole (80.0 mg, 396 μmol), benzyl azide (52.7 mg, 198 μmol) copper(II) acetate monohydrate (3.59 mg, 19.8 μmol) in MeOH (4 mL). The crude was purified by flash column chromatography (50 – 100% ethyl acetate in hexane) to give the desired product as an off-white solid (90.0 mg, 268 μmol, 68%).

^{1}H NMR (500 MHz, DMSO) δ 8.14 (s, 1H), 8.09 (s, 1H), 7.49 – 7.31 (m, 8H), 7.28 – 7.15 (m, 5H), 7.09 (d, *J* = 5.1 Hz, 2H), 5.58 (s, 2H).

^{13}C NMR (101 MHz, $CDCl_3$) δ 141.9, 133.5, 130.8, 129.7, 129.0, 128.9, 128.9, 128.7, 128.7, 128.6, 128.6, 128.1, 128.0, 128.0, 128.0, 127.7, 127.6, 126.6, 115.7, 54.5.

HR-MS (ESI) $C_{24}H_{19}N_5^+$ calculated 378.1713, found 378.1708.

IR ν_{max} (cm^{-1}) 3120 (C-H), 3057 (C-H), 1580 (C=C).

2.5.5 Single Crystal X-ray Diffraction

All crystallographic measurements were made with monochromatic Cu radiation (λ = 1.54184 Å) using a Rigaku Synergy-i diffractometer. Raw data processing utilised the program CrysalisPro. All structures were solved using direct methods and were refined against F^2 to convergence using all unique reflections and the program Shelxl, as implemented within WinGX. All non-H atoms were refined anisotropically. H atoms bound to N or to O were

placed as found and refined isotropically. H atoms bound to C were placed in geometrically expected positions and refined in riding modes. Selected crystallographic and refinement parameters are given for each structure obtained below.

2.5.5.1 Compound 2.64

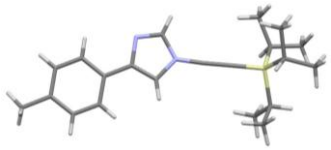

Table 2.4. Crystal data and structure refinement for **2.64**

Empirical formula	C21 H30 N2 Si
Formula weight	338.56
Temperature	100(2) K
Wavelength	1.54184 Å
Crystal system	Triclinic
Space group	P -1
a (Å)	16.2916(5)
b (Å)	18.6274(7)
c (Å)	19.3406(4)
α (°)	78.150(3)
β (°)	72.397(2)
γ (°)	66.057(3)
Volume (Å^3)	5090.0(3)
Z	10
Density (calculated)	1.104 Mg/m^3
Absorption coefficient	1.026 mm^{-1}
F(000)	1840
Crystal size	0.25 x 0.10 x 0.05 mm^3
Theta range for data collection	3.061 to 69.999°.
Index ranges	-19<=h<=19, -22<=k<=22, -

	23<=l<=18
Reflections collected	59735
Independent reflections	19247 [R(int) = 0.0528]
Completeness to theta = 69.999°	99.7%
Absorption correction	Semi-empirical from equivalents
Max. and min. transmission	1.00000 and 0.63354
Refinement method	Full-matrix least-squares on F^2
Data / restraints / parameters	19247 / 0 / 1116
Goodness-of-fit on F^2	1.065
Final R indices [I>2sigma(I)]	R1 = 0.0662, wR2 = 0.1989
R indices (all data)	R1 = 0.1116, wR2 = 0.2365
Extinction coefficient	n/a
Largest diff. peak and hole	0.526 and -0.541 e.Å^{-3}

2.5.5.2 Compound 2.68

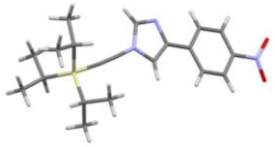

Table 2.5. Crystal data and structure refinement for **2.68**

Empirical formula	C20 H27 N3 O2 Si
Formula weight	369.53
Temperature	100(2) K
Wavelength	1.54184 Å
Crystal system	Triclinic
Space group	P -1
a (Å)	7.6708(2)

b (Å)	14.1055(4)
c (Å)	19.4704(5)
α (°)	83.068(2)
β (°)	79.665(2)
γ (°)	80.831(2)
Volume ($Å^3$)	2036.82(10)
Z	4
Density (calculated)	1.205 Mg/m^3
Absorption coefficient	1.161 mm^{-1}
F(000)	792
Crystal size	0.22 x 0.11 x 0.02 mm^3
Theta range for data collection	2.317 to 71.532°.
Index ranges	-7<=h<=9, -17<=k<=17, -23<=l<=23
Reflections collected	21512
Independent reflections	7853 [R(int) = 0.0407]
Completeness to theta = 70.000°	99.7%
Absorption correction	Semi-empirical from equivalents
Max. and min. transmission	1.00000 and 0.74667
Refinement method	Full-matrix least-squares on F^2
Data / restraints / parameters	7853 / 0 / 481
Goodness-of-fit on F^2	1.026
Final R indices [I>2sigma(I)]	R1 = 0.0496, wR2 = 0.1351
R indices (all data)	R1 = 0.0596, wR2 = 0.1436
Extinction coefficient	n/a
Largest diff. peak and hole	0.525 and -0.351 $e.Å^{-3}$

2.5.5.3 Compound 2.69

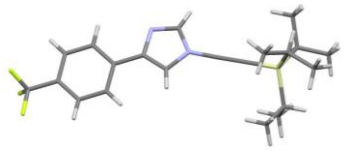

Table 2.6. Crystal data and structure refinement for **2.69**

Empirical formula	C21 H27 F3 N2 Si
Formula weight	392.53
Temperature	100(2) K
Wavelength	1.54184 Å
Crystal system	Triclinic
Space group	P -1
a (Å)	9.9832(3)
b (Å)	11.4277(3)
c (Å)	19.5556(5)
α (°)	103.081(2)
β (°)	99.475(2)
γ (°)	96.052(2)
Volume ($Å^3$)	2119.69(10)
Z	4
Density (calculated)	1.230 Mg/m^3
Absorption coefficient	1.267 mm^{-1}
F(000)	832
Crystal size	0.20 x 0.08 x 0.02 mm^3
Theta range for data collection	2.365 to 71.625°.
Index ranges	-12<=h<=12, -14<=k<=11, -23<=l<=24
Reflections collected	21072

Independent reflections	8173 [R(int) = 0.0454]
Completeness to theta = 70.000°	99.8%
Absorption correction	Semi-empirical from equivalents
Max. and min. transmission	1.00000 and 0.74400
Refinement method	Full-matrix least-squares on F^2
Data / restraints / parameters	8173 / 18 / 511
Goodness-of-fit on F^2	1.073
Final R indices [I>2sigma(I)]	R1 = 0.0576, wR2 = 0.1520
R indices (all data)	R1 = 0.0823, wR2 = 0.1626
Extinction coefficient	n/a
Largest diff. peak and hole	0.554 and -0.369 e.Å^{-3}

2.5.5.4 Compound 2.74

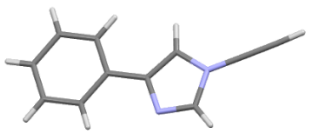

Table 2.7. Crystal data and structure refinement for **2.74**

Empirical formula	C11 H8 N2
Formula weight	168.19
Temperature	100(2) K
Wavelength	1.54184 Å
Crystal system	Orthorhombic
Space group	P n a 2_1
a (Å)	8.4429(2)
b (Å)	18.7436(5)
c (Å)	5.6123(2)

α (°)	90
β (°)	90
γ (°)	90
Volume	888.15(4) $Å^3$
Z	4
Density (calculated)	1.258 Mg/m^3
Absorption coefficient	0.604 mm^{-1}
F(000)	352
Crystal size	0.20 x 0.04 x 0.02 mm^3
Theta range for data collection	4.718 to 71.321°.
Index ranges	-10<=h<=7, -20<=k<=22, -6<=l<=6
Reflections collected	4252
Independent reflections	1530 [R(int) = 0.0254]
Completeness to theta = 70.000°	100.0%
Absorption correction	Semi-empirical from equivalents
Max. and min. transmission	1.00000 and 0.69707
Refinement method	Full-matrix least-squares on F^2
Data / restraints / parameters	1530 / 1 / 122
Goodness-of-fit on F^2	1.074
Final R indices [I>2sigma(I)]	R1 = 0.0303, wR2 = 0.0746
R indices (all data)	R1 = 0.0317, wR2 = 0.0753
Absolute structure parameter	-0.3(3)
Extinction coefficient	n/a
Largest diff. peak and hole	0.106 and -0.172 $e.Å^{-3}$

2.5.5.5 Compound 2.76

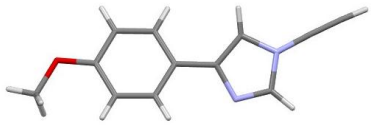

Table 2.8. Crystal data and structure refinement for **2.76**

Empirical formula	C12 H10 N2 O
Formula weight	198.22
Temperature	100(2) K
Wavelength	1.54184 Å
Crystal system	Monoclinic
Space group	P 2_1/c
a (Å)	8.1268(2)
b (Å)	5.67200(10)
c (Å)	21.1801(4
α (°)	90
β (°)	96.641
γ (°)	90
Volume	969.75(3) $Å^3$
Z	4
Density (calculated)	1.358 Mg/m^3
Absorption coefficient	0.716 mm^{-1}
F(000)	416
Crystal size	0.15 x 0.04 x 0.02 mm^3
Theta range for data collection	4.203 to 71.562°.
Index ranges	-9<=h<=9, -6<=k<=6, -26<=l<=26
Reflections collected	3139
Independent reflections	3139 [R(int) = 0.0377]
Completeness to theta = 70.000°	100.0%

Absorption correction	Semi-empirical from equivalents
Max. and min. transmission	1.00000 and 0.96351
Refinement method	Full-matrix least-squares on F^2
Data / restraints / parameters	3139 / 0 / 150
Goodness-of-fit on F^2	1.066
Final R indices [I>2sigma(I)]	R1 = 0.0373, wR2 = 0.0982
R indices (all data)	R1 = 0.0436, wR2 = 0.1022
Extinction coefficient	n/a
Largest diff. peak and hole	0.169 and -0.279 e.Å^{-3}

2.5.5.6 Compound 2.77

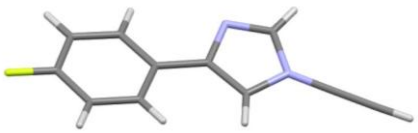

Table 2.9. Crystal data and structure refinement for **2.77**

Empirical formula	C11 H7 F N2
Formula weight	186.19
Temperature	100(2) K
Wavelength	1.54184 Å
Crystal system	Triclinic
Space group	P -1
a (Å)	5.7116(2)
b (Å)	11.1479(6)
c (Å)	13.8116(5)
α (°)	81.770(4)°.
β (°)	89.081(3)°.

γ (°)	89.954(4)
Volume	870.25(6) $Å^3$
Z	4
Density (calculated)	1.421 Mg/m^3
Absorption coefficient	0.845 mm^{-1}
F(000)	384
Crystal size	0.18 x 0.10 x 0.04 mm^3
Theta range for data collection	3.233 to 71.436°.
Index ranges	-6<=h<=6, -13<=k<=13, -16<=l<=16
Reflections collected	7508
Independent reflections	3310 [R(int) = 0.0269]
Completeness to theta = 70.000°	99.5%
Absorption correction	Semi-empirical from equivalents
Max. and min. transmission	1.00000 and 0.94986
Refinement method	Full-matrix least-squares on F^2
Data / restraints / parameters	3310 / 0 / 261
Goodness-of-fit on F^2	1.023
Final R indices [I>2sigma(I)]	R1 = 0.0416, wR2 = 0.1090
R indices (all data)	R1 = 0.0524, wR2 = 0.1174
Extinction coefficient	n/a
Largest diff. peak and hole	0.175 and -0.224 $e.Å^{-3}$

2.5.6 HPLC Assay for Metal Free Reactions

2.5.6.1 Procedure for analysis of metal free HPLC reactions

1-ethynyl-5,6-dimethyl-1*H*-benzo[*d*]imidazole (**2.5**) (10.0 mg, 6.0 μmol, 1.00 equiv), benzyl azide (7.00 mg, 60.0 μmol, 1.00 equiv) and metal salt (60.0 μmol, 1.00 equiv) were stirred in solvent (1 mL) for 16 – 24 h. 40.0 μL of the reaction mixture was placed into 96 μL of MeOH and analysed by HPLC.

For reactions containing a chelating agent, reaction was carried out as above but with the addition of the metal chelating agent (60.0 μmol, 1.00 equiv).

2.5.6.2 Instrument, Method and Quantification

HPLC was carried out on a Dionex UltiMate 3000 HPLC.
Column Specifications: Luma Omega 3 μm polar C19 100 x 4.6 mm
Column Temperature: 24 °C
Mobile Phase A: 0.1% v/v TFA in water
Mobile Phase B: 0.1% TFA in MeCN
Flow rate: 1.2 mL/min

Example Gradient Profile:

Time (min)	B%
0 – 17	25 – 45
17 – 18	45 – 95
18 – 21	95 – 95
21 – 22	95 – 25
22 – 26	25

To determine the conversion, the peak area of the product was divided by the peak area of the starting material.

2.5.7 NMR Analysis of Metal Free Reactions

1-ethynyl-5,6-dimethyl-1*H*-benzo[*d*]imidazole (**2.5**) (10.0 mg, 60.0 μmol, 1.00 equiv), benzyl azide (7.00 mg, 60.0 μmol, 1.00 equiv) and metal salt (60.0 μmol, 1.00 equiv) were stirred in

solvent (1 mL) for 16 – 24 h. DCM (4 mL) and water (4 mL) were added to the reaction vial and shaken vigorously. The organic layer was extracted and solvent removed by an air stream. The residue was dissolved in $CDCl_3$ (500 μL) for ^1H NMR analysis.
NMR traces were analysed by MestReNova.

Chapter 3

Exploration of the Molecular Determinants of Ynamine Reactivity in (3+2) Cycloaddition Reactions

3.1 Introduction

3.1.1 Terminal Alkyne Reactivity in CuAAC

Despite the efforts made to unravel the mechanistic insights of the CuAAC, there has not been many studies focusing on the reactivity of terminal alkynes in this type of reactions. Kislukhin *et al.* investigated the differences the performance of common non-Micheal reactive alkyne building blocks, such as propiolamides, propargyl derivatives and longer chain alkynes and aromatic alkynes.[44] The results showed that moderate changes in the electronic nature of the alkyne do not have a dramatic effect on the CuAAC rate when good accelerating ligands are used. Exemplar substrates which showed good reactivity are given in Figure 3.1A. The most comprehensive study was carried out by Zhang *et al.* where it was hypothesised that the acidity of the C-H terminal alkyne could be related to the reactivity of the alkyne in CuAAC reactions.[185] Considering the mechanistic insights indicating that the deprotonation of alkyne to form copper(I) acetylide is the turnover-limiting step in CuAAC reactions, an electron-withdrawing group that lowers the pK_a value of the Csp-H bond should augment the reactivity of the alkyne.[25,27,43,186] The tested alkynes were divided in three groups: electron-withdrawing group-bearing alkynes (**3.4 – 3.8**), alkynes with potentially copper-binding moieties (**3.11 – 3.12**) and control alkynes that contain none of those features (**3.9** and **3.10**) (Figure 3.1B).

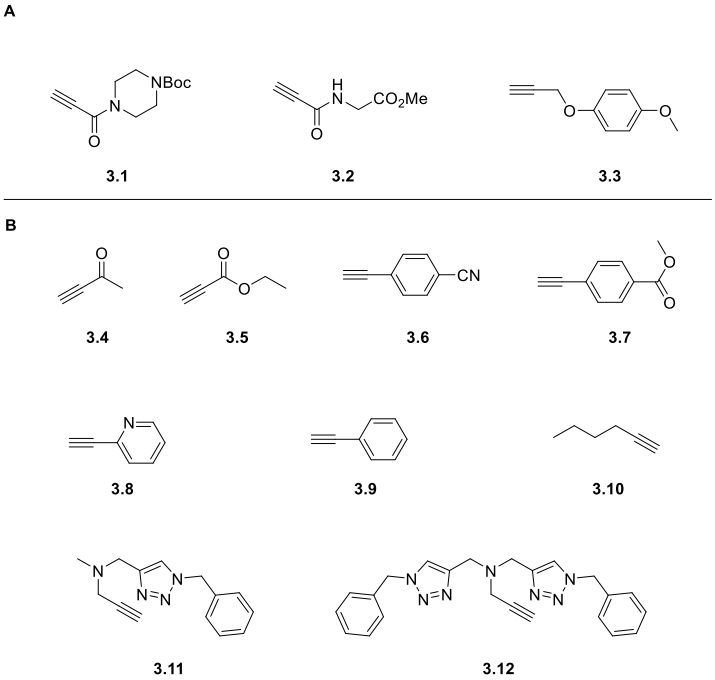

Figure 3.1. A selection of the alkynes tested in literature. **A)** Alkynes tested in work by Kislukhin *et al.*[44]; **B)** Alkynes tested in work by Zhang *et al.* [185]

This study confirmed that C-H acidic terminal alkynes exhibit relatively high reactivity in CuAAC reactions.[185] Additionally, it was observed that alkynes that are precursors of CuAAC-accelerating poly(triazolylmethyl) ligands (**3.11** and **3.12**) demonstrated enhanced reactivity despite their low acidity. Alkyne deprotonation and azide binding to copper were identified as the slow steps in the CuAAC pathway, significantly influencing the overall reaction rate.[185] Consequently, it is understandable that acidic alkynes and chelating azides such as 2-picolyl azide have high reactivity in CuAAC reactions.[187]

3.1.2 Mechanistic Studies on Dimethylbenzimidazole Ynamine Reactivity

In the case of the benzimidazole ynamine (**3.13**), which has been found to have enhanced reactivity in the CuAAC, the interaction between copper and the benzimidazole through N3 lowers the acetylinic pK_a, resulting in rapid Cu-acetylide formation.[183] The final key factor to consider is the reactivity of the ynamine in the homocoupling Glaser-Hay, crucial to generate Cu(I) for the CuAAC to proceed. Both Cu-catalysed reactions work in concert to produce the final 1,4-triazole products.

Previous work in the group analysed the mechanistic origin of rate-independent chemoselectivity in CuAAC reactions of the dimethylbenzimidazole ynamine (**3.13**).[183] Kinetic investigations revealed a shift in the RDS of the reaction from Cu-acetylide formation to azide ligation, attributed to a rapid Lewis acid-assisted acetylide formation step. The unusual reactivity of ynamines was the origin of its chemo-selectivity in the CuAAC reaction over a range of alkynes, even in the presence of alkyne substrates that individually exhibited faster overall rates. However, these studies did not clarify the role of the $Cu(OAc)_2$, or the potential *in situ* generation of Cu(I) *via* a Glaser-Hay coupling forming a diyne as a side product.

Concurrent mechanistic studies were conducted within the group simultaneously with the progress of this thesis and were the basis of the reactivity studies described in this chapter.[188] The key finding highlighted how the interplay of two reactions, the Glaser-Hay alkyne coupling and CuAAC, is mediated by the choice of Cu catalyst and the alkyne substrate (Figure 3.2). The initiation of the reaction occurs through the Glaser-Hay alkyne reaction to form the Cu(I) species (Figure 3.2A). This happens through the coordination of the $Cu(OAc)_2$ to the N3 of the benzimidazole, forming complex **3.14**. This homocoupling produces diyne **3.15** and a Cu(I) complex (assumed to be **3.17**). Complex **3.18** is formed as a result of the coordination of $Cu(OAc)_2$ and this forms a binuclear Cu-acetylide species. The azide ligation of **3.19** is followed by protodemetallation of the Cu-triazole. A final protonation occurs, which may occur *via* the dissociated acetic acid or by a build-up of **3.19** as triazole **3.20** forms.

During the reaction, the benzimidazole is believed to play several key roles: assisting in C-H activation, Cu-coordination, and the formation of a post-reaction resting state Cu complex. It is therefore important that the benzimidazole is optimised for the reaction.

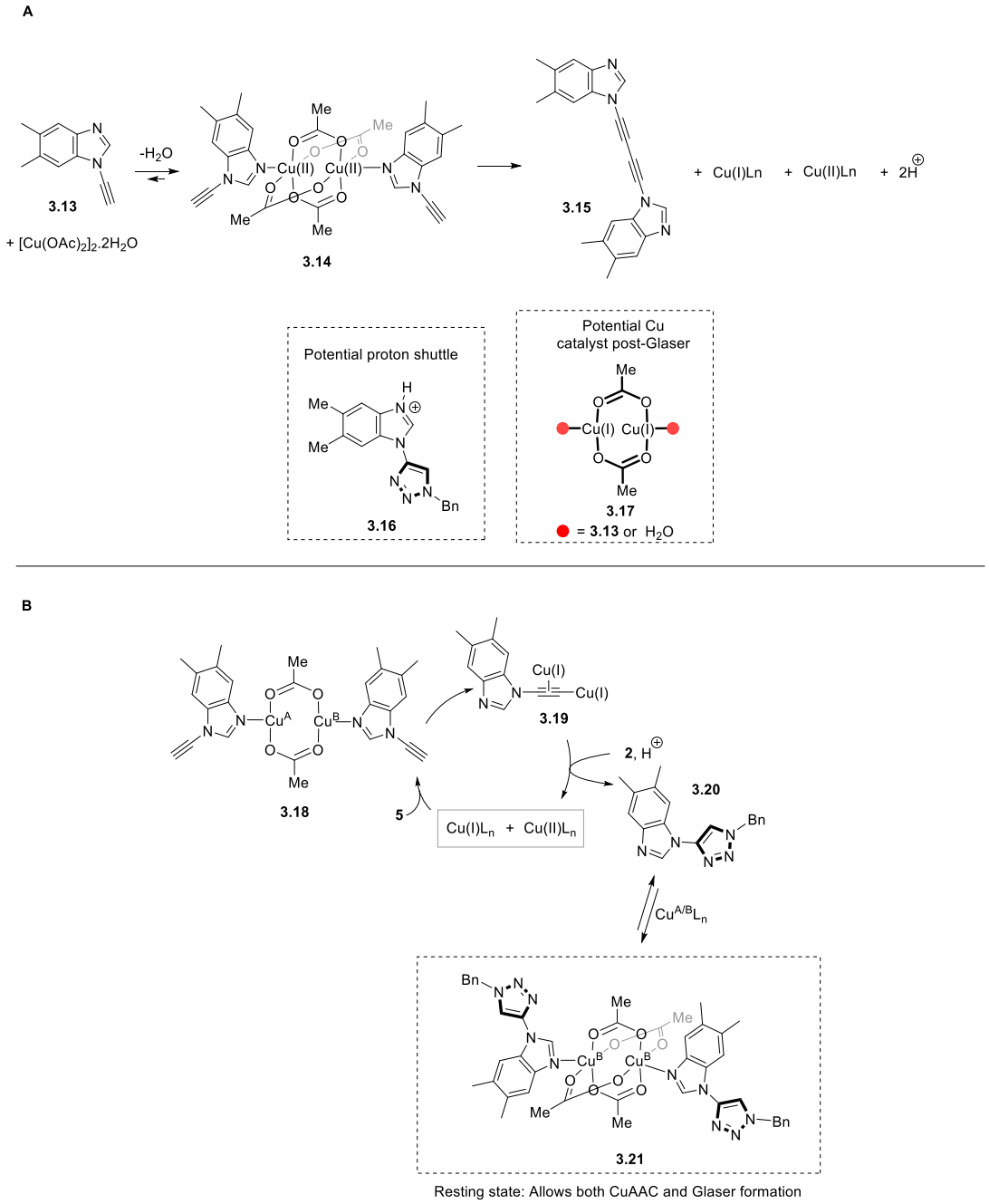

Figure 3.2. The revised mechanism for the aromatic ynamine CuAAC. **A**) The reaction initiation showing Glaser-Hay formation (**3.15**), the generation of Cu(I) and a possible Cu(I) catalyst structure; **B)** The CuAAC mechanism showing catalysis and the Cu oxidation resting state (**3.21**)

Hydrogen Deuterium Exchange (HDE) NMR experiments with different Cu sources in acetonitrile showed how the exchange was promoted predominantly by the acetate ligand. Additionally, the presence of the N3 in the benzimidazole was crucial for the HDE and the initiation of the CuAAC. Further NMR experiments and crystallographic work established that the N3 coordinates Cu(II) at the apical position of the paddlewheel (Figure 3.3). The ability of the N3 to act as Cu(I) and Cu(II) ligand opened the possibility of exploring how the variation in substitution on the benzene ring of the benzimidazole would affect the coordination event and therefore the kinetics of the reaction.

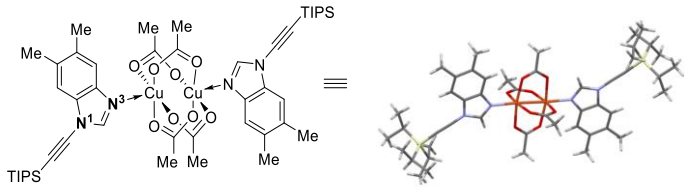

3.22

Figure 3.3. Asymmetric unit cell of Cu(II) complexation *via* N3 of the TIPS-protected ynamines using $Cu(OAc)_2$.

Taken collectively all these mechanistic findings, changes in the alkyne substrates could influence multiple factors in the reaction kinetics and mechanistic pathway. Different electron donating or electron withdrawing groups would affect the following factors:

- Ability of the ynamine to initially coordinate to Cu(II) *via* N3.
- pK_a of the ynamine alkyne.
- Changes in HOMO and LUMO alkyne orbitals.
- Glaser-Hay product rate formation.
- Ability of the ynamine to coordinate to Cu(II)/Cu(I) species during reaction.
- Shift of the RDS depending on the substrate and/or solvent.
- Change in the kinetics of the protodemetallation step.
- Coordination of the triazole to Cu(I) and/or Cu(II).

3.1.3 Choice of Ynamines for the Reactivity Studies

In the previous chapter, a wide range of aromatic alkynes were synthesised. Following the results obtained for the ynamine **3.13** given above, a broader scope of ynamines will be investigated. The ynamines that will be probed in more detail in this chapter are given in Figure 3.4. For the benzimidazole series, ynamines **3.24** and **3.25** were chosen due to their differing electronic properties (EDG *vs*. EWG). Ynamines **3.26** and **3.27** were chosen to explore the

differences in the substitution properties on the ynamine, with the methoxy group chosen as the substituent to explore this with. The effect of conjugation of the ynamine properties was explored using ynamines **3.30** and **3.31**.

For the palette of imidazole ynamines, a wider range of functional groups were chosen. Imidazoles **3.34**, **3.35** and **3.37** were selected due to similar groups with the benzimidazole ynamines tested. Imidazole **3.33** allowed the exploration of the reaction without the electronic effects of any substituents. To broaden the range of groups tested, imidazoles **3.39**, **3.38** and **3.36** were used. Imidazole **3.40** was used to begin an initial study into the effect of sterics on the reaction, by the introduction of the second phenyl group.

The large skewing of the substituents chosen towards EWGs for both benzimidazoles and imidazoles follows on from the results by Zhang *et al.* previously discussed.[185] It was assumed that the EWGs would help to increase the acidity of the alkyne.

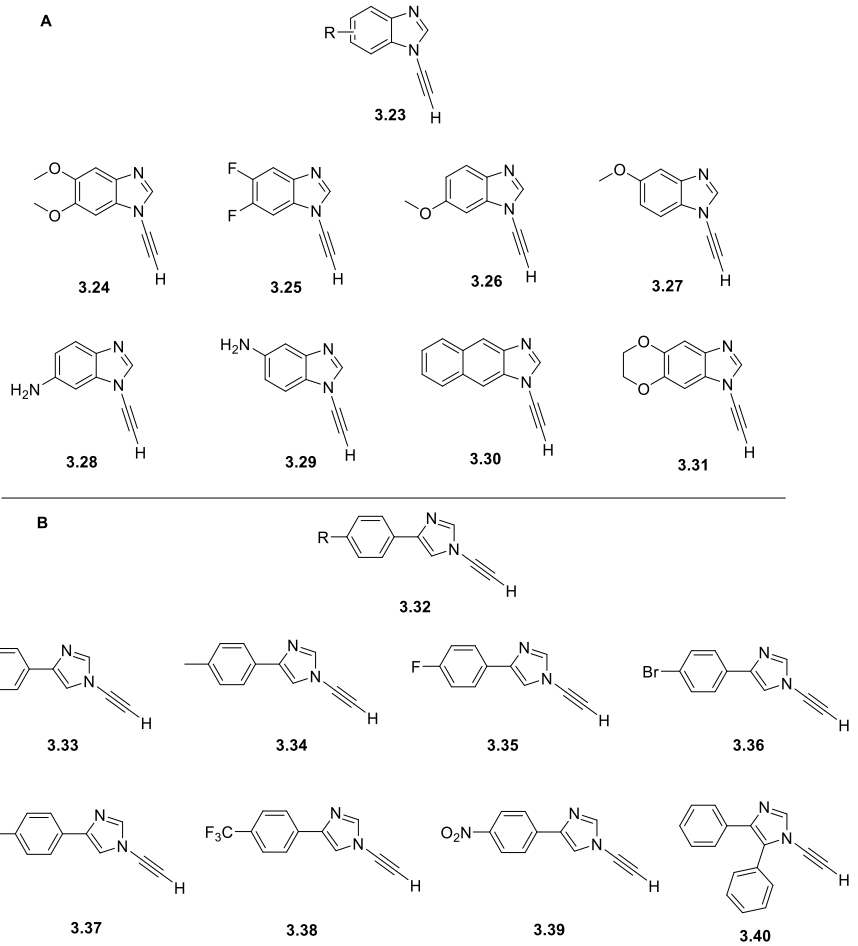

Figure 3.4. Selected ynamines for reactivity analysis. **A)** Benzimidazole ynamines; **B)** Imidazole ynamines.

3.2 Aims of Chapter 3

The aims of this chapter are to:

(i) probe the reactivity of the ynamine alkyne using HDE exchange.

(ii) investigate any differences between benzimidazoles and imidazole ynamines in the reactivity of CuAAC reactions

(iii) investigate how the differences between solvents can affect the CuAAC reaction

3.3 Results & Discussion

3.3.1 Ynamine Hydrogen-Deuterium Exchange (HDE) experiments

In the parallel mechanistic study carried out in the group it was postulated that an interaction between copper and the benzimidazole through the N3 lowers the acetylenic pK_a, resulting in a rapid acetylide formation.[188] The hypothesis is that the base catalysed HDE rate constant $K_{H/D}$ increases in the presence of $Cu(OAc)_2$ (Scheme 3.1A).

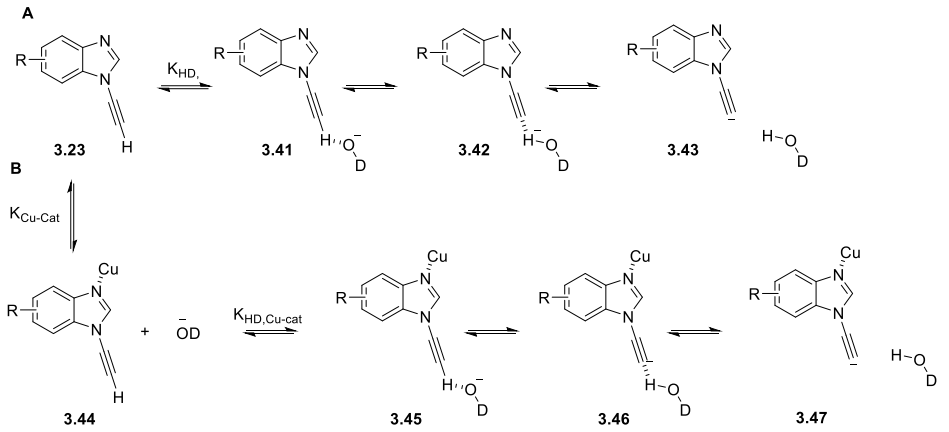

Scheme 3.1. A) Proposed base catalysed mechanism for the HDE of the benzimidazole ynamines. **B)** Proposed mechanism for the HDE of the benzimidazole ynamines in the presence of Cu.

As is shown, the mechanism is the same using Cu (Scheme 3.1B), however, owing to the presence of the Cu, the energy barrier (K_{HD}) will be different. The Cu chelates to the N3 of the benzimidazole core, altering the electron density of the alkyne, allowing the O^-D to bond to the alkyne proton to form a HDO molecule, and this results on the negative charge being on the alkyne. This is based on the base-catalysed HDE process given by Bi *et al*.[189]
It is also mentioned in this paper that hydrogen bond formation may slow down the HDE. This could be affecting the HDE of the ynamines as the crystal structures obtained show H-bonding within the structure and at the alkyne proton.

The introduction of substituents on the benzimidazole or imidazole could also influence the acetylenic proton acidity, having an impact on the general ynamine reactivity. Therefore, HDE of the terminal alkyne proton of the selected ynamines was investigated in a mixture of CD_3CN : D_2O (9 : 1) as function of a 5 mol% $Cu(OAc)_2$.

3.3.1.1 Benzimidazole Ynamines HDE

The HDE of the benzimidazole ynamines was investigated first. Ynamines **3.24** – **3.28, 3.30** and **3.31** were dissolved in CD_3CN and a solution of $Cu(OAc)_2$ in D_2O was added to reach a final copper concentration of 5 mol% and a solvent ration of CD_3CN : D_2O (9 : 1). The sample was immediately placed in the NMR for spectrum acquisition and the formation of the deuterated products monitored by ^{1}H-NMR (Figure 3.5). Ynamine **3.29** was insoluble in the solvent system and no HDE was attempted.

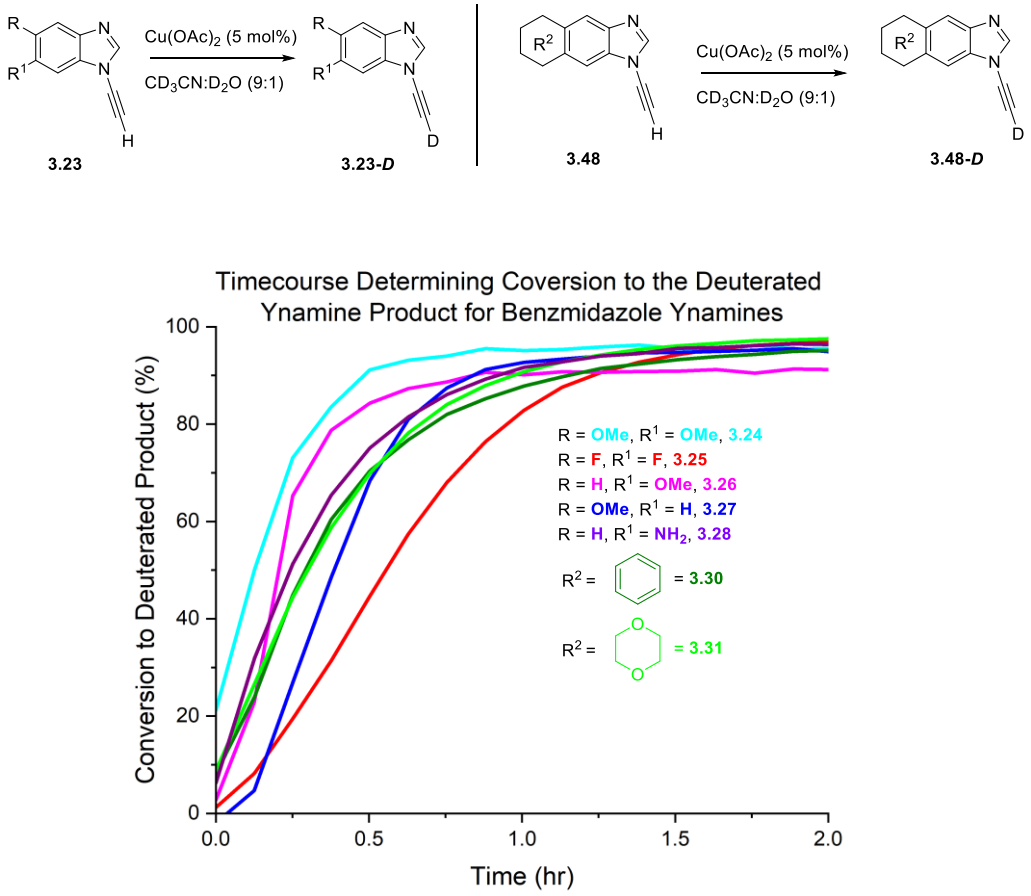

Figure 3.5. Time course of HDE of benzimidazole ynamines with varying substituents in 9 : 1 CD_3CN : D_2O with 5 mol% $Cu(OAc)_2$.

As can be seen in Figure 3.5, the majority of ynamines plateaued at 75 min, apart from ynamine **3.25**. The fastest HDE observed was with **3.24,** forming 90% **3.24-*D*** after 30 min. Interestingly, the slowest HDE was **3.25** which was complete after 90 min. Differences between different substrates are not very pronounced, but are present, and electron withdrawing groups (EWG) (**3.25**) generally slowed down the HDE while electron donating

groups (EDG's), such as **3.24**, accelerated the process. Also observed were the differences between the two isomers of the OMe ynamine, **3.26** and **3.27**. Faster HDE was observed for **3.26**, with the methoxy group at position 7, than for **3.27** with substitution in position 6. As shown in Scheme 3.1, it is hypothesised that the Cu binding to the N3 of the benzimidazole will alter the electron density, but also the functional groups present will affect the alkyne, changing the $K_{HD\ Cu\text{-}cat}$ observed.

Control HDE experiments were carried out on the ynamines without the presence of the Cu catalyst (Figure 3.6).

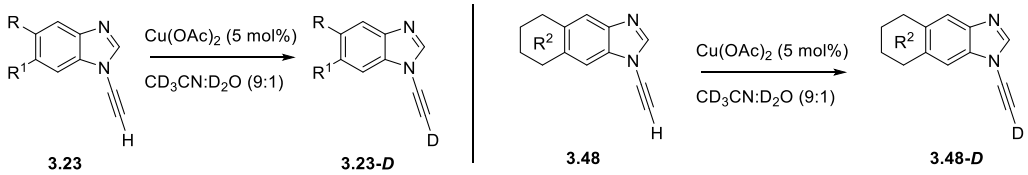

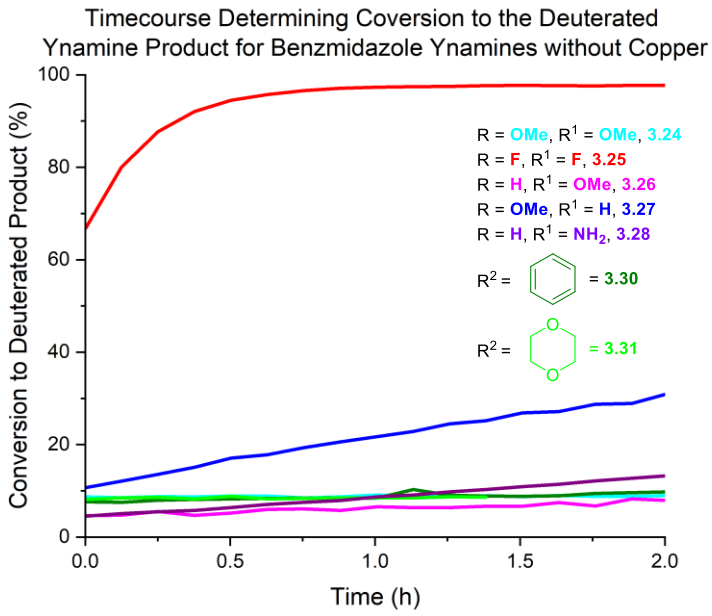

Figure 3.6. Time course of HDE of benzimidazole ynamines with varying substituents in 9 : 1 CD_3CN : D_2O without 5 mol% $Cu(OAc)_2$.

The majority of ynamines tested have slow HDE when there is no copper catalyst present. However, the main exception to this is ynamine **3.25**, which reaches an exchange plateau after approx. 45 min. Surprisingly, this is quicker than the reaction with 5 mol% $Cu(OAc)_2$. This experiment was repeated to investigate whether it was an experimental error or an issue with the batch of ynamine synthesised, however, the results remained consistent. These results

suggest that the EWG is increasing the alkyne acidity. There are no changes in the other proton signals (such as line broadening/peak shifts). This may be due to the electron withdrawing nature of the fluorine atoms, as no other ynamines with strong electron withdrawing natures were tested. Additionally, potential bonding was observed between the molecules in the structure on the crystal structure (Figure 3.7B). The unusual contacts between different parts of the molecule suggests that the presence of the two fluorine atoms in **3.25** could be changing the electron density, affecting the acidity of the alkyne.

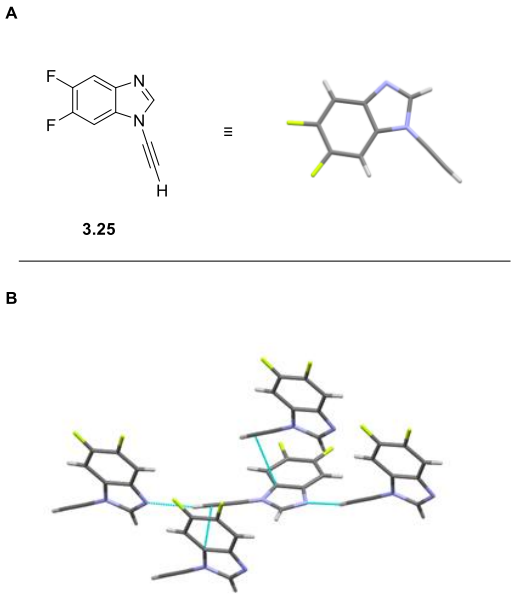

Figure 3.7. A) Single crystal structure of **3.25**; **B)** Shortest contacts in the crystal structure.

Other ynamines, such as **3.27** and **3.28** show a slight increase in the HDE as the reaction progresses, however, this is not as pronounced. **3.27** is the second slowest in the HDE with Cu. In the absence of Cu there is a reverse trend, suggestive of copper binding activating the alkyne more than the intrinsic electronics of the molecule. Again, there is a difference observed with the two isomers **3.26** and **3.27**. This time the opposite effect, with **3.27** giving higher rates of exchange.

A hypothesis for the unexpected trends in reactivity of the benzimidazoles in the HDE and the controls could be due to differential copper binding of the functionalised ynamines, with electron-rich ynamines (such as OMe) rendering the N3 more electron-rich, resulting in better binding to Cu, which in turn could result in a stronger activation of the acetylene proton upon binding. It has been shown that EWG increase the alkyne acidity, as shown with ynamine **3.25**, and that EDG can increase the Cu binding.

It was also postulated that the pK_a of the molecule might play into the differences observed in the HDE. The pK_a values for the benzimidazoles were calculated using Marvin Sketch software (Table 3.1). In previous work, the pK_a of the ynamine **3.13** proton in MeCN has been determined as 27.9, higher than the estimated values given in this table.[183] If the pK_a values were to be determined experimentally, the alkyne proton pK_a could be obtained by NMR titration, and the N3 by a separate method in which the ynamine is dissolved in several aqueous buffer solutions at varying pHs, allowing the determination of a UV spectra as a result of pH.[190] As can be seen, there is a small difference in the pK_a values of the alkyne H, however, this does not correlate to the trends observed in the HDE. There is a larger difference in the pK_a values of the N3, however, this also does not correlate with the reactivity.

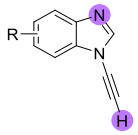

Table 3.1. pKa values calculated by Marvin Sketch. N3 and alkyne H are highlighted in purple.

Ynamine	Functional Group	N3 pK_a	Alkyne H pK_a
3.13	DiMe	5.10	23.89
3.24	DiOMe	5.27	23.90
3.25	DiF	4.69	23.88
3.26	H, OMe	4.75	23.89
3.27	OMe, H	4.92	23.87
3.28	H, NH_2	5.22	23.93
3.29	NH_2, H	5.97	23.88
3.30	ArAr	4.35	23.87
3.31	$ArOCH_2$	5.24	23.90

When performing the HDE experiments, there was evolution of the NMR signals for all the ynamine substrates after the addition of $Cu(OAc)_2$. The benzimidazole peaks exhibit a broadening and a shift in ppm when Cu(II) was added that gradually reversed as the HDE progressed. As exemplified in the spectra of the HDE of ynamine **3.24** shown in Figure 3.8,

there is a difference in the appearance of the peaks in the NMR spectra if Cu(II) is present. The red spectra, showing the control sample with no $Cu(OAc)_2$, has sharp peaks. Upon addition of $Cu(OAc)_2$ (green spectra), these peaks are broadened and shift downfield, with aromatic protons being more affected than the methoxy protons. The benzimidazole proton is particularly affected (8.00 ppm in the control sample). However, after exchange is complete, the peaks shifted back to their original positions and remain sharp.

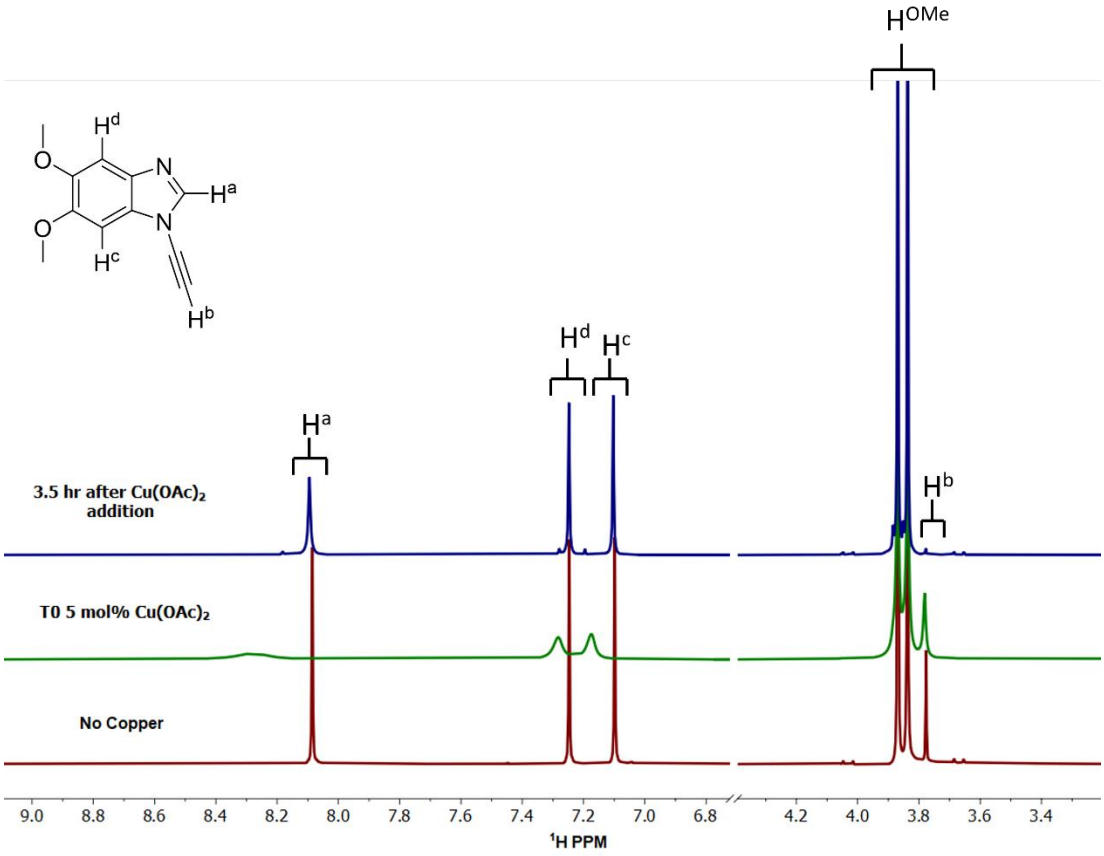

Figure 3.8. Stacked NMR spectra of the ynamine **3.24** undergoing HDE. The red line is the control sample of **3.24** without $Cu(OAc)_2$, the green line is the first spectra obtained immediately after addition of the $Cu(OAc)_2$ and the blue line is the last spectra obtained (3.5 hr).

Cu(II) is paramagnetic which can affect both the chemical shift and the relaxation time of the protons, causing line broadening and shifting of the signals. This effect correlates with the observation of the benzimidazole signals broadening immediately after the addition of $Cu(OAc)_2$. The fact that over time the NMR signals shift back to their initial positions and the sharp signals are restored could indicate that Cu(II) is being reduced to Cu(I) during the HDE (possible by diyne formation). This is supported by the published research into ynamine **3.13** which behaves in a similar manner, and further experimental analysis showed that diyne

formation is involved.[188] This hypothesis is also supported by the colour change of the solution, from light blue to light yellow indicating a change in the oxidation state of copper ions (Figure 3.9).

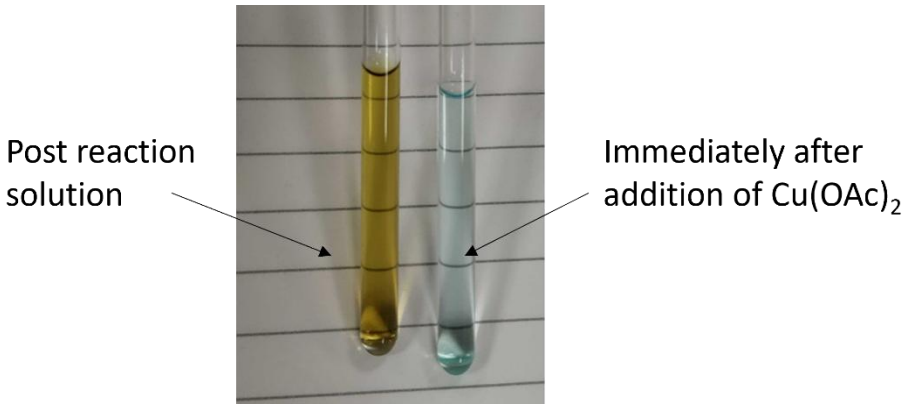

Figure 3.9. Picture showing colour change from immediately after the addition of 5 mol% $Cu(OAc)_2$ in D_2O to a solution of ynamine **3.24** in MeCN (blue) to the colour of the reaction after completion (yellow).

3.3.1.2 Imidazole Ynamines HDE

The HDE NMR was performed in the same conditions with the imidazole ynamines **3.34-3.40** (Figure 3.10). Most of the imidazole ynamine substrates plateaued by 3.5 h, except for the **3.39**, containing the nitro substituent, which did not exchange fully in the time monitored. The fastest imidazole to exchange is **3.33**, which has no substituents present on the para position.

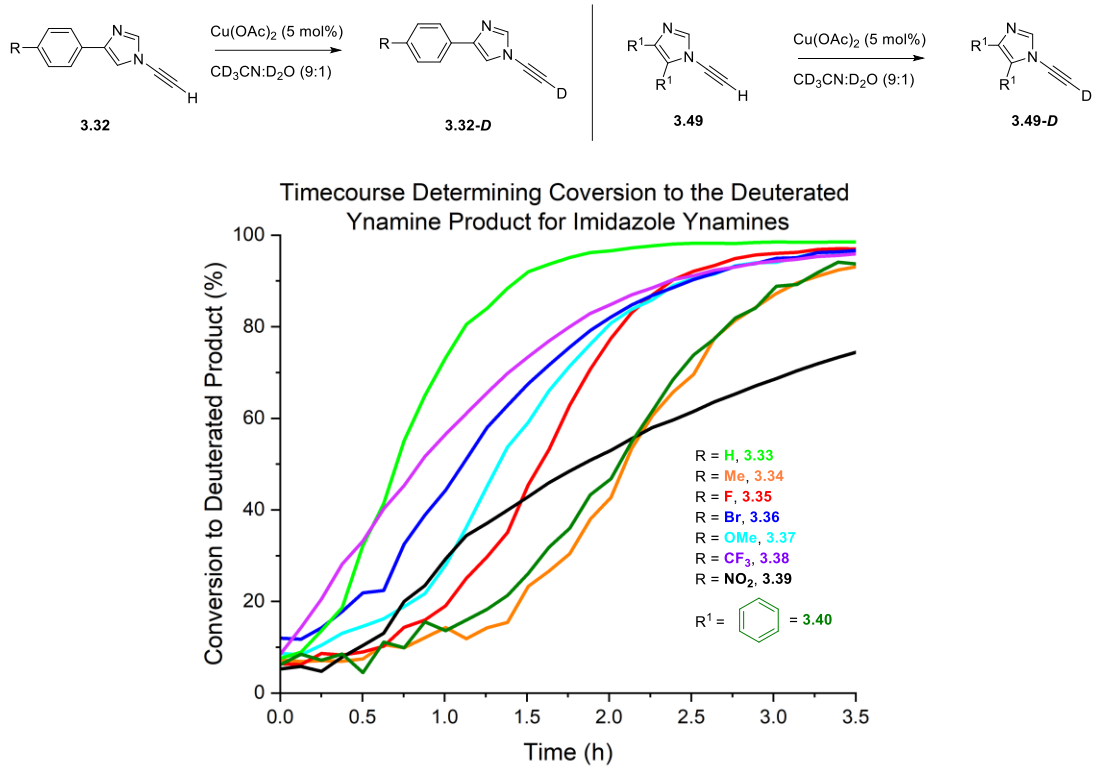

Figure 3.10. Time course of HDE of imidazole ynamines with varying substituents in 9 : 1 CD_3CN : D_2O with 5 mol% $Cu(OAc)_2$.

When compared to the benzimidazole ynamines there are two main differences: the exchange time and the shape of the curve.

The length of time that it takes to reach the exchange plateau differs for the benzimidazoles and the imidazoles. Most benzimidazoles fully exchange within the first 90 min, however, most imidazoles require twice that amount of time.

The second difference is in the shape of the exchange curve. The observed HDE of imidazole mainly results in a sigmoidal curve with an initial induction period. This change could be indicative of a change in the mechanism of the HDE, potentially due to low initial formation of an imidazole Cu(II) complex or the slower rate of the Glaser formation and therefore, production of Cu(I). The exchange could be then accelerated by the presence of Cu(I), which might be a better binder of imidazole.

Control experiments without copper were also carried out for the imidazoles (Figure 3.11). Unlike the benzimidazole ynamines, there is not a substrate that has a high exchange without Cu present. Only the imidazole **3.37** with the methoxy group, exhibited a small amount of HDE, as was observed for the benzimidazoles.

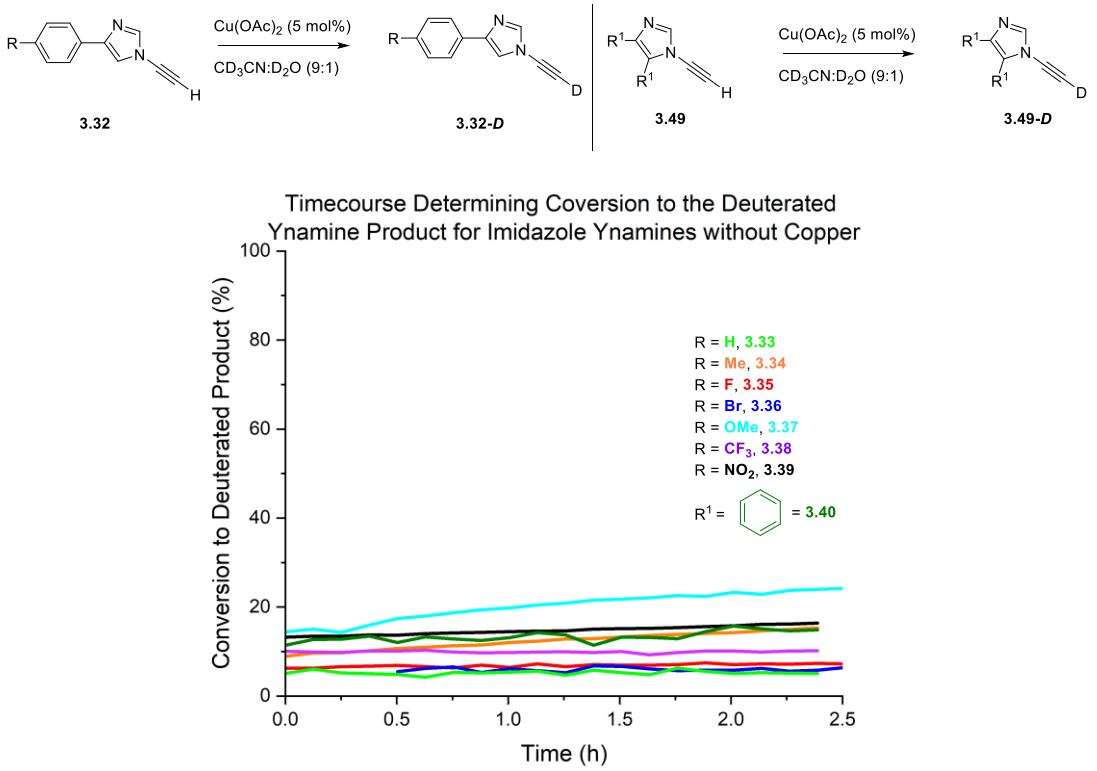

Figure 3.11. Time course of HDE of imidazole ynamines with varying substituents in 9 : 1 CD_3CN : D_2O without 5 mol% $Cu(OAc)_2$.

As with the benzimidazoles, a hypothesis was that the pK_a of the alkyne proton was affecting the exchange. The values for the imidazoles were determined using MarvinSketch. As shown in Table 3.2, the calculated pK_a values for the imidazole are not influenced significantly by the ring substituent. This contrasts with the benzimidazoles. This difference can be rationalised due to the conjugation within the systems: for the imidazoles, the phenyl ring is not in conjugation with the imidazole ring, causing the substituents to affect the electronics of the molecule less.

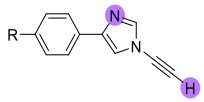

Table 3.2. pK_a values as determined by MarvinSketch software. N3 and alkyne H are highlighted in purple.

Ynamine	Functional Group	N3	Alkyne H
No sub – hydrogen	Hydrogen	4.57	23.98
Methyl	CH_3	4.57	23.98
Methoxy	OMe	4.57	23.98
Fluoro	F	4.57	23.98
Bromo	Br	4.57	23.98
Nitro	NO_2	4.56	23.98
Trifluoro methyl	CF_3	4.57	23.98
Biphenyl	Ar	4.39	23.92

The effects of the $Cu(OAc)_2$ on the NMR peak shape is different for the imidazoles in comparison to the benzimidazoles. As is shown in Figure 3.12 for imidazole **3.37**, the initial peaks pre $Cu(OAc)_2$ addition are well resolved. Upon addition of the catalyst (T0), a broadening is observed without the change in ppm as observed in the benzimidazoles. After reaction completion, the peaks are more resolved, however, they have not reverted to their original sharpness. As shown in the spectra, the peaks remain at their broadest from 15 min, with a small increase in resolution becoming visible at 1 h 15 min, slowly increasing until the final spectra recorded at 3.5 h. The broad peak shapes at 15 - 38 min indicate that there is complex formation between the imidazole and the Cu, which corresponds to the start of the HDE exchange. This is significantly slower compared to benzimidazoles, which experiences peak broadening immediately after copper addition. These differences are indicative of the $Cu(OAc)_2$ having a different effect on the benzimidazole ynamine than the imidazole ynamine, possibly that there is slow initial copper complexation. The chelation effect of the copper to N3 may differ depending on the heterocycle, especially if there are changes in pK_a between them.[191] The difference in the peak resolution after the reaction has finished could indicate the Cu remains bound in greater proportions imidazole substrates causing the protons to remain slightly broader than their benzimidazole counterparts.

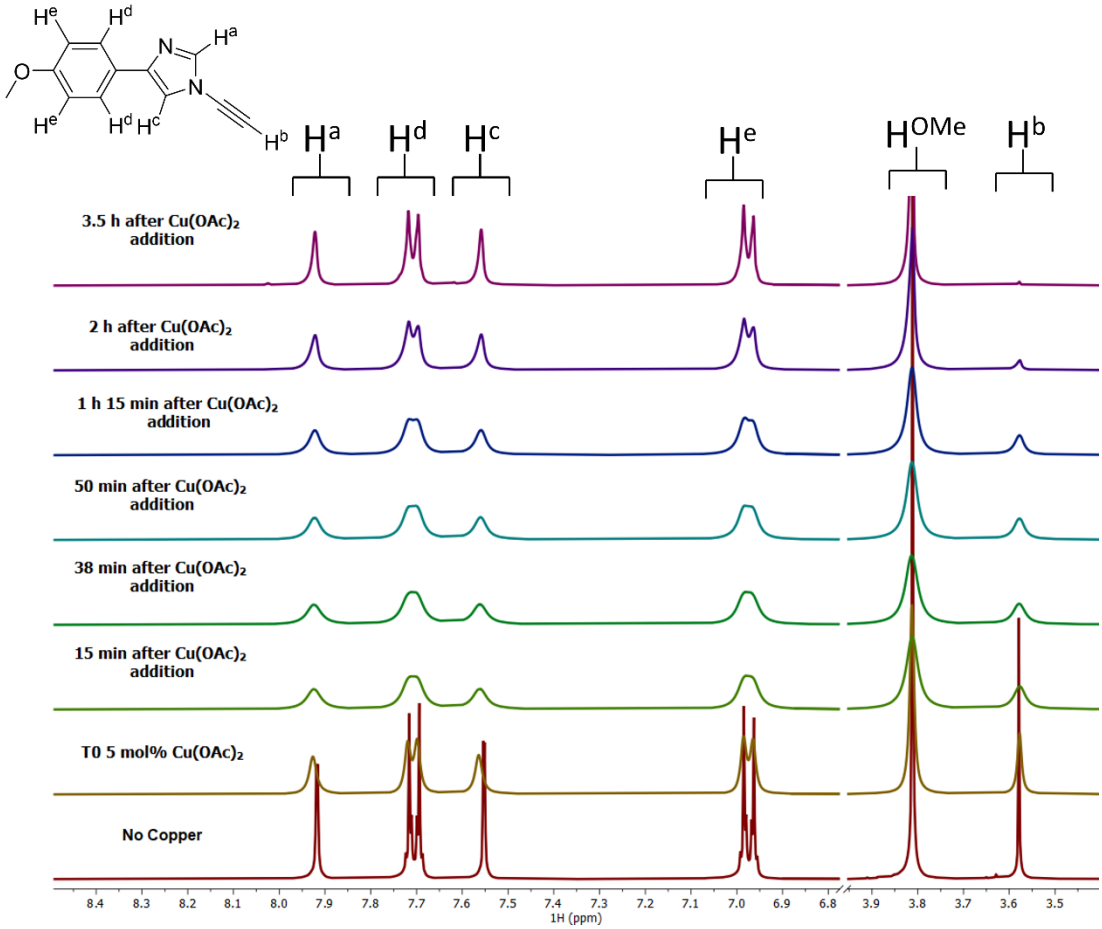

Figure 3.12. Stacked ^{1}H NMR spectra of the methoxy imidazole ynamine undergoing HDE. The red line is the control sample without $Cu(OAc)_2$, with other lines showing how the broadening changes at selected times during the reaction, from the initial addition of $Cu(OAc)_2$ to the final spectra obtained.

When the broadening in Figure 3.12 is compared to the progress of the HDE for **3.37**, there are similarities. As observed in Figure 3.10, the ynamine undergoes a slower induction/lag phase between 0 and 50 min, when the lines are at their broadest, before the sigmoidal slope increases in gradient, overlapping with the period in which the peak resolution starts to slowly reappear. This suggest that the slow complex formation is hindering the HDE, and potentially, once a critical point is reached the HDE speed increases.

To investigate the effect of the Cu oxidation state, a control experiment was undertaken using methyl imidazole **3.34** and CuOAc as the Cu(I) catalyst under identical conditions as used for $Cu(OAc)_2$. For comparison, experiments with and without $Cu(OAc)_2$ were added to Figure 3.13. Despite the initially higher rate of exchange, the reaction with CuOAc does not reach full conversion – unlike when $Cu(OAc)_2$ is used as a catalyst. This could be because there is

faster initial binding of the Cu(I) to the N3, however, this is less activating than the Cu(II) resulting in less of the deuterated product formed.

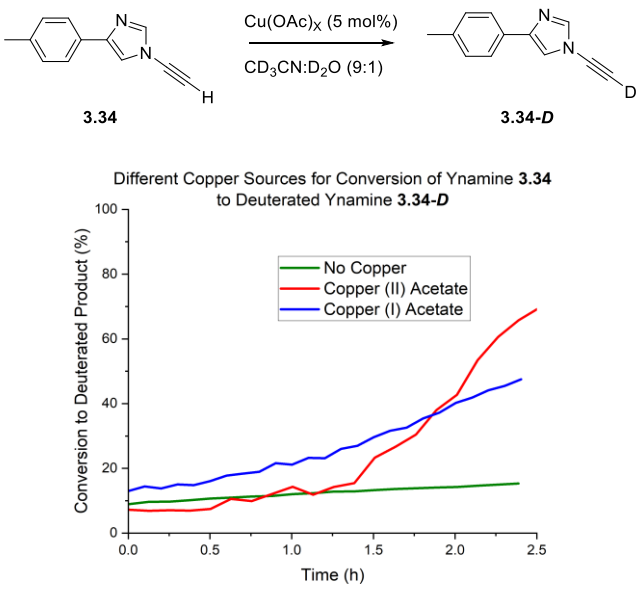

Figure 3.13. HDE of Imidazole **3.34** with 5 mol% $Cu(OAc)_2$, 5 mol% CuOAc and without copper catalyst.

3.3.1.3 Diyne Formation During HDE

Alongside the broadening of the peaks, the formation of additional, smaller peaks were also observed on the NMR spectra. These were identified as the formation of the Glaser-Hay coupling product. Typically, diyne (**3.51**) is formed using a Cu(I) source from alkyne (**3.50**), however, there is literature precedent for the formation of the diyne product using $Cu(OAc)_2$ (Scheme 3.2A).[192] In the HDE experiments, Cu(II) is initially present (Scheme 3.2B), and in the parallel work ongoing within the group, it was confirmed that this was forming the diyne.[188]

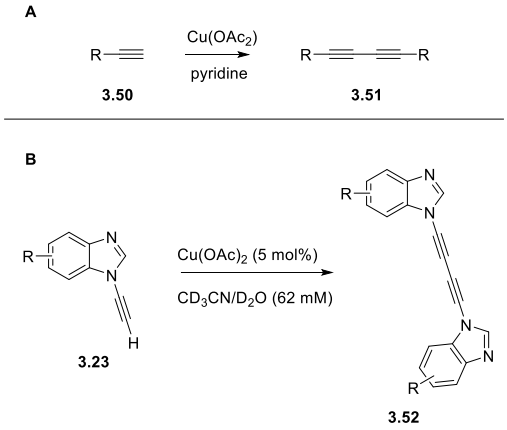

Scheme 3.2. The formation of diyne in the HDE. **A)** Formation of diyne **3.51** using Glaser-Eglinton conditions. **B)** Conditions that diyne **3.52** is formed in in the HDE experiments.

Diyne formation in this reaction suggests that the Cu(II) is being reduced to Cu(I). The diyne peaks are small peaks (observed in the red spectra) next to the parent ynamine peak. An example of the diyne formation for ynamine **3.27** is given (Figure 3.14).

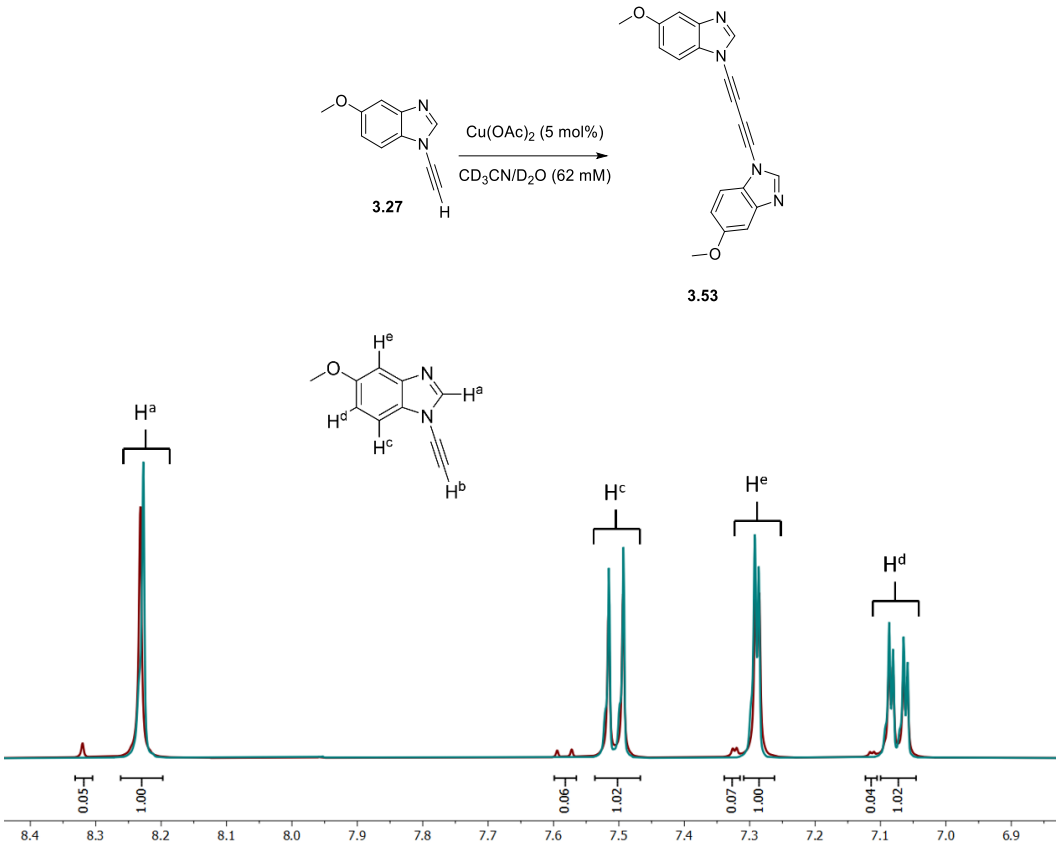

Figure 3.14. ^{1}H NMR spectra of formation of the diyne **3.53** during the HDE. Diyne peaks are observed in red.

As can be seen in Figure 3.14, the small peaks observed at 8.53, 8.33 and 8.17 ppm indicate formation of the Glaser-Hay product under HDE conditions. The integration gives a ratio of 0.05:1 consistent with the 5mol% catalytic loading of Cu(II) added to the reaction and is observed for all benzimidazoles. However, the diyne product formed in the case of the imidazoles varies: several substrates demonstrate a small amount of the diyne forming (such as **3.37**), however, for the remaining substrates no diyne side product is observed (Figure 3.15 and Table 3.3).

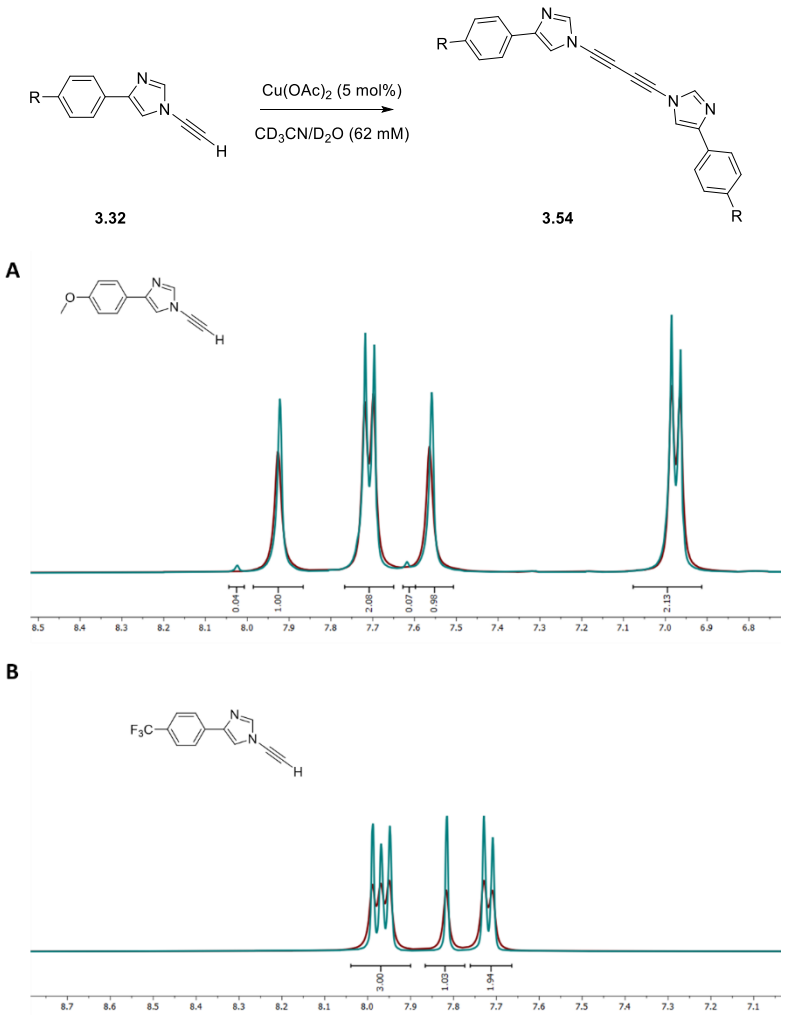

Figure 3.15. A) ^{1}H NMR spectra showing formation of diyne for **3.37**; **B)** ^{1}H NMR spectra showing no diyne formation for **3.38**.

Table 3.3. Diyne Integration on final NMR spectra of HDE

Ynamine	Functional Group	Diyne integration
3.37	Methoxy	0.04
3.36	Bromo	0.03
3.38	$-CF_3$	None observed
3.34	Me	0.03
3.35	F	0.04**
3.33	H	0.02
3.39	$-NO_2$	None observed
3.40	Biphenyl	None observed

*relative to the aromatic protons

**overlaps with the main peak

This could lead to several hypotheses including that the Cu(II) is not being reduced to Cu(I), or, alternatively, the amount of Cu(I) is small. Despite no diyne being observed, line broadening then sharpening still occurs, suggesting that the formation is happening, just at lower levels that cannot be detected. Additionally, no diyne formation was observed on the spectra when CuOAc was used. A hypothesis of this is that the imidazole is interfering with the formation of the Cu paddlewheel (**3.14**) which is needed for the formation of the diyne. The imidazole substrate could be more intrinsically activated for the CuAAC, and therefore lower amounts of Cu(I) are required to initiate the reaction, resulting in less detectable diyne formation. This may be substrate dependent, as shown by the varying levels for each ynamine. The change in curve shape for the imidazoles is also suggestive of a difference in the oxidation state of the Cu(I).

3.3.1.4 HDE Conclusions

In conclusion, monitoring the alkyne HDE of the benzimidazoles and imidazoles gave an insight into a potential difference in reactivity between the two heterocyclic series and between the substrates in both.

Substituents on the benzimidazole ring influenced the HDE, with EDGs increasing the rate of HDE and EWG reducing the rate. Difluoro ynamine **3.25** exemplified that copper binding overrules intrinsic electronic properties and leads to a stronger activation of the alkyne proton.

For imidazoles, the HDE displayed a sigmoidal curve, with an observable induction period. The HDE for methylimidazole **3.34** with CuAOc was slower than with $Cu(OAc)_2$.
This points to a difference in how benzimidazoles and imidazoles interact with $Cu(OAc)_2$. For the benzimidazole series, the rapid line broadening followed by line sharpening suggests rapid binding to $Cu(OAc)_2$ followed by reduction of Cu(II) to Cu(I) by Glaser-Hay coupling. For imidazoles, the lack of line broadening, the observed induction period and the lack of Glaser formation suggest a slower interaction with Cu(II).

3.3.2 Influence of Ynamine Substituents on CuAAC Reactivity with Benzyl Azide

To further explore the impact of substituents on ynamine reactivity and potentially establish a correlation between the alkyne reactivity and HDE, HPLC analysis was employed to monitor the CuAAC reaction of both benzimidazoles and imidazoles. HPLC was chosen over NMR due to its enhanced sensitivity and low limit of detection, facilitating the detection of side products generated during the reaction (*e.g.* Glaser-Hay side product). Additionally, HPLC enabled the collection of timepoints to be at shorter time intervals expediting the monitoring of the reaction initiation. These quick measurements would not have been possible *via* NMR, as exemplified by a test reaction using ynamine **3.24** (Experimental Figure 3.33).

During previous work within the group, a HPLC procedure for monitoring the CuAAC reaction has been established. The procedure for this involved carrying out the reaction in small vials using 500 µL of 62 mM reactant solution and taking 10 µL aliquots at consistent timed intervals. These aliquots were then quenched with an EDTA solution that had been optimised for Cu quenching ability. 610 µl of quench solution were used to dilute the aliquot to an appropriate concentration for the HPLC detection.

An internal standard (IS) was used in the reaction to minimise any errors. 1,3,5-Trimethoxy benzene had previously been chosen as in tests it had not interfered in the CuAAC reaction and tended to have a retention time that did not overlap with any of the starting materials or products. Calibration curves were also made to allow the ynamine and triazole in the reaction to be converted to concentration. Calibration curves can be found in the Experimental Figure 3.35.

Parallel mechanistic work carried out within the group focused on the reactivity of the dimethyl ynamine **3.13**.[188] That study showed different ynamine reactivity as function of solvent, copper loading and water content. An interesting finding was the solvent effect on the

ynamine reactivity (Figure 3.16). The CuAAC reaction was performed using 5 mol% $Cu(OAc)_2$ in MeCN, (polar aprotic solvent), IPA, methanol (polar protic solvents) and HFIP, a polar strong hydrogen bond donating solvent. IPA showed a dramatic increase of the reaction rate for the dimethyl ynamine click relative to performing the reaction in methanol or acetonitrile. No triazole product **3.56** was observed when HFIP was used as the corresponding solvent (Figure 3.16A). Surprisingly, when the reaction was performed in a mixture of HFIP with 40% water the ynamine CuAAC reaction reached full conversion to **3.56** within 2 h. The reaction was in this case quicker than when using IPA with 40% water (Figure 3.16B). Another interesting fact found with the dimethyl ynamine when using HFIP was that no side products were observed.

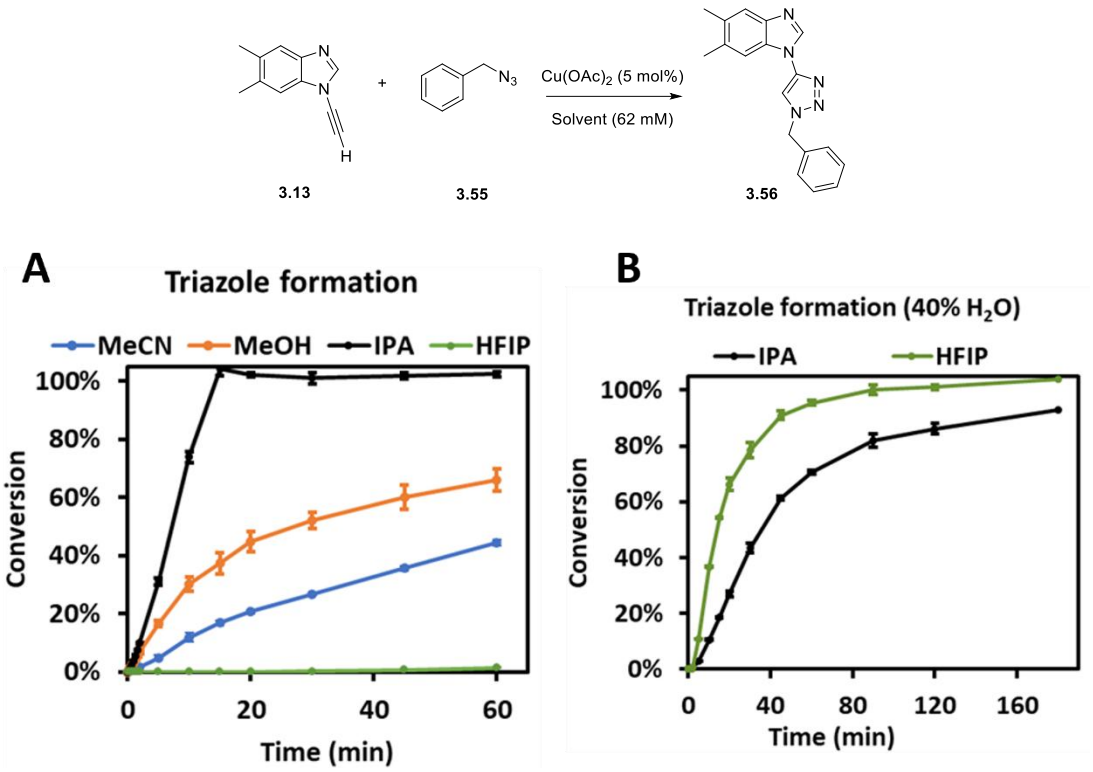

Figure 3.16. A) Formation of **3.56** in the presence MeCN, MeOH, IPA and HFIP; **B)** Formation of **3.56** in the presence of IPA/H_2O (60/40) and HFIP/H_2O (60/40). Work in this figure performed by Roderick Bunschoten.

HFIP has recently gained attention in organic synthesis due its potential to transfer protons, stabilise ionic species or other intermolecular interactions.[193] HFIP is often superior to other alternative solvents however the underlying reasons for that are still unclear. Its slight acidity (with a pK_a of 9.3) primarily enhances its role as a hydrogen bond donor within the solvent, particularly when bolstered by larger molecular assemblies that effectively boost the solvent's

capacity for forming hydrogen bonds. However, the addition of water decreases those hydrogen bonding networks with itself and competes with it. The HFIP/water mixtures play a key role in solvolytic studies and are known to change mechanism pathways depending on the percentage mixture.[194]

Based on these findings, time courses of all the new ynamine substrates in the three solvent systems (MeCN, IPA, HFIP:H_2O (60:40, by volume) were carried out using 5 mol% $Cu(OAc)_2$.

3.3.2.1 Influence of Solvent and Substituent on CuAAC reactivity of Benzimidazole Ynamines

The reactivity of the benzimidazole ynamines (**3.24-3.31**) was tested using MeCN, IPA and HFIP/water (40/60) with 5 mol% $Cu(OAc)_2$. Good solubility was observed for both the ynamines and the triazole products. The results are given in Figure 3.17 for monitoring triazole formation (Graphs for ynamine depletion are given in Experimental Figure 3.39).

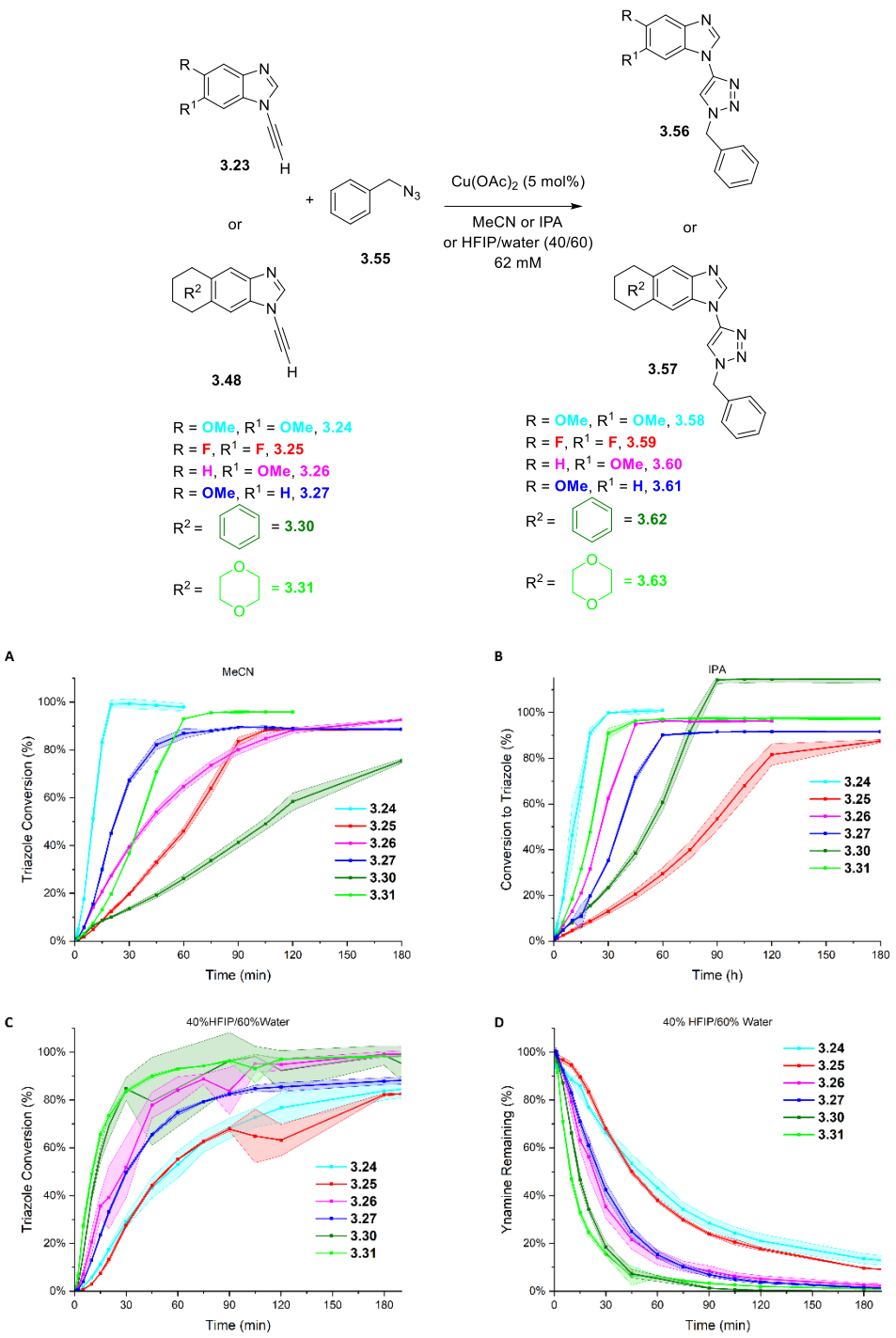

Figure 3.17. Triazole formation and ynamine depletion of the CuAAC reaction of benzimidazole ynamines using 5 mol% $Cu(OAc)_2$ in varying solvents. **A)** Triazole formation in MeCN; **B)** Triazole formation in IPA; **C)** Triazole formation in HFIP/water; **D)** Ynamine depletion in HFIP/water

As is shown in Figure 3.17A, the CuAAC reaction kinetics in MeCN for each ynamine is very different, with all of them reaching significant conversions after 2 h. In accordance with the

HDE data, the dimethoxy ynamine **3.24** is the fastest, reaching completion between 15 and 20 min. Contrary to what was observed by Zhu *et al*.[185] with a different range of alkynes there are not significant induction periods. The dioxino ynamine (**3.24**) reached full conversion within 1 h followed by one of the methoxy isomers (**3.27**). The difluoro ynamine (**3.25**) is one of the slowest only reaching full conversion after 1 h and 45 min, and the slowest napthoimidazole (**3.30**) does not reach completion within the monitoring time of 5 h. One interesting observation is the difference in the reactivity of both methoxy regioisomers (**3.26** and **3.27**) in the varying solvents. Isomer **3.27** was fastest in MeCN, however, was the slowest isomer in IPA. This suggests that the electronic effects of the OMe in positions 6 and 7 are having different effects on the reactivity in the CuAAC. The rate of the reaction in MeCN was tested for the two isomers containing amino functional groups (**3.28** and **3.29**) and the rates were very similar (Experimental Figure 3.36), suggesting that the unique reactivity of the OMe group is the cause of this disparity.

Unexpectedly, the kinetics of CuAAC for benzimidazole ynamines underwent a shift when transitioning to a protic solvent such as IPA (pK_a 17.1) (Figure 3.17B). Notably, the dimethoxy ynamine **3.24** exhibited a slight deceleration, now completing in approximately 45 min. Furthermore, the two OMe isomers exchanged positions, with isomer 1 **3.26** displaying the fastest reaction rate. In general, all the ynamines with electron donating substituents (**3.24, 3.26, 3.27, 3.31**) reached full conversion in 1 h. The difference in reactivity of this substrates is much pronounced in acetonitrile than in IPA, potentially indicating a switch in the RDS of the CuAAC. However, the most significant difference was observed with the difluoro ynamine **3.25**, which proved to be the slowest, reaching full conversion only after 3 hours.

Switching the reaction solvent to HFIP/water (40%/60%) resulted in a change in the reactivity profile. When carrying out the reactions it was observed that the reactants, or products, were not as soluble in the HFIP/water mixture as in other solvents. For some of the reactions, there was insoluble material, believed to be triazole, present after the reaction had started running that may have resulted in errors in pipetting, and therefore larger errors in HPLC analysis of the triazole product formation. In this case, both, triazole formation and ynamine depletion graphs are shown (Figure 3.17C and D). Unexpectedly, in this case the dimethoxy ynamine **3.24** is as slow as the difluoro **3.25** (not reaching completion in 2 h) and **3.30** became the quickest reaching full conversion in 1 h and 30 min. This surprising change of trend could come from the different interactions of the ynamine substrates with the solvent. If the

interaction *via* hydrogen bonding with HFIP and water forms stable clusters with the ynamine, the reaction would be slower. **3.30** is also the most lipophilic ynamine, potentially suggesting that "on-water" effect could be impacting the reaction. This showcases that the reaction kinetics not only depends on the electronic properties of the ynamine substituents but on other factors like interaction with the solvent, steric properties, or copper complexation ability.

The nature of the substituents influences on the ynamine reactivity, however, contrary to what has been reported previously, it does not correlate with the alkyne acidity, with the exceptions of the fastest and slowest extremes **3.24** and **3.30** in MeCN. This observation could be related though with the ability of the alkyne to form the homocoupling product and therefore reduce Cu(II) to Cu(I) for the reaction to proceed. Another potential reasoning for the changes between the substrates could be that the electronic effects of the substituents are causing alterations in the HUMO and LUMO. However, it was previously found that although the ynamine causes a higher lower LUMO than an aliphatic alkyne, the change in substituents does not have a major effect and so subsequently this can be ruled out as a cause of the difference in reactivity. Looking individually each ynamine, it becomes clearer the impact of the solvent as function of the substituent (Figure 3.18).

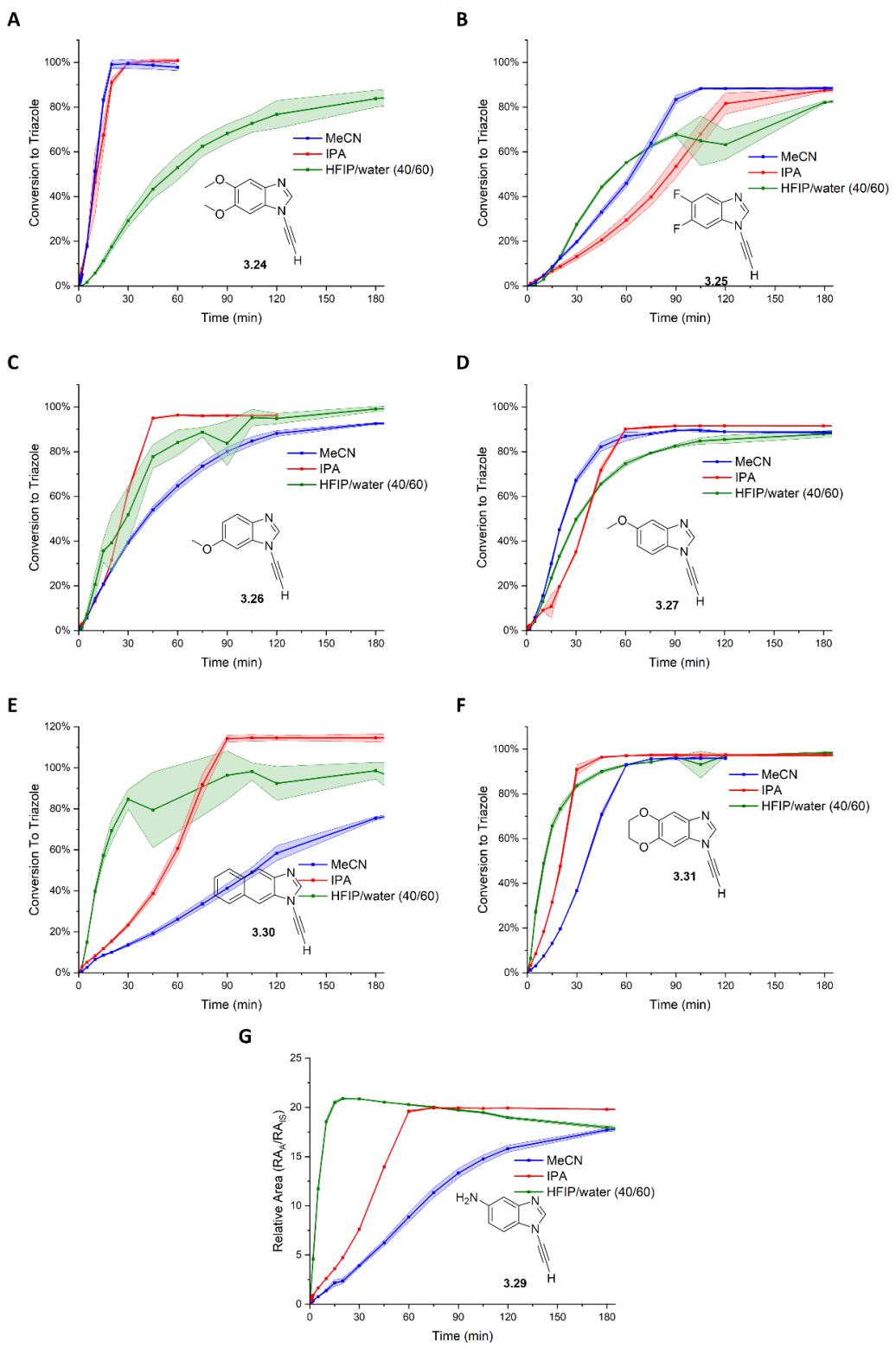

Figure 3.18. Differences in the formation of the triazole product for each benzimidazole ynamine in the CuAAC in differing solvents using 5 mol% $Cu(OAc)_2$.**A)** Ynamine **3.24; B)** Ynamine **3.25**; **C)** Ynamine **3.26**; **D)** Ynamine **3.27**; **E)** Ynamine **3.30**; **E)** Ynamine **3.31; G)** Ynamine **3.29**.

The influence of the solvent is dramatic for the dimethoxy ynamine **3.24** (Figure 3.18A) and **3.30** (Figure 3.21E), whereas compounds **3.25, 3.26, 3.27** and **3.31** are only weakly affected. Ynamines **3.24** and **3.30** exhibited opposite reactivities. Dimethoxy **3.24** has the quickest reaction rates in both MeCN and IPA, however, HFIP/H_2O slows down the reaction becoming one of the slowest overall. Naphto **3.30**, exhibits the slowest rate in MeCN not reaching completion in 2 h, the reaction is accelerated in IPA, and shows the quickest rate in HFIP/ H_2O.

Ynamine **3.29**, a benzimidazole containing an amine functional group, is given in Figure 3.18G. Due to solubility issues when obtaining a calibration curve, data from this ynamine was unable to be plotted in Figure 3.17, instead, the area of the analyte of interest in relation to the internal standard is plotted. The reactivity in HFIP is extremely fast compared to MeCN. Potentially, this can be explained by the acidity of HFIP which might lead to the protonation of the aniline nitrogen and prevention of futile copper catalyst binding.
The comparison between the dioxino **3.31** and the dimethoxy **3.24** is even more unexpected. **3.31** is not slowed down by the solvent change to HFIP/water. The obvious difference between both is the restricted conformation that **3.31** confers to the ynamine (Figure 3.19A). HFIP, could be interacting *via* hydrogen bonding between both OMe in the dimethoxy and not allowing the interaction with Cu(II) as illustrated in Figure 3.19B.

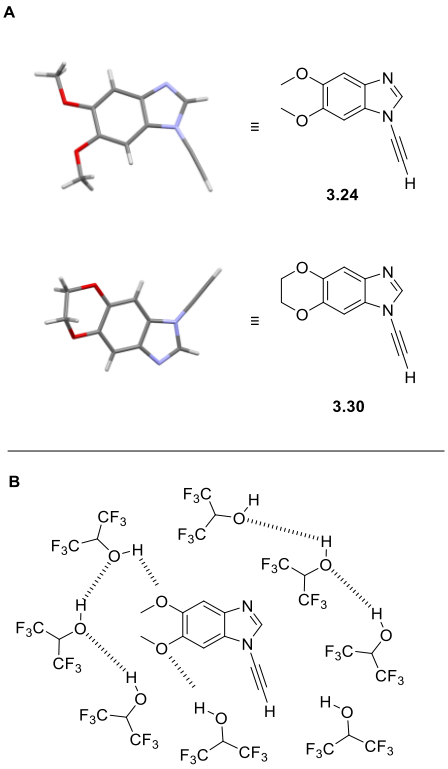

Figure 3.19. A) Single crystal structure of **3.24** and **3.30; B)** Potential ynamine/HFIP hydrogen bond network

Conversely, **3.30** reacted more rapidly in IPA compared to MeCN. The crystal structure of **3.30** indicated the potential for π-stacking (Figure 3.20B). IPA could be disruptive to the bond system, whereas MeCN is not. However, it is important to note that the crystal structures are obtained in a solid crystalline form, and addition of solvent can dramatically alter the characteristics of the molecule.

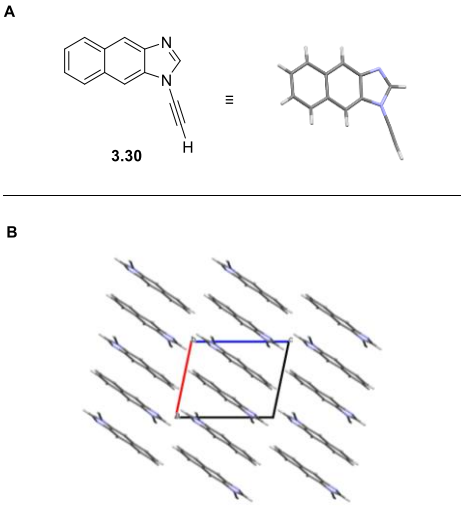

Figure 3.20. A) Crystal structure of **3.30; B)** Packing view of **3.30.**

A further potential possibility that was explored for the difference between the substrates was the length of the alkyne C≡C bond and the terminal C-H bond. The crystal structures that were obtained were used for this, however, there was no significant changes in length of these bond (Data given in Experimental 3.5.5.7).

3.3.2.2 Benzimidazole Side Product Formation during CuAAC

During the monitoring by HPLC, the formation of other peaks was observed. During previous work within the group on the dimethyl ynamine (**3.13**), side products **3.15** and **3.64** were isolated and the mass ion of **3.65** was observed on LC-MS. The structures are shown in Figure 3.21.

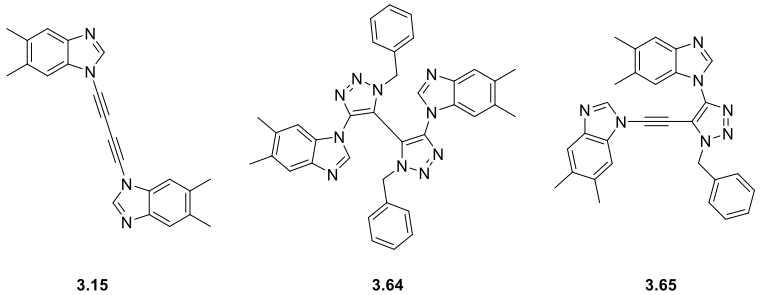

Figure 3.21. Side products formed during the CuAAC. The Glaser-Hay product **3.15**, the triazole complex **3.64** and the ynamine-triazole complex **3.65**.

The Glaser-Hay coupling is expected from the reduction of Cu(II) to Cu(I) as part of the mechanism. However, the other side products were unexpected by-products and are likely to

have formed before the protodematallation step (Figure 3.2), when Cu is chelating to the triazole (**3.21**) as Cu is also a ligand.[195,196] For 2 benzimidazole ynamines (**3.24** and **3.25**), sufficient quantities of the ynamine were synthesised to allow for a Glaser-Hay coupling reaction (Scheme 3.3) to give **3.67** and **3.68** respectively. Following the reaction, a basic work up was attempted, and the product obtained dried, however, a detailed analysis of the product was not carried out due to limited solubility and mass. The existence of the diyne **3.67** or **3.68** was confirmed by either ^{1}H NMR, HRMS or LCMS. The data is given in the Experimental Section 3.6.4.

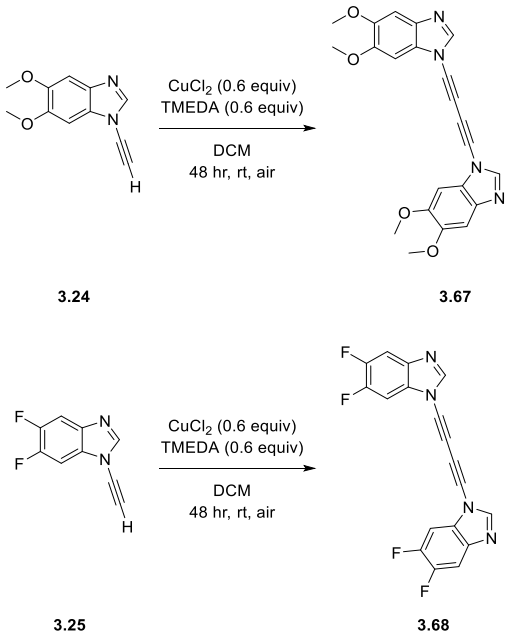

Scheme 3.3. Formation of diyne for ynamines **3.24** and **3.25**. Reaction conditions: $CuCl_2$ (0.6 equiv), TMEDA (0.6 equiv), DCM, rt, 48 h.

The retention times of the diyne products **3.67** and **3.68** were obtained by analysing a sample in the quench mixture used for the HPLC reaction on the HPLC using the same methods. This allowed the comparison of diyne formation in MeCN and IPA for ynamines **3.24** and **3.25** (Figure 3.22A and B). As no calibration curve has been obtained, the peak areas were divided by the area of the IS, therefore, the numbers are not quantitative and cannot be compared between the different ynamines, as they may give different UV readouts. HPLC traces can clearly show the formation of the diyne, in addition to other side products. The HPLC trace for **3.24** in IPA (Figure 3.22C) shows the diyne product as the latter smaller peak of the two side products, and the other side product formed overlaps with the benzyl azide peak. The HPLC trace for **3.25** in MeCN (Figure 3.22D) shows two side products with very similar RT.

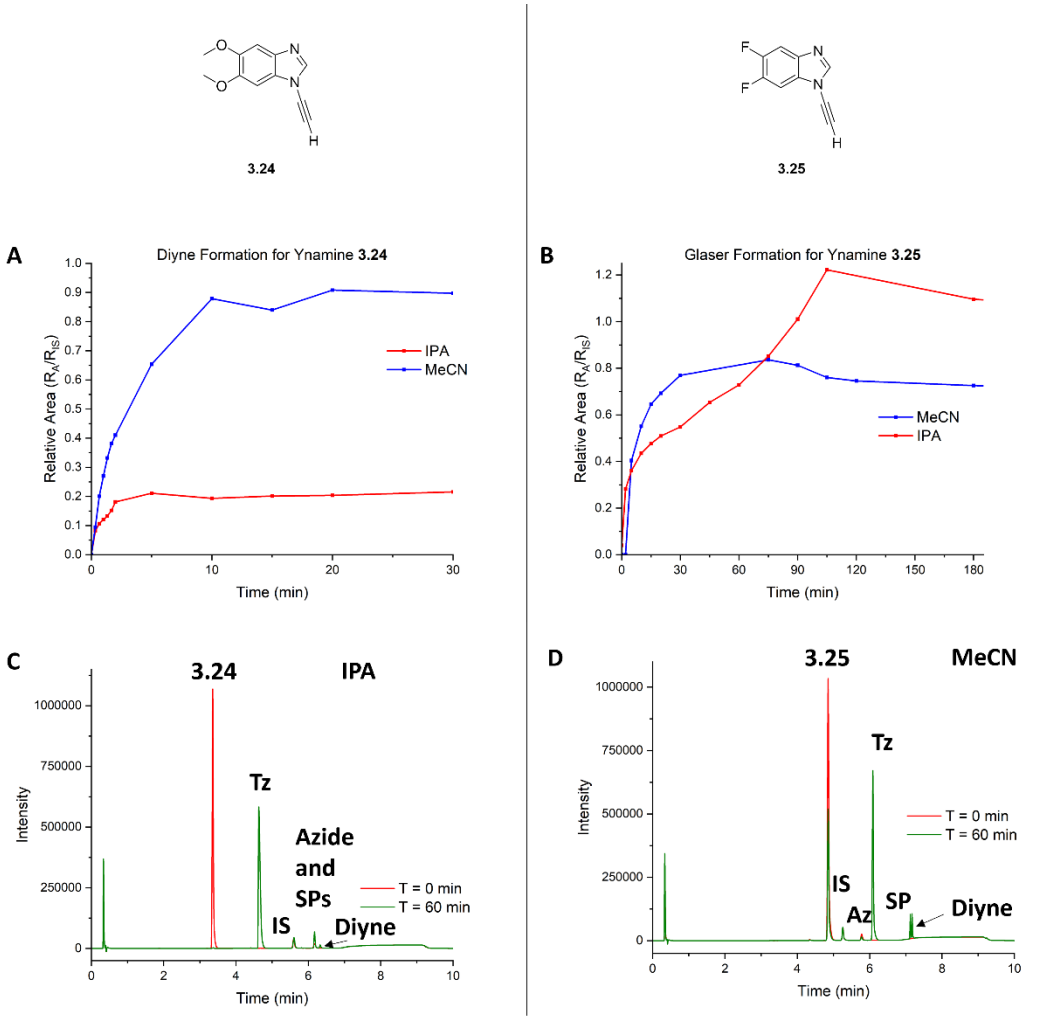

Figure 3.22. Side product formation and HPLC traces for ynamines **3.24** and **3.25**. **A)** Diyne formation during the CuAAC for **3.24** in IPA and MeCN; **B)** Diyne formation during the CuAAC for **3.25** in IPA and MeCN; **C)** HPLC trace for the CuAAC for **3.24** in IPA at T = 0 min (red) and T = 60 min (green); **D)** HPLC trace for the CuAAC for **3.25** in MeCN at T = 0 min (red) and T = 60 min (green).

Ynamine **3.24** produces more diyne in MeCN than in IPA, however, in MeCN, the diyne is slower, despite MeCN being the fastest reaction. This suggests that the rate of the reaction may align more closely with diyne formation in MeCN than in IPA. For ynamine **3.25**, the formation of diyne in MeCN also levels off after an hour and then experiences a slight fall. The difference between these two benzimidazole ynamines and the formation of diyne suggests that this could be playing a role in the reactivity differences.

However, when a HFIP/water (40/60) system is used, there is no side product formation (Experimental Figure 3.40). The presence of the diyne for the other solvents suggests that the

Cu(I) species is present in the reaction, however, for the HFIP/water system the lack of diyne formation suggests that there may be no Cu(I) present in the reaction: the solvent could mediate a different mechanism for the ynamine-alkyne reaction. This hypothesis has not been further explored in this work.

3.3.2.3 Benzimidazole Summary

A summary of the results for the benzimidazoles is given in Figure 3.23.

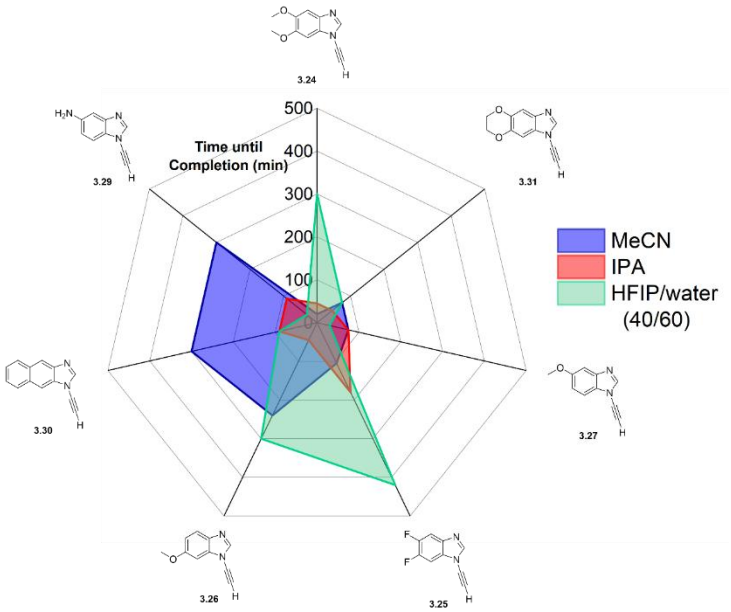

Figure 3.23. Summary of the benzimidazole ynamine results for the CuAAC in IPA, MeCN and HFIP/water (40/60), by time until completion.

From this, the differences between the solvents are clear. IPA, although not the fastest for each individual ynamine (*e.g.* **3.24**), can generally be found to have fast reaction rates. MeCN is more variable, and a HFIP/water solvent system is best avoided due to erratic reaction rates and insolubility, unless a clean reaction profile without small percentages of side products is required.

3.3.2.4 Influence of Solvent and Substituent on CuAAC reactivity of Imidazole Ynamines

Following on from the successful testing of the benzimidazole ynamines, the imidazole ynamines were tested in the same way. Graphs showing the formation of the corresponding imidazole triazole are given in Figure 3.24, and the fastest to slowest imidazoles for each solvent are illustrated.

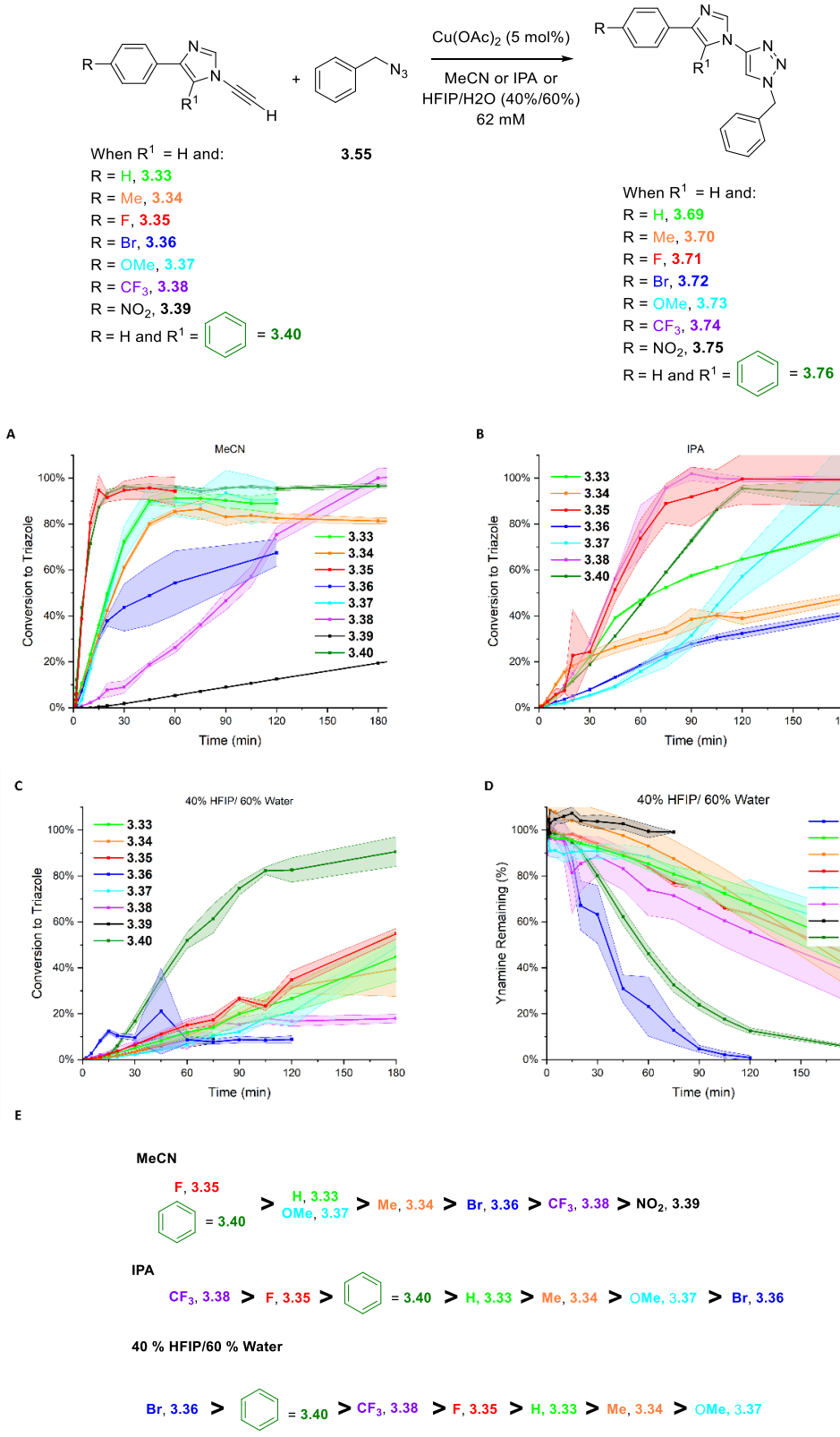

Figure 3.24. CuAAC of the imidazole ynamines in 5 mol% $Cu(OAc)_2$. **A)** Triazole formation in MeCN; **B)** Triazole formation in IPA; **C)** Triazole formation in 40% HFIP/Water; **D)** Ynamine depletion in HFIP/water (40/60); **E)** Ranking of the substituents in each solvent.

The first observation when comparing the imidazole ynamine kinetic plots with the benzimidazole ones is the larger error bars in MeCN and IPA (Figure 3.24A and B). During these set of time courses, a precipitate appearance was noticed as the reaction proceeded, forming triazole products insoluble in the reaction solvent. This phenomenon suggested that the imidazole triazole is more insoluble than the ynamine substrate and Cu complexes. The graphs showing ynamine depletion for these show a gradual depletion of the ynamine without the large error bars (Experimental Figure 3.38). The precipitation could affect the kinetic process therefore the data for the imidazole ynamines can be taken as semi-quantitative.

All the imidazole ynamines except the nitro and bromo (**3.39** and **3.36**) reached full conversion in less than 1 h using MeCN. The fastest in MeCN is the imidazole **3.35** with a fluorine group, followed closely by the bulky biphenyl imidazole **3.40**. The methoxy imidazole **3.37** is slower compared to the dimethoxy benzimidazole **3.24**, however, it is similar to OMe isomer 2, **3.27**, which has a similar electronic effect due to the placing of the para OMe to the ynamine. The slowest imidazole tested in MeCN is the imidazole containing the EW nitro group **3.39**. This imidazole was monitored for 7 hours and did not reach completion. The second slowest was imidazole **3.38**, containing the strongly electron withdrawing trifluoromethyl group. The bromo imidazole **3.36** does not go to completion based on the triazole formation, however, the ynamine is fully depleted – this one was quite insoluble. The alkyne acidity, as determined by HDE, does not correlate with fast reaction kinetics in the CuAAC. The fastest in HDE is **3.33**, which is the third fastest in MeCN. This, in addition to the strong EWGs being slow, suggests that there is the potential for the functional groups to be affecting the electronics from their extended system, and influencing parts of the reaction.

In IPA, the reaction rate for most substrates decreases. Interestingly, the trifluoromethyl imidazole **3.38** is the fastest, reaching completion within 90 min, faster than the reaction in MeCN.

In HFIP/water, the system was affected by solubility, with some of the ynamines and triazoles tested having low solubility, hence the ynamine depletion is also shown. The bromo imidazole **3.36** depletes in a controlled fashion suggesting a quick reaction. The biphenyl imidazole **3.40** appears to be the most soluble, given the smaller error bars and the reaction reaching completion through the monitoring of the triazole formation. This suggests that the increased

lipophilicity of the ynamine may increase speed in HFIP/H_2O as was observed with benzimidazole **3.30**.

Looking individually each ynamine, it becomes clearer the impact of the solvent as function of the substituent (Figure 3.25).

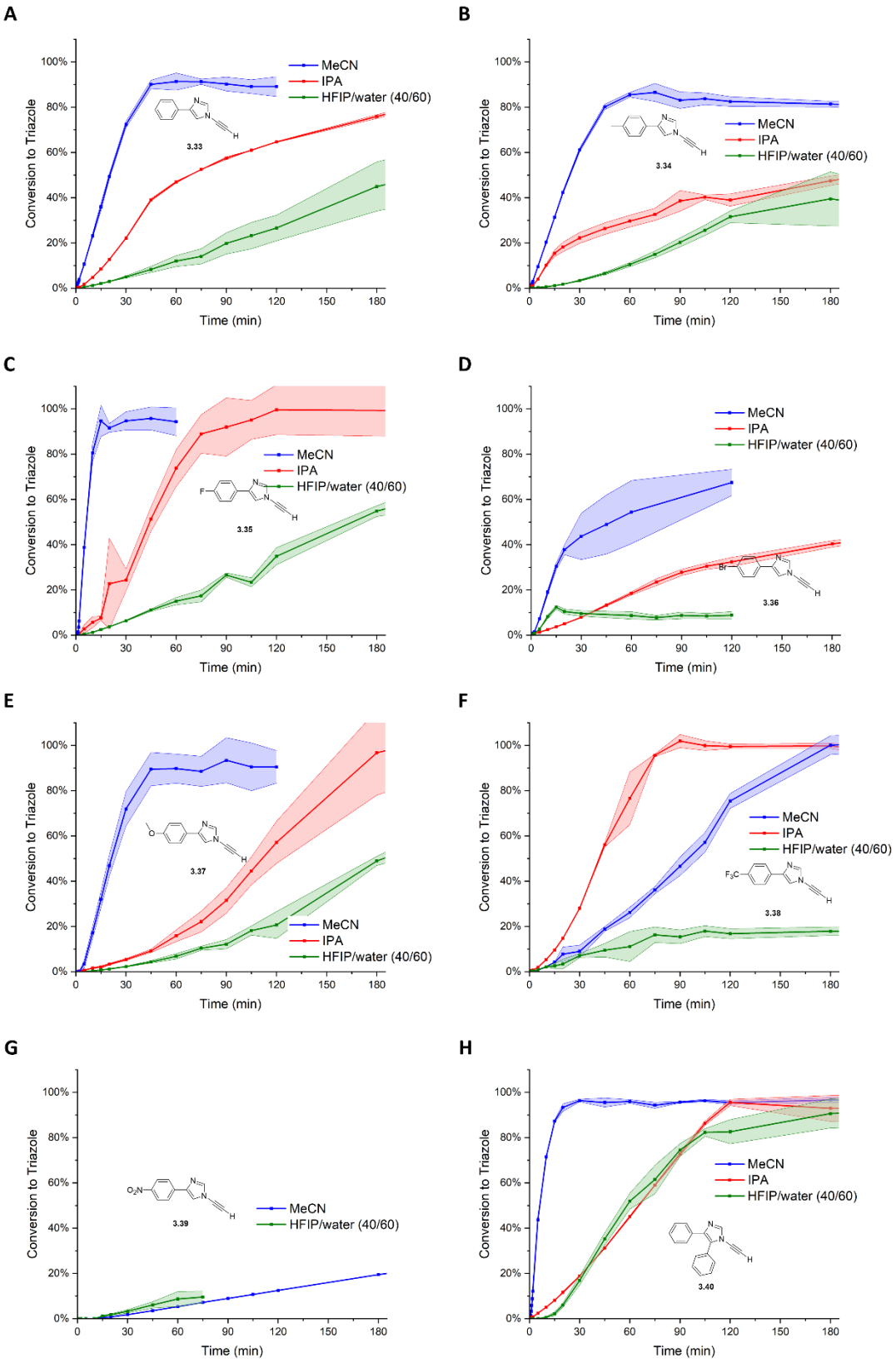

Figure 3.25. Differences in the formation of the triazole product for each ynamine in the CuAAC in differing solvents using 5 mol% Cu(OAc)

With the exception of ynamine **3.39** with the nitro group and **3.36** with the CF_3 modality (Figure 3.25F and G), MeCN is the superior solvent for fast reaction kinetics of the imidazole ynamine. Other solvents could be potentially influenced by solubility issues. The differences indicate that the RDS is influenced by the solvent, similar to the observation with the benzimidazoles.

For the bromo imidazole **3.36** (Figure 3.25D), the product never reaches completion, however, the ynamine depletion (Experimental Figure 3.38), shows that any potential benefit the imidazole has in reaction rate, is lost in the insolubility of the product. This is unfortunate, and other solvent systems could be investigated for the bromine group, as the halogen is a useful handle for further chemistry.

The fluoro imidazole **3.35** (Figure 3.25C) appears to be largely affected by the solvent, with MeCN being very fast (15 min), other systems slower. This speed in MeCN differs from the comparable benzimidazole. The methoxy imidazole **3.37** (Figure 3.25E) is also affected by the solvent to a large extent, suggesting that the electron donating *vs*. electron withdrawing abilities of the substrate may not be the main contributor in each solvent.

Another interesting imidazole is the biphenyl imidazole **3.40** (Figure 3.25H), which is extremely fast in MeCN (completion within 30 mins) and the time of completion significantly slows in IPA (2 h) and HFIP/water (3 h). Additionally, a lag phase in HFIP/water is observed which is not present in the other solvents. Imidazole **3.34** containing the methyl group (Figure 3.25B) also appears to display a lag phase for HFIP/water. The observation of a lag phase only for a select few conditions could suggest that the mechanism of the reaction is substrate (and solvent) dependent.

3.3.2.5 Imidazole Side Product Formation during CuAAC

Similar to the benzimidazole counterparts, the imidazole ynamines also form side products in MeCN and IPA. The diyne product (**3.77**) of **3.35** was synthesised (Scheme 3.4) to be used to attempt to determine which side product was diyne and which was the other unidentified side products. The product only underwent a work-up prior to running on the HPLC to determine RT, and hence LC-MS was used to determine formation of desired product **3.77** (Experimental Figure 3.46).

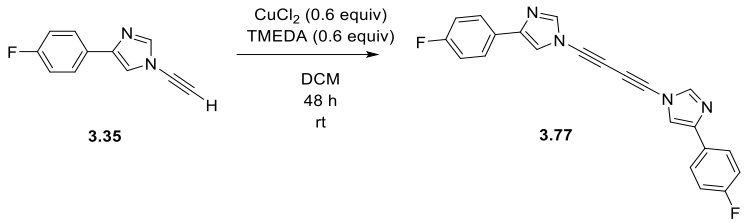

Scheme 3.4. Synthesis of **3.77** for determination of diyne formation in HPLC analysis of the CuAAC.

The CuAAC reaction of **3.35** in MeCN showed diyne formation, however, IPA did not show any diyne formation (Figure 3.26A). The reaction of **3.35** in MeCN resulted in two side product peaks appearing at retention times of 12.23 and 12.33 min (Figure 3.26B). The diyne product **3.77** gave a retention time of 12.36, so it is assumed that the peak at 12.33 min is the diyne, the relative formation of which is shown in Figure 3.26A. For the reaction carried out in IPA, only one side product was formed, at 12.2 min. however, this did not appear to be diyne (HPLC trace in Experimental Figure 3.42).

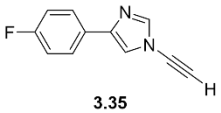

3.35

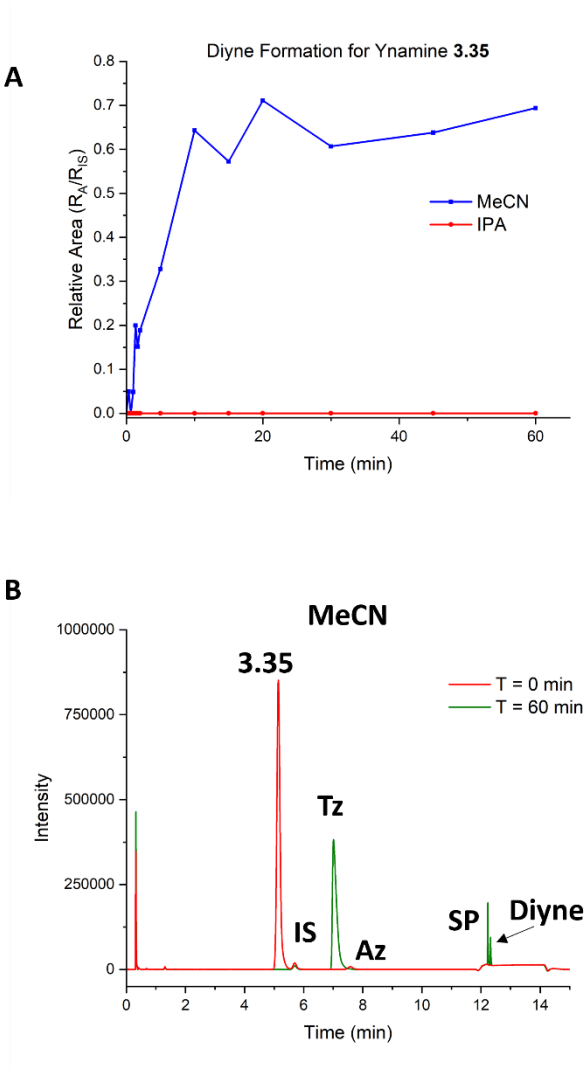

Figure 3.26. Side product formation and HPLC trace for ynamines **3.35** **A)** Diyne formation during the CuAAC for **3.35** MeCN; **B)** HPLC trace for the CuAAC for **3.35** in MeCN at T = 0 min (red) and T = 60 min (green).

Diyne is only forming in MeCN, suggesting that the Glaser reaction is not the source of Cu(I) in IPA. Potentially, Cu(I) could be formed by alcohol oxidation as suggested by Kuang *et al.*[43] The second side product peak could not be identified by LC-MS as no mass was observed due to insufficient sensitivity.

A reaction using methyl imidazole **3.34** in MeCN allowed the observation of an additional side products formed (through LC-MS analysis), in addition to the diyne (Experimental Figure 3.47). The assumed structure for the side product is the same as formed for the benzimidazole

ynamine, confirming that the overall mechanism is the same, but that solvent and substituents can have an effect on the RDS and the rate of each of the steps. A reaction using imidazole **3.38** in IPA was analysed by LC-MS, and consistent with the results obtained for **3.35**, no diyne was observed, however, m/z relating to the other two side products was observed (Figure 3.48). The ynamine-triazole side product was also observed in MeCN.

3.3.2.6 Imidazole Summary

A summary of the results for the imidazoles in each of the three solvents is given in Figure 3.27.

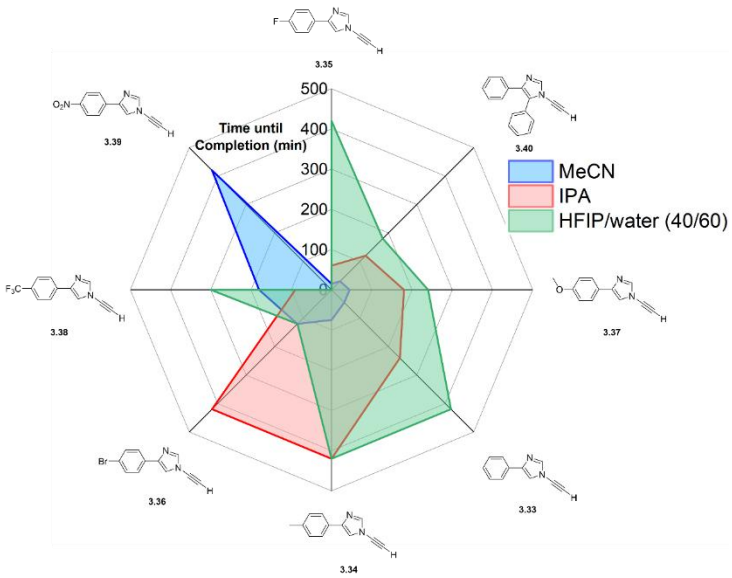

Figure 3.27. Summary of the imidazole ynamine results for the CuAAC in IPA, MeCN and HFIP/water (40/60), by time until completion.

There is large variability between the solvent and the substituent on the imidazole ynamine. MeCN appears to be consistently fast, bar the two ynamines with strong EWGs (**3.38** and **3.39**). The other solvents all vary, and this can be partly attributed to the solubility, mainly of the triazole product.

3.3.3 Influence on Copper Loading on Ynamine CuAAC Reactivity

The toxicity of copper catalyst and the major drawback of the CuAAC for bioconjugation is well documented, and as such the copper-free SPAAC is an attractive alternative method of forming a triazole. A reduction in the levels of catalyst required in the CuAAC may open it up

to more applications and reduce the likelihood of adverse side effects caused by copper. In previous experiments, 5 mol% $Cu(OAc)_2$ has been used as the catalyst. However, with the high speed of some of these reactions it was postulated that the lowering of the catalyst loading may not adversely impact reaction speed to a large degree.

The CuAAC with selected ynamines (**3.24-3.26, 3.30, 3.31**) in MeCN with 2.5 mol% $Cu(OAc)_2$ was therefore undertaken. As shown in the graphs below, ynamine **3.24** rate decreases from completion in twenty minutes to completion within forty-five. Ynamine **3.31** reaches completion within 2 h, however, the other substrates failed to reach completion within the investigated timeframe.

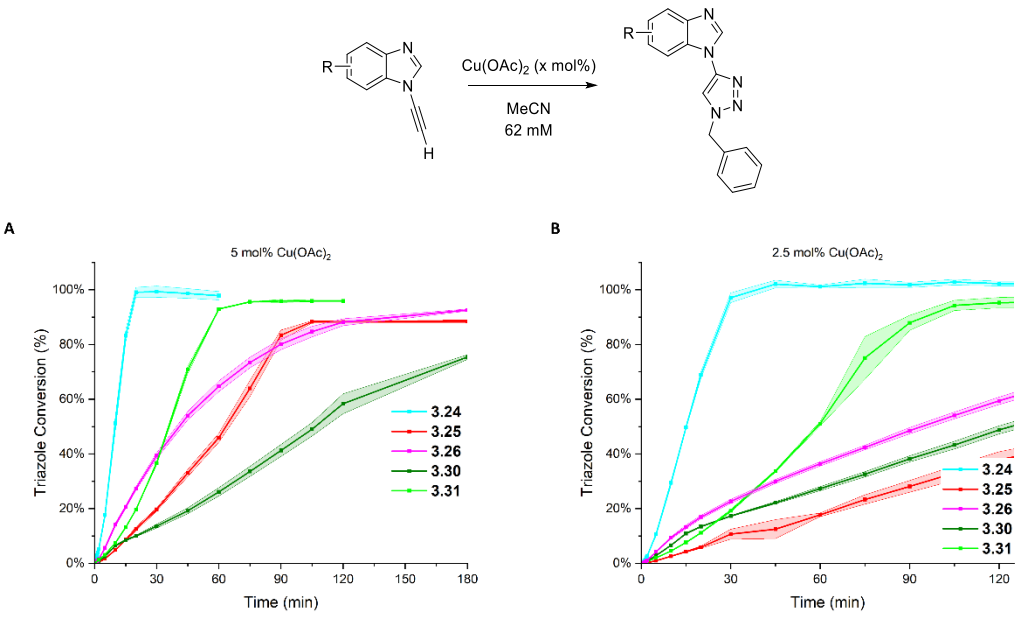

Figure 3.28. A) 5% mol $Cu(OAc)_2$; **B)** 2.5 mol% $Cu(OAc)_2$

When the lowered $Cu(OAc)_2$ conditions were applied to the imidazoles, the results varied. The imidazole with the fluorine substituent speed slowed by almost double, however, others, such as the imidazoles containing the methoxy group and with no substitution, did not show any changes in the rate (Figure 3.29).

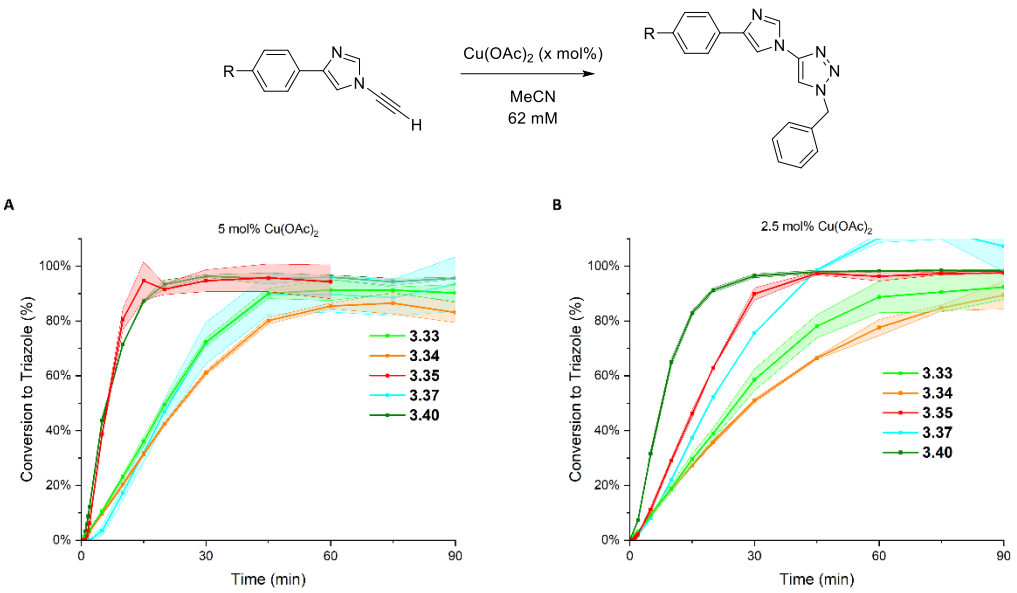

Figure 3.29. A) 5 mol% $Cu(OAc)_2$; **B)** 2.5 mol% $Cu(OAc)_2$.

This disparity between the benzimidazole and the imidazole substituent could add further evidence for differences in how the substituents react with Cu, either in its Cu(I) or Cu(II) state.

As it was observed that, for selected ynamines, lowering the copper loading did not significantly change the reaction rate, a representative benzimidazole (**3.24**) and imidazole (**3.37**) ynamine were chosen to be a part of further investigations. Copper loading was to be sequentially reduced to investigate where the limit for Cu mol% was relative to the rate. The benzimidazole **3.24** was chosen due to it being the fastest benzimidazole. The copper mol% was reduced up to 0.156 mol% $Cu(OAc)_2$ (Figure 3.30A) to investigate the limit of reactivity. The reduction in $Cu(OAc)_2$ lowering was repeated for the methoxy imidazole ynamine, but for fewer $Cu(OAc)_2$ concentrations (Figure 3.30B) due to insufficient material. The methoxy imidazole was chosen due to it being one of the imidazole that did not show a change in the reaction time on the initial halving of $Cu(OAc)_2$.

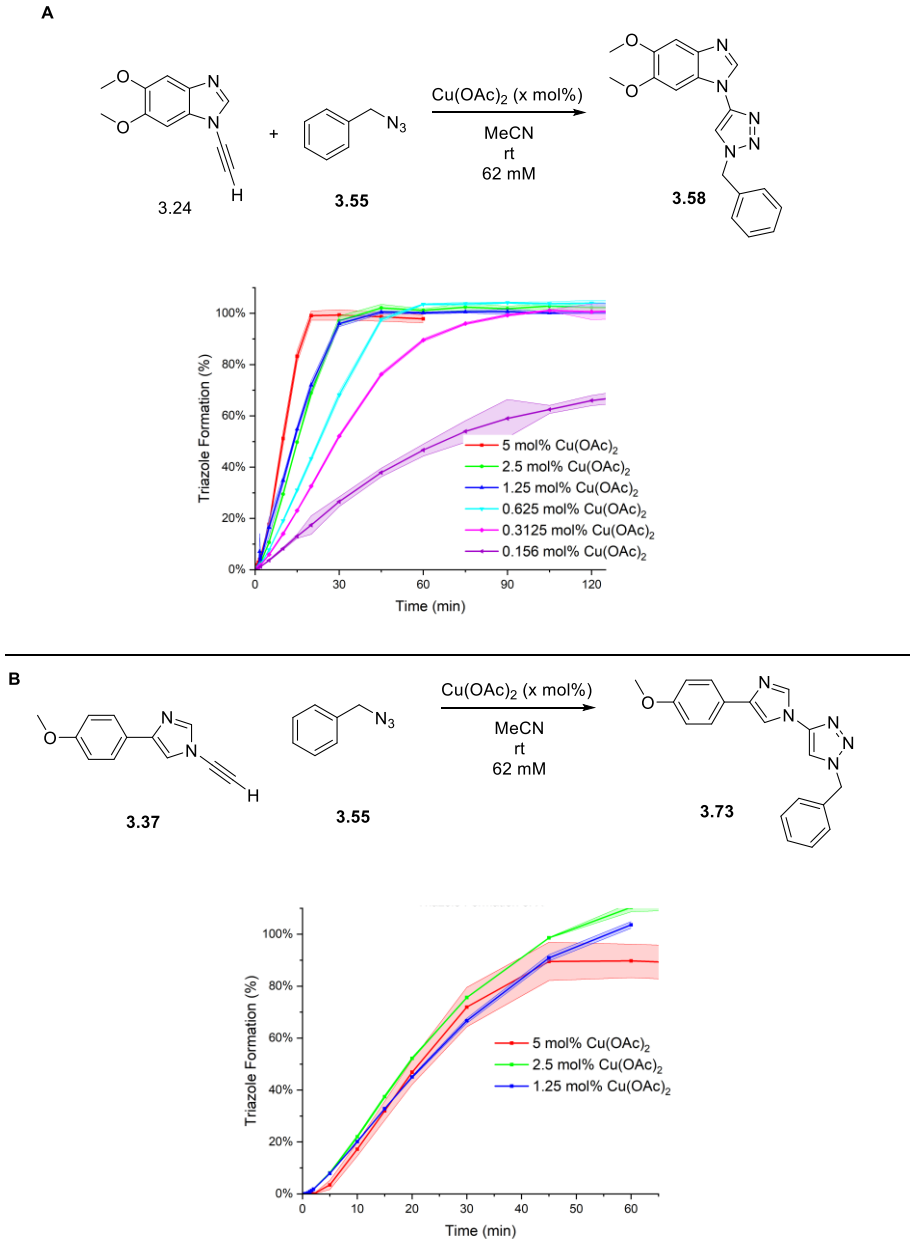

Figure 3.30. Graphs showing the conversion to triazole at varying concentrations of $Cu(OAc)_2$ in MeCN. **A)** Formation of triazole **3.58** from ynamine **3.24** and **3.55**; **B)** Formation of triazole **3.73** from **3.37** and **3.55**

As has been shown previously, the reaction is fastest in 5 mol% $Cu(OAc)_2$ for ynamine **3.24**. However, interestingly, the values for 2.5 mol% $Cu(OAc)_2$ and 1.25 mol% $Cu(OAc)_2$ are both similar, reaching completion at approximately 45 min. The reaction slows down slightly with 0.625 mol% $Cu(OAc)_2$, completing within 60 min, and for 0.312 mol% completed within 2 to 3 h. The reaction slows considerably when the copper concentration is reduced further to 0.165 mol% $Cu(OAc)_2$, with the reaction not reaching completion in 6 hours.

In contrast, lowering the copper concentration from 5 mol% to 1.25 mol% $Cu(OAc)_2$ does not have a significant effect of the rate of the reaction for the methoxy imidazole **3.35** (Figure 3.30B).

Lowering the $Cu(OAc)_2$ concentration was also explored for IPA for the dimethoxy benzimidazole **3.24** and for the fluoro imidazole **3.35** (Experimental Figure 3.39). Lowering the Cu loading from 5 mol% $Cu(OAc)_2$ to 2.5 mol% $Cu(OAc)_2$ does decrease the reaction rate slightly, from completion in approx. 20 mins to 30 mins. However, the reaction is still faster than for 2.5 mol% $Cu(OAc)_2$ in MeCN. This further suggests that in IPA, the rate of Cu(I) is not reliant on Glaser formation but potentially through alcohol oxidation. Data for the fluoro imidazole **3.35** was also obtained and the reduction to 2.5 mol% $Cu(OAc)_2$ resulted in a decrease in the rate by approx. 50%. These results indicate that the solvent choice has an impact on the reaction and shows that the copper loading can be tuned dependent on the solvent used.

3.3.4 Competition Experiments

Competition experiments were carried out with selected ynamines, specifically chosen for their contrasting electronics (*i.e.* **3.24** *vs*. **3.25**). One equiv of each ynamine, together with benzyl azide (1 equiv) and $Cu(OAc)_2$ (5 mol%) was monitored for both starting material depletion and product formation by HPLC.

3.3.4.1 Competition Experiments between Benzimidazole Ynamines

Initially, the dimethoxy ynamine and the difluoro ynamine were tested in a competition experiment in MeCN, then in IPA (Figure 3.31). These two ynamines were chosen due to their contrasting speeds in MeCN and IPA, with **3.24** showing higher reactivity than **3.25** in both solvents when tested individually.

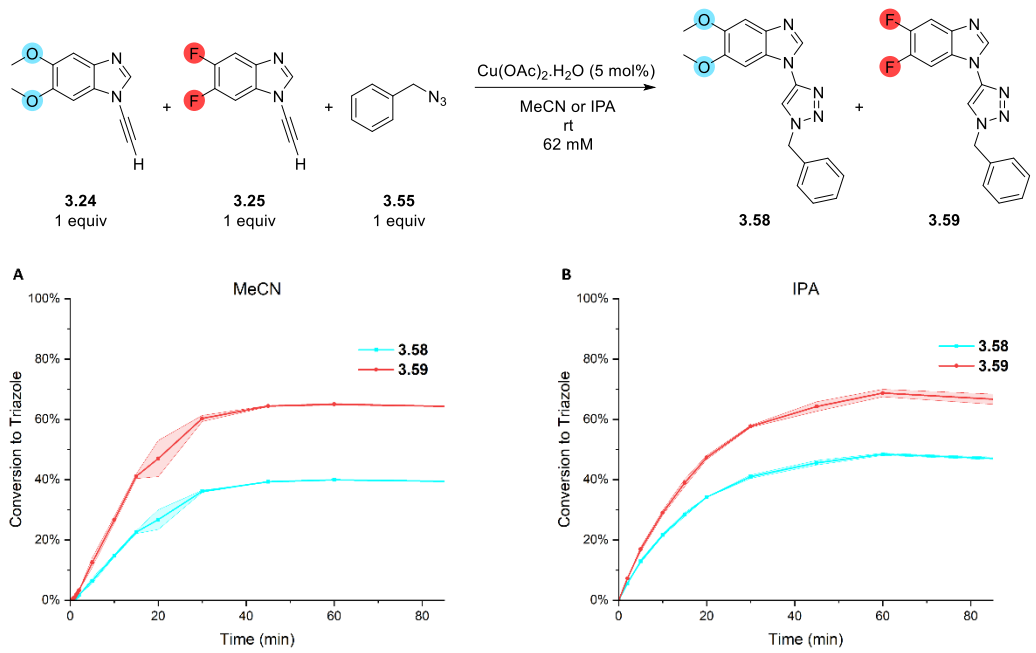

Figure 3.31. Formation of triazoles **3.58** and **3.59** from ynamines **3.24** and **3.25** and **3.55** in MeCN or IPA using 5 mol% $Cu(OAc)_2.H_2O$.

As is shown in Figure 3.31A, after benzyl azide **3.55** has been consumed at approx. 60 mins there is over 60% conversion to the difluoro triazole **3.59**, compared to just under 40% conversion to dimethoxy triazole **3.58**. These results vary largely from when the ynamines are reacted individually and the dimethoxy ynamine **3.24** is complete within 20 min and difluoro ynamine **3.25** within 60 min.

The competition experiment was repeated using NMR monitoring in *d*-MeCN and the results were consistent, with approx. 33% of the triazole of **3.24** formed and 66% of the triazole of **3.25** formed (Experimental Figure 3.34).

These results are suggestive that the mechanism governing the kinetics for the triazole formation are complex. Both the rate of Cu(I) formation (either through Glaser coupling or alcohol oxidation) and the inherent CuAAC reactivity of the substrates determine reactivity. In isolation, the methoxy ynamine **3.24** is superior to **3.25** in diyne formation and the CuAAC rate is not limited by access to Cu(I). In combination, difluoro ynamine **3.25** can benefit from the accelerated Cu(I) formation based on its inherent higher reactivity. Additionally, the fact that the triazole products could also act as CuAAC accelerating ligands further complicates

the competition experiments and could result in difluoro ynamine **3.25** outcompeting dimethoxy **3.24.**

3.3.4.2 Competition Experiments between Fastest Benzimidazole and Fastest Imidazole

The competition experiment was carried out with dimethoxy benzimidazole **3.24** and fluoro imidazole **3.35**. These were chosen as they are the fastest in each of their heterocycle categories (**3.24** completing in 20 min in MeCN and **3.35** completing in 15 min in MeCN).

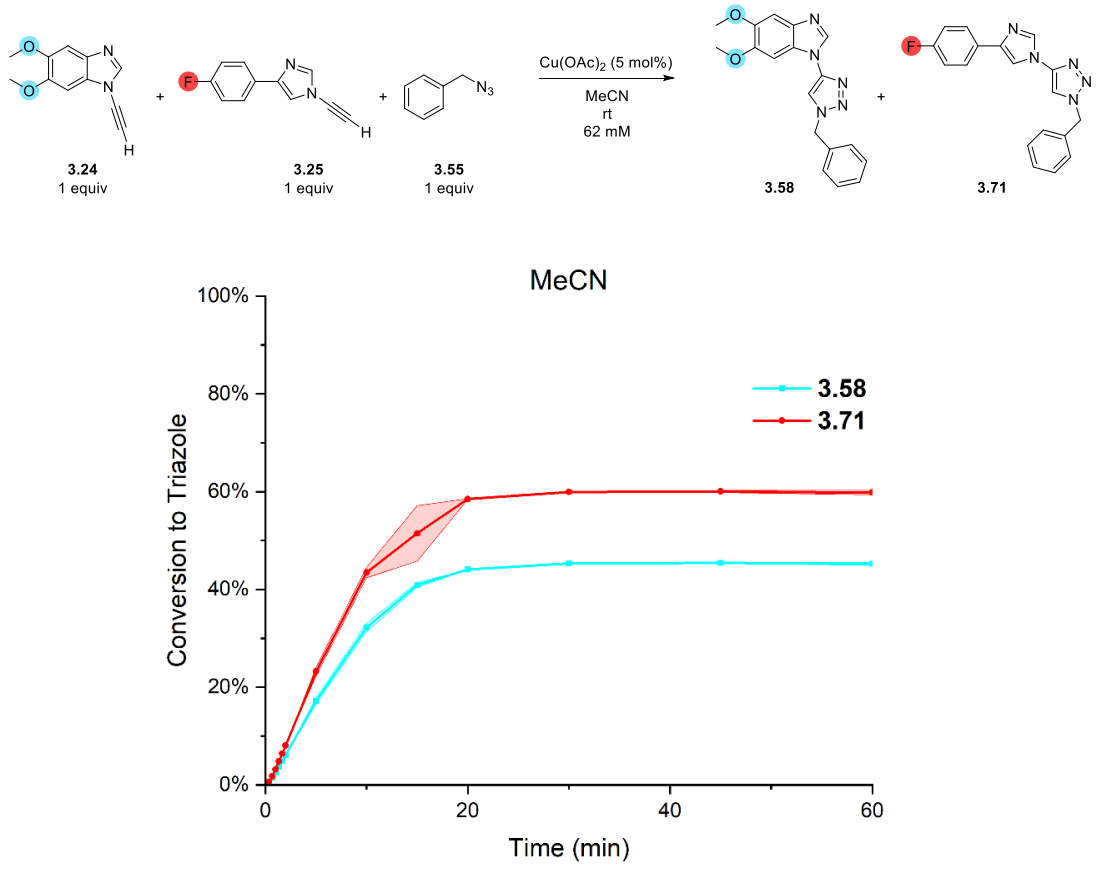

Figure 3.32. Formation of triazoles **3.58** and **3.71** from ynamines **3.24** and **3.71** and azide **3.55** in MeCN using 5 mol% $Cu(OAc)_2.H_2O$.

Figure 3.32 shows that the dimethoxy ynamine **3.24** is outcompeted again, forming just over 40% of the respective triazole **3.58**. However, the fluoro forms approx. 60% of **3.71**. The reaction is also over within 20 mins. This again suggests that **3.24** might be a good sacrificial reductant to form Cu(I) and could act as a good ligand for the CuAAC reaction. LC-MS analysis of the reaction mixture was inconclusive.

In the future, several experiments could be performed:
(1) the reactions could be repeated with a Cu(I) source to eliminate the diyne coupling as a variable;
(2) a small amount of triazole product of the dimethoxy ynamine (**3.58**) could be added to a reaction of difluoro **3.25** to test the triazole product ability as a ligand.

3.4 Summary and Future Work

In conclusion, the CuAAC reactivity of several novel ynamines was investigated. Variations included the type of heterocycle (imidazole *vs*. benzimidazole), substituent pattern, substitution electronics, the solvent used and the catalyst loading.

The initial investigation focused on the acidity of the alkyne using HDE monitoring by ^{1}H NMR spectroscopy. Electron-donating ynamines displayed faster HDE compared to electron-withdrawing substrates. Ynamine **3.24**, containing methoxy groups, outperformed **3.25**, with two fluorine's. However, upon conducting the reaction with no copper catalyst, the HDE progressed faster than with $Cu(OAc)_2$ present, suggesting that the interaction of the ynamine with $Cu(OAc)_2$ dominates over any inherent reactivity. Additionally, the rate of HDE differed between benzimidazoles and imidazoles with imidazoles displaying a sigmoidal HDE trend. There was a difference in curve shape, ppm shifts of the signal when Cu(II) is present, and diyne formation. During the HDE, upon addition of $Cu(OAc)_2$, the benzimidazole ynamines displayed a broadening of the peaks and a shift in ppm; for the imidazoles, this shift in ppm was not observed, although peak broadening was. The presence of diyne after completion of the HDE was pronounced, with more typically being detected with the benzimidazole ynamines.

Following the HDE experiments, the CuAAC was investigated using HPLC. Different solvents were tested for each ynamine with benzyl azide. It was found that the solvent used played a large part in the reaction, and that triazole solubility varied for each substituent in each ynamine. For imidazole ynamines, typically, MeCN was the faster solvent and had less solubility issues. The substrates on the ynamine scaffold can have an effect, however, it was not possible to determine if this effect comes from copper binding to the functional group, or the electronics altering N3 binding of copper. Further work is necessary to determine this. The side products formed in each solvent system indicates that the solvent is impacting on the

mechanism of the reaction. The lack of any side products in HFIP/water shows that, despite solubility issues, this solvent system is useful if a mostly clean reaction profile is required.

Lowering $Cu(OAc)_2$ loading generally decreased reaction rate, but reasonable reaction rate could still be achieved with a catalyst loading as low as 0.3 mol% using dimethoxy ynamine **3.24**. The outlier was imidazole **3.37** which did not decrease in reactivity upon reducing $Cu(OAc)_2$ from 5 to 1.25 mol%. These results are encouraging for potential application in a biological setting.

The competition experiments showed that the reactivity of an ynamine in a (3+2) cycloaddition reaction is influenced by the presence of other ynamine substrates. For the dimethoxy ynamine **3.24**, the introduction of the difluoro ynamine **3.25** slowed down its reaction, and the reverse was true for **3.25** which saw it reacting faster. This is an interesting phenomenon, which could be caused by several factors, such as rate of diyne formation, inherent ynamine reactivity and the ability of triazoles to act as CuAAC ligands.

Further work could explore these differences in reactivity. A full solvent screen on selected representative ynamines, such as **3.24** and **3.35** due to their high rates in MeCN, may provide clarity about what types of solvents accelerate these reactions. Exploring more of the reaction using a part aqueous system, such as $MeCN/H_2O$ could explore the potential "on-water" effect further for ynamine **3.30**. A Hammett plot for the imidazole ynamines may provide more insight into the impacts of electronics on the rate of reaction. Further substrates could also be synthesised, with groups added at the 8 and 5 position of the benzimidazole, and ortho and meta on the imidazole substrate. This study would investigate the electronic effects of the substituents. The methoxy group would be a useful functional group to initially investigate, due to differences observed between the 6,7-substitutued and the 6- and 7- singular substituted benzimidazole.

Until now, the literature published on ynamine reactivity in the CuAAC has focused on the benzimidazole scaffold. However, this chapter has shown that the reactivity of the ynamine can differ when different heterocycles are used and that there could be interesting mechanistic investigations to be made when studying the imidazole ynamines on a deeper level.

Following investigation into the reactivity of the ynamine described in this chapter, the potential biological applications of the ynamine scaffold can be considered. For use in a biological application, the ynamine will ideally contain an imaging part, so it can be easily monitored.

3.5 Experimental

3.5.1 NMR Experimentation and Reaction Monitoring

3.5.1.1 Hydrogen-Deuterium Exchange (HDE)

The HDE capacity for the ynamines tested was investigated in a 9:1 CD_3CN / D_2O solution at a concentration of 62.0 mM. A 69.0 mM alkyne stock solution was prepared in CD_3CN, and a Cu catalyst solution of 31.0 mM was prepared in D_2O. NMR samples were prepared by transferring 450 μL alkyne stock to a clean NMR tube, and then adding 50 μL of the Cu catalyst stock. This gave the alkyne a concentration of 62.0 mM with 5.00 mol% catalyst. ^{1}H-spectra were acquired immediately on a AVIIIHD Nanobay400 NMR spectrometer (parameters: TE = 300 K, NS = 16, D1 = 5 sec, RG = 203). Samples were measured using the *multi_zgvd2* command that included a *topshim_1dfast* shim after each acquisition. Experiments had a fixed delay of 300 s, n = 20 to 30 to monitor every 5 min for up to 3 h. Due to acquisition times, spectra were obtained approximately every 7 min. For selected ynamines that a slow HDE was anticipated, the number of experiments was increased. Deuteration was calculated by monitoring and integrating the alkyne proton, normalised against non-exchangeable protons.

For experiments where no copper catalyst was present, the procedure was identical with the exception that the Cu catalyst stock was not prepared and 50 μL of D_2O was instead added to the NMR tube in place of the catalyst solution.

3.5.1.2 Data processing protocol

Stacking 1D Spectra: spectra were individually referenced to the respective solvent. Phase correction was performed automatically and adjusted manually where appropriate. The baseline was automatically adjusted using the Whittaker Smoother. Spectra of interest were then selected, stacked and analysed.

Integrating Stacked 1D Spectra: graphs were generated with MNova using the *Advanced* > *Data Analysis* > *Create* > *Integrals Graph* tool. The integrated area was adjusted for drifting. The generated report table was then copied to Microsoft Excel for further processing.

3.5.1.3 [3+2] Cycloaddition Reaction Monitoring Example

A time course experiment used to monitor the [3+2] cycloaddition reaction for ynamine **3.24** using NMR. Stock solutions were prepared in *d*-MeCN following the amounts in Table 3.4

Table 3.4. Stock Solution Preparation for NMR Reaction Monitoring

	Analyte		Catalyst
	Ynamine **3.24**	Azide	$Cu(OAc)_2.H_2O$
Stock Volume (mL)	1		0.62
Mass (mg)	14.02	-	4.15
Volume (μL)	-	8.6	-

A reference sample was first prepared:
To 400 μL of analyte stock in a clean and dry NMR tube was added 100 μL of *d*-MeCN to give a concentration of analyte of 62.0 mM. The sample was shaken, placed in the magnet, tuned, shimmed, locked and a proton spectrum was acquired to study the quality of the shims. This sample was used as a control for the reaction prior to catalyst addition.

A separate reaction sample was prepared:
To 400 μL of analyte stock in a clean and dry NMR tube was added 100 μL of catalyst stock, giving a concentration of analyte of 62.0 mM. The sample was shaken and placed into the probe. Time course experiments were recorded using experiments that were automated utilising the *multi_zgvd2* command with a fixed delay of 300 s, n = 20.
The data obtained is given in Figure 3.33.

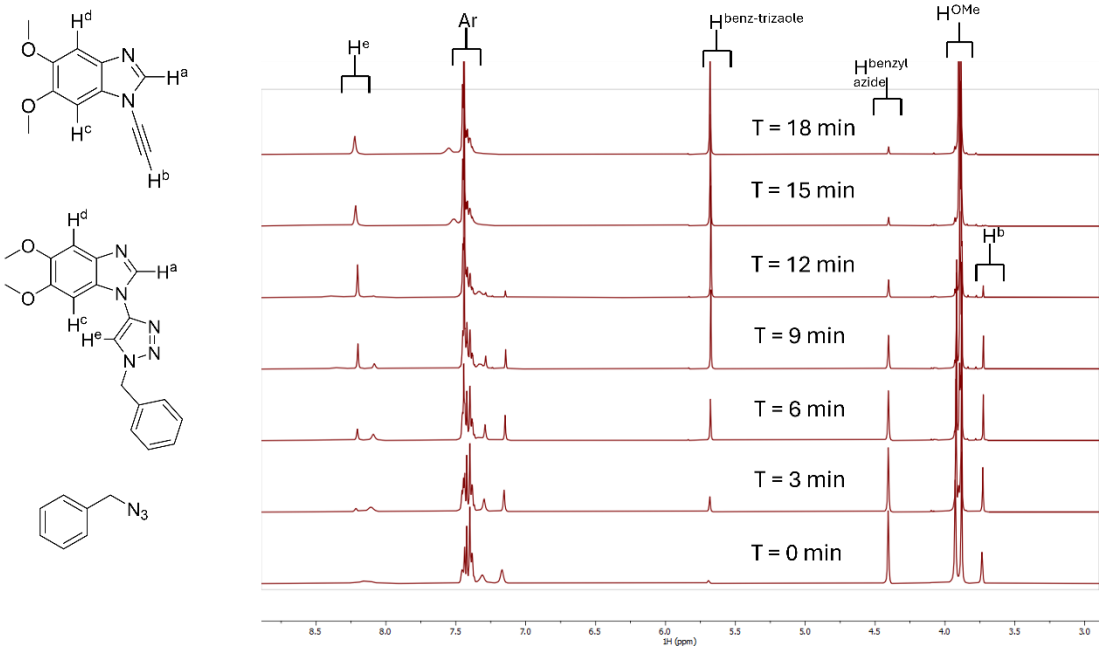

Figure 3.33. NMR spectra for the time course of the CuAAC of **3.24** with benzyl azide.

3.5.1.4 [3+2] Cycloaddition Competition Reaction Monitoring Example

The protocol from 3.6.1.3 was repeated, with the exception that two ynamines were in the analyte stock solution with benzyl azide (Table 3.5)

Table 3.5. Stock Solution Preparation for NMR Competition Reaction Monitoring

	Analyte			Catalyst
	Ynamine **3.24**	Ynamine **3.25**	Azide	$Cu(OAc)_2.H_2O$
Stock Volume (mL)	1			0.62
Mass (mg)	14.02	12.35	-	4.15
Volume (µL)	-		8.6	-

The final spectra obtained is given in Figure 3.34.

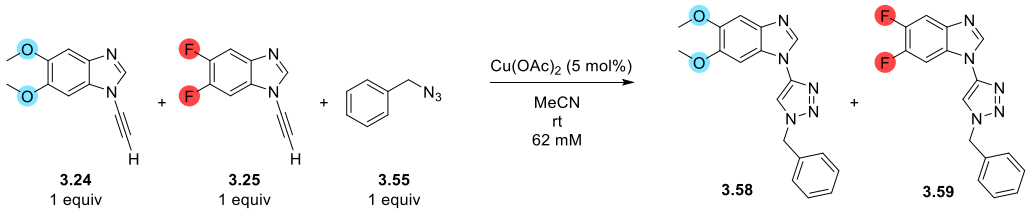

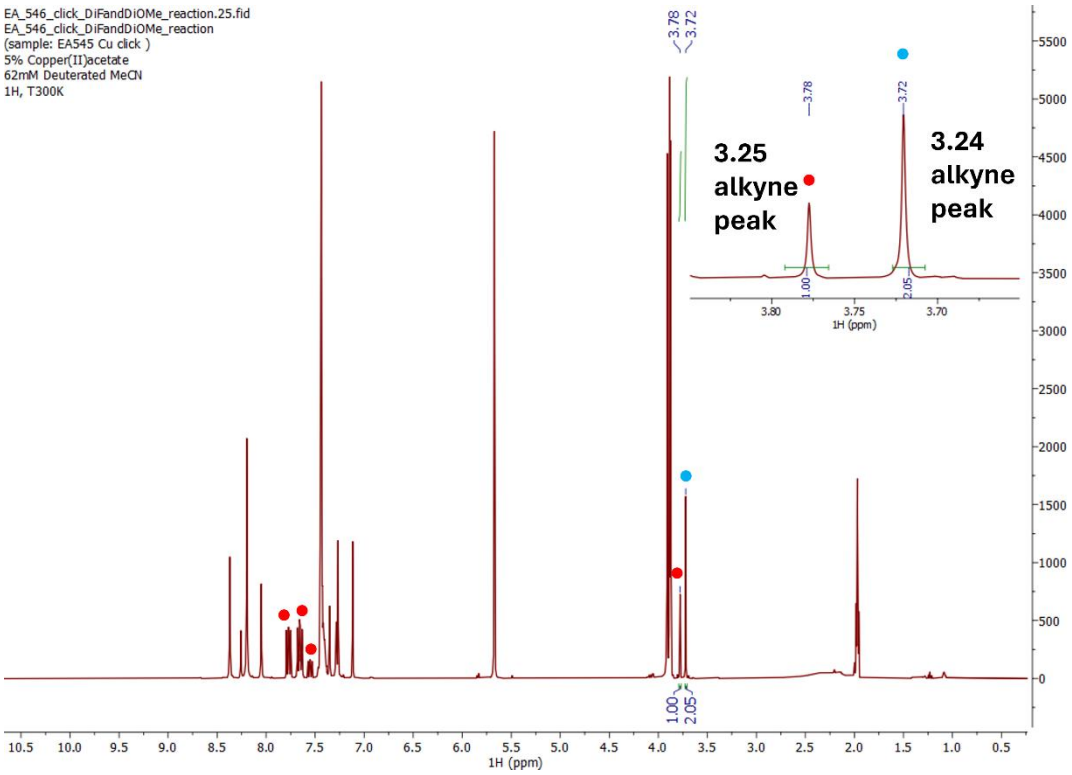

Figure 3.34. Final spectra obtained for the competition experiment between **3.24** and **3.25.**

3.5.2 HPLC Analysis

3.5.2.1 Instruments and Methods

HPLC was carried out on a Shimadzu Prominence LC System.

Typical HPLC conditions are described below:

Column Specification: Kinetix C18 100 Å, 50 x 4.6 mm, 2.6 µm

Mobile Phase A: 0.1% v/v TFA in water

Mobile Phase B: 0.1% v/v TFA in MeCN

Flow rate: 1.5 mL/min

Injection volume: 10 µL

UV detection signal was recorded at 254 nm.

The gradient was optimised for each ynamine. An example gradient profile for the 5-60% Kinetix 10 min method is given below:

Time (min)	B%
0 – 5.8	5 - 60
5.8 – 6.0	60 - 95
6 – 8.1	95 – 95
8.1 – 8.2	95 – 5
8.2 – 10.0	5 - 5

The HPLC methods used for each ynamine are given in Table 3.6.

Table 3.6. HPLC Methods for the Ynamine Substrates

Ynamine	Method Used
3.24	5 – 40% B Kinetix 10 min
3.25	5 – 50% B Kinetix 10 min
3.26	5 – 60% B Kinetix 10 min
3.27	5 – 60% B Kinetix 10 min
3.28	5 – 60% B Kinetix 10 min
3.29	5 – 60% B Kinetix 10 min
3.30	20 – 40% B Kinetix 10 min
3.31	5 – 60% B Kinetix 10 min
3.33	10 – 50% B Kinetix 10 min
3.34	40 - 80% Phenylhexyl 15min
3.35	20 – 30% B Kinetix 15 min
3.36	20 – 60% B Kinetix 10 min
3.37	5 – 50% B Kinetix 10 min
3.38	5 – 95% B Kinetix 10 min
3.39	20 – 50% B Kinetix 10 min
3.40	20 – 50% B Kinetix 10 min

3.5.2.2 Calibration Curve Preparation

Stock solutions for each ynamine and triazole were prepared. A representative example for the mass of analyte and internal standard required and volume of solvent is given in Table 3.7 for ynamine **3.24** and triazole **3.58**.

Table 3.7. Stock solutions for HPLC Calibration in MeCN

	Analyte Stock		**IS Stock**
	Ynamine 3.24	**Triazole 3.58**	**1,3,5-TMB**
MW (g/mol)	202.21	335.37	168.19
Volume (mL)	25	25	25
Concentration (1.50 mM)	1.5	1.5	5
Mass (mg)	7.58	12.58	21.02

The premade stock solutions were then used to prepare calibration curves in MeCN according to the volumes given in Table 3.8.

Table 3.8. Volumes of each stock used in calibration curve formation

Vial no.	**Total Volume (µL)**	**Volume of Analyte Stock (µL)**	**Volume of IS Stock (µL)**	**Volume of MeCN (µL)**
1	500	400	100	0.00
2	500	360	100	40.0
3	500	280	100	120
4	500	200	100	200
5	500	120	100	280
6	500	40.0	100	360
7	500	0.00	100	400

The samples were injected undiluted. The results were plotted in ratios where:

C_A = concentration of the analyte

C_{IS} = concentration of the internal standard

R_A = response of the analyte

R_{IS} = response of the internal standard

The calibration graphs for each ynamine and triazole are given below in Figure 3.35.

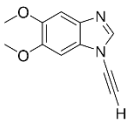

3.24

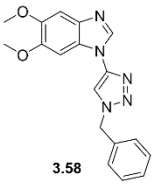

3.58

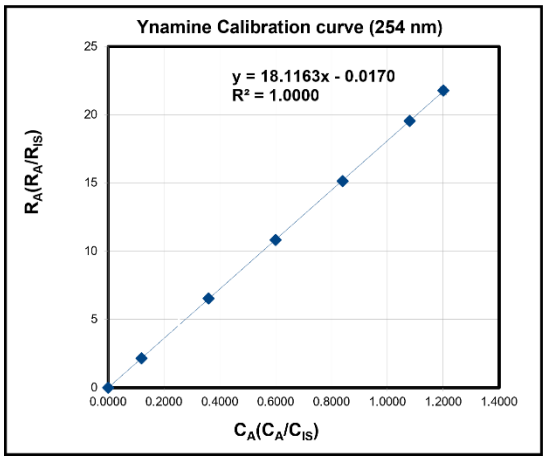

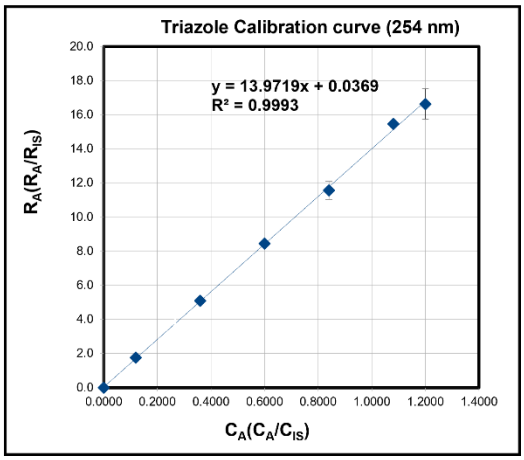

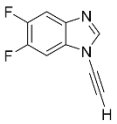

3.25

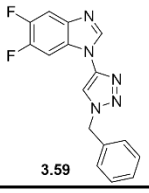

3.59

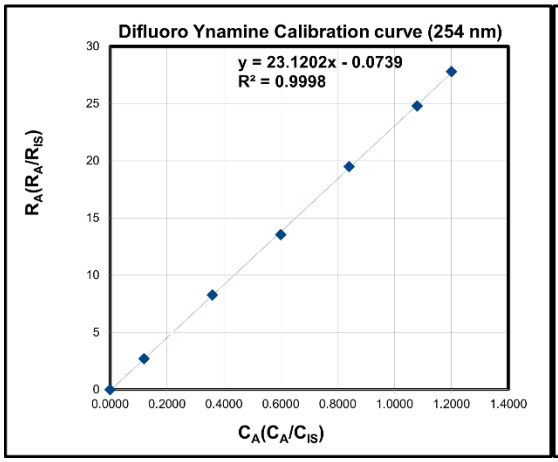

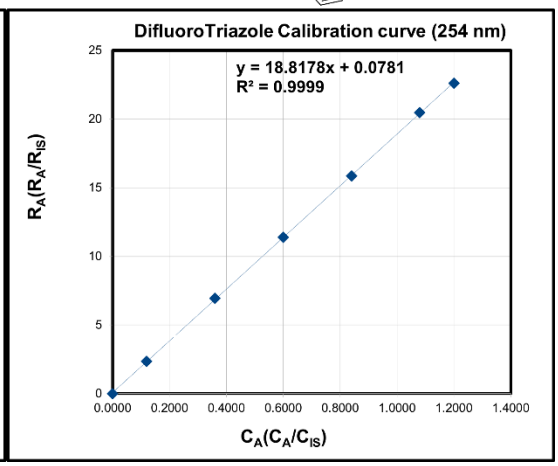

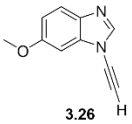

3.26

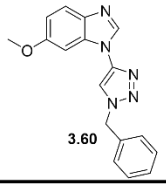

3.60

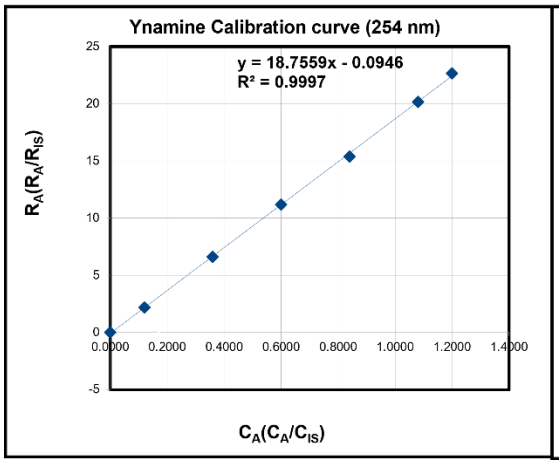

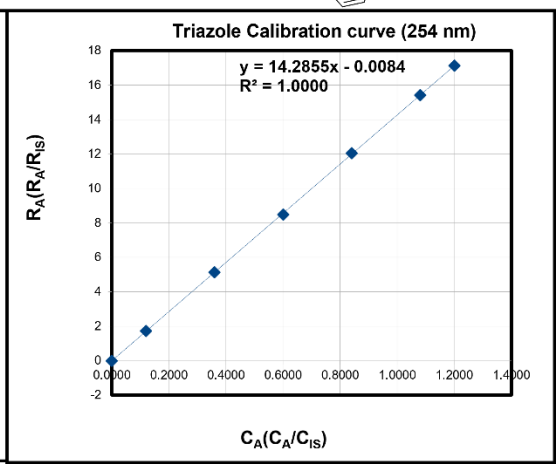

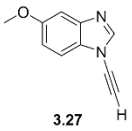

3.27

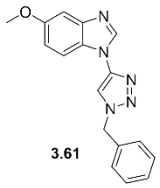

3.61

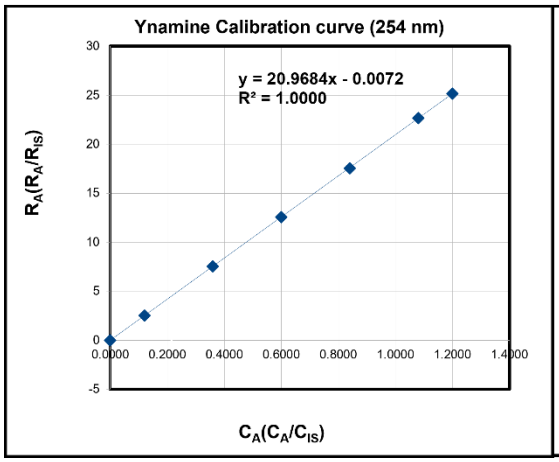

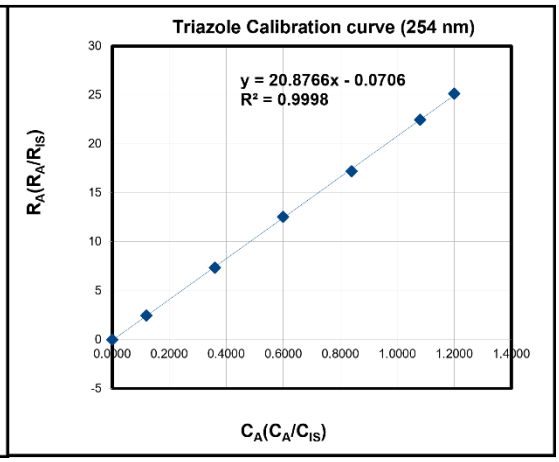

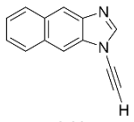

3.30

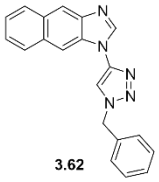

3.62

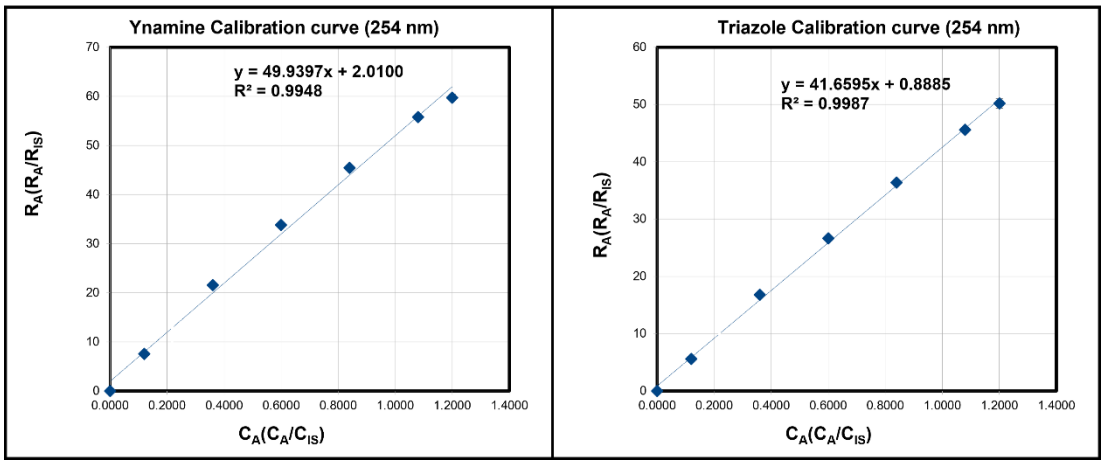

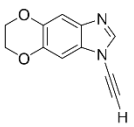

3.31

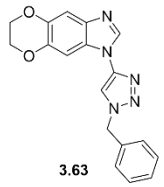

3.63

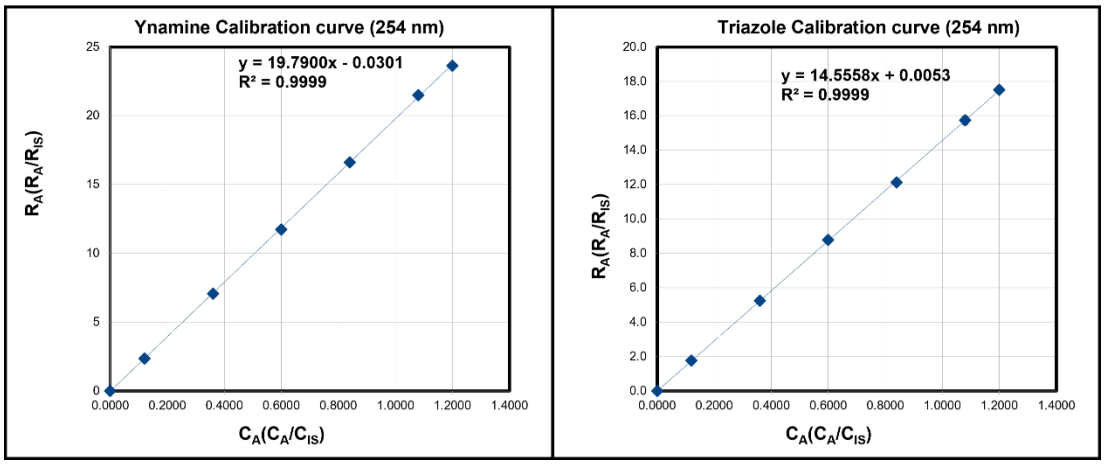

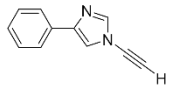

3.33

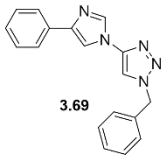

3.69

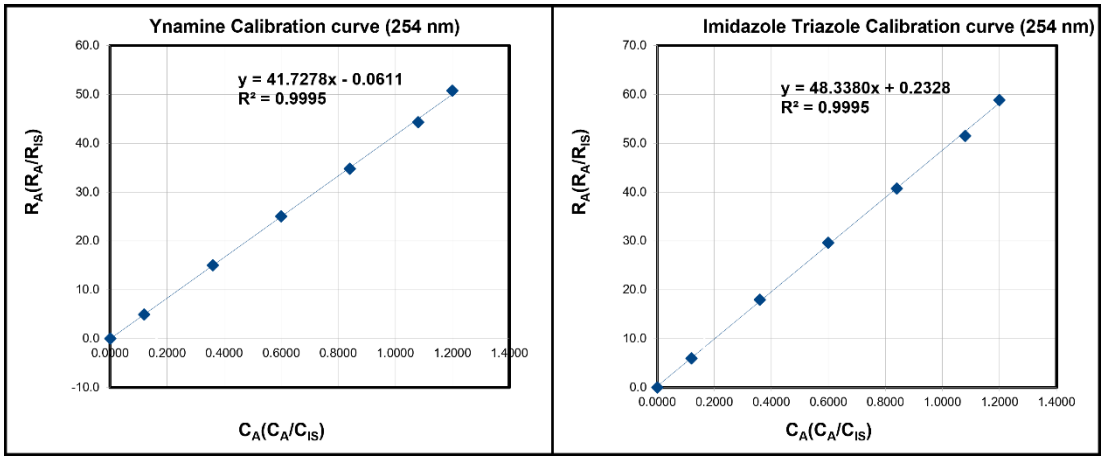

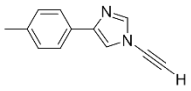

3.34

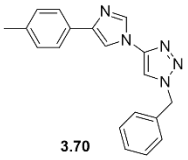

3.70

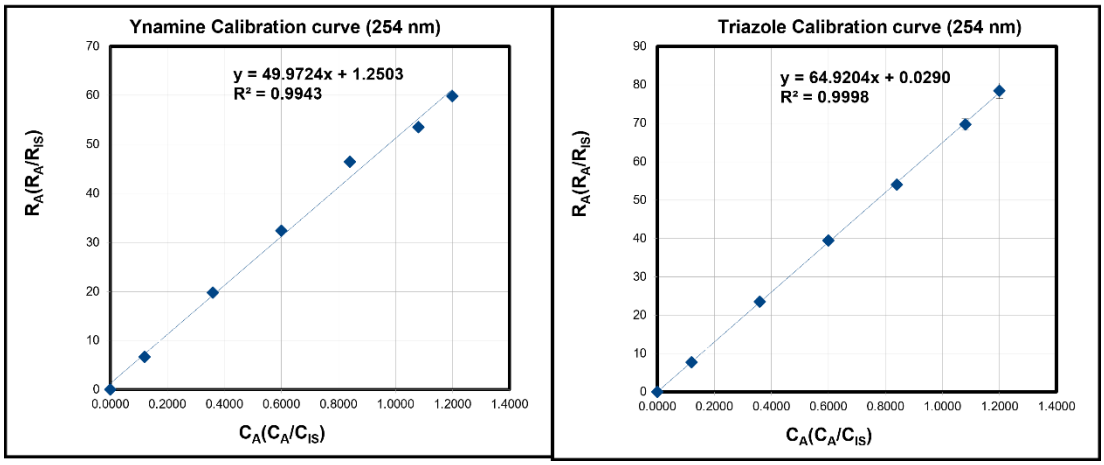

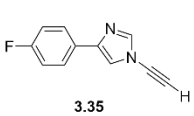
F
N
N
H

3.35

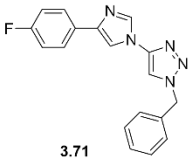
F
N
N
N
N

3.71

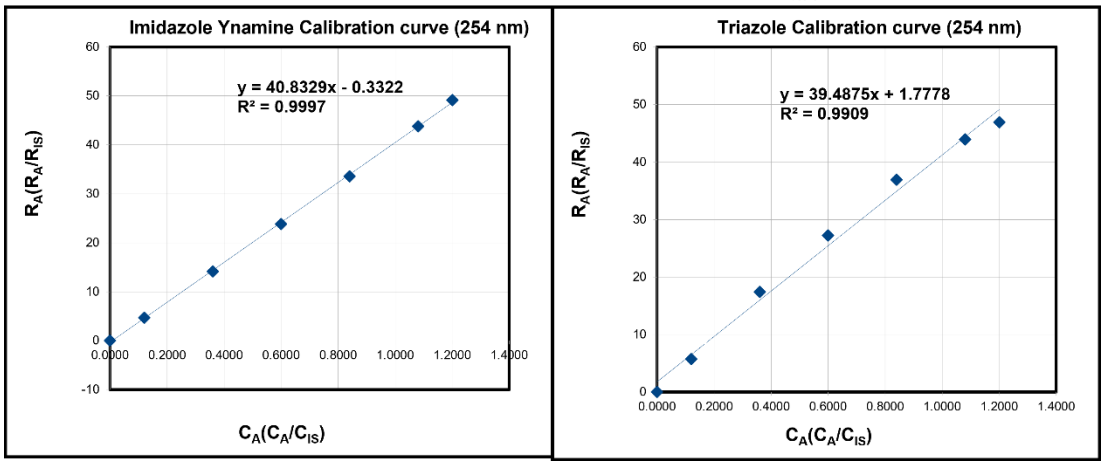
Imidazole Ynamine Calibration curve (254 nm)
y = 40.8329x - 0.3322
R² = 0.9997
RA(RA/RIS)
CA(CA/CIS)
60
50
40
30
20
10
0
-10
0.0000
0.2000
0.4000
0.6000
0.8000
1.0000
1.2000
1.4000
Triazole Calibration curve (254 nm)
y = 39.4875x + 1.7778
R² = 0.9909
RA(RA/RIS)
CA(CA/CIS)
60
50
40
30
20
10
0
0.0000
0.2000
0.4000
0.6000
0.8000
1.0000
1.2000
1.4000

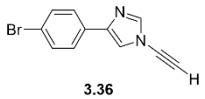

3.36

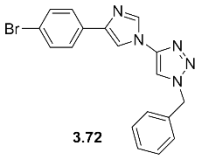

3.72

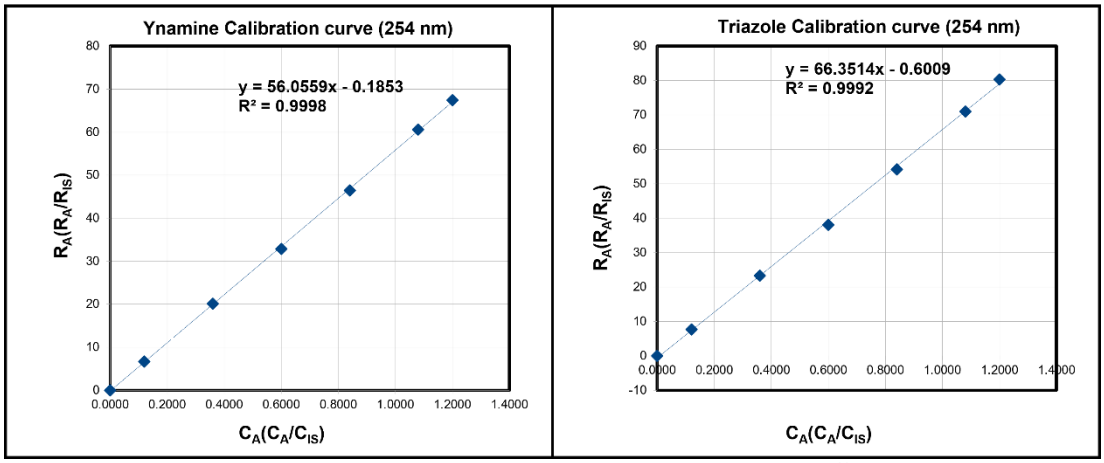

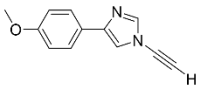

3.37

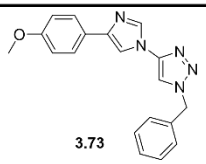

3.73

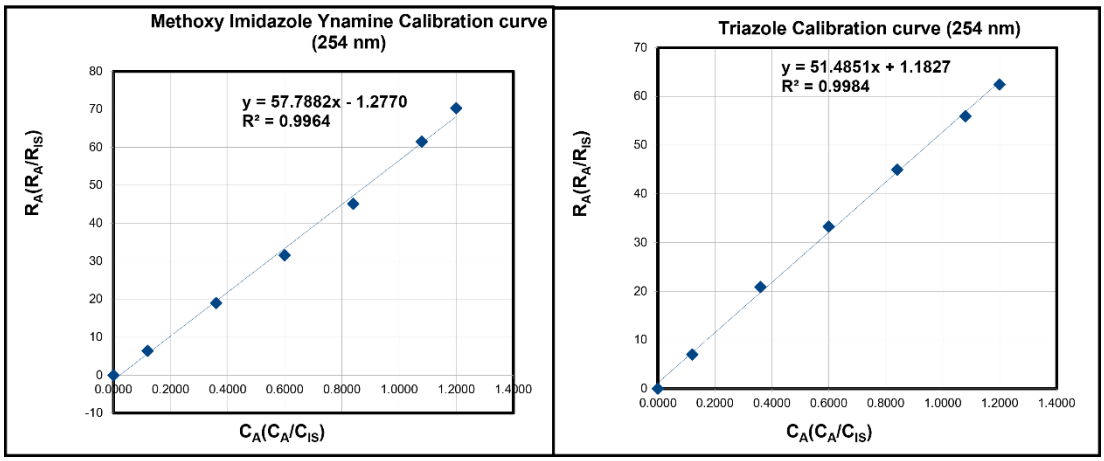

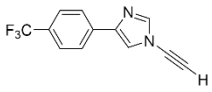

3.38

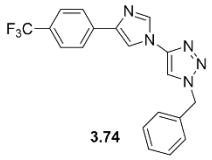

3.74

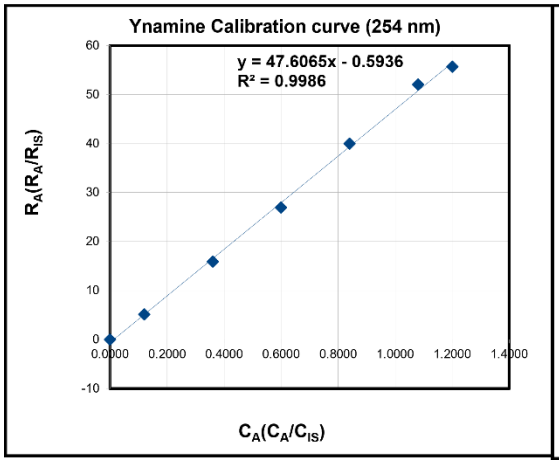

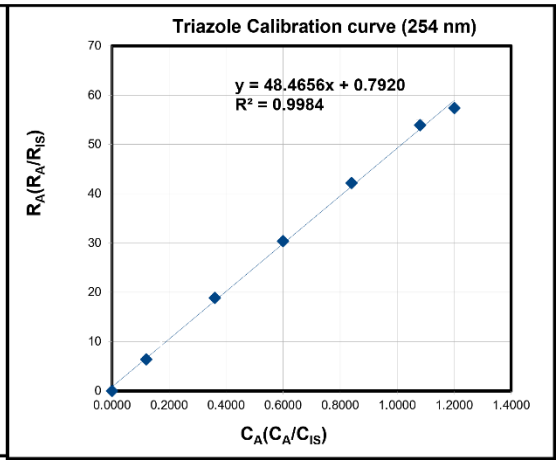

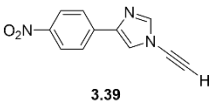

3.39

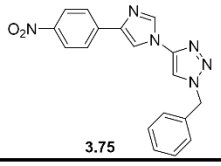

3.75

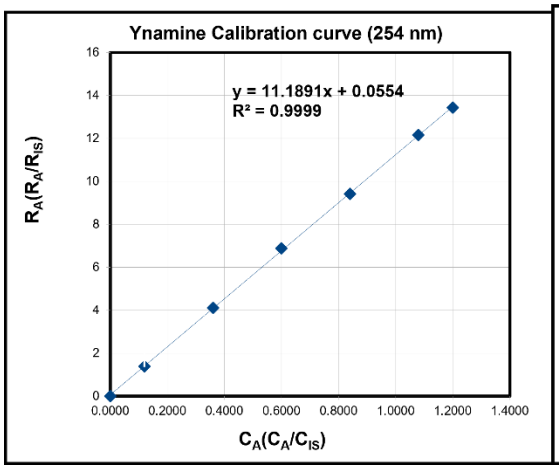

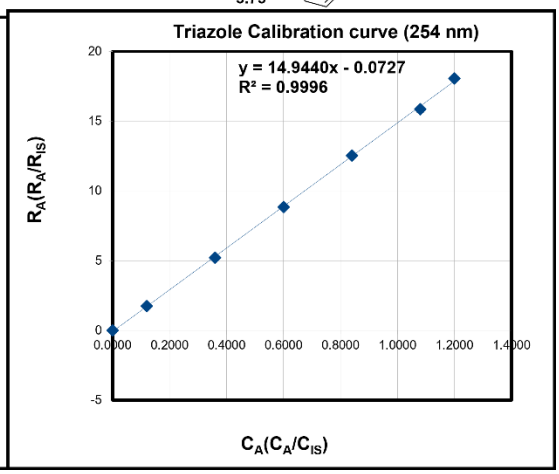

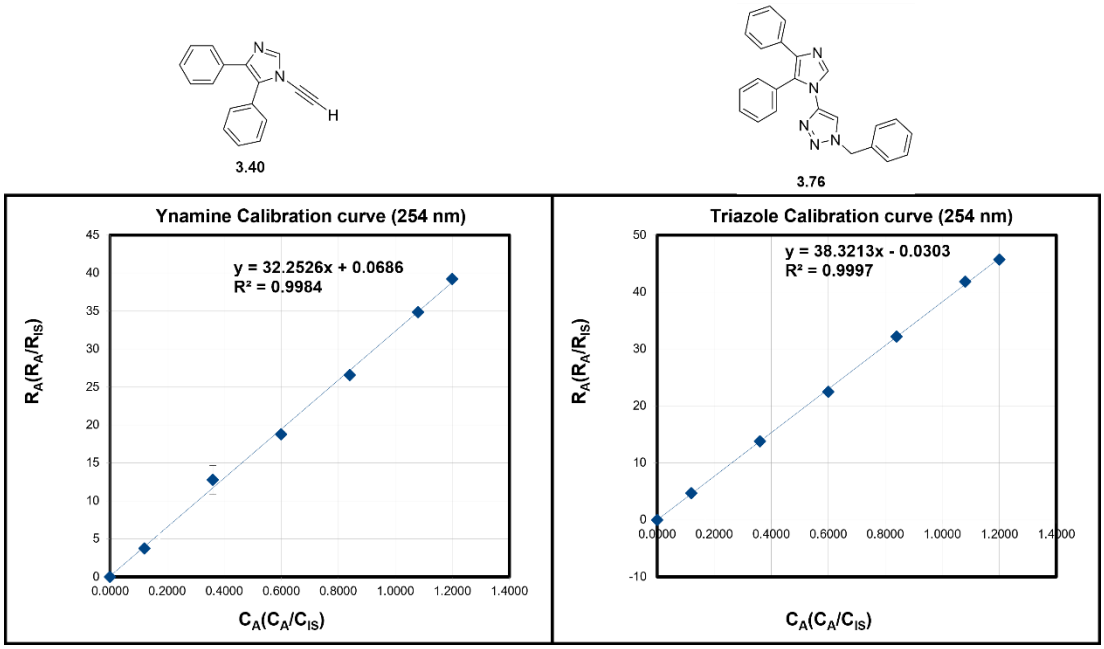

Figure 3.35. HPLC calibration graphs for each ynamine and triazole.

3.5.2.3 [3+2] Cycloaddition Reaction Monitoring Procedure MeCN

The following protocol describes an example of a time course experiment that was used to monitor [3+2] cycloaddition reactions in MeCN. Stock solutions were prepared in MeCN. Ynamine **3.25** is used as an exemplar in Table 3.9.

Table 3.9. Example of a time course stock solution preparation for a reaction in MeCN with 5 mol% $Cu(OAc)_2$

Stock	Analyte			Catalyst
	Ynamine **3.25**	Azide **3.55**	1,3,5-TMB	$Cu(OAc)_2.H_2O$
MW (g/mol)	202.21	133.15	168.19	199.65
Concentration (mM)	77.5	77.5	77.5	15.5
Stock Volume (mL)	1.8			1
Mass (mg)	28.23	18.57	23.46	3.09
Density (g/mL)	-	1.0655	-	-
Volume (µL)	-	17.43	-	-

To a stirring solution of analyte stock (400 µL) in a small vial was added catalyst stock (100 µL) to give a reaction concentration of 62.0 mM ynamine, 62.0 mM azide, 62.0 mM 1,3,5-TMB and 5mol% catalyst. After the addition of the catalyst, 10.0 µL aliquots were taken at

timed intervals, and diluted to 1.00 mM with a quench solution (610 µL, 49/33/18 v/v% MeCN, water, EDTA solution (10% in water pH ≈ 10, NaOH). To a second smaller vial was added analyte stock (400 µL) and MeCN (100 µL). A 10.0 µL aliquot was taken and diluted to 1 mM with a quench solution (610 µL, 49/33/18 v/v% MeCN, water, EDTA solution (10% in water pH ≈ 10, NaOH). This was used at the t = 0 s measurement. The quenched samples were then injected into the HPLC and results analysed.

3.5.2.4 [3+2] Cycloaddition Reaction Monitoring Procedure IPA

The following protocol describes an example of a time course experiment that was used to monitor [3+2] cycloaddition reactions in IPA. Stock solutions were prepared in IPA. Ynamine C is used as an exemplar in Table 3.10

Table 3.10. Example of a time course stock solution preparation in IPA with $Cu(OAc)_2$

Stock	Analyte			Catalyst
	Ynamine **3.24**	Azide **3.55**	1,3,5-TMB	$Cu(OAc)_2.H_2O$
MW (g/mol)	202.21	133.15	168.19	199.65
Concentration (mM)	103.3	103.3	103.3	7.75
Stock Volume (mL)	1.3			2
Mass (mg)	27.14	18.57	23.46	6.19
Density (g/mL)	-	1.065	-	-
Volume (µL)	-	17.43	-	-

To a stirring solution of analyte stock (300 µL) in a small vial was added catalyst stock (200 µL) to give a reaction concentration of 62.0 mM ynamine, 62.0 mM azide, 62.0 mM 1,3,5-TMB and 5mol% catalyst. After the addition of the catalyst, 10.0 µL aliquots were taken at timed intervals, and diluted to 1.00 mM with a quench solution (610 µL, 49/33/18 v/v% MeCN, water, EDTA solution (10% in water pH ≈ 10, NaOH). To a second smaller vial was added analyte stock (400 µL) and MeCN (100 µL). A 10.0 µL aliquot was taken and diluted to 1 mM with a quench solution (610 µL, 49/33/18 v/v% MeCN, water, EDTA solution (10% in water pH ≈ 10, NaOH). This was used at the t = 0 s measurement. The quenched samples were then injected into the HPLC and results analysed.

3.5.2.5 [3+2] Cycloaddition Reaction Monitoring Procedure HFIP/Water

The following protocol describes an example of a time course experiment that was used to monitor [3+2] cycloaddition reactions in HFIP/water. Stock solutions were prepared in HFIP and H_2O. Ynamine C is used as an exemplar in Table 3.11

Table 3.11. Example of a time course stock solution preparation in HFIP/water

Stock	Analyte			Catalyst
	Ynamine **3.24**	Azide **3.55**	1,3,5-TMB	$Cu(OAc)_2.H_2O$
MW (g/mol)	202.1	133.15	168.19	199.65
Concentration (mM)	310	310	310	15.5
Volume of solvent (mL)	0.5			0.5
Mass (mg)	31.34	20.64	26.07	1.55
Density (g/mL)	-	1.0655	-	-
Volume (µL)	-	19.37	-	-

To a stirring solution of analyte stock (100 µL), HFIP (100 µL), water (200 µL) in a small vial was added catalyst stock (100 µL) to give a reaction concentration of 62.0 mM ynamine, 62.0 mM azide, 62.0 mM 1,3,5-TMB and 5mol% catalyst. After the addition of the catalyst, 10.0 µL aliquots were taken at timed intervals, and diluted to 1.00 mM with a quench solution (610 µL, (49/33/18 v/v% MeCN, water, EDTA solution (10% in water pH ≈ 10, NaOH)) and 500 µL water). To a second smaller vial was added analyte stock (400 µL) HFIP (200 µL), water (200 µL). A 10.0 µL aliquot was taken and diluted to 1 mM with a quench solution (610 µL, 49/33/18 v/v% MeCN, water, EDTA solution (10% in water pH ≈ 10, NaOH). This was used at the t = 0 s measurement. The quenched samples were then injected into the HPLC and results analysed.

3.5.2.6 [3+2] Cycloaddition Reaction Monitoring Procedure for Ynamine Competition Analysis

The protocol for monitoring the competition experiments was identical to the protocol for monitoring the reaction for a singular ynamine. Both ynamines were dissolved in the same analyte stock.

3.5.2.7 Additional HPLC Data

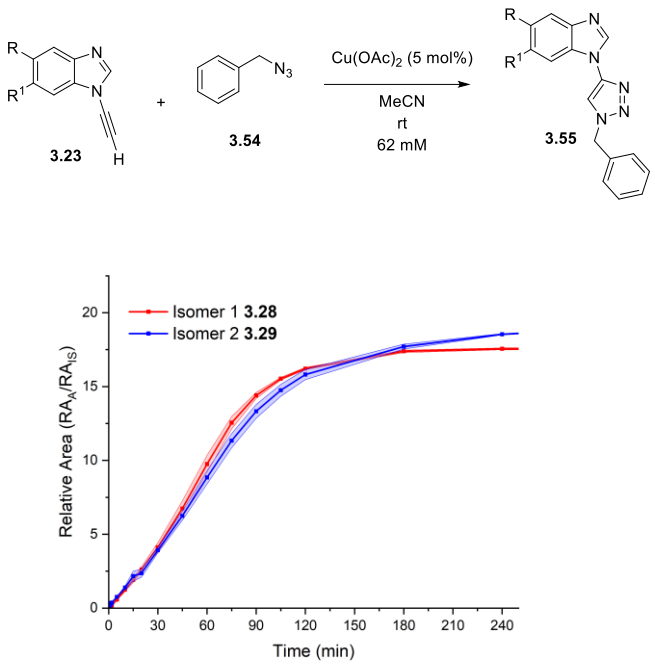

Figure 3.36. Comparison of the formation of the triazole product of amino benzimidazole isomers **3.28** and **3.29** in MeCN.

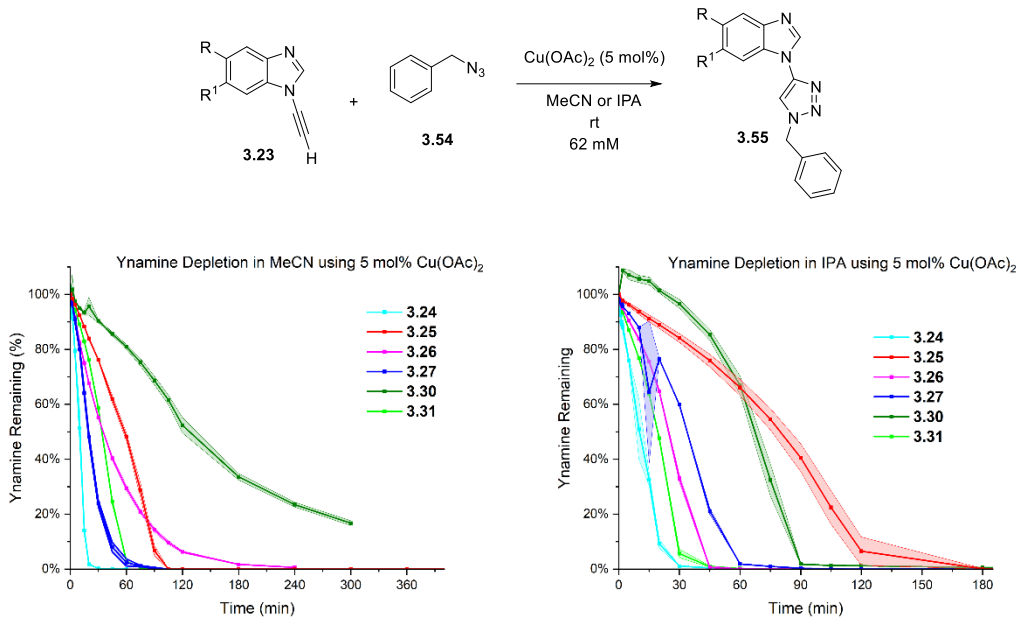

Figure 3.37. A) Ynamine depletion for benzimidazoles in MeCN; **B)** Ynamine depletion for benzimidazoles in IPA.

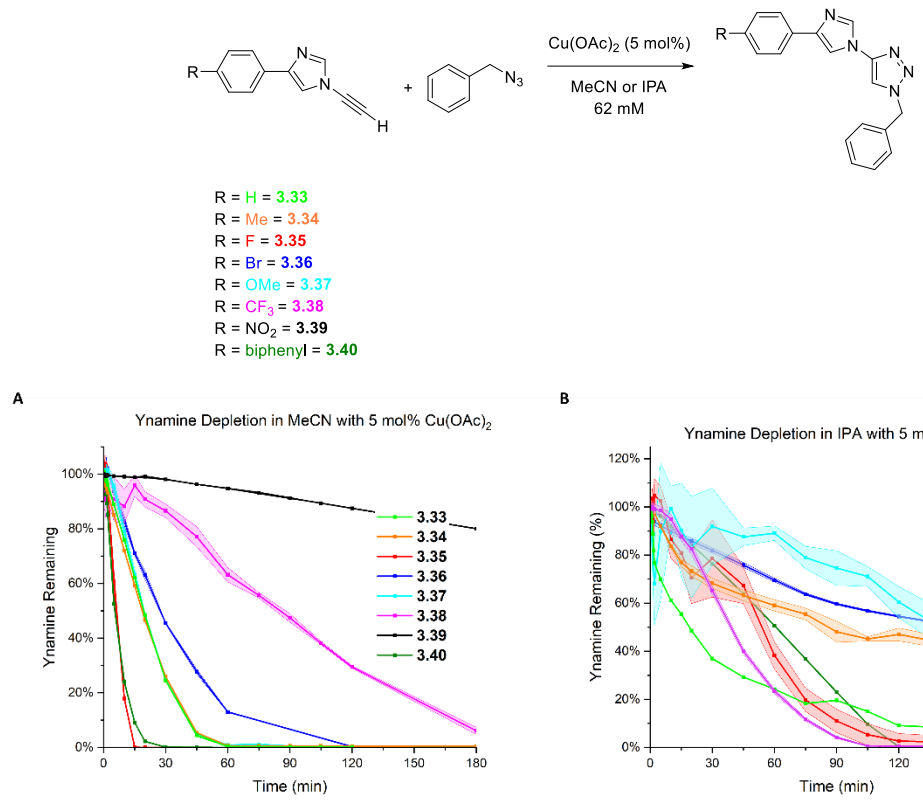

Figure 3.38. A) Ynamine depletion for imidazoles in MeCN; **B)** Ynamine depletion for imidazoles in IPA.

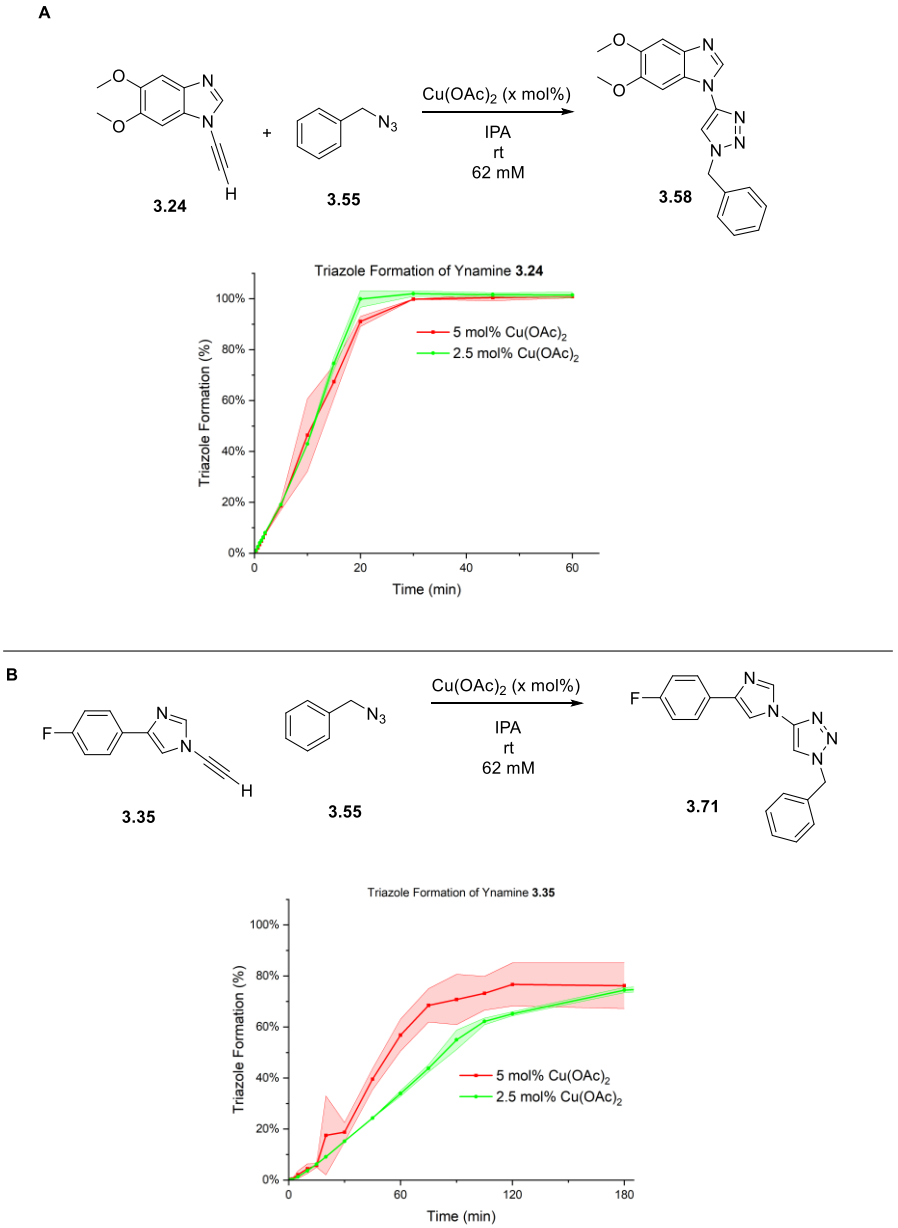

Figure 3.39. A) Triazole formation in IPA for ynamine **3.24**; **B)** Triazole formation in IPA for ynamine **3.35.**

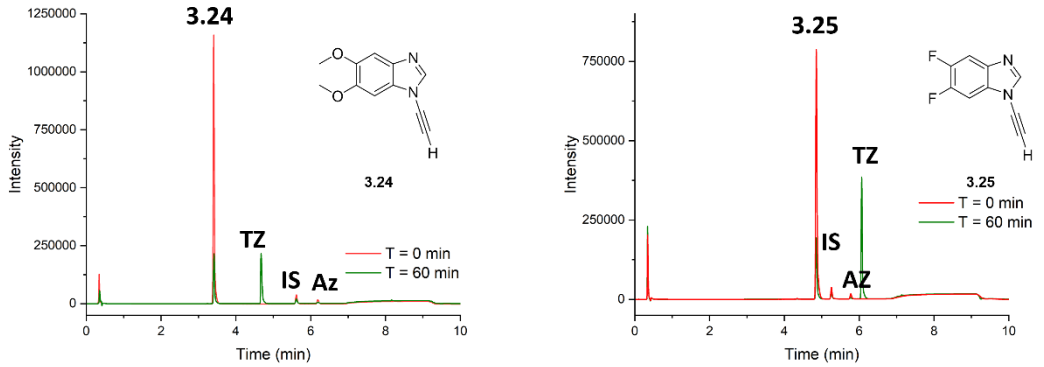

Figure 3.40. HPLC traces for ynamines **3.24** and **3.25** in HFIP/water (40/60)

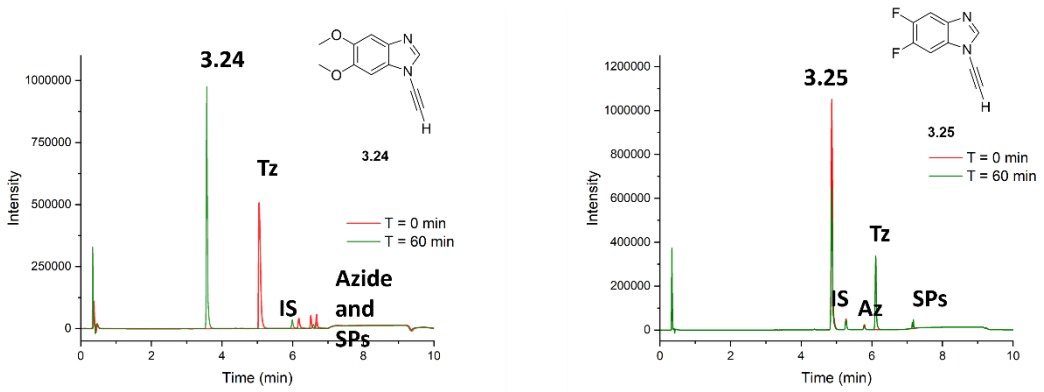

Figure 3.41. HPLC traces for the CuAAC for **3.24** in MeCN and **3.25** in IPA.

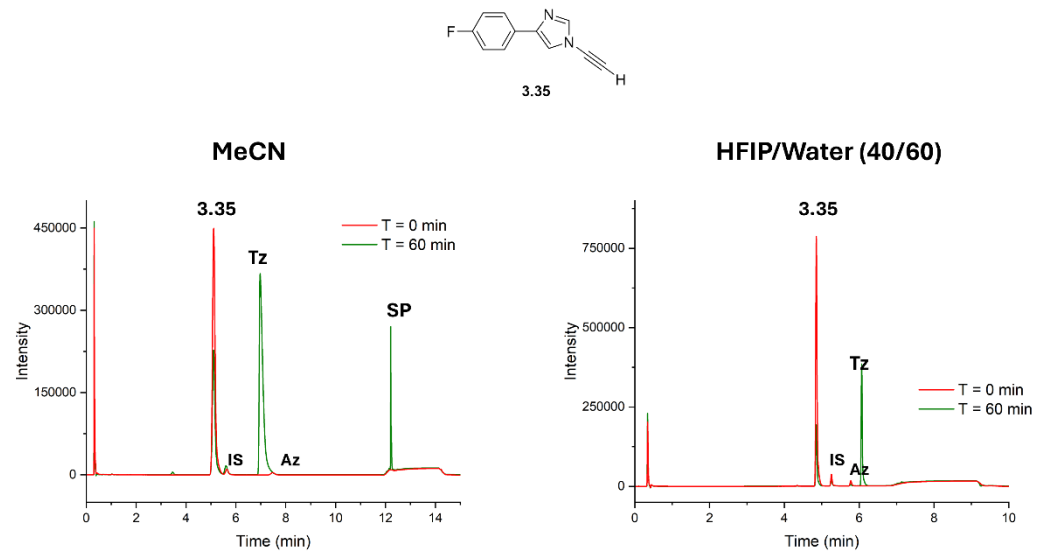

Figure 3.42. HPLC traces for the CuAAC for **3.35** in IPA and HFIP/water.

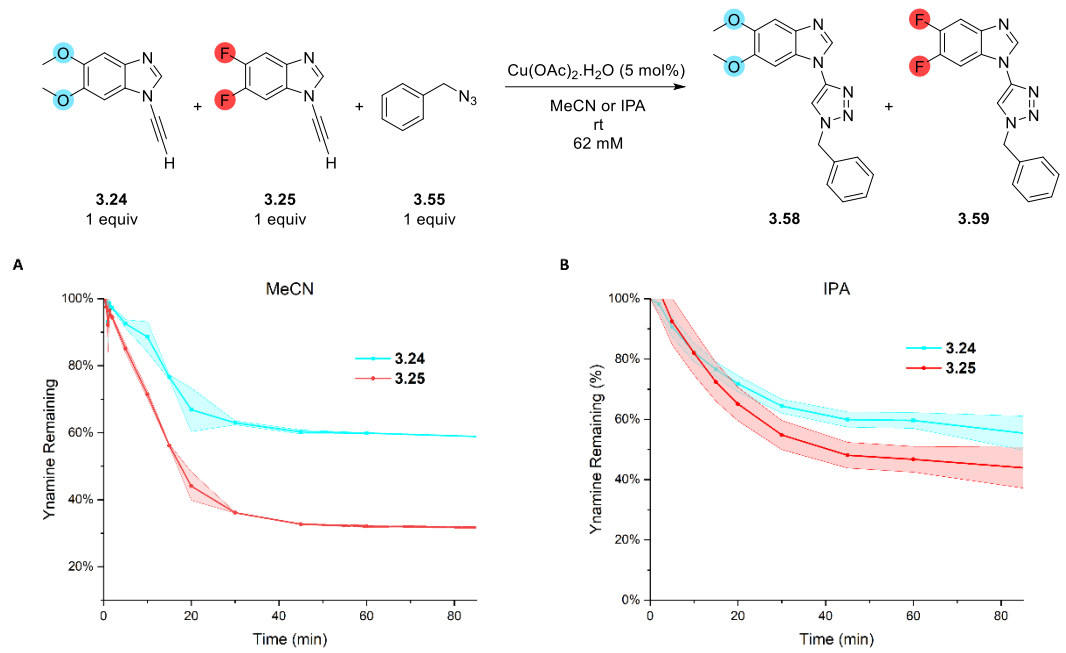

Figure 3.43. Ynamine depletion of **3.24** and **3.25** and azide **3.55** in MeCN (**A**) and IPA (**B**) using 5 mol% $Cu(OAc)_2.H_2O$.

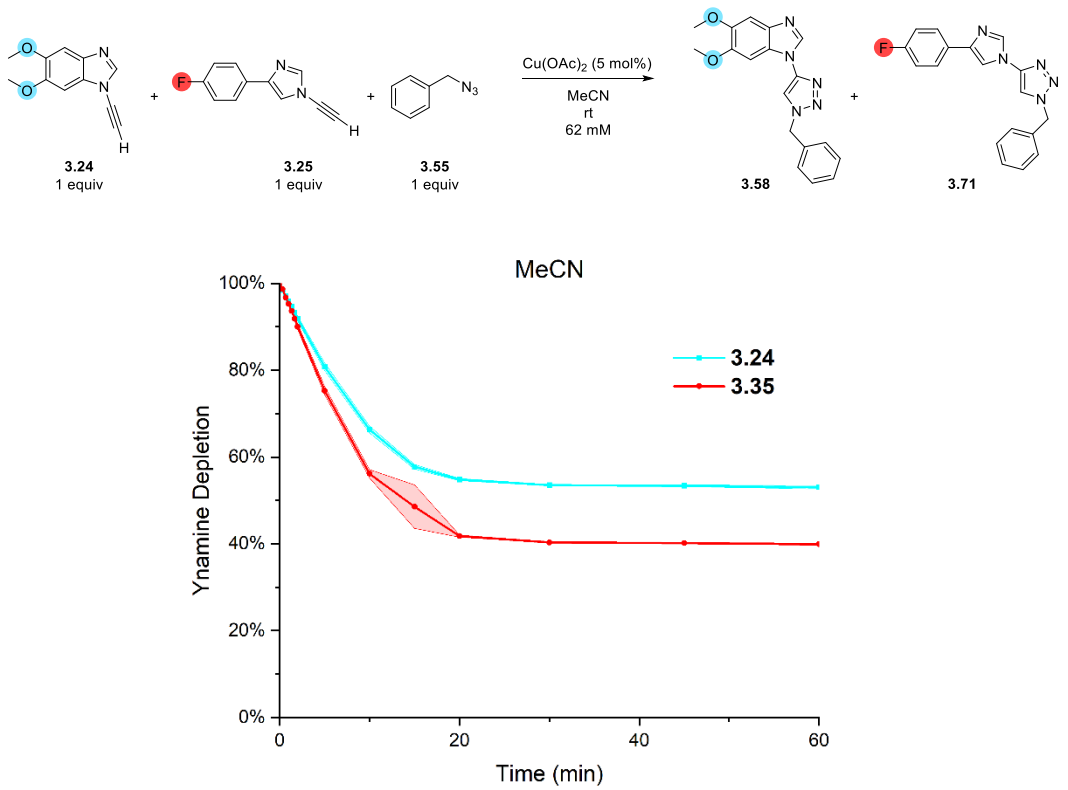

Figure 3.44. Ynamine depletion of **3.24** and **3.35** and azide **3.55** in MeCN using 5 mol% $Cu(OAc)_2.H_2O$

3.5.3 Synthesis of Diyne for HPLC Reference

General Procedure:

To a solution of ynamine (1 equiv) dissolved in DCM was added a solution of copper(II) chloride (0.06 equiv) and TMEDA (0.6 equiv) in DCM. Air was bubbled through the reaction for 30 min and the reaction stirred at rt overnight. The reaction was diluted with DCM and the washed with sat. EDTA solution. The organic layers were combined, washed with brine and dried over anhydrous sodium sulphate. The solution was filtered and the solvent removed *in vacuo* to give a crude diyne product. For each diyne formation, characterisation methods were used to confirm product formation.

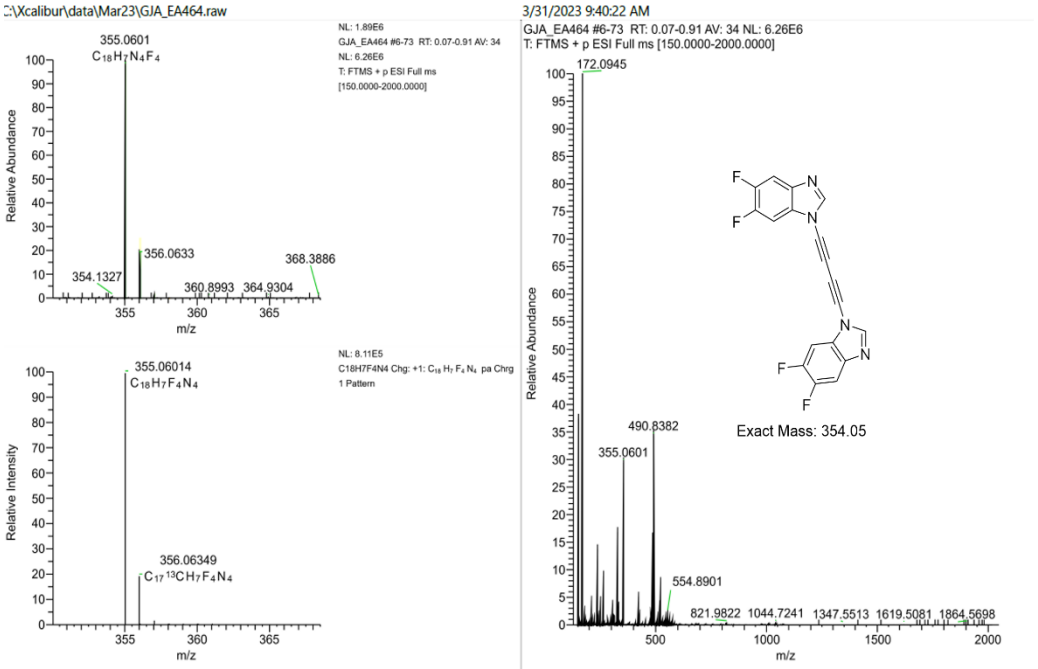

Peak Mass	Display For...	S Fit	RDB	Delta [ppm]	Theo. mass	Rank	Combined S...	# Matched I...	# Missed Iso.	MS Cov. [%]	Pattern Cov....	MSMS Matc.
355.0601	$C_{16}H_4N_{10}F$	73.69624288 44521	19.50	0.67	355.05989	1	98.07	3	0	99.42	100	(Collection)
355.0601	$C_{18}H_7N_4F_4$	48.49190675 33135	15.50	-0.01	355.06014	2	96.74	4	0	99.42	99.91	(Collection)

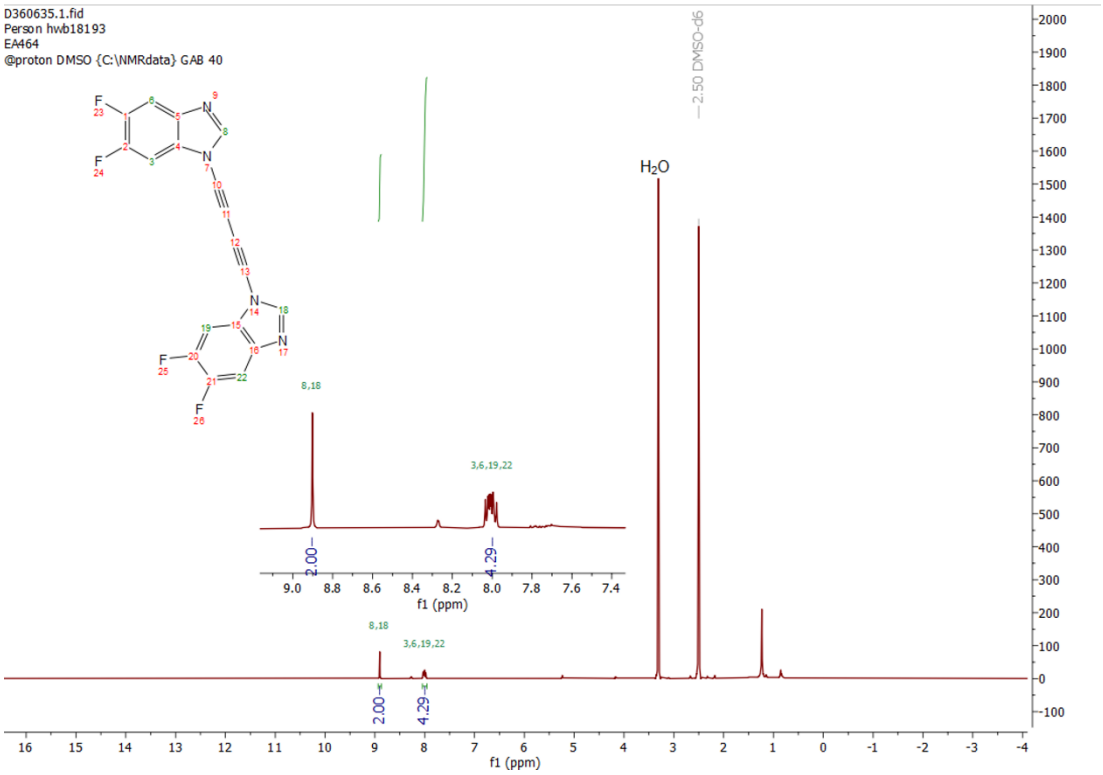

Figure 3.45. HR-MS and NMR for the formation of diyne **3.68**.

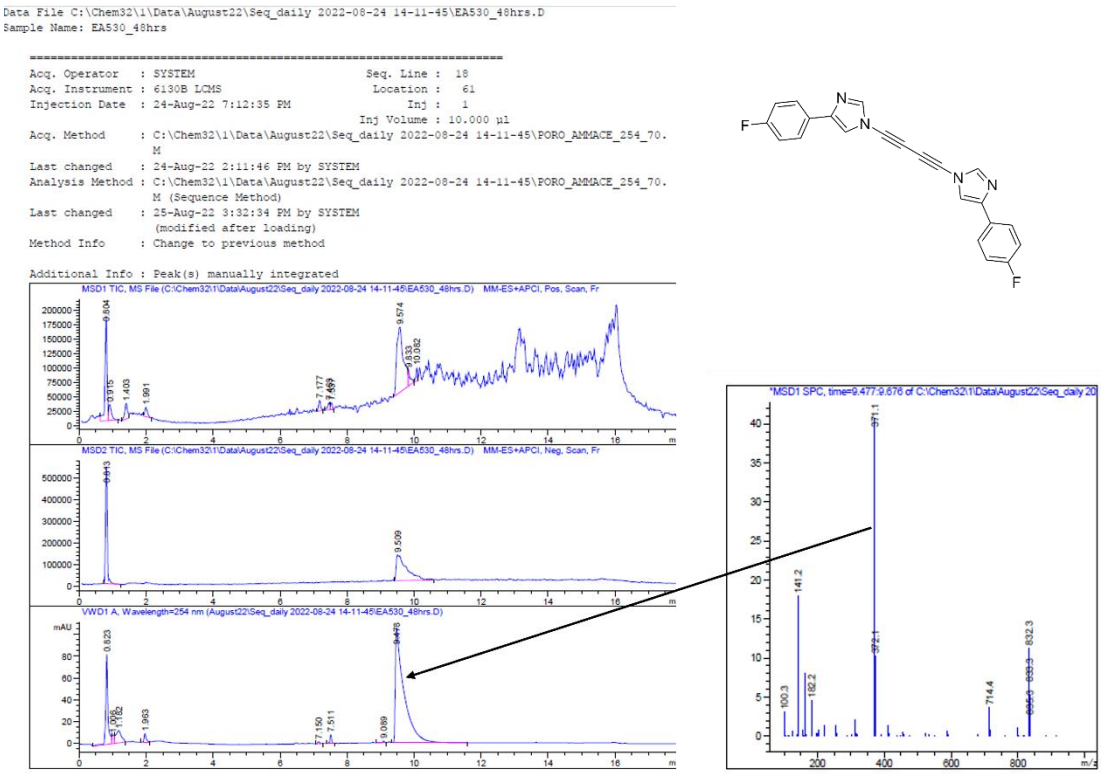

Figure 3.46. LCMS trace for the formation of diyne **3.77**, confirming the formation of the desired product.

3.5.4 Side Product Analysis

LC-MS analysis of the reaction of imidazole **3.34** in MeCN with 5 mol% $Cu(OAc)_2$ showed the formation of the diyne and of another side product (Figure 3.47)

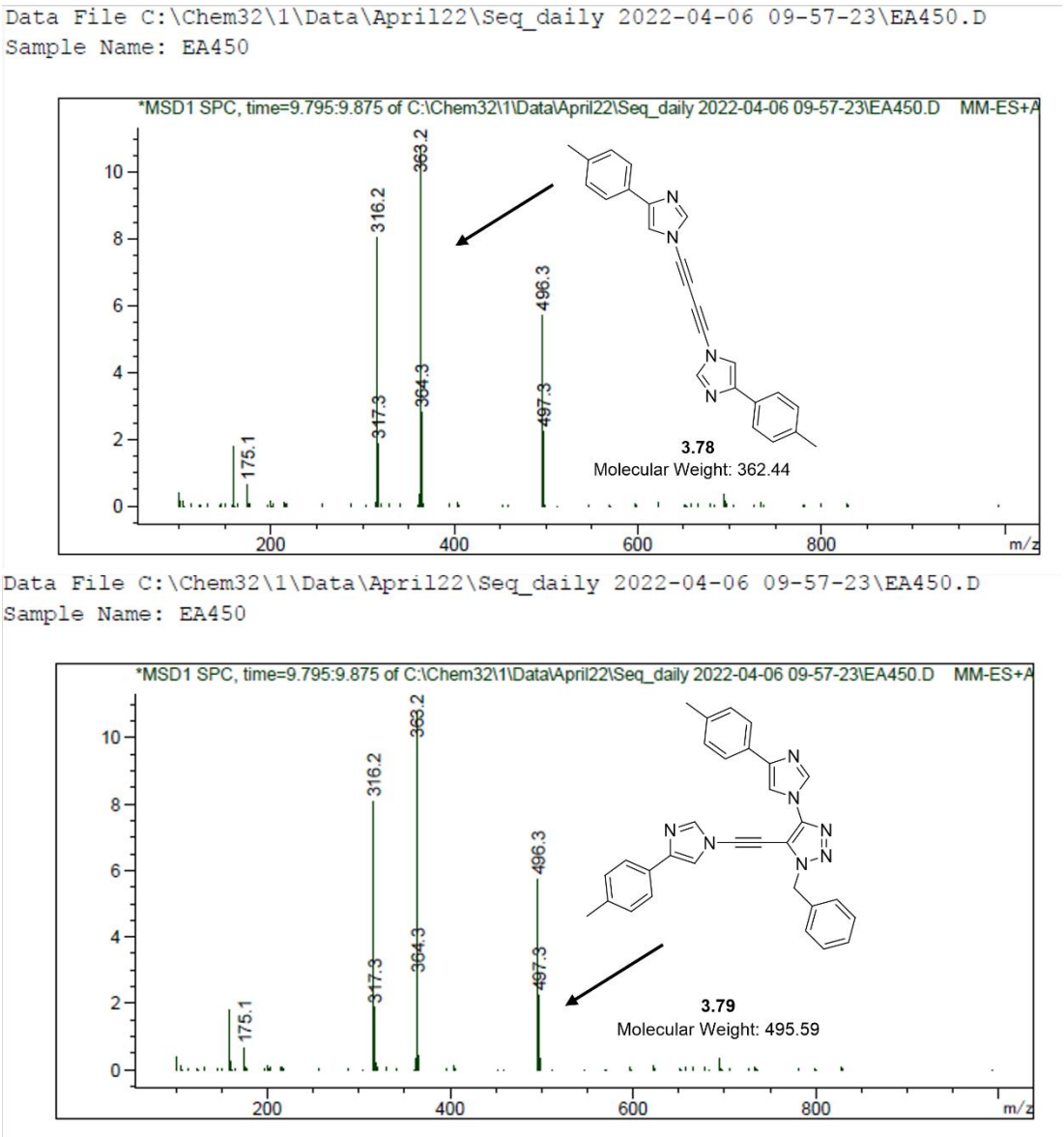

Figure 3.47. LC-MS traces of the reaction of methyl imidazole **3.34** with benzyl azide **3.55** in MeCN with 5 mol% $Cu(OAc)_2.H_2O$ showing the mass peak of the diyne **3.78** and another side product, assumed to be **3.79**.

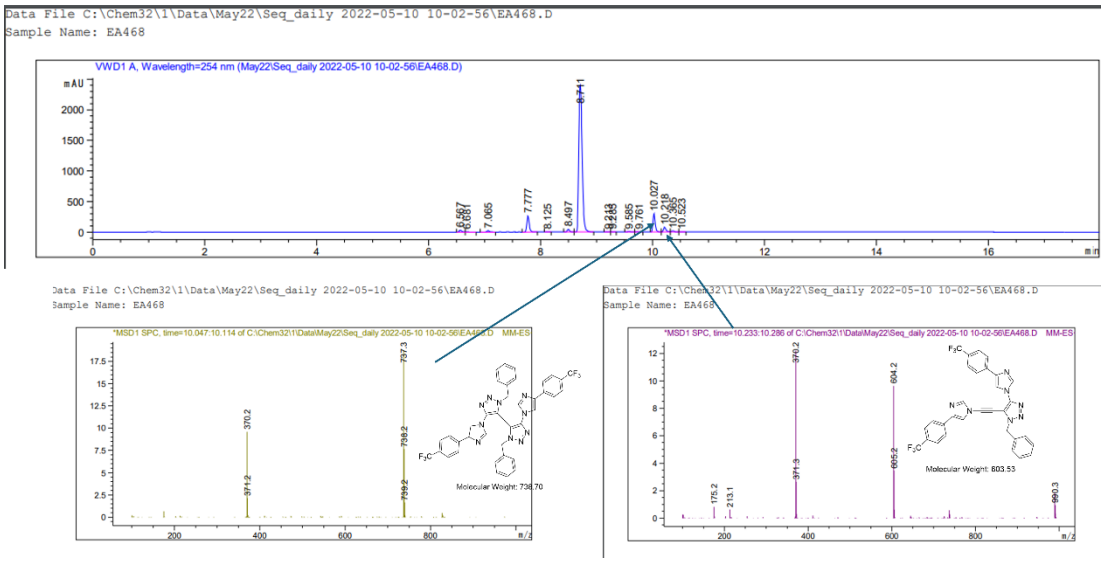

Figure 3.48. LC-MS traces of the reaction of imidazole **3.38** with benzyl azide **3.55** in IPA with 5 mol% $Cu(OAc)_2.H_2O$ showing the mass peak of two side products, as shown.

3.5.5 Single Crystal X-Ray Diffraction

All crystallographic measurements were made with monochromatic Cu radiation (λ = 1.54184 Å) using a Rigaku Synergy-i diffractometer. Raw data processing utilised the program CrysalisPro. All structures were solved using direct methods and were refined against F^2 to convergence using all unique reflections and the program Shelxl, as implemented within WinGX. All non-H atoms were refined anisotropically. H atoms bound to N or to O were placed as found and refined isotropically. H atoms bound to C were placed in geometrically expected positions and refined in riding modes. Selected crystallographic and refinement parameters are given for each structure obtained below.

3.5.5.1 Compound **3.22**

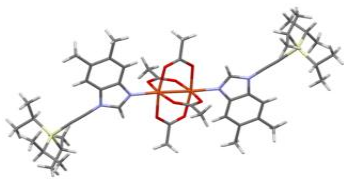

Compound	**13**
CCDC	2274320
Formula	$C_{48}H_{72}Cu_2N_4O_8Si_2$
Form. Wt.	1016.35

Space Group	P-1
Crystal system	Triclinic
Temp. (K)	100(2)
a (Å)	8.5416(1)
b (Å)	11.7320(1)
c (Å)	13.2393(1)
α (°)	96.411(1)
β (°)	98.152(1)
γ (°)	99.188(1)
Volume (Å^3)	1284.153(2)
Z	1
Z'	0.5
Measured Reflections	45754
Unique Reflections	4961
2θmax (°)	142.666
R_{int}	0.0493
Observed Reflections [I>2σI]	4730
No. Parameters	299
S	1.089
R [on *F*, obs refs only]	0.0403
ωR [on F^2, all data]	0.1190
Largest diff. peak /hole (eÅ^{-3})	0.911/-0.850

3.5.5.2 Compound **3.24**

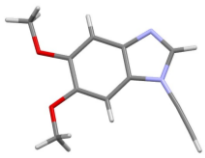

Table 3.12. Crystal data and structure refinement for **3.24.**

Empirical formula	C11 H10 N2 O2
Formula weight	202.21
Temperature	100(2) K
Wavelength	1.54184 Å
Crystal system	Orthorhombic
Space group	P n a 2_1
a (Å)	13.41220(10)
b (Å)	17.0940(2)
c (Å)	4.21320(10)
α (°)	90
β (°)	90
γ (°)	90
Volume (Å^3)	965.95(3)
Z	4
Density (calculated)	1.390 Mg/m^3
Absorption coefficient	0.807 mm^{-1}
F(000)	424
Crystal size	0.13 x 0.08 x 0.06 mm^3
Theta range for data collection	4.190 to 71.434°.
Index ranges	-16<=h<=16, -19<=k<=21, -5<=l<=5
Reflections collected	17661
Independent reflections	1698 [R(int) = 0.0249]
Completeness to theta = 70.000°	100.0%
Absorption correction	Semi-empirical from equivalents
Max. and min. transmission	1.00000 and 0.93133
Refinement method	Full-matrix least-squares on F^2
Data / restraints / parameters	1698 / 1 / 147

Goodness-of-fit on F^2	1.069
Final R indices [I>2sigma(I)]	R1 = 0.0285, wR2 = 0.0790
R indices (all data)	R1 = 0.0291, wR2 = 0.0796
Absolute structure parameter	-0.01(12)
Extinction coefficient	0.0029(6)
Largest diff. peak and hole	0.146 and -0.141 e.$Å^{-3}$

3.5.5.3 Compound **3.25**

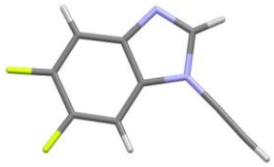

Table 3.13. Crystal data and structure refinement for **3.25**

Empirical formula	C9 H4 F2 N2
Formula weight	178.14
Temperature	100(2) K
Wavelength	1.54184 Å
Crystal system	Orthorhombic
Space group	P n a 2_1
a (Å)	8.4036(2)
b (Å)	14.2825(3)
c (Å)	6.32560(10)
α (°)	90
β (°)	90
γ (°)	90
Volume	759.23(3) $Å^3$
Z	4
Density (calculated)	1.558 Mg/m^3

Absorption coefficient	1.135 mm^{-1}
F(000)	360
Crystal size	0.2 x 0.2 x 0.05 mm^3
Theta range for data collection	6.110 to 70.920°.
Index ranges	-10<=h<=10, -17<=k<=16, -7<=l<=7
Reflections collected	3235
Independent reflections	1130 [R(int) = 0.0215]
Completeness to theta = 70.000°	100.0%
Absorption correction	Semi-empirical from equivalents
Max. and min. transmission	1.00000 and 0.25446
Refinement method	Full-matrix least-squares on F^2
Data / restraints / parameters	1130 / 1 / 135
Goodness-of-fit on F^2	1.071
Final R indices [I>2sigma(I)]	R1 = 0.0278, wR2 = 0.0754
R indices (all data)	R1 = 0.0280, wR2 = 0.0756
Absolute structure parameter	0.08(18)
Extinction coefficient	n/a
Largest diff. peak and hole	0.140 and -0.223 e.$Å^{-3}$

3.5.5.4 Compound **3.26**

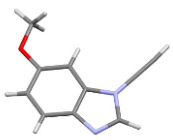

Table 3.14. Crystal data and structure refinement for **3.26**

Empirical formula	C10 H8 N2 O

Formula weight	172.18
Temperature	100(2) K
Wavelength	1.54184 Å
Crystal system	Monoclinic
Space group	C 2/c
a (Å)	9.0956(5)
b (Å)	15.2670(12)
c (Å)	13.0260(8)
α (°)	90
β (°)	103.858(6)
γ (°)	90
Volume	1756.2(2) $Å^3$
Z	8
Density (calculated)	1.302 Mg/m^3
Absorption coefficient	0.708 mm^{-1}
F(000)	720
Crystal size	0.14 x 0.07 x 0.04 mm^3
Theta range for data collection	5.788 to 71.580°.
Index ranges	-11<=h<=9, -18<=k<=18, -16<=l<=15
Reflections collected	4707
Independent reflections	1645 [R(int) = 0.0344]
Completeness to theta = 70.000°	97.1%
Absorption correction	Semi-empirical from equivalents
Max. and min. transmission	1.00000 and 0.86558
Refinement method	Full-matrix least-squares on F^2
Data / restraints / parameters	1645 / 0 / 127
Goodness-of-fit on F^2	1.037

Final R indices [I>2sigma(I)]	R1 = 0.0471, wR2 = 0.1270
R indices (all data)	R1 = 0.0569, wR2 = 0.1352
Extinction coefficient	n/a
Largest diff. peak and hole	0.279 and -0.264 e.Å^{-3}

3.5.5.5 Compound **3.30**

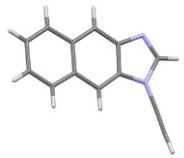

Table 3.15. Crystal data and structure refinement for **3.30**

Empirical formula	C13 H8 N2
Formula weight	192.21
Temperature	100(2) K
Wavelength	1.54184 Å
Crystal system	Triclinic
Space group	P -1
a (Å)	7.3567(3)
b (Å)	7.7447(4)
c (Å)	9.1200(4)
α (°)	99.474(4)
β (°)	98.631(4)
γ (°)	105.938(4)
Volume (Å^3)	482.27(4)
Z	2
Density (calculated)	1.324 Mg/m^3
Absorption coefficient	0.630 mm^{-1}
F(000)	200
Crystal size	0.12 x 0.10 x 0.06 mm^3

Theta range for data collection	5.024 to 71.350°.
Index ranges	-8<=h<=7, -9<=k<=9, -11<=l<=11
Reflections collected	4048
Independent reflections	1849 [R(int) = 0.0154]
Completeness to theta = 70.000°	99.9%
Absorption correction	Semi-empirical from equivalents
Max. and min. transmission	1.00000 and 0.97483
Refinement method	Full-matrix least-squares on F^2
Data / restraints / parameters	1849 / 0 / 144
Goodness-of-fit on F^2	1.076
Final R indices [I>2sigma(I)]	R1 = 0.0347, wR2 = 0.0897
R indices (all data)	R1 = 0.0387, wR2 = 0.0932
Extinction coefficient	n/a
Largest diff. peak and hole	0.137 and -0.214 e.Å^{-3}

3.5.5.6 Compound **3.31**

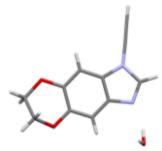

Empirical formula	C11 H10 N2 O3
Formula weight	218.21
Temperature	100(2) K
Wavelength	1.54184 Å
Crystal system	Monoclinic
Space group	I 2/a

a (Å)	18.3370(8)
b (Å)	3.9506(2)
c (Å)	27.4613(8)
α (°)	90
β (°)	92.930(3)
γ (°)	90
Volume	1986.75(14) $Å^3$
Z	8
Density (calculated)	1.459 Mg/m^3
Absorption coefficient	0.907 mm^{-1}
F(000)	912
Crystal size	.34 x .10 x .02 mm^3
Theta range for data collection	4.830 to 71.431°.
Index ranges	-22<=h<=22, -4<=k<=3, -33<=l<=33
Reflections collected	18120
Independent reflections	1920 [R(int) = 0.0869]
Completeness to theta = 70.000°	99.9%
Absorption correction	Semi-empirical from equivalents
Max. and min. transmission	1.00000 and 0.64677
Refinement method	Full-matrix least-squares on F^2
Data / restraints / parameters	1920 / 2 / 161
Goodness-of-fit on F^2	1.049
Final R indices [I>2sigma(I)]	R1 = 0.0514, wR2 = 0.1502
R indices (all data)	R1 = 0.0526, wR2 = 0.1520
Extinction coefficient	n/a

Largest diff. peak and hole	0.335 and -0.350 e.Å^{-3}

3.5.5.7 Comparison of Bond Length

From the structures, the bond lengths of some of the key bonds were obtained. The main bonds chosen to analyse were related to the alkyne: the N-C bond, the C-C bond and the C-H bond. The results are given in the table below:

Table 3.16. Bond lengths

Bond	**Ynamine**					
	3.24	**3.25**	**3.30**	**3.31**	**3.33**	**3.37**
N(1)-C(2)	1.363(3)	1.362(3)	1.3544(13)	1.356(2)	1.366(2)	1.366(2)
C(1)-C(2)	1.186(3)	1.187	1.1863(15)	1.186(3)	1.185(3)	1.183(2)
C(1)-H(1)	0.97(3)	0.91(3)	0.941(14)	0.91(2)	0.99(3)	0.97(2)

Weighted standard deviation (WSD) was used to estimate if there was a significant difference between bond lengths. Using ynamine **3.24** and **3.25** as an exemplar:

$WSD = ((0.03)^2 + (0.03)^2)^{1/2}$

$WSD = 0.042$

3 times WSD = 0.126

0.06 (sum of the two bond lengths added together) < 0.126 therefore not significant.

Upon calculating this for other bonds and for the other ynamines, no significant differences were found.

Chapter 4

Developments Towards the Synthesis of a New Ynamine BAPTA Calcium Probe

4.1 Introduction

In previous chapters, the synthesis of new ynamine scaffolds and their subsequent reactivity in the CuAAC reaction has been investigated. It was found that the synthesis of these ynamines tends to be facile, however, the reactivity between substrates differs significantly. The reactivity of these ynamines also varies in the solvent used, resulting in a system that can have the reactivity of the ynamine in the CuAAC tuned. It was hypothesised that the ynamine could be utilised in a biological system. Calcium probes are typically composed of two moieties, a BAPTA chelating core and a fluorophore, and the introduction of a handle for easy functionalisation can be difficult. The addition of an ynamine, with a bioorthogonal alkyne handle, would allow for the efficient (in yield and in reaction time) addition of a fluorophore or functional handle. By using a model system of ynamines **4.1** and **4.2** (Figure 4.1), the incorporation of this useful moiety into the system was attempted.

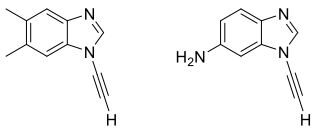

Figure 4.1. Ynamine scaffolds used in this chapter.

4.1.1 Routes Towards BAPTA Ca^{2+} Probes

Despite the number of commercially available calcium probes, and additionally, those published in research, they tend to have structural similarities.[114] This is due to the design considerations mentioned in Chapter 1.3.2, as the BAPTA scaffold does not tolerate many modifications without the alteration of the properties of the probe.

Typically, the BAPTA scaffold requires a functional handle to allow conjugation to the fluorophore, and designing this can be difficult due to the limitations.[114] However, there are a few scaffolds, including the hydroxyl (**4.3**), amine (**4.4**) and aldehyde (**4.5**) that have been used more extensively. A selection of scaffolds is shown in Figure 4.2.

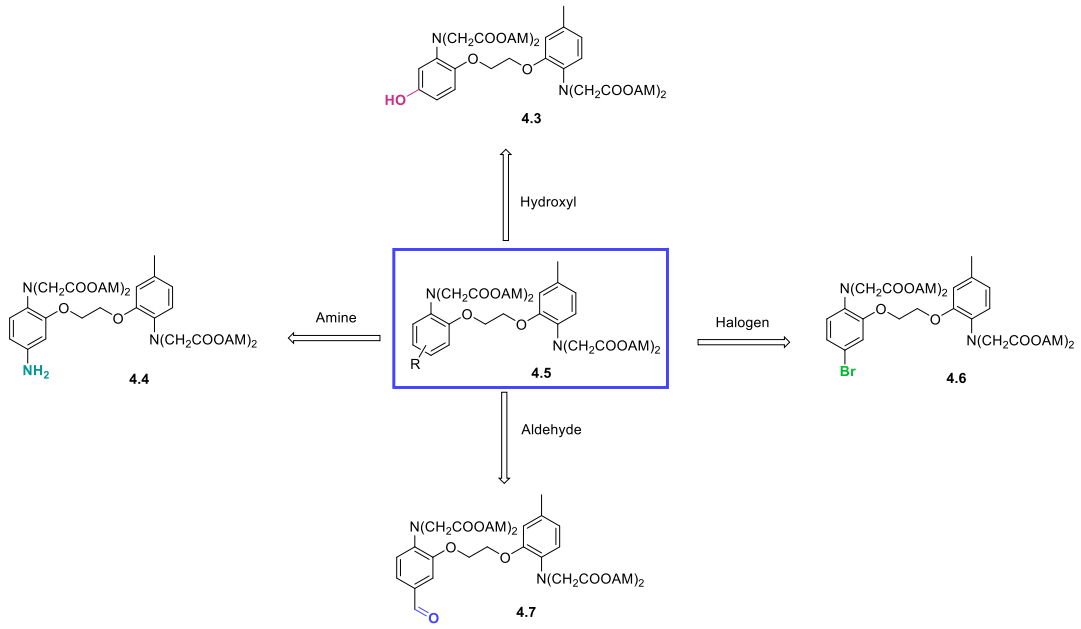

Figure 4.2. Different strategies that can be employed to functionalise the BAPTA scaffold for the synthesis of calcium probes.

The BAPTA moiety **4.5** can bear several reactive handles allowing further conjugation with the fluorophore. The presence of an alcohol (**4.3**), obtained through various synthesis can then lead to the formation of a chelator with an expanded ring system (Section 4.1.1.2). The introduction of an amine group (**4.4**) facilitates the use of amide couplings with acidic fluorophores. A halogen group can also be incorporated (**4.4**) which can then be involved in cross-couplings for C-C bond formation. One of the more versatile functional groups is an aldehyde (**4.7**), which, upon incorporation, can be utilised to introduce groups such as acids and alkynes. The synthesis of these, amongst others, is described in the following sections.

The synthesis of probes tends to be linear and does not allow for a large extent of conjugation. This poses limitations for the fluorescence emission properties, as the more conjugation in a compound, the longer the fluorescence wavelength.[197] The synthesis of most typical, successful, calcium probes can fall into two strategies:

1. A convergent synthesis, where the BAPTA handle, and the fluorophore, are synthesised in parallel with reactive handles and then conjugated together.
2. A linear synthesis, where the fluorophore is synthesised using the BAPTA scaffold.

4.1.1.1 Functionalisation Using Aldehyde

As shown in Figure 4.3, the installation of an aldehyde group enables the incorporation of several different functional groups to the BAPTA core.

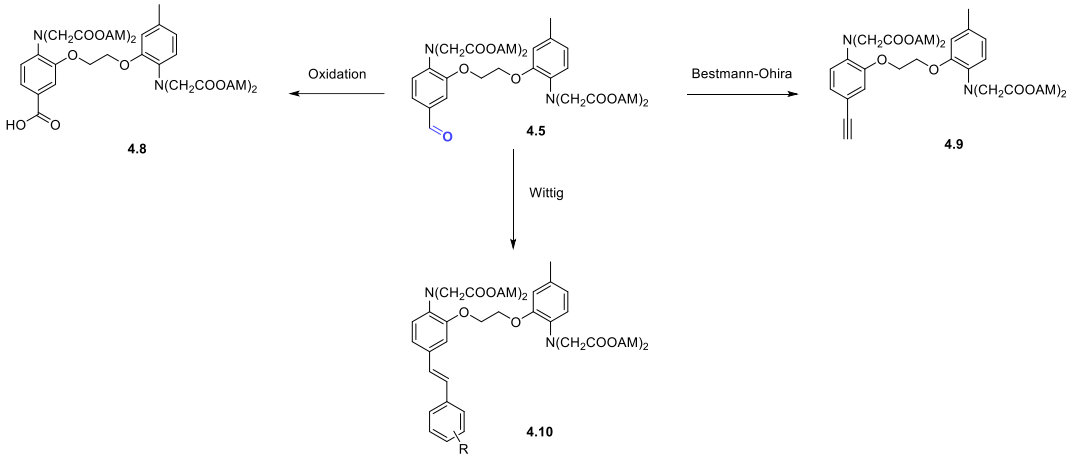

Figure 4.3. Different reactions that an aldehyde handle (**4.5**) can undergo.

The synthesis for the aldehyde linker was first reported in 1985 by Grynkiewicz *et al.* on scale (Scheme 4.1).[132] The synthesis begins with the formation of the aromatic scaffold before the Ca^{2+} chelators' core is added (can be esters or AM esters depending on the substrate and further use), which is followed by functionalisation.

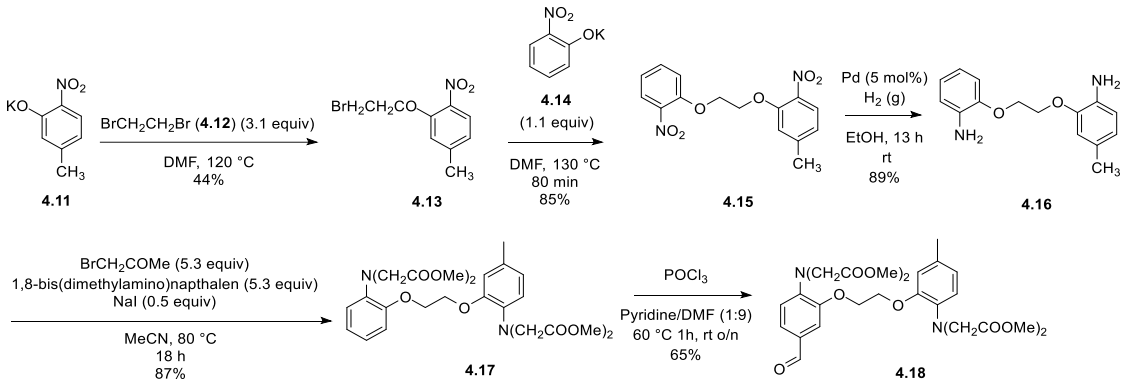

Scheme 4.1. Reported multi-step synthesis of aldehyde **4.18**.

The alkylation of the nitrophenol derivative (**4.11**) by dibromoethane (**4.12**), and the further alkylation using **4.14** forms the biaryl core (**4.15**). The nitro groups are then reduced *via* hydrogenation to amines (**4.16**) followed by an *N*-alkylation using a bromoacetyl derivative before a Vilsmeier-Haack to form the aldehyde (**4.18**).

The aldehyde has then been used for a variety of functionalisations to give calcium probes (Scheme 4.2).[132,198–200] In the synthesis of indo-1 (**4.23**), a Wittig reaction occurs to give **4.21**

before cyclisation to form an indole (**4.22**).[132] The ester groups are then removed using KOH to give indo-1 in the desired form (**4.32**).

The synthesis of TP-BAPTA probe **4.26** follows a similar synthesis to **4.23**, with the aldehyde being formed (**4.19**), followed by a Wittig reaction to give **4.25** and then the ester cleavage to give the final probe **4.26**.[199]

The aldehyde formed can also be oxidised to a carboxylic acid through a Pinnick reaction. Barandov *et al.* used the acid **4.27** in an amide coupling with a PEG linker.[201]

An aldehyde (**4.8**) can also be used to form an alkyne (**4.29**) using the Bestman-Ohira reagent. This was attempted by Schwarze *et al.* to form a triazole coumarin **28**.[200]

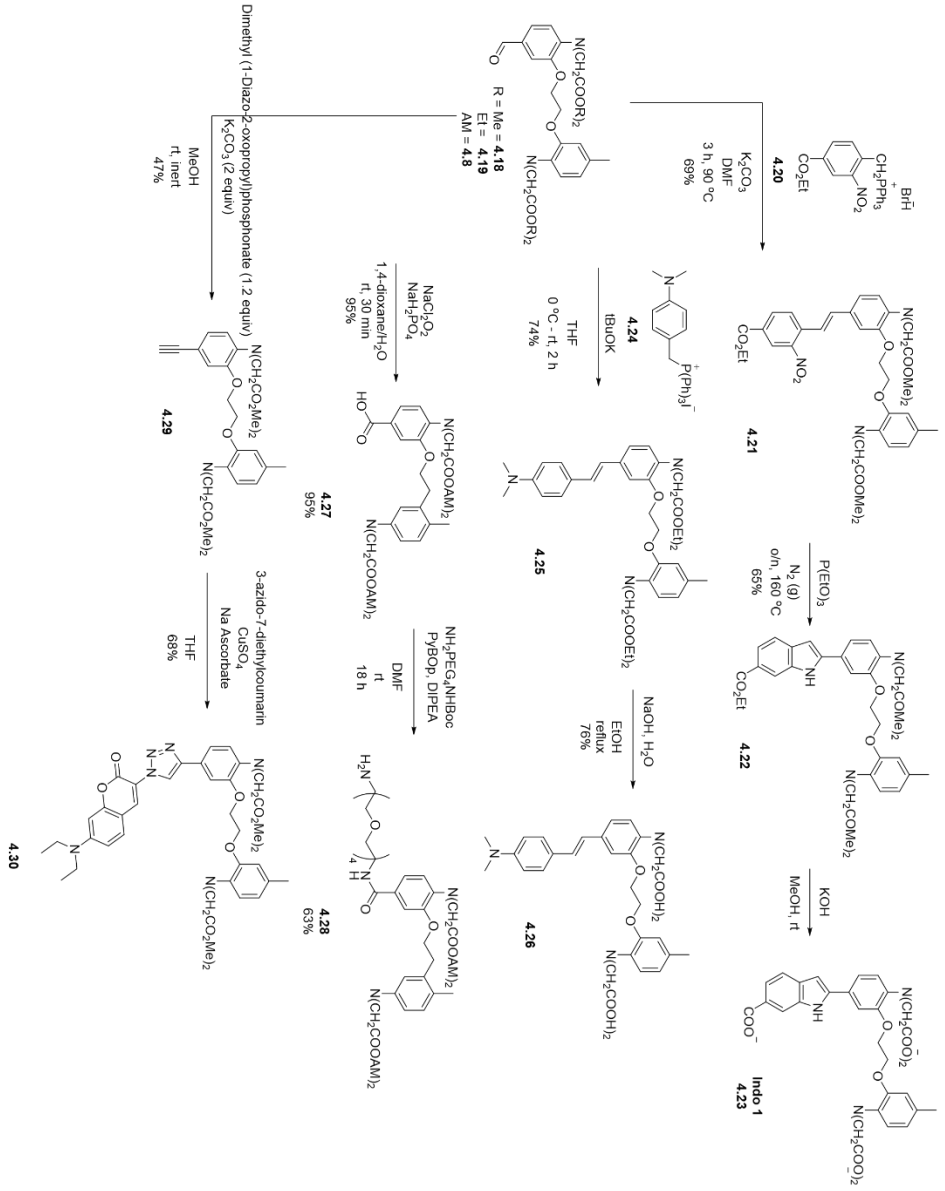

Scheme 4.2 Various routes of functionalisation of the aldehyde to give probes.

The series of probes termed calcium rubies developed by Collet *et al.* add the fluorophore moiety through a reaction with an aldehyde.[137] However, the BAPTA chelating core is synthesised through an adapted route (Scheme 4.3) to allow for the inclusion of the azide arm (**4.40**) that is used for further functionalisation of these probes.

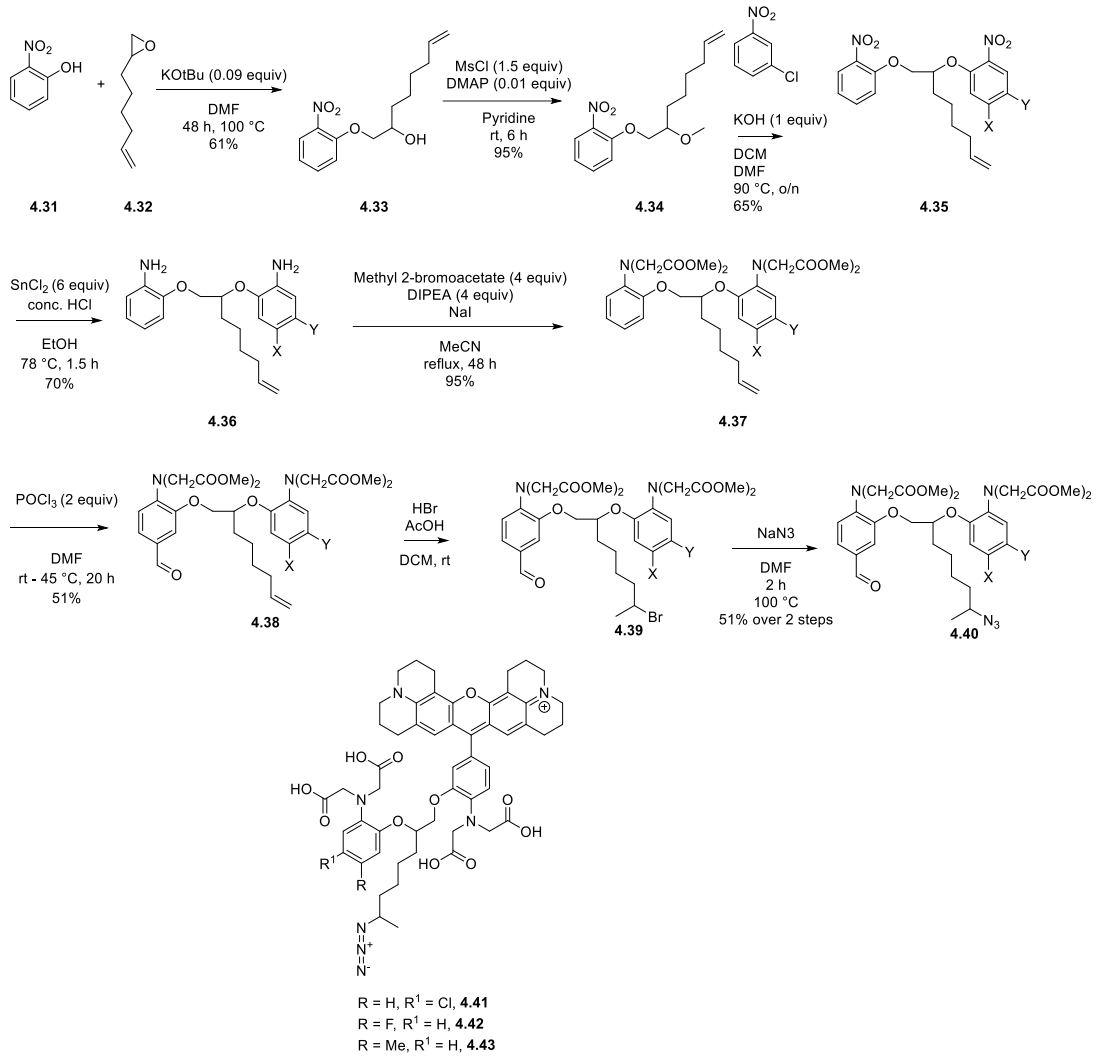

Scheme 4.3. Synthesis of **4.40** the aldehyde moiety of the Calcium Rubies (**4.41 – 4.43**).

As shown above, the BAPTA core is built up first with the inclusion of an alkene arm (**4.33**), followed by the methylation of the alcohol (**4.34**) and addition of the second aromatic group (**4.35**). The nitro groups are then reduced using Sn(II) chloride and HCl to give the amine groups (**4.36**) which are subsequently transformed into esters (**4.37**). The aldehyde is than added as before (**4.38**). Following the addition of the aldehyde, the terminal alkene on the chain is transformed to a bromine and then the desired azide. Following the installation of the azide (**4.40**), acetalization occurs to add the fluorophore to give the probes **4.41 – 4.43.**

4.1.1.2 Linear Synthetic Strategies Using Aldehydes

The fluorophore can also be incorporated into the BAPTA by using a linear synthetic strategy. In this case, the fluorophore is built into the BAPTA core instead of being added in a one-step reaction. This increases the number of steps in the synthesis and can result in lower overall yields. These probes use an aldehyde that is installed in the ring in conjunction with a phenol group to undergo a condensation reaction forming a ring system conjugated to the BAPTA core.[132] This is a longer synthesis, 10 steps to obtain the final probes, and 8 steps to the common core (Scheme 4.4). The synthesis begins from the *p*-hydroquinone (**4.44**) where the alcohols are benzyl protected (**4.45**) using benzyl chloride. Nitration can be achieved at the 2-position (**4.46**) before selective debenzylation of the phenol group ortho to the nitro (**4.47**). An alkylation joins the cores together (**4.49**) and hydrogenation with platinum reduces the nitro groups to amines (**4.50**). The aldehyde is then formed using a Vilsmeier-Haack reaction before deprotection of the phenol (**4.452**).

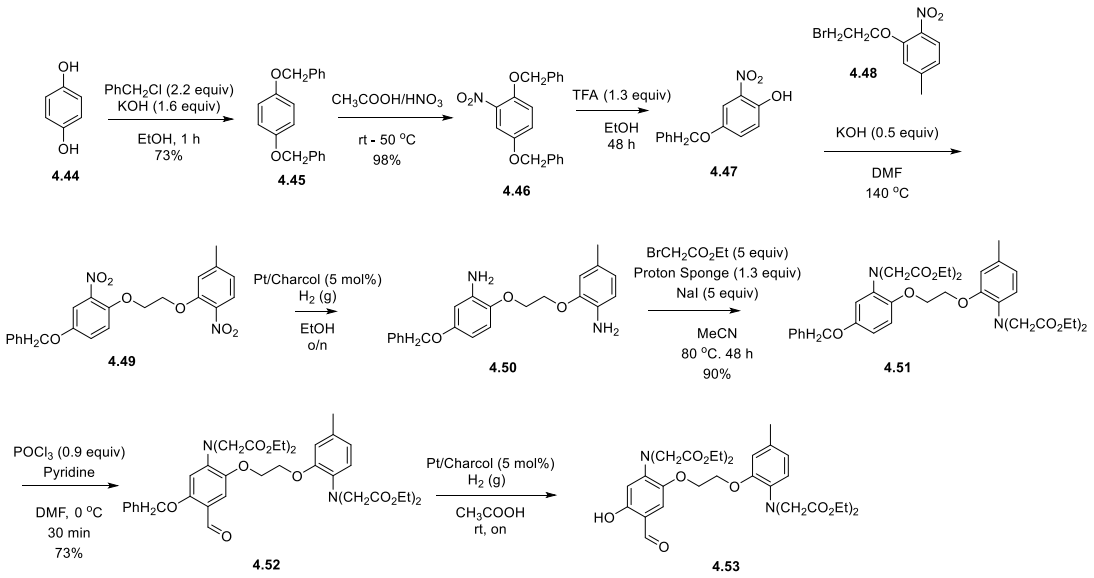

Scheme 4.4. First reported synthesis of a core (**4.53**) for the beginning of fluorophore building.

In the synthesis of the fura-analogues, a Knoevenagel condensation forms the benzofuran ring (**4.54**) before the ester cleavage to give the probes **4.56 – 4.58 (**Scheme 4.5).[132]

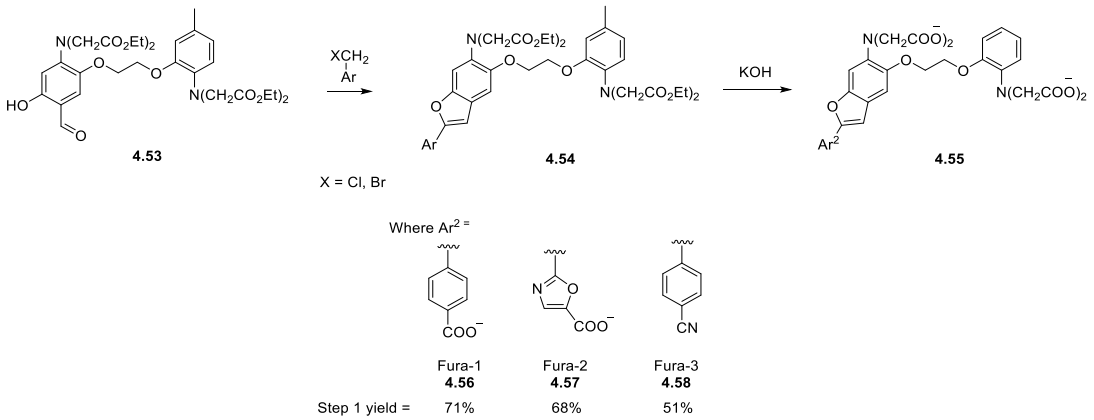

Scheme 4.5. Synthesis of the Fura series (**4.56 – 4.58**) from the common core **4.53.**

Following the success of the fura series of probes, other probes have also been synthesised using built-up ring systems. Komatsu *et al.* uccessfully synthesised KCM-1 (Scheme 4.6).[202] The same core building block was used to obtain **4.59**, with the only difference being the fluorine group in place of the methyl. The synthesis of the aromatic extended core involves the condensation reaction between **4.59** and the malonic acid dibenzyl to give coumarin-like **4.60**. The acid is deprotected using H_2 and Pd/C (**4.61**). Esterification occurs before the formation of the AM esters (**4.63**).

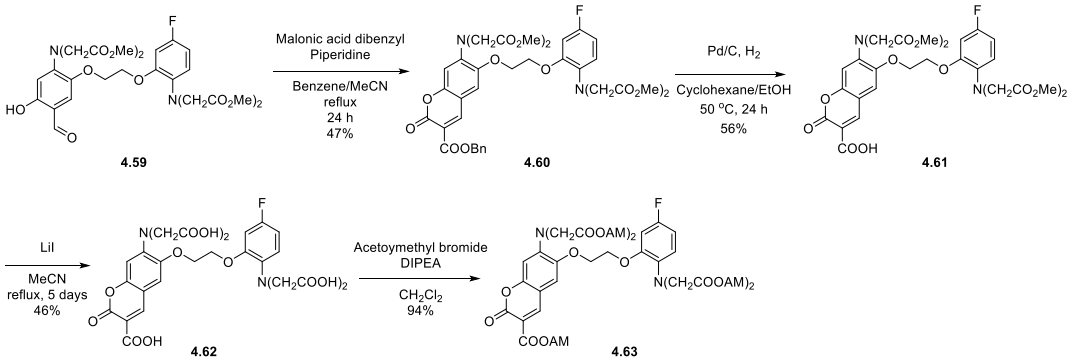

Scheme 4.6. Multi-step synthesis of KCM-1 (**4.63**).

Another core synthesised probe is NitroAzidoFuraRed (**4.69**), also a ura derivative (Scheme 4.7).[203] The route was adapted from the original synthesis by Grynkiewicz *et al.* but producing an intermediate that does not contain a methyl group on the aromatic core of the BAPTA.[132]

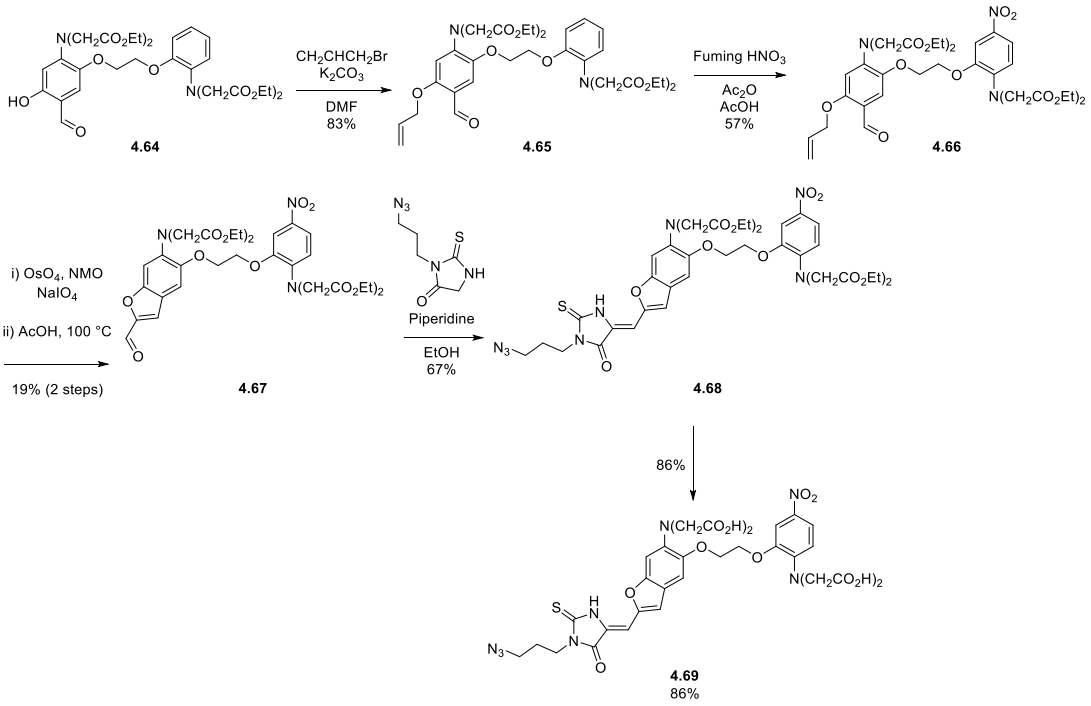

Scheme 4.7. Final steps of the synthesis of NitroAzidoFuranRed **4.69.**

As shown in Scheme 4.7, an allyl group was introduced to phenol **4.64**. The nitration was then achieved to give **4.66**. Oxidation and cyclisation of **4.66** using osmium tetroxide and sodium periodate followed by acid gave **4.67**. The thiohydantoin was added using a Knoevangel condensation (**4.68**) and following saponification of the esters, NitroAzidoFuraRed (**4.69**) was synthesised. From **4.64** to **4.69**, the overall yield is 5%.

4.1.1.3 Amine Formation

A further method of attaching a fluorophore to the BAPTA core is by incorporating an amine on the core to subsequently form an amide. The route towards the amine involves the nitration of synthesised BAPTA core (**4.70**) followed by hydrogenation of the nitro to give the amine (**4.72**, Scheme 4.8).[116,204]

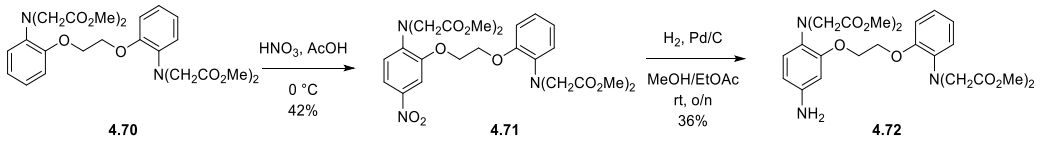

Scheme 4.8. Synthesis of an amine on the BAPTA core (**4.72**).

This synthesis was used in the examples given in Figure 4.4 which all contain an amide linker.[204–206]

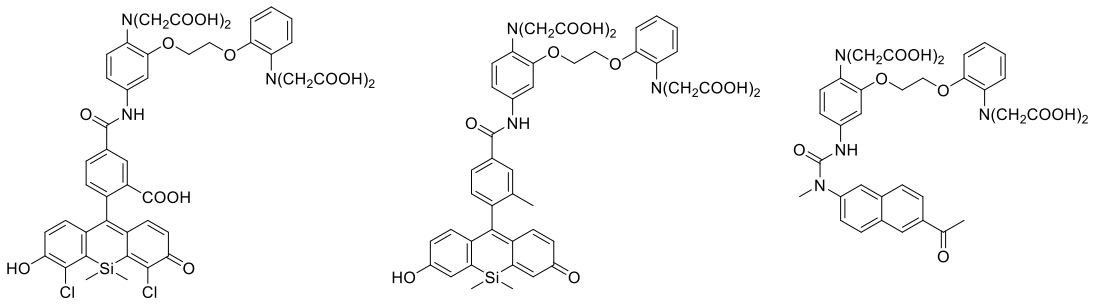

Figure 4.4. Probes containing an amide linker. CaTM (**4.73**), CaSIR (**4.74**), Ace-1 (**4.75**).

4.1.1.4 Use of Halogen-based reactive handles

Fluorophores have also been added to a BAPTA core by using a halogen as a reactive handle. The core **4.76** was formed *via* bromination of **4.77** with elemental bromine (Scheme 4.9).[125]

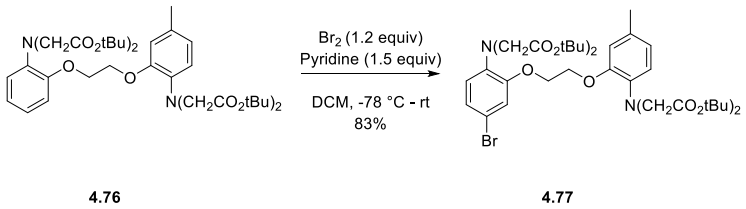

Scheme 4.9. Bromination of core **4.76** to produce **4.77**.

From the brominated core, the fluorophore is incorporated through a lithiation on the aryl bromide to form a nucleophile that then attacks the ketone and eliminates (Scheme 4.10).[207] This method gives **4.79**, a BAPTA-fluorophore conjugate.

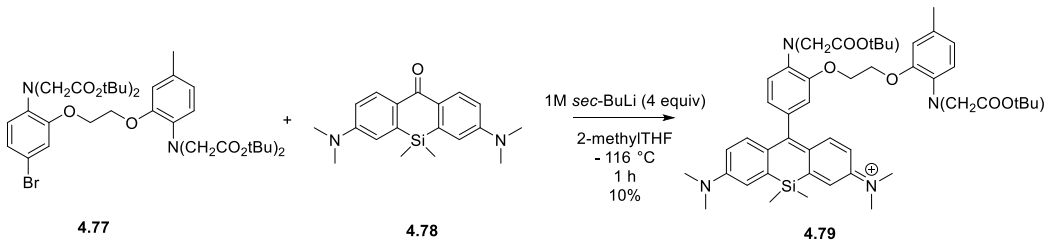

Scheme 4.10. Addition of a fluorophore (**4.78**) to a brominated core (**4.77**) to give the BAPTA fluorophore conjugate **4.79**.

A brominated BAPTA analogue is also used in the synthesis of a HaloTag calcium indicator (Scheme 4.11).[139] From the brominated core **4.80**, a Buchwald-Hartwig reaction was used to form **4.82**. This probe varies from the norm in that it does not contain a fluorophore owing to the HaloTag that is added on further into the synthesis, however, it displays further potential uses for the bromine moiety.

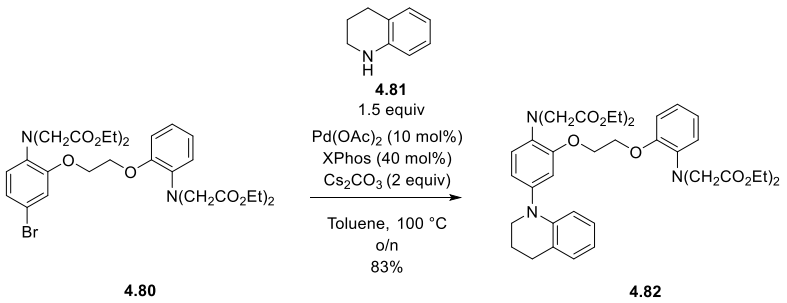

Scheme 4.11. Synthesis of HaloTag probe intermediate **4.82** from **4.80**.

4.1.2 Summary of Existing Strategies to Prepare Calcium Imaging Probes

As has been shown, synthesis of the BAPTA scaffold takes several steps, and the synthesis has not undergone much optimisation since the initial publication by Grynkiewicz *et al*.[132] To synthesise an aldehyde handle is 5 steps, with an overall yield of 19%. Linear synthesis then takes between 2-4 additional steps to give a final probe, including esterification, and some of these steps can be low yielding, dependent on the substrate. Convergent synthesis tends to take 10 steps to the final compound (including initial aldehyde synthesis), resulting in a lengthy and time-consuming synthesis. Total yields for the syntheses are also low, showing that there is still room for improvements in the synthetic procedures.

Click chemistry, in particular the CuAAC, is a high yielding reaction with maximum atom efficiency that forms a single regioisomer. Due to the many alkynes and azides that are commercially available, it can form part of a modular system, allowing facile changes in the R groups.

The aldehyde has been shown to be the most versatile handle and is the most used. It opens up various synthetic possibilities such as a Wittig reaction and oxidation to the acid. The amine handle however, despite the apparent simplicity in the approach, is less well used as a linking group. This could be attributed to the lack of diversity that can be obtained from the amine groups, as well as the lack of conjugation to the system though the bond. Cross-couplings, whilst not currently well used, are not ideal due to the bulky scaffold of the BAPTA, and potential interference in the catalytic cycle.

4.2 Hypothesis of Chapter 4

It is hypothesised that the developments of ynamine-based click chemistry can be applied to the BAPTA scaffold to form a probe. The ynamine can have two functional handles: the alkyne (for a CuAAC reaction), and the substituent group on the ynamine scaffold. It was therefore hypothesised that the ynamine can be attached to the BAPTA scaffold and have different ways in which a fluorophore, for imaging, or a targeting moiety, could be attached (Figure 4.5).

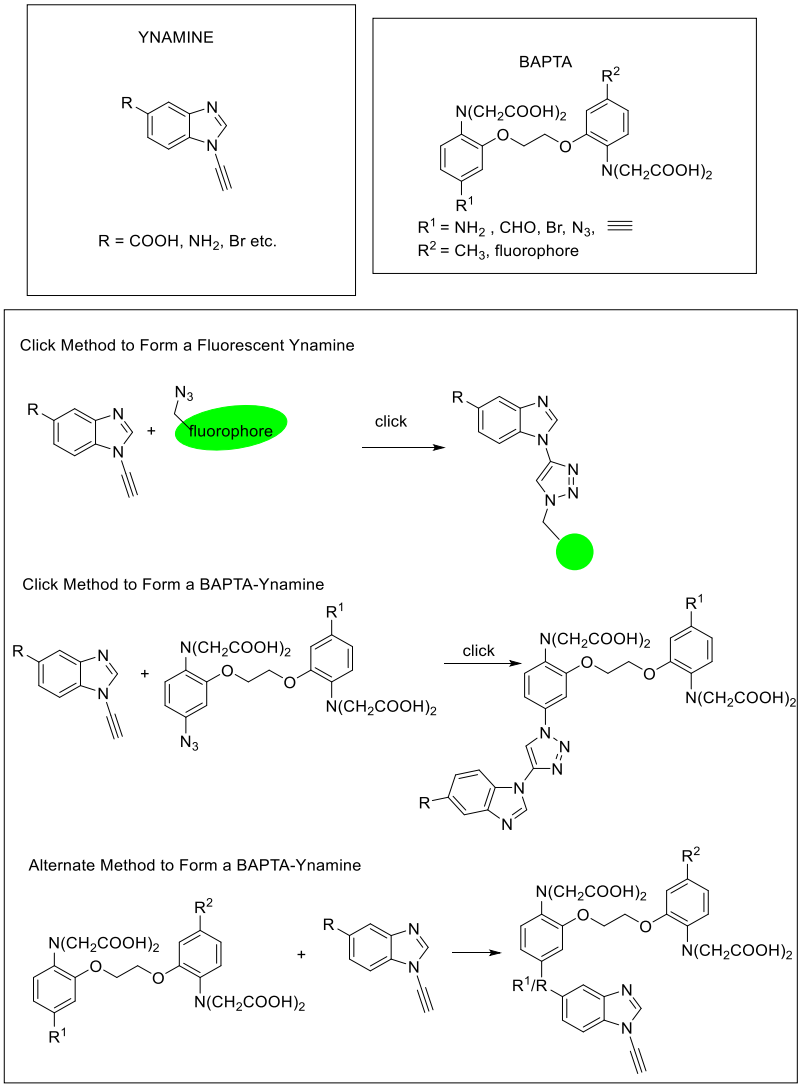

Figure 4.5. Potential uses of the ynamine in a BAPTA scaffold.

4.3 Aims of Chapter 4

The aims of this chapter are:

i) To synthesise a calcium chelator core that will allow for facile modulation.

ii) To functionalise a calcium chelator framework with an aromatic ynamine.

4.4 Results & Discussion

It was initially postulated, after a literature search, that there were different routes to the synthesis of a calcium chelator (Chapter 4.1) and modification of these could allow for the insertion of an ynamine (Figure 4.6). The synthesis of an amine scaffold **4.84** would allow for amine couplings, potentially through a linker or through an ynamine with a carboxylic acid functionality (**4.85**) (Figure 4.6A). A halogen handle, **4.89,** could allow for benzimidazoles to attach through a cross coupling (Figure 4.6B). This would allow the alkyne to be free for fluorophore addition or an organelle targeting moiety. The aldehyde **4.92** would open the most options, with further formation of an acid (**4.91**) allowing addition of the ynamine **4.2** (Figure 4.6C). The amide route, on paper, appears to be the simplest. However, this would result in a break in the conjugation system of the fluorophore, and to develop fluorophores towards the NIR zone, increased conjugation is a key factor.[208]

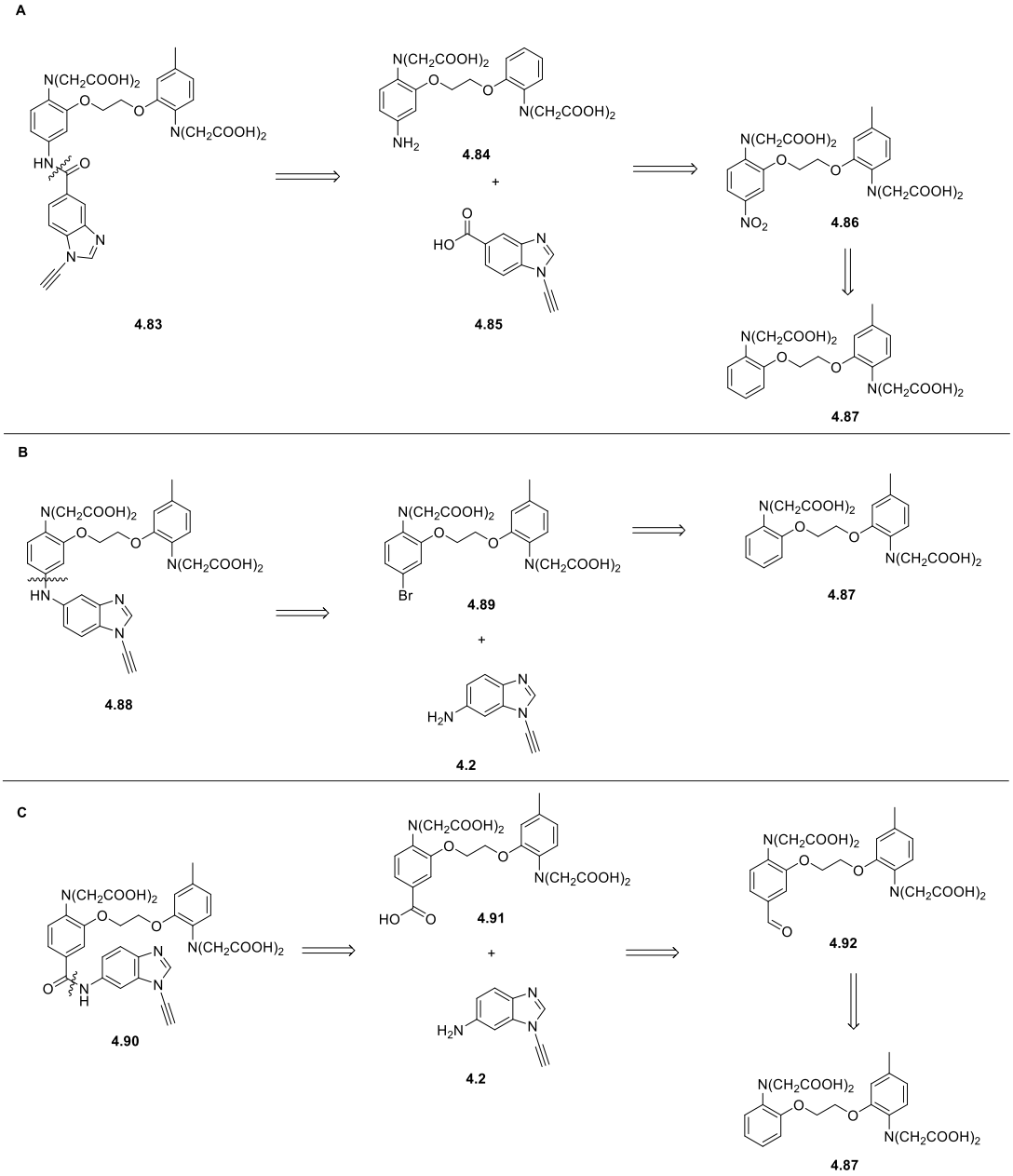

Figure 4.6. Potential scaffolds to utilise the ynamine scaffold in a BAPTA probe. **A)** Use of an amide to form an amide bond; **B)** Use of a halogen handle for a cross-coupling reaction; **C)** Use of an acid for an amide bond formation.

One method commonly employed in literature that was not considered was the building up of an extended aromatic core as seen in the fura series[132] (Scheme 4.5) as this would not have allowed for facile inclusion of an ynamine moiety.

4.4.1 Synthesis of an Amine Functional Handle

As a starting point, due to the simple nature of the route, the nitration of a commercially available BAPTA scaffold (**4.93**) was attempted. It was hypothesised that the nitration of the core, followed by reduction to the amine, would allow for the easy addition of ynamines and various linking groups. Taking literature conditions for nitration of the commercially available scaffold **4.93**, glacial acetic acid and nitric acid were used.[116] However, the reaction was unsuccessful (Scheme 4.12).

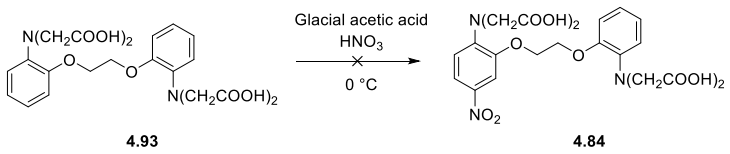

4.93 **4.84**

Scheme 4.12. Failed synthesis of a nitrated BAPTA core **4.84**.

Upon attempting the reaction, degradation appeared. Multiple spots were observed on TLC and LC-MS analysis did not show product mass. The route was taken no further and other methods to develop a linking moiety were investigated through the synthesis of a halogen handle and an aldehyde group. On reflection, protection of the acid groups with an ester moiety observed in other synthesis should have been attempted. This would have been able to troubleshoot whether the nitration conditions were posing an issue or, if it was the free acid groups. Commercially available **4.93,** without a directing methyl group, was used as an initial starting point to test the reaction, due to the number of steps required to synthesise BAPTA core **4.18** for a test reaction that may yield poor quantities and where the regioselectivity may struggle to be controlled.

4.4.2 Synthesis of a Halogen Functional Handle

An attempt to use a halogen for the addition of functional groups, in this case a bromine, was investigated. Following the successful build-up of the Br-BAPTA core (**4.88**), it was envisaged that the addition of a bromine would allow cross-coupling additions of an ynamine to take place (Scheme 4.13).

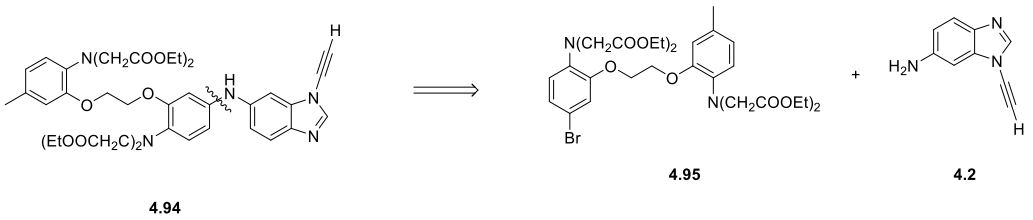

Scheme 4.13. The anticipated retrosynthesis of **4.94**.

Two initial routes to the Br-BAPTA were tested, the first, the alkylation of the brominated nitrophenol (**4.96**) with **4.12** to give **4.97** (Scheme 4.14).

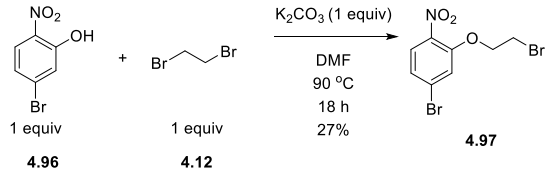

Scheme 4.14. Synthesis of a brominated nitrophenol derivative **4.97**.

On a small-scale reaction (2.3 mmol), the substitution as shown in Scheme 4.14 gave a yield of 27%. However, when the reaction was scaled up to 14 mmol, the yield dropped significantly to 12%. The reaction may have needed longer to run, or an increase in the equivalents of the reactants.

After the successful synthesis of **4.97**, the second step of the reaction involved the addition of either the methyl-nitrophenol **4.98** or the nitrophenol **4.100**. The nitrophenol **4.100** was used to assess whether there was any difference in the synthesis when using a des-methylated analogue.

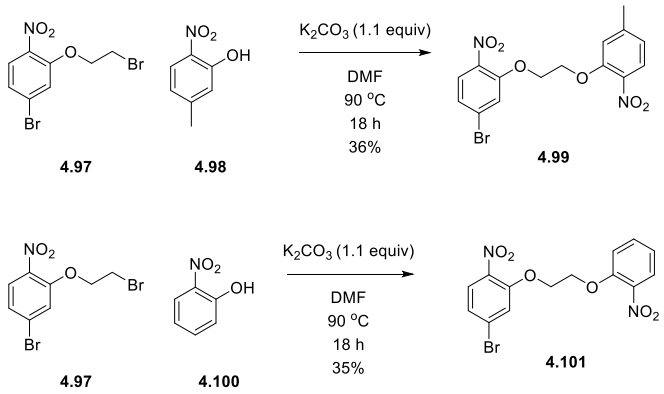

Scheme 4.15. Synthesis of a methylated (**4.99**) and des-methyl (**4.101**) BAPTA core.

As the synthesis of the brominated core (**4.99**) gave low yields, a second method was attempted, where **4.98** was alkylated to give **4.13** before the formation of **4.99**. This synthesis gave a good yield of 93% for the alkylation of the brominated **4.93** (Scheme 4.16).

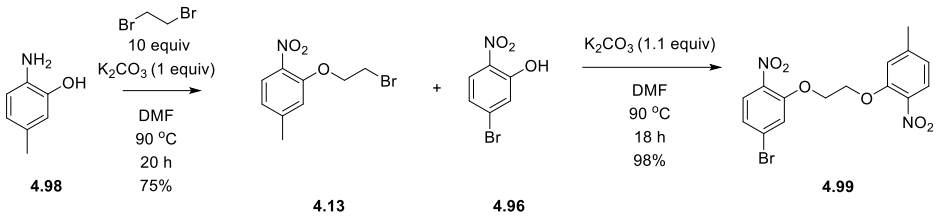

Scheme 4.16. Formation of a brominated core **4.95**

The nitro groups were then reduced to amine groups using iron powder and ammonium chloride (Scheme 4.17). The previous method of reduction using hydrogen and Pd/C could not be used due to the halogen present. This gave a yield of 23% (Scheme 4.17). The reaction was stopped after 30 min due to the iron forming a coating on the stirrer bar. The addition of more iron powder, or more vigorous stirring, may have facilitated pushing the reaction closer to completion. Examination of the characterisation data showed that an amide salt may have formed, and that iron may be remaining in the product.

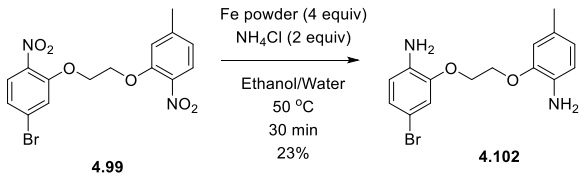

Scheme 4.17. Reduction of nitro groups to amines using iron to form **4.102**.

The next step in the synthesis was the addition of ester groups to the methyl to form **4.104** (Scheme 4.18).

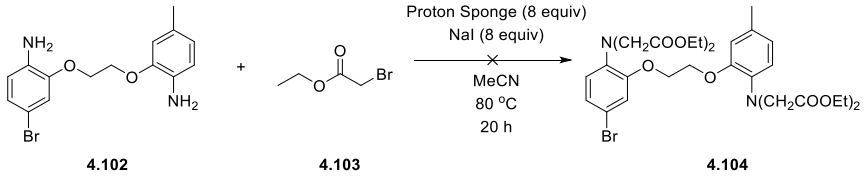

Scheme 4.18. Attempted synthesis of **4.86**.

However, using these conditions, the reaction does not go to completion. Instead, the LC-MS trace is showing multiple peaks with between 2-4 equivalents of ester groups added on. To

attempt to push the reaction towards completion more equivalents of the proton sponge, ethyl 2-bromoacetate and sodium iodide were added. The reaction was also heated for longer. This resulted in more of the fully esterified product being formed, however, it still was not the main product. Further equivalents could be added to push the reaction further and obtain the desired product as the major product. In future, the reaction will be done on a larger scale to allow for isolation of the intended product for further reactions, and, also to determine which amine group the ester adds on to first. Unfortunately, no more attempts were taken at this stage and the synthesis was not optimised.

4.4.3 Synthesis of the Aldehyde BAPTA Scaffold

Following the attempts at the other handles, it was decided to follow literature in the synthesis of a core that is used in many BAPTA probes, the aldehyde handle.[201] As shown in 4.1.1.1, the route towards an aldehyde handle is lengthy, however, it allows the formation of a versatile, reactive handle. This a multi-step synthesis that involves building up the core and then adding functional groups (Scheme 4.19).

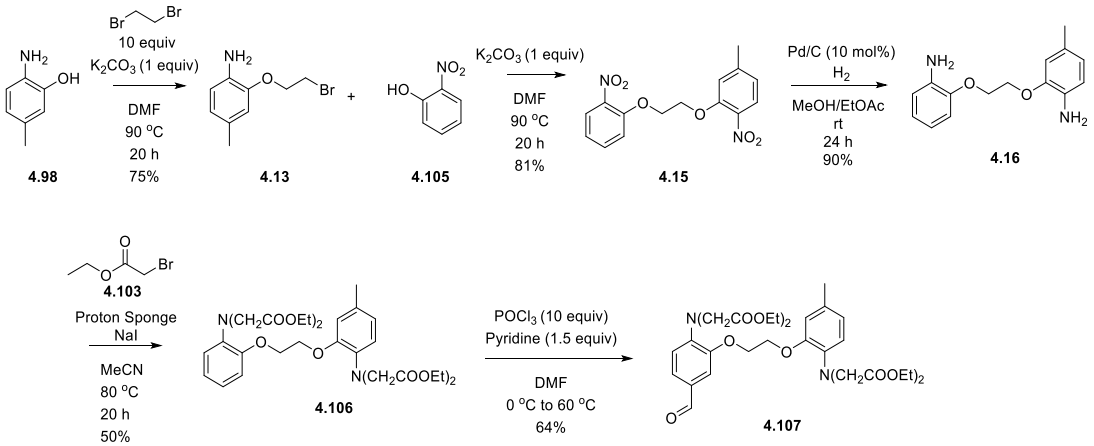

Scheme 4.19. 5 step synthesis to form a BAPTA core with an aldehyde functional group (**4.107**) with an overall yield of 17%.

Following literature conditions, the first step, alkylation of **4.98** tended to typically yield around 50%, with a large amount of the starting 5-methyl-2-nitrophenol **4.98** remaining. The equivalents of KOH and the 1,2-dibromoethane were increased resulting in a yield increase to 75%. Yields were required to be as high as possible due to the multi-step synthesis involved. The second step gave high yields, greater than 80%, with no column chromatography needed as the product formed a precipitate upon the addition of water. The third step, the hydrogenation, gave yields consistently at 90% after overnight stirring. Step 4, to give **4.106**

also displayed low yields when following literature precedent. Upon increasing the number of equivalents of the proton sponge and **4.103**, the reaction proceeds well. The Vilsmeier-Haack reaction to form the aldehyde gave low-moderate yields ranging from 20 - 64%. This was a key step in the synthesis as the aldehyde is required for the linker and so low yields posed a problem for the scale up of the synthesis.

For delivery into the cell, an AM ester is the ideal version. The ester allows the probe to easily enter the cell, and on entry, esterases cleave the ester, trapping the charged molecule in the cell. To install the AM ester, the ester group of **4.18** has to be saponified and the AM ester added (Scheme 4.20). However, whilst the cleavage of the ester **4.107** was successful to give **4.192** as an intermediate, the subsequent addition of the carboxylic acid to give **4.108** was not.

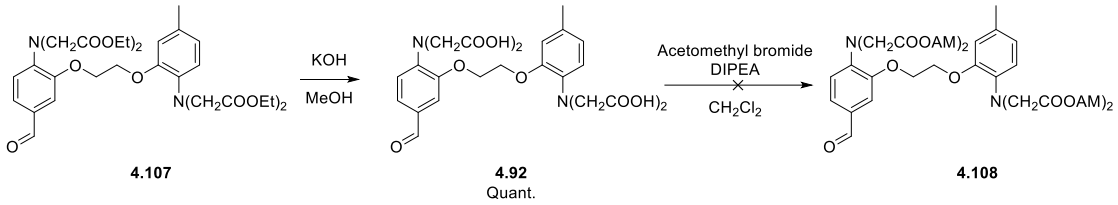

Scheme 4.20. Ester cleavage of **4.107** and attempted addition of an AM ester to **4.92**.

Due to this failure, the Et ester **4.107** will be used for test reactions, and once a suitable workflow has been established, then the cleavage and esterification will be attempted in the last steps in a probe synthesis, provided that there is not a base labile group present.

Following the successful synthesis of the BAPTA core with the aldehyde group (**4.107**), the first attempted functionalisation was to form an acid (**4.109**) (Scheme 4.21).

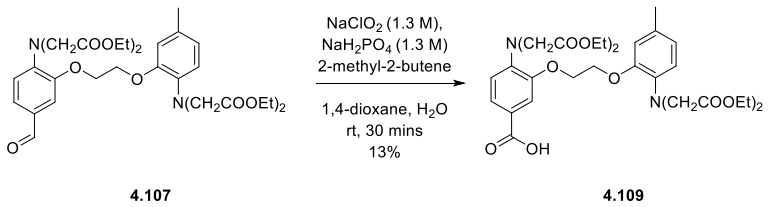

Scheme 4.21. Formation of BAPTA-acid **4.109**.

The acid (**4.109**) was formed in 13% yield. In an initial test, 3 additions of aqueous solutions of NaH_2PO_4 (1.3 M) and $NaClO_2$ (1.3 M) were carried out 30 min apart and the reaction monitored by TLC. After 5 h, the reaction was still progressing and so was left overnight. It is

not known if the extended reaction time caused the degradation or unknown side product peaks that were seen on the crude NMR. However, on the second attempt, the reaction was not left for as long and quenched when the acid (**4.109**) was visible on TLC. This resulted in **4.109** being successfully isolated in a 13% yield. The acid **4.109** can then be used for amide couplings to conjugate to the ynamine.

Another modification reported in literature was the conversion of the aldehyde to an alkyne using the Bestmann-Ohira regent. In literature, this was used to couple coumarin azide to a BAPTA chelator, as well as various other metal chelators.[200] It was hypothesised that other fluorescent azides could be added to the indicators or linkers used to add the ynamine in another way. The synthesis is given in Scheme 4.22

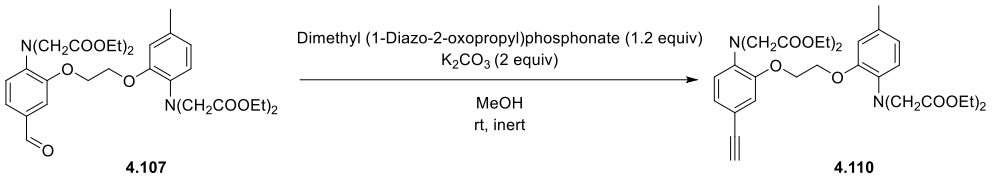

Scheme 4.22. Attempted synthesis of an alkyne from an aldehyde using the Bestmann-Ohira reagent. Traces of the product were detected by LC-MS, however, no **4.110** was isolated.

On a small-scale test reaction, a new spot forming was observed *via* TLC and the product mass was identified *via* LC-MS. However, when the reaction was scaled up the synthesis was unsuccessful. Instead, three peaks were formed, none bearing the product mass (Figure 4.7).

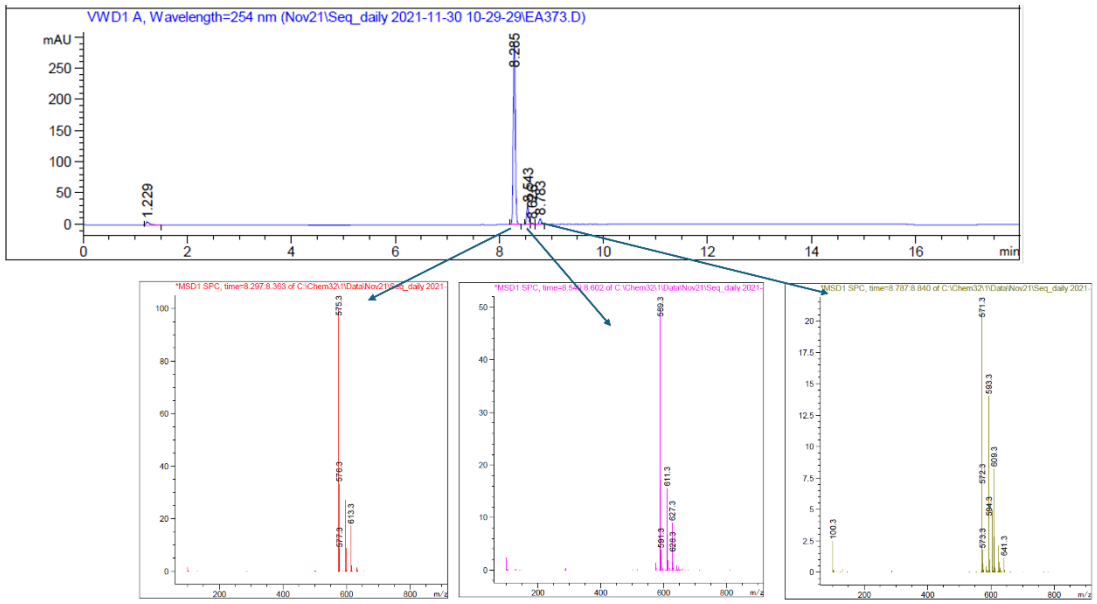

Figure 4.7. LCMS trace showing the formation of the three peaks and the corresponding masses of the peaks.

As can be seen in Figure 4.7, no peak bearing either starting material (mass = 630.69) or the desired product (mass = 626.70) is found. The mass consistent with the largest peak is consistent with the loss of two ester groups, potentially due to the presence of base and MeOH. However, alternative conditions could not be found in literature. No further attempts were made to synthesise the alkyne. The use of EtOH as the solvent instead of MeOH would be tested in any follow up reactions, to avoid the cleavage of the ethyl ester and the formation of a methyl ester.

4.4.4 Ynamine-Fluorophore-BAPTA Conjugates

The acid (**4.109**) was then used for amide couplings. The aniline ynamine (**4.111**) was chosen as the amine in the coupling. This was because it was hoped that the ynamine could be used as the alkyne handle in a click reaction for the addition of a fluorophore. An initial amide coupling using literature conditions for **4.109**, PyBOP (1 equiv) and DIPEA (1.3 equiv) in DMF, only gave trace amounts of product formation (Scheme 4.23).[201]

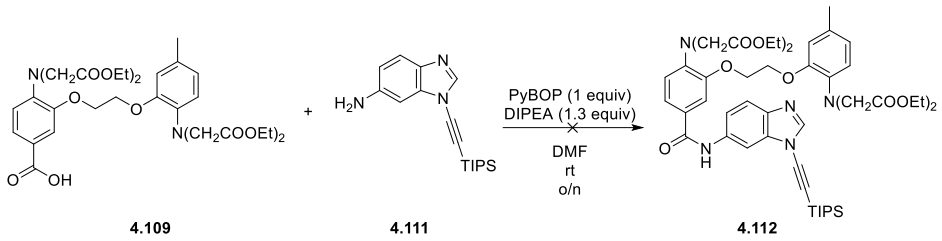

4.109 4.111 4.112

Scheme 4.23. Attempted amide coupling between acid **4.109** and amine **4.111** to form **4.112.**

Following the unsuccessful reaction, several other conditions (Table 4.1) were tested without the amine present and the formation of the activated ester monitored. After 30 minutes, the amine was added and the product formation tested by LC-MS.

Table 4.1. Amide coupling conditions tested and observation by LCMS. All reactions were attempted in DMF (10 mM). Entries 2 and 4(*) did not progress to amine addition due to the activated ester not being formed.

Amide Coupling Reagents	Product Formation (4.110) Observed
COMU (1.1 equiv), DIPEA (2 equiv)	No
DIC (1.1 equiv), HOAt (1.1 equiv)	No activated ester*
EDC (1.1 equiv), HOBt (1.1 equiv)	A small peak
DIC (1.5 equiv), HOBt (1.1 equiv)	No activated ester*
HATU (1.2 equiv), DIPEA (2 equiv)	A small peak

As observed in the table above, two of the amide conditions tested resulted in product formation, however, these peaks were small. Additional unidentified peaks were also formed in all cases. If further tests were being carried out, the deprotected ynamine would be used to avoid having to carry out the deprotection on the BAPTA scaffold. Conditions tested would also vary the number of equivalents used and reaction concentration in an attempt to find optimum conditions.

However, despite successful conditions being tested, the reaction was not done on a larger scale due to a lack of the BAPTA acid **4.109.**

The synthesis of ynamine-fluorophore conjugates was attempted. The aim of this section was therefore to synthesise a modular system with a fluorescent moiety which can be either in the ynamine or the azide.

Initially, the TIPS-protected ynamine **4.113** was used as it had a functional handle to easily carry out amide couplings (Scheme 4.24). The synthesis of **4.115 -4.117** was successful.

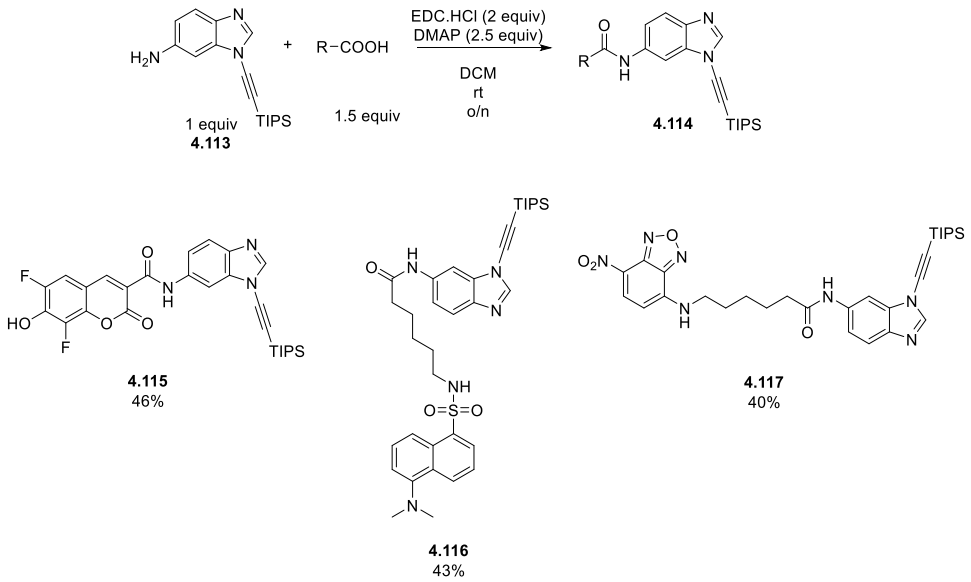

Scheme 4.24. Synthesis of ynamine-fluorophore conjugates **4.115, 4.116** and **4.117**.

Alongside the addition of a fluorophore to the ynamine, the synthesis of a fluorescent moiety that could be added *via* an azide with a click reaction was attempted. Coumarin azide (**4.117**) is a turn-on fluorescent azide; it is non-fluorescent when an azide and when in the triazole form, it is fluorescent (Scheme 4.25).[209]

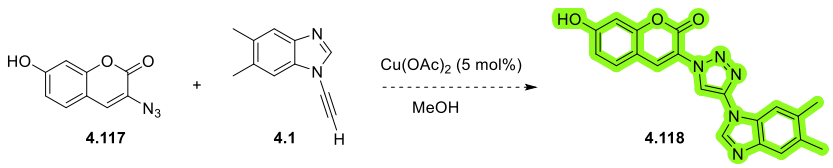

Scheme 4.25. The hypothesised fluorescent turn-on activity of coumarin azide.

The synthesis of coumarin azide is a multistep two-pot synthesis that is reported in literature.[209] The first step involves the condensation of 2,4-dihydroxybenzaldehde (**2.129**) and *N*-acetyl glycine (**2.130**) in acetic anhydride. Using literature conditions of reflux for 4 h, only trace product was formed. To increase the yield, the reaction was left at reflux for 16 h, giving a yield of 3%. Therefore, different literature conditions were attempted (Scheme 4.26) which involved heating the reaction at 140 °C for 4 h. This was successful in increasing the yield to 29%. Further optimisation could have been carried out by increasing the reaction time,

lowering the reaction temperature to avoid degradation or using microwave conditions, however, sufficient material had been obtained.

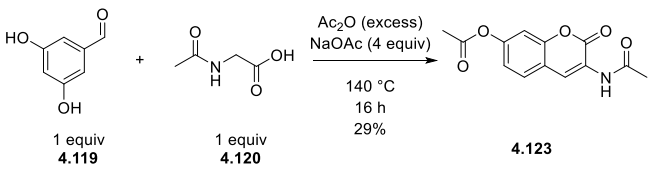

Scheme 4.26. First step in the synthesis of coumarin azide.

To form the desired azide **4.117**, **4.123** was hydrolysed to form the amine **4.124**, which then underwent diazotization and subsequent displacement to the azide **4.117**. LC-MS was used to confirm that the first step was successful before moving onto the next steps. Over the three steps the product was obtained in a 50% yield (Scheme 4.27).

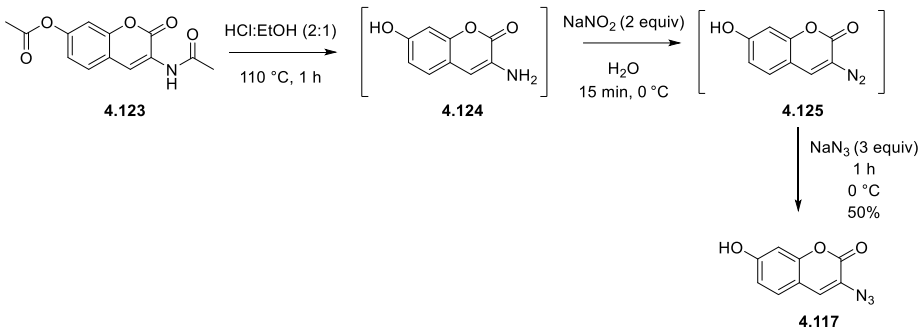

Scheme 4.27. Synthesis of **4.118**.

Triazole **4.126** was formed using standard conditions for the Cu-catalysed ynamine (3+2) azide-alkyne cycloaddition (Scheme 4.28). A poor yield (12%) was achieved for this reaction, most likely due to issues in the purification as the triazole had poor solubility in most solvents. Alternative purification methods such as precipitation or preparative HPLC might improve the purification.

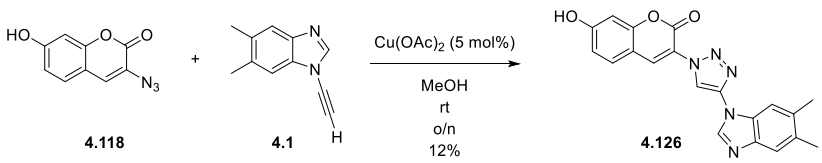

Scheme 4.28. Formation of the fluorescent triazole (**4.126**) using standard click conditions.

Two further fluorescent azides (**4.129** and **4.130**) were synthesised based on the dansyl fluorophore (**4.127**). The dansyl azide fluorophore **4.129** was synthesised from 3-azidopropan-

1-amine (**4.128**) and dansyl chloride **4.127** and obtained in good yield (95%) (**4.129**) (Scheme 4.29). Another dansyl azide with a sulfunyl azide moiety (**4.130**) was also synthesised for comparison in further tests.

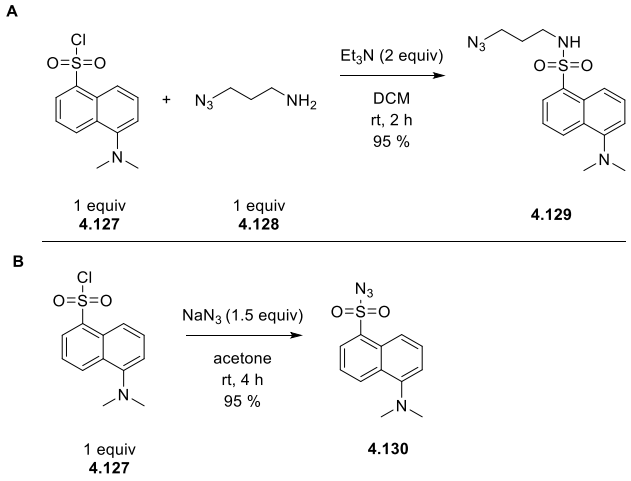

Scheme 4.29. Synthesis of dansyl azides **4.129 (A)** and **4.130 (B)**.

4.5 Summary and Future Work

In conclusion, there was no success in the attempted synthesis of a BAPTA-ynamine probe. The synthesis of an amine (**4.84**) was the first initial route attempted through the nitration of **4.93** and did not work as per literature conditions.[116] This led to the formation of an aldehyde (**4.107**) for further functionalisation being the main route under consideration. Attempts at forming the aldehyde (**4.107**) and the optimisation of early parts of the synthesis to achieve high yields were successful and so a handle was achieved for further attempts to form the BAPTA-ynamine conjugate.

The aldehyde handle led to the successful synthesis of an acid (**4.109**) and attempts at amide couplings were carried out. Several amide coupling conditions were attempted, and EDC and HOBt or HATU and DIPEA were identified as potential coupling partners to be used in further amide couplings relating to the BAPTA scaffold. Unfortunately, the synthesis of the alkyne (**4.110**) was unsuccessful, potentially due to cleavage of the ester groups. To identify if this was the source of the failed attempts, the reaction could be carried out with the acid groups already in place instead of the ester.

Further work then led to the attempted synthesis of a Br-BAPTA core (**4.95**), to use the halogen as a coupling partner. Following optimisation of this synthesis, work stalled at the addition of

the ester groups to the amines (**4.104**). Further optimisation and large-scale synthesis of this stage would have led to the successful optimisation of the product.

There is still a large amount of unexplored work within the development of a calcium probe using bioorthogonal chemistry. There were unexplored modifications to the aldehyde that were not investigated. These included a reductive amination which would have given the opportunity to add the amino-ynamine directly to the core (Scheme 4.30).

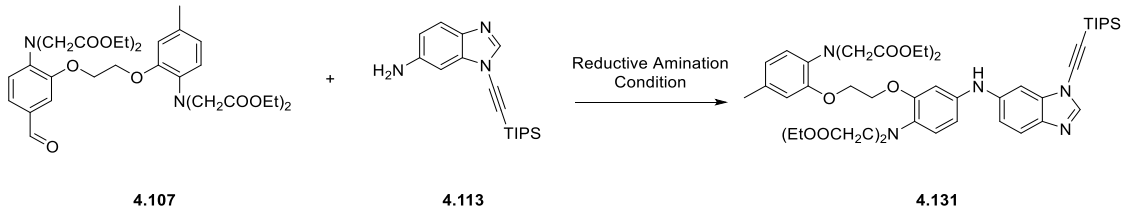

4.107 **4.113** **4.131**

Scheme 4.30. Proposed reductive amination of **4.107**.

Other potential substrates for the reductive amination are given in Figure 4.8. These include a bromo substrate (**4.132**) for alkylation reactions or cross-couplings, and acid (**4.133**) for attempts at an amide coupling with a linker bridging the BAPTA core and the ynamine substrate (**4.113**). The addition of an azide partner (**4.134**) would allow an ynamine to be added through a CuAAC reaction. Each of these (**4.132 – 4.134**) could have a different carbon chain length between the amine group for reductive amination and the other functional handle, allowing a small investigation into the importance of the linker between the BAPTA core and other group (whether an ynamine or a fluorescent moiety). An analogue of each containing the alkene could also be tested to investigate the effects of conjugation.

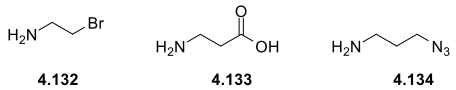

4.132 **4.133** **4.134**

Figure 4.8. Potential substrates for a reductive amination.

One of the hypothesised compounds for synthesis was an azide incorporated into the BAPTA scaffold (Figure 4.5). This was not attempted, however, if the formation of an amine on the BAPTA core was successful, the Sharpless method of azide formation (Scheme 4.31A) could be utilised to form a BAPTA azide (Scheme 4.31B).[210] The subsequent CuAAC with an ynamine would be anticipated to form **4.136** in high yields.

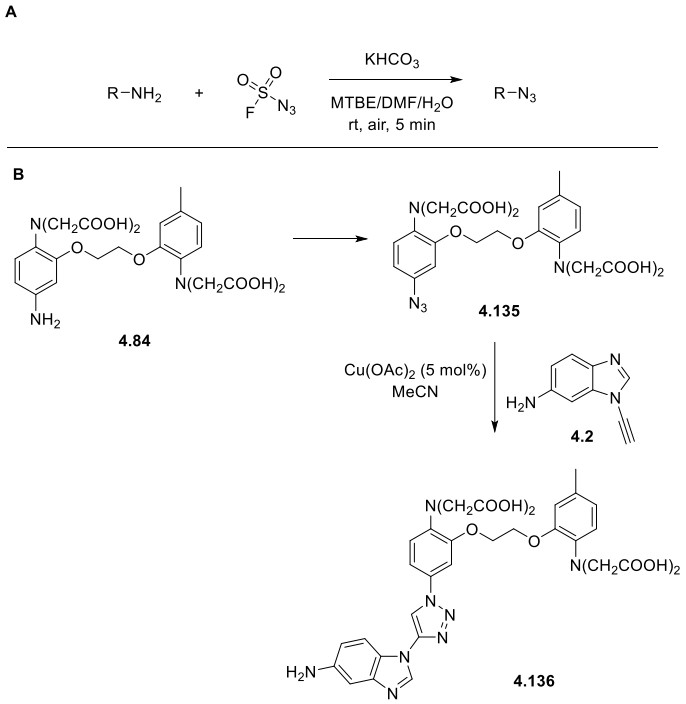

Scheme 4.31. A) Formation of an azide using a diazotising agent; [210] **B)** Formation of BAPTA azide **4.135** and click reaction to form **4.136**

The azide (**4.135**) could also be used to click with functionalised ynamines or with an azido-fluorophore. This method, however, relies on the successful synthesis of the BAPTA-amine **4.77**.

Following an anticipated successful synthesis of a BAPTA-ynamine probe, by one of the methods described, the compounds spectral properties and ability to chelate calcium to be an effective imaging would be tested. This would involve obtaining absorption and emission spectra using a UV-vis spectrometer and fluorescence measurements on a fluorescence spectrometer. To measure the dissociation constant of the probe with Ca^{2+}, absorption and emission spectra of the probe can be measured in the presence of various concentrations of free Ca^{2+}.

4.6 Experimental

4.6.1 General Experimental Techniques and Procedures

4.6.1.1 Reagents and Solvents

All reagents and solvents were used as supplied from commercial sources and used without further purification unless otherwise stated.

4.6.1.2 Column Chromatography

Thin layer chromatography (TLC) was carried out using Merck silica plates coated with fluorescent indicator UV254. TLC plates were analysed under 254 nm UV light or developed using potassium permanganate solution. Normal-phase flash chromatography was carried out using ZEOprep 60 HYD 40-63 μm silica gel. Automatic purification was carried out on an Interchim PuriFLASH XS52Plus system, using Silicycle 230-400 mesh 40-63 μm silica columns of various sizes.

4.6.1.3 NMR Spectroscopy

NMR spectroscopy was carried out using either a Bruker 400 UltraShield™ B-ACS 60 spectrometer, Bruker AV500 spectrometer at 500 MHz (^{1}H) and 126 Hz (^{13}C) or Bruker AV600 spectrometer at 156 Hz (^{13}C). All chemical shifts (δ) in $CDCl_3$ were referenced at 7.26 (^{1}H) and 77.06 ppm (^{13}C), in $(CD_3)_2SO$ at 2.50 (^{1}H) and 39.52 (^{13}C), in D_2O at 4.79 ppm (^{1}H) and in CD_3CN at 1.94 (^{1}H) and 118.26 ppm (^{13}C) and reported in parts per million (ppm). Coupling constants are quoted in hertz (Hz). Abbreviations for splitting patterns are s (singlet), br. s (broad singlet), d (doublet), dd (doublet of doublets), ddd (doublet of doublets of doublets), t (triplet), td (triplet of doublets), app. t (apparent triplet), q (quartet) and m (multiplet). All NMR data was processed using Mestrenova 11.0 software. Proton and carbon chemical shifts were assigned using proton (^{1}H), carbon (^{13}C), Heteronuclear Single Quantum Coherence (HSQC), Heteronuclear Multiple-Bond Correlation Spectroscopy (HMBC) and Correlation Spectroscopy (COSY) and Nuclear Overhauser Effect Spectroscopy (NOESY) whenever possible.

4.6.1.4 High Resolution Mass Spectrometry

High-resolution mass spectra were recorded on a ThermoScientific Exactive™ Plus Orbitrap Mass Spectrometer at the University of Strathclyde or a Bruker Micro TOF II at The University of Edinburgh.

4.6.1.5 IR Spectroscopy

IR data was collected on either an Agilent or Shimadzu FTIR spectrometer and the data processed using the proprietary software. Only major absorbances were reported.

4.6.2 Liquid Chromatography-Mass Spectrometry (LC-MS) and Ultra-Performance-Mass-Spectrometry (UPLC-MS)

LC-MS was carried out on an Agilent HPLC instrument in conjunction with an Agilent Quadrupole mass detector on an Agilent Poroshell 120 C18 column (75 mm × 4.6 mm, 2.7 μm). UPLC-MS was carried out on an AVANT UPLC with an Advion Expression CMS L attached for mass detection on a Phenomenex Kinetex C18 column (30 mm × 2.1 mm, 2.7 μm). Electrospray ionization (ESI) was used in all cases.

4.6.3 Synthetic Procedures

*2-(2-Bromoethoxy)-4-methyl-1-nitrobenzene (**4.13**)*

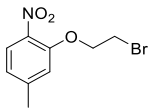

5-Methyl-2-nitrophenol (5.02 g, 32.7 mmol) and potassium carbonate (4.51 g, 32.7 mmol) were dissolved in anhydrous DMF and stirred at 90 °C for 20 min. 1,2-dibromoethane (60.8 g, 324 mmol) was added and the mixture was stirred at 90 °C for 18 h. The solution was allowed to cool to rt and the solvent was removed *in vacuo.* The crude product was purified with column chromatography (5% ethyl acetate in petroleum ether) to give the product as a yellow solid (6.41 g, 24.7 mmol, 75%).

^{1}H NMR (400 MHz, $CDCl_3$) δ 7.78 (d, *J* = 8.6 Hz, 1H), 6.91 – 6.84 (m, 2H), 4.39 (t, *J* = 6.5 Hz, 2H), 3.67 (t, *J* = 6.5 Hz, 2H), 2.41 (s, 3H).

^{13}C NMR (101 MHz, $CDCl_3$) δ 151.4, 145.7, 137.8, 125.7, 121.9, 115.8, 69.4, 27.9, 21.7.

Values correspond to literature values[201]

*4-Methyl-1-nitro-2-(2-nitrophenoxy)ethoxy)benzene (**4.15**)*

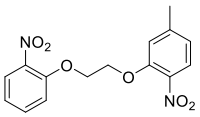

2-(2-Bromoethoxy)-4-methyl-1-nitrobenzene (3 g, 11.5 mmol), 2-nitrophenol (1.67 g, 12 mmol) and potassium carbonate (0.98 g, 7 mmol) were stirred in anhydrous DMF (10 mL) at 90°C for 5 h. The reaction was allowed to cool to room temperature and distilled water (100

mL) was added dropwise. The resulting solid was filtered and washed with water then diethyl ether. The product was fired to give a white solid (3.02 g, 9.50 mmol, 82%).

^{1}H NMR (500 MHz, DMSO) δ 7.87 – 7.83 (m, 1H), 7.77 (d, *J* = 8.3 Hz, 1H), 7.69 – 7.62 (m, 1H), 7.44 (d, *J* = 8.5 Hz, 1H), 7.26 (s, 1H), 7.17 – 7.11 (m, 1H), 6.94 (d, *J* = 8.3 Hz, 1H), 4.56-4.52 (m, 4H), 2.39 (s, 3H).

^{13}C NMR (126 MHz, DMSO) δ 151.3, 150.9, 145.7, 139.8, 137.3, 134.3, 125.0, 124.8, 121.5, 120.97, 116.0, 115.6, 68.1, 68.0, 21.3.

Values correspond to literature values[201]

*2-(2-(2-Aminophenoxy)ethoxy)-4-methylaniline (**4.16**)*

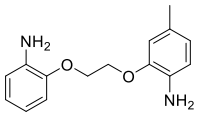

4-Methyl-1-nitro-2-(2-nitrophenoxy)ethoxy)benzene (1.50 g, 5.20 mmol) and Pd/C (55.0 mg, 52.0 μmol) were suspended in a mixture of EtOAc/MeOH (45 mL/80mL). The reaction was stirred under hydrogen atmosphere at rt for 18 h. The catalyst was filtered off over celite and washed with MeOH. The solvent was removed under vacuum to give the product as a pale-yellow solid (1.12 g, 5.81 mmol, 90%)

^{1}H NMR (500 MHz, DMSO) δ 6.86 (d, *J* = 7.3 Hz, 1H), 6.72 – 6.67 (m, 2H), 6.64 (dd, *J* = 7.8, 1.8 Hz, 1H), 6.55 – 6.49 (m, 3H), 4.67 (s, 2H), 4.45 (s, 2H), 4.26 (app.s, 4H), 2.16 (s, 3H).

^{13}C NMR (126 MHz, $CDCl_3$) δ 146.35, 136.98, 134.27, 128.09, 122.20, 122.01, 118.45, 115.48, 115.44, 113.68, 112.66, 67.62, 67.57, 21.00.

Values correspond to literature values[201]

*4-Bromo-2-(2-bromoethoxy)-1-nitrobenzene (**4.97**)*

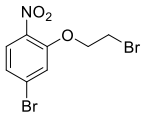

5-Bromo-2-nitrophenol (1 g, 4.59 mmol) and potassium carbonate (630 g, 4.56 mmol) were dissolved in anhydrous DMF (10 mL) and stirred at 90 °C for 20 min. 1,2-dibromoethane (860 mg, 4.59 mmol) was added and the mixture was stirred at 90 °C for 3 h. The solution was allowed to cool to rt and stirred for a further 13 h. The solvent was removed *in vacuo* and the crude product was purified with column chromatography (5% ethyl acetate in petroleum ether) to give the product as a yellow solid (401 mg, 1.24 mmol, 27%).

^{1}H NMR (500 MHz, $CDCl_3$) δ 7.78 – 7.72 (m, 1H), 7.25 – 7.22 (m, 2H), 4.41 (t, *J* = 6.4 Hz, 2H), 3.68 (t, *J* = 6.4 Hz, 2H).

IR ν_{max} (cm^{-1}) 3107 (ar. C-H), 1605 (C=C ar.), 1515 (C-O stretch), 1258 (C-O), 750 (C-Br).

*4-Bromo-2-(2-(5-methyl-2-nitrophenoxy)ethoxy)-1-nitrobenzene (**4.99**)*

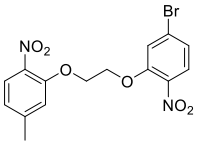

To a solution of 2-(2-bromoethoxy)-4-methyl-1-nitrobenzene (2.00 g, 7.69 mmol) in DMF (10 mL) was added K_2CO_3 (1.17 g, 8.46 mmol) and 5-bromo-2-nitrophenol (1.68 g, 7.69 mmol). The reaction was heated to 90 ˚C and left to stir for 7 h. The reaction was allowed to cool to rt, and water (30 mL) was added. The yellow precipitate formed was recovered through vacuum filtration and dried under vacuum to give the desired product as a yellow solid (2.83 g, 7.12 mmol, 93%).

^{1}H NMR (500 MHz, DMSO) δ 7.83 (d, *J* = 8.6 Hz, 1H), 7.77 (d, *J* = 8.2 Hz, 1H), 7.70 (d, *J* = 1.8 Hz, 1H), 7.36 (dd, *J* = 8.6, 1.8 Hz, 1H), 7.26 (s, 1H), 6.95 (d, *J* = 8.3 Hz, 1H), 4.64 – 4.48 (m, 4H), 2.39 (s, 3H).

IR ν_{max} (cm^{-1}) 3107 (ar. C-H), 1603 (ar. C=C), 1513 (C-O stretch), 1355 (NO_2), 1260 (NO_2), 752 (C-Br).

*2-(2-(2-Amino-5-bromophenoxy)ethoxy)-4-methylaniline (**4.102**)*

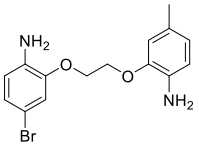

To a solution of 4-bromo-2-(2-(5-methyl-2-nitrophenoxy)ethoxy)-1-nitrobenzene (500 mg, 1.26 mmol) in EtOH (25 mL) was added iron powder (281 mg, 5.04 mmol). The reaction was heated to 40 °C and a solution of water (25 mL) and ammonium chloride (135 mg, 2.52 mmol) added. The reaction was heated to 80 °C for 30 mins. After cooling to rt, the solution was filtered over celite, and solvent removed *in vacuo* to give the desired product as a brown solid (97.6 mg, 290 mmol, 23%).

^{1}H NMR (500 MHz, DMSO) δ 7.04 (s, 1H), 6.87 (s, 1H), 6.73 (s, 1H), 6.59 (dd, *J* = 29.5, 13.0 Hz, 3H), 4.80 (s, 4H), 4.42 – 4.20 (m, 4H), 2.19 (s, 3H).

LC-MS (ESI) RT = 7.44 min, m/z = 339.1.

IR ν_{max} (cm^{-1}) 3427 (N-H), 3118 (N-H stretch of amine salt), 3029 (ar. C-H), 2947 (ar. C-H), 1504 (ar. C=C), 1396 (C-O), 1223 (C-O).

*Diethyl 2,2'-((2-(2-(2-(bis(2-ethoxy-2-oxoethyl)amino-5-methylphenoxy)ethoxy)phenyl)azanediyl)diacetate (**4.106**)*

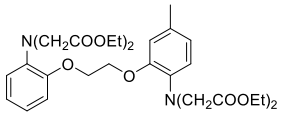

2-(2-(2-Aminophenoxy)ethoxy)-4-methylaniline (1.11 g, 4.30 mmol), proton sponge (4.6 g, 215 mmol) and ethyl bromoacetate (3.59 g, 21.5 mmol) were dissolved in anhydrous MeCN (43 mL) and NaI (3.41 g, 2.28 mmol) was added. The mixture was heated to reflux and stirred for 21 h. The reaction was allowed to cool down to room temperature and diluted with DCM (150 mL). The mixture was washed with saturated aqueous solutions of NaH_2PO_4 (100 mL), $NaHCO_3$ (100 mL) and brine (100 mL). The organic phase was dried over anhydrous sodium sulphate and reduced *in vacuo*. The residue was purified by column chromatography (10 – 20% ethyl acetate in petroleum ether) to give the product (1.29 g, 2.14 mmol, 50%).

^{1}H NMR (500 MHz, $CDCl_3$) δ 6.92 – 6.81 (m, 4H), 6.76 – 6.72 (m, 1H), 6.69 – 6.65 (m, 2H), 4.28 (hept, *J* = 2.7 Hz, 4H), 4.14 (d, *J* = 17.4 Hz, 8H), 4.05 (dq, *J* = 9.8, 7.1 Hz, 8H), 2.26 (s, 3H), 1.15 (td, *J* = 7.2, 3.3 Hz, 12H).

IR ν_{max} (cm^{-1}) 2980 (ar. C-H), 2915 (ar. C-H), 1731 (C=O), 1510 (ar. C=C), 1242 (C-N), 1175 (C-O), 1027 (C-O).

Values correspond to literature values[201]

*Diethyl 2,2'-((2-(2-(2-(bis(2-ethoxy-2-oxoethyl)amino)-5-formylphenoxy)ethoxy)-4-methylphenyl)azanediyl)diacetate (**4.107**)*

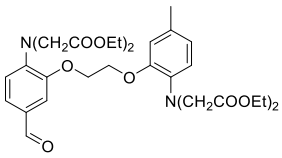

Diethyl 2,2'-((2-(2-(2-(bis(2-ethoxy-2-oxoethyl)amino-5-methylphenoxy)ethoxy)phenyl)azanediyl)diacetate (1.5 g, 2.50 mmol) and pyridine (0.29 g, 3.71 mmol) were dissolved in anhydrous DMF (15 mL). The reaction was placed under argon and cooled to 0°C. $POCl_3$ (3.78 g, 24.0 mmol) was added dropwise. The reaction was stirred at 0°C or 15 mins and then heated to 60 °C for 4 h. The reaction was allowed to cool to room

temperature and was diluted with DCM (20 mL). The diluted solution was slowly added to a solution of NaOH with crushed ice. The DCM layer was extracted, further diluted with additional DCM (20 mL) and washed with saturated $NaHCO_3$ (50 mL) and brine (50 mL). The organic layer was dried over anhydrous sodium sulphate and solvent was removed *in vacuo*. The crude residue was purified using column chromatography (ethyl acetate (20-50%:hexane) to give the product as an orange solid (1.03 g, 1.65 mmol, 64%).

^{1}H NMR (400 MHz, $CDCl_3$) δ 9.79 (s, 1H), 7.41 – 7.36 (m, 2H), 6.79 – 6.73 (m, 2H), 6.71 – 6.64 (m, 2H), 4.34 – 4.26 (m, 4H), 4.23 (s, 4H), 4.11 (s, 4H), 4.10 – 4.00 (m, 8H), 2.26 (s, 3H), 1.15 (td, *J* = 7.1, 2.5 Hz, 12H).

^{13}C NMR (101 MHz, $CDCl_3$) δ 190.7, 171.7, 171.0, 150.3, 149.9, 145.4, 137.2, 132.2, 130.1, 126.7, 122.9, 119.6, 116.8, 114.7, 111.3, 67.6, 67.0, 61.3, 60.8, 53.9, 53.7, 21.1, 14.2, 14.2. Values correspond to literature values[201]

*4-(Bis(2-ethoxy-2-oxoethyl)amino)-3-(2-(2-(bis(2-ethoxy-2-oxoethyl)amino)-5-methylphenoxy)ethoxy)benzoic acid (**4.109**)*

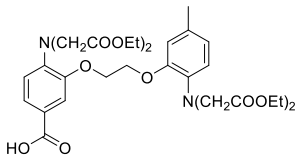

To a solution of diethyl 2,2'-((2-(2-(2-(bis(2-ethoxy-2-oxoethyl)amino)-5-formylphenoxy)ethoxy)-4-methylphenyl)azanediyl)diacetate (200 mg, 317 µmol) was dissolved in 1,4-dioxane (2.5 mL) was added a solution of $Na_2H_2PO_4$ (90 mg, 634 µmol) in water (0.5 mL) followed by a solution of $NaClO_2$ (55 mg, 610 µmol) in water (0.5 mL). The reaction was stirred at rt for 30 min and analysed by TLC. $Na_2H_2PO_4$ (90 mg, 634 µmol) in water (0.5 mL) and $NaClO_2$ (55 mg, 610 µmol) in water (0.5 mL) were added sequentially. The reaction was stirred at rt for a further 1 h. The reaction was quenched with water (10 mL) and the aqueous layer extracted with ethyl acetate (3 x 10 mL). The organic extracts were combined, washed with brine (10 mL), dried over anhydrous sodium sulphate and the solvent removed *in vacuo*. The crude obtained was purified by flash column chromatography (40 – 80% ethyl acetate in hexane) to give the desired product as a dark orange viscous oil (26.7 mg, 42.2 µmol, 13%).

^{1}H NMR (400 MHz, $CDCl_3$) δ 7.66 (dd, *J* = 8.4, 1.8 Hz, 1H), 7.56 (d, *J* = 1.9 Hz, 1H), 7.28 (d, *J* = 7.8 Hz, 1H), 6.79 – 6.69 (m, 3H), 4.45 – 3.94 (m, 20H), 2.33 (s, 3H), 1.29 – 1.08 (m, 12H) (exchangeable COOH proton not observed).

^{13}C NMR (101 MHz, $CDCl_3$) δ 170.7, 170.4, 167.8, 161.7, 161.4, 153.2, 148.9, 143.7, 140.3, 129.8, 125.7, 124.4, 121.4, 121.2, 116.6, 114.3, 113.1, 66.6, 66.3, 61.0, 60.7, 60.5, 59.9, 53.3, 48.1, 21.1, 13.7, 13.6, 13.6, 13.1.

*6,8-Difluoro-7-hydroxy-2-oxo-N-(1-((triisopropylsilyl)ethynyl)-1H-benzo[d]imidazol-6-yl)-2H-chromene-3-carboxamide (**4.115**)*

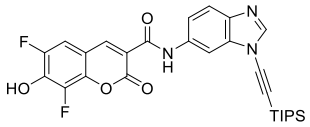

A solution of 1-((triisopropylsilyl)ethynyl)-1*H*-benzo[*d*]imidazol-6-amine (50.0 mg, 159 µmol), pacific blue (38.7 mg, 159 µmol), EDC.HCl (61.0 mg, 320 µmol) and DMAP (5.00 mg, 400 µmol) in DCM (5 mL) was stirred for 18 h. The reaction was diluted with ethyl acetate and washed with $NaHCO_3$, NaOH and brine. The organic phase was dried over sodium sulphate and then concentrated *in vacuo*. The residue was then purified by column chromatography (2% MeOH in DCM (1% triethylamine)) to give the product as a green solid (40.0 mg, 73.4 µmol, 46%).

^{1}H NMR (500 MHz, DMSO) δ 10.92 (s, 1H), 8.71 (s, 1H), 8.61 (s, 1H), 8.43 (d, J = 2.0 Hz, 1H), 8.25 – 8.18 (m, 1H), 7.74 (d, J = 8.5 Hz, 1H), 7.57 (d, J = 10.8 Hz, 1H), 7.35 (dd, J = 8.7, 2.0 Hz, 1H), 7.02 – 6.94 (m, 1H), 1.18 – 1.15 (m, 21H).

^{19}F NMR (471 MHz, DMSO) δ -135.24.

*6-((5-(Dimethylamino)naphthalene)-1-sulfonamido)-N-(1-((triisopropylsilyl)ethynyl)-1H-benzo[d]imidazol-6-yl)hexanamide (**4.116**)*

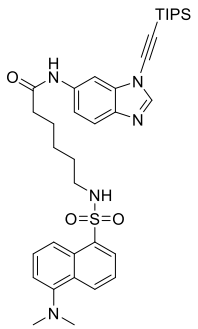

A solution of 1-((triisopropylsilyl)ethynyl)-1*H*-benzo[*d*]imidazol-6-amine (43.0 mg, 140 µmol), 6-((5-(dimethylamino)naphthalene)-1-sulfonamide)hexanoic acid (53.0 mg, 150 µmol), DMAP (3.00 mg, 2.50 µmol) and EDC.HCl (48.0 mg, 250 µmol) in DCM (5 mL) was covered in foil and stirred for 48 h at rt. The reaction was extracted into ethyl acetate, washed with $NaHCO_3$, NaOH and brine. The organic layer dried with anhydrous sodium sulphate and

concentrated *in vacuo*. The residue was then purified by column chromatography (40 – 60% ethyl acetate in petroleum ether) to give the desired product as a green solid (40.8 mg, 61.0 mmol, 43%).

^{1}H NMR (500 MHz, DMSO) δ 10.04 (s, 1H), 8.54 (s, 1H), 8.44 (d, *J* = 8.5 Hz, 1H), 8.30 (d, *J* = 8.7 Hz, 1H), 8.20 (s, 1H), 8.09 (dd, *J* = 7.3, 1.2 Hz, 1H), 7.87 (t, *J* = 5.8 Hz, 1H), 7.67 (s, 1H), 7.59 (dt, *J* = 13.3, 8.3 Hz, 2H), 7.34 (dd, *J* = 8.7, 2.0 Hz, 1H), 7.23 (d, *J* = 7.5 Hz, 1H), 2.81 (s, 7H), 2.80 – 2.74 (m, 3H), 2.18 (t, *J* = 7.5 Hz, 2H), 1.44 – 1.24 (m, 6H), 1.14 (d, *J* = 4.7 Hz, 22H).

*3-Azido-7-hydroxy-2H-chromen-2-one (**4.117**)*[209]

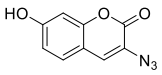

To a solution of 3-acetamido-2-oxo-2*H*-chromen-7-yl acetate (1.03 g, 3.94 mmol) in ethanol (12.5 mL) was added dropwise hydrochloric acid (25 mL) at rt. The reaction was then heated to 105 °C for 1 h. The reaction was cooled to rt before being placed in an ice bath and then diluted with ice cold deionised water (25 mL). Sodium nitrite (520 mg, 7.53 mmol) was added and left to stir for 15 mins. Sodium azide (750 mg, 11.5 mmol) was added portion wise, and the reaction left to stir for 1 h. The reaction was filtered, and the brown precipitate washed with cold deionised water (3 x 25 mL). The desired product was obtained as a brown solid (389 mg, 1.91 mmol, 50%).

^{1}H NMR (500 MHz, DMSO) δ 10.52 (s, 1H), 7.60 (s, 1H), 7.48 (d, *J* = 8.5 Hz, 1H), 6.81 (dd, *J* = 8.5, 2.3 Hz, 1H), 6.76 (d, *J* = 2.3 Hz, 1H).

Values correspond to literature values[209]

*3-(4-(5,6-Dimethyl-1H-benzo[d]imidazol-1-yl)-1H-1,2,3-triazol-1-yl)-7-hydroxy-2H-chromen-2-one (**4.118**)*

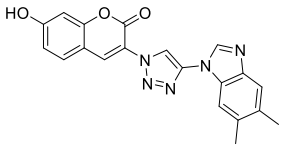

A mixture of 3-azido-7-hydroxy-2*H*-chromen-2-one (59.5 mg, 0.292 mmol), 1-ethynyl-5-6-dimethyl- 1*H*-benzo[*d*]imidazole (51.2 mg, 0.2937 mmol) and copper(II) acetate (2.20 mg, 0.01 mmol) in methanol (50 mL) was left to stir for 48 h. EDTA (10 mL) and ethyl acetate (10 mL) were added and the resulting precipitate filtered and washed with ethyl acetate (3 x 10 mL) to give the desired product as a brown solid (12.9 mg, 0.035 mmol, 12%).

^{1}H NMR (500 MHz, DMSO) δ: 11.00 (s, 1H), 9.16 (s, 1H), 8.74 (s, 1H), 7.82 (d, 1H, *J* = 8.6 Hz*),* 7.73 (broad s, 1H), 7.58 (broad s, 1H), 6.96 (dd, 2H, *J* = 8.5, 2.5 Hz,*),* 6.91 (d, 1H, 2.1 Hz), 2.39 (s, 3H), 2.36 (s, 3H).

^{13}C NMR (125 MHz, DMSO*)* δ 142.3, 135.3, 134.3, 133.6, 129.4, 128.3, 118.7, 114.7, 112.4, 55.3, 20.5, 20.3 (5 carbons not observed).

Values correspond to literature values[211]

*3-Acetamido-2-oxo-2H-chromen-7-yl acetate (**4.123**)*

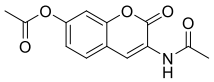

To a solution of 2,4-dihydroxybenzaldehyde (2.01 g, 14.6 mmol) and *N*-acetyl glycine (1.68 g. 14.3 mmol) in acetic anhydride (12 mL) was added anhydrous sodium acetate (5.00 g, 60.9 mmol) and the reaction mixture was heated to 115 °C for 4 h. Upon cooling to rt, the resulting solid was triturated with cold deionised water (30 mL), filtered and washed with cold deionised water (3 x 30 ml). The solid was sonicated in ethyl acetate (12 ml) and filtered to give the desired product as an orange solid (1.09 g, 29%).

^{1}H NMR (500 MHz, DMSO) δ 9.76 (s, 1H), 8.63 (s, 1H), 7.75 (d, *J* = 8.5 Hz, 1H), 7.27 (d, 2.2 Hz, 1H), 7.13 (dd, *J* = 8.5 Hz, 2.2 Hz, 1H), 2.31 (s, 3H), 2.18 (s, 3H).

^{13}**C NMR** (125 MHz, DMSO) δ 175.4, 174.1, 162.5 156.2, 155.1, 133.8, 129.3, 124.2, 122.7, 114.9, 29.1, 26.1.

Values correspond to literature values[209]

*N-(3-azidopropyl)-5-(dimethylamino)naphthalene-1-sulfonamide (**4.129**)*[212]

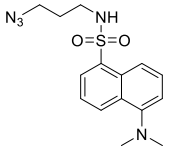

3-Azido-propan-1-amine (119 mg, 1.19 mmol) was added dropwise to a solution of 5-(dimethylamino)mapthalene-1-sulfonyl chloride (322 mg, 1.19 mmol) and triethylamine (241 mg, 2.39 mmol) in DCM (5 mL) under argon and stirred at room temperature for 1.5 h. The reaction mixture was concentrated *in vacuo* and absorbed onto celite for purification by silica gel flash-column chromatography (70% hexane in ethyl acetate). The product was obtained as a green solid (376 mg, 1.13 mmol, 95%).

^{1}H NMR (500 MHz, $CDCl_3$) δ 8.56 (d, *J* = 8.6 Hz, 1H), 8.30 (d, *J* = 8.6 Hz, 2H), 7.58 – 7.54 (m, 2H), 7.197 (d, *J* = 7.5 Hz, 1H), 5.15 (broad s, 1H), 3.24 (s, *J* = 6.4 Hz, 2H), 2.98 (q, *J* = 6.4 Hz, 2H), 2.89 (s, 6H), 1.55 (quint, *J* = 12.9 Hz, 2H).
^{13}C NMR (125 MHz, $CDCl_3$) δ 151.9, 136.3, 130.0, 129.6 128.9, 128.3, 124.1, 119.5, 115.6, 48.3, 45.3, 29.0.
Values correspond to literature values [212]

*5-(Dimethylamino)naphthalene-1-sulfonyl azide (**4.130**)*[213]

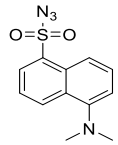

A solution of dansyl chloride (272 mg, 1.01 mmol) in acetone (6 mL) was added to a solution of sodium azide (97.5 mg, 1.50 mmol,) in water (2 mL). The reaction was stirred for 4 h at rt and then diluted with ammonium chloride. The solution was extracted into ethyl acetate (3 × 10 mL) and the organic phase was dried with anhydrous sodium sulphate. The solvent was removed *in vacuo* to give a green/yellow gel (280 g, 1 mmol, 95%).
^{1}H NMR (500 MHz, DMSO) δ 8.66 (d, *J* = 8.4 Hz, 1H), 8.37 (dd, *J* = 7.4, 1.2 Hz, 1H), 8.04 (d, *J* = 8.6 Hz, 1H), 7.78 – 7.71 (m, 2H), 7.35 (d, *J* = 7.3 Hz, 1H), 2.86 (s, 6H).
^{13}C NMR (126 MHz, DMSO) δ 151.9, 132.7, 130.3, 129.6, 129.1, 128.7, 123.7, 117.6, 115.9, 45.0 (2 carbons not observed).
IR ν_{max} (cm^{-1}): 3943 (N-H), 2152 (N_3),1361 (C-N), 1146 (S=O).
Values correspond to literature values [213]

*6-((5-(Dimethylamino)naphthalene)-1-sulfonamide)hexanoic acid (**4.136**)*[214]

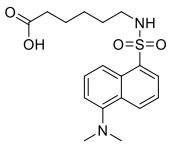

6-Aminohexanoic acid (0.21 g, 1.60 mmol) was dissolved in sodium hydroxide (2 mL) and added to a solution of dansyl chloride (403 mg, 1.5 mmol) in THF (13 mL) and stirred for 1.5 h at rt. The solution was acidified using 10% HCl. The solution was extracted into ethyl acetate and the organic layer dried with anhydrous sodium sulphate and the solvent removed *in vacuo*. The crude residue was purified using silica gel column chromatography (6% MeOH in DCM) to give the product as a green solid (202 mg, 0.56 mmol, 37%).

^{1}H NMR (500 MHz, $CDCl_3$) δ 8.55 (d, *J* = 8.5 Hz, 1H), 8.29 (d, *J* = 8.6 Hz, 1H), 8.25 (dd, *J* = 7.4, 1.3 Hz, 1H), 7.54 (ddd, *J* = 17.1, 8.6, 7.4 Hz, 2H), 7.20 (d, *J* = 7.5 Hz, 1H), 2.90 (d, *J* = 3.3 Hz, 7H), 2.18 (t, *J* = 7.3 Hz, 2H), 1.41 (m, 5H), 1.26 (s, 1H), 1.24 – 1.14 (m, 3H) (Exchangeable COOH and NH protons not observed).

Values correspond to literature values [214]

Chapter 5

Conclusions and Future Directions

5.1 Conclusions and Future Directions

The aim of this thesis was to expand on the scope of ynamines for the CuAAC reaction and investigate the influence of substituents and solvents on reactivity. To showcase the potential of aromatic ynamines in bioconjugation, a calcium sensor approach was explored.

First, various ynamines based on both benzimidazoles and imidazole scaffolds containing EWD and EDGs were synthesised. The synthetic yields of the TIPS-protected ynamines varied, dependent on substrate and reaction conditions. Ynamine synthesis attempts on a substrate containing an amine were consistently low, for both the imidazole and benzimidazole scaffold.
Next, following on from preliminary findings within the group, it was attempted to perform the azide-alkyne cycloaddition using metal salts that did not contain copper. The results obtained in this were highly variable, and no clear trends could be established. The source of the reactivity was not identified in these experiments, and despite efforts to reduce the likelihood of copper contamination, it is a potential that there may be a trace contamination, potentially from the salts used.

Next, the HDE rate of each ynamine alkyne was investigated. Substituents on the benzimidazole ring influenced the reactivity, however, the differences in reactivity were more pronounced for the imidazoles, with the electron withdrawing nitro substituent (**3.39**) not showing full exchange in the time observed (3.5 h), and the bare aromatic imidazole completing in 1.5 h. A unique reactant was the difluoro benzimidazole **3.25**, which exhibited faster exchange without the presence of copper. Further differences between the benzimidazoles and the imidazoles observed included faster formation of diyne for benzimidazoles, and for some of the imidazoles, no diyne formation was observed. There was also a difference in the exchange curve shape (imidazoles display a sigmoidal shape and benzimidazoles do not) and the peak broadening upon copper addition for the two heterocycles, with benzimidazole peaks broadening and shifting temporarily downfield, and imidazole peaks not shifting, only broadening. These observations point to a fundamental difference between benzimidazoles and imidazoles in how they interact with the copper catalyst.
The effect of the substituents on the ynamines reactivity in CuAAC in 3 different solvents: MeCN, IPA and HFIP/water (40/60), was probed by HPLC analysis. For benzimidazole ynamines, dimethoxy benzimidazole ynamine **3.24** was the fastest in MeCN, reaching

completion in 20 min in MeCN and 45 min in IPA. However, the reaction was slowed down in the HFIP/water system, reaching completion in over 3 h. The difluoro ynamine **3.25** was amongst the slowest benzimidazoles for all solvents, completing in 90 min in MeCN, 3 h in IPA and over 3 h in HFIP/water. This suggest that EDGs are faster than EWGs, and this is further shown with the other methoxy variants (**3.26** and **3.27)** also being fast. To confirm this hypothesis, further EWGs would need to be tested. For imidazoles, the fluoro imidazole **3.35** was the fastest substrate in MeCN, completing in 15 min. However, changing the solvent to IPA reduced the speed to completion to 2 h. When HFIP/water is used, the low solubility of the triazole products interfere with the HPLC analysis and caused low reproducibility due to precipitation, this was particularly prevalent for the imidazole series tested.

In MeCN and IPA two side products typically formed, in addition to diyne, which were putatively identified as **3.64** and **3.65** (as illustrated for the dimethyl ynamine **3.13**). For benzimidazoles, diyne was formed in both solvents, but for imidazoles, it was only found in quantifiable levels in MeCN. The other side products formed were unidentified but presumed to be either an ynamine-triazole complex or a bis-triazole molecule based on previous work within the group. For the HFIP/water system, no side product formation was observed.

Next, influence of copper catalyst concentration on reactivity was tested. Preliminary results using 2.5 mol% $Cu(OAc)_2$ for benzimidazole ynamines tested showed that reducing the copper levels tended to double the reaction rate (*e.g.* **3.24** and **3.31**). For the imidazole ynamines, it did not significantly affect the reaction rates, with reaction rates for most (*e.g.* **3.37** and **3.40**) tested only dropping by a small margin. One benzimidazole (**3.24**) and one imidazole (**3.37**) were then tested with further lower concentrations of $Cu(OAc)_2$. Benzimidazole **3.24** decreased in the reaction rate as the $Cu(OAc)_2$ concentration was sequentially decreased to 0.156% $Cu(OAc)_2$. The lowest concentration did not reach completion in the time monitored (2 h) however, 0.625% $Cu(OAc)_2$ still allowed the reaction to go to completion in 1 hour. This loss in rate could be perceived as a small trade-off for the reduction of copper in the reaction. In contrast, imidazole **3.37** did not show a significant decrease in rate on the lowering of $Cu(OAc)_2$, from 5 mol% to 1.25 mol% suggesting that if low levels of copper are required, the use of imidazole ynamines may be best.

Finally, attempts were made to form a BAPTA core that an ynamine could be conjugated. Despite attempting literature conditions, conversion to a suitable linker was not synthesised. The formation of an aldehyde handle was successful, but attempts to form an alkyne failed. Initial test reactions were performed using successfully synthesised acid-BAPTA **4.109**, but

these were not scaled up to isolate product. A halogen handle was introduced, but synthesis stalled when there were issues with the addition of the ester groups to the brominated core.

A number of further investigations can be proposed to expand on the findings presented in this thesis:

i) *Investigation of potential mechanistic differences between the imidazole and the benzimidazole* - The HDE experiments suggested that there was a potential difference between the benzimidazole ynamines and the imidazole ynamines. The role of the N3 in the benzimidazole ynamines has been extensively studied in a separate set of work, however the imidazole has not.[188] The synthesis of a ^{15}N-labelled imidazole ynamine would allow for probing by NMR of the binding of copper to the N3. This could be compared to work ongoing in parallel within the group and recently published, which uses isotopically labelled benzimidazole ynamine for NMR investigations.[188]

ii) *Further investigations of the substrate effect* – Despite the studies performed in Chapter 3, there are still unknowns into the exact impact on the mechanism that the substrate effects have. To investigate the copper binding, the use of crystal structures could be exploited. By attempting to crystalise the alkynes, and the triazole products with $Cu(OAc)_2$, the binding of Cu will hopefully be observed. Initial attempts were made to form crystals of the ynamine substrates in the presence of $Cu(OAc)_2$, however, these were unsuccessful and only limited solvents were tested (MeCN and EtOAc). Investigating more solvents, and different concentrations of $Cu(OAc)_2$ may give successful crystals. For the imidazole ynamines, a Hammett plot could be established, if rate constants for the reactions can be obtained, that would give a further insight into the effect of the electronic properties of the substituents.[215,216]

iii) *Investigation into the solvent effect* – The reasoning for the differences between the effects of the solvents has not been fully explored. Whilst it can be placed to differences in the polarity of the solvent, HFIP is the outlier. One potential could be to carry out increased mechanistic studies in deuterated HFIP to investigate the effects of this solvent. The investigation of the CuAAC using a Cu(I) catalyst in the HFIP/water system should also be investigated.

iv) *Identification of the CuAAC side products* – To interrogate the proposed mechanism further, isolation of the side products formed would provide information. To do this, selected ynamines, such as benzimidaole **3.24** and imidazole **3.35** which have been shown to form the assumed side products, could be scaled up to a large enough scale (≈ 1 g) to isolate the side products. Full characterisation of these side products and the rate that they form would inform the mechanistic studies.

v) *Investigating the effect of diyne formation on the CuAAC* – The CuAAC could be performed with Cu(I) salts. This would allow the effect of Glaser formation on the reaction to be investigated. The reaction could also be performed with the addition of a small amount of isolated diyne during the reaction. This would allow the influence of the diyne to be observed, and would work best on a slower reaction (such as the difluoro ynamine **3.**24 in MeCN). Various diynes could be added, such as its own, or the diyne of the fastest benzimidazole **3.24.** Repeating this with the imidazole ynamines would also prove an interesting way to investigate the differences between the heterocycles.

vi) *Incorporation of the ynamine into BAPTA scaffolds* – Despite the unsuccessful attempts to utilise an ynamine in a BAPTA probe, other routes could be attempted. One potential focus could be the incorporation of the ynamine scaffold into the BAPTA (Figure 5.1A). However, this synthesis may prove difficult due to the likely large numbers of steps required, and anticipated low yields, including, the Ullmann of the ynamine synthesis, which was shown in Chapter 2 to give variable yields and be less efficient on increasingly functionalised ynamines. Another option would be to incorporate an ynamine into a fluorogenic scaffold, without disrupting the fluorescence capabilities (Figure 5.1B). A first choice for this would be a coumarin (**5.3**), due to its similar aromatic profile and large amounts of derivates that have been researched previously.[217–219] This would hypothetically form a fluorescent molecule which could undergo an ynamine CuAAC reaction.

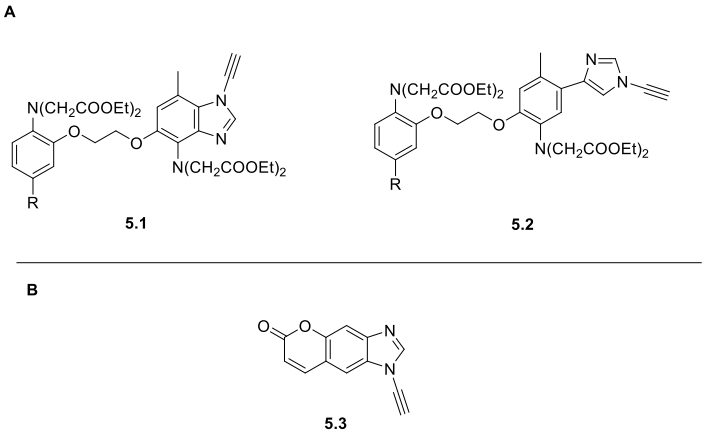

Figure 5.1. A) Potential new BAPTA chelators incorporating the ynamine scaffold; **B)** An ynamine incorporated into a coumarin scaffold.

List of References

(1) Sletten, E. M.; Bertozzi, C. R. Bioorthogonal Chemistry: Fishing for Selectivity in a Sea of Functionality. *Angew. Chem., Int. Ed.* **2009**, *48* (38), 6974–6998.

(2) Sletten, E. M.; Bertozzi, C. R. From Mechanism to Mouse: A Tale of Two Bioorthogonal Reactions. *Acc. Chem. Res.* **2011**, *44* (9), 666–676.

(3) Saxon, E.; Armstrong, J. I.; Bertozzi, C. R. A "Traceless" Staudinger Ligation for the Chemoselective Synthesis of Amide Bonds. *Org. Lett.* **2000**, *2* (14), 2141–2143.

(4) Rostovtsev, V. V.; Green, L. G.; Fokin, V. V.; Sharpless, K. B. A Stepwise Huisgen Cycloaddition Process: Copper(I)-Catalyzed Regioselective "Ligation" of Azides and Terminal Alkynes. *Angew. Chem., Int. Ed.* **2002**, *41* (14), 2596–2599.

(5) Agard, N. J.; Prescher, J. A.; Bertozzi, C. R. A Strain-Promoted [3 + 2] Azide-Alkyne Cycloaddition for Covalent Modification of Biomolecules in Living Systems. *J. Am. Chem. Soc.* **2004**, *126* (46), 15046–15047.

(6) Blackman, M. L.; Royzen, M.; Fox, J. M. The Tetrazine Ligation: Fast Bioconjugation Based on Inverse-Electron-Demand Diels-Alder Reactivity NIH Public Access. *J. Am. Chem. Soc.* **2008**, *130* (41), 13518–13519.

(7) Bird, R. E.; Lemmel, S. A.; Yu, X.; Zhou, Q. A. Bioorthogonal Chemistry and Its Applications. *Bioconjug. Chem.* **2021**, *32* (12), 2457–2479.

(8) Smeenk, M. L. W. J.; Agramunt, J.; Bonger, K. M. Recent Developments in Bioorthogonal Chemistry and the Orthogonality Within. *Curr. Opin. Chem. Biol.* **2021**, *60*, 79–88.

(9) Hong, V.; Presolski, S. I.; Ma, C.; Finn, M. G. Analysis and Optimization of Copper-Catalyzed Azide–Alkyne Cycloaddition for Bioconjugation. *Angew. Chem., Int. Ed.* **2009**, *48* (52), 9879–9883.

(10) Kaur, J.; Saxena, M.; Rishi, N. An Overview of Recent Advances in Biomedical Applications of Click Chemistry. *Bioconjug Chem* **2021**, *32* (8), 1455–1471.

(11) Staudinger, H.; Meyer, J. Über Neue Organische Phosphorverbindungen III. Phosphinmethylenderivate Und Phosphinimine. *Helv. Chim. Acta* **1919**, *2* (1), 635–646.

(12) Gololobov, Y. G.; Nesmeyanov, A. N.; Kasukhin, L. F. Recent Advances In The Staudinger Reaction. *Tetrahedron* **1992**, *48* (8), 1353–1406.

(13) Saxon, E.; Bertozzi, C. R. Cell Surface Engineering by a Modified Staudinger Reaction. *Science* **2000**, *287* (5460), 2007–2010.

(14) Bednarek, C.; Wehl, I.; Jung, N.; Schepers, U.; Brä, S. The Staudinger Ligation. *Chem. Rev.* **2020**, *120* (10), 4301–4354.

(15) Lin, F. L.; Hoyt, H. M.; Van Halbeek, H.; Bergman, R. G.; Bertozzi, C. R. Mechanistic Investigation of the Staudinger Ligation. *J. Am. Chem. Soc.* **2005**, *127* (8), 2686–2695.

(16) Heiss, T. K.; Dorn, R. S.; Prescher, J. A. Bioorthogonal Reactions of Triarylphosphines and Related Analogues. *Chem. Rev.* **2021**, *121* (12), 6802–6848.

(17) Köhn, M.; Breinbauer, R. The Staudinger Ligation—A Gift to Chemical Biology. *Angew. Chem., Int. Ed.* **2004**, *43* (24), 3106–3116.

(18) Nilsson, B. L.; Kiessling, L. L.; Raines, R. T. Staudinger Ligation: A Peptide from a Thioester and Azide. *Org. Lett.* **2000**, *2* (13), 1939–1941.

(19) Soellner, M. B.; Nilsson, B. L.; Raines, R. T. Reaction Mechanism and Kinetics of the Traceless Staudinger Ligation. *J. Am. Chem. Soc.* **2006**, *128* (27), 8820–8828.

(20) Lang, K.; Chin, J. W. Bioorthogonal Reactions for Labeling Proteins. *ACS Chem. Biol.* **2014**, *9* (1), 16–20.

(21) Carroll, L.; Evans, H. L.; Aboagye, E. O.; Spivey, A. C. Bioorthogonal Chemistry for Pre-Targeted Molecular Imaging – Progress and Prospects. *Org. Biomol. Chem.* **2013**, *11* (35), 5772–5781.

(22) Mamat, C.; Gott, M.; Steinbach, J. Recent Progress Using the Staudinger Ligation for Radiolabeling Applications. *J. Label. Compd. Radiopharm.* **2018**, *61* (3), 165–178.

(23) Huisgen, R. 1,3-Dipolar Cycloadditions. Past and Future. *Angew. Chem., Int. Ed.* **1963**, *2* (10), 565–598.

(24) Tornøe, C. W.; Christensen, C.; Meldal, M. Peptidotriazoles on Solid Phase: [1,2,3]-Triazoles by Regiospecific Copper(I)-Catalyzed 1,3-Dipolar Cycloadditions of Terminal Alkynes to Azides. *J. Org. Chem.* **2002**, *67* (9), 3057–3064.

(25) Jin, L.; Tolentino, D. R.; Melaimi, M.; Bertrand, G. Isolation of Bis(Copper) Key Intermediates in Cu-Catalyzed Azide-Alkyne "Click Reaction." *Sci. Adv.* **2015**, *1* (5).

(26) Iacobucci, C.; Reale, S.; Gal, J.; De Angelis, F. Dinuclear Copper Intermediates in Copper(I)-Catalyzed Azide–Alkyne Cycloaddition Directly Observed by Electrospray Ionization Mass Spectrometry. *Angew. Chem., Int. Ed.* **2015**, *54* (10), 3065–3068.

(27) Rodionov, V. O.; Fokin, V. V.; Finn, M. G. Mechanism of the Ligand-Free Cu(I)-Catalyzed Azide–Alkyne Cycloaddition Reaction. *Angew. Chem., Int. Ed.* **2005**, *44* (15), 2210–2215.

(28) Worrell, B. T.; Malik, J. A.; Fokin, V. V. Direct Evidence of a Dinuclear Copper Intermediate in Cu(I)-Catalyzed Azide-Alkyne Cycloadditions. *Science* **2013**, *340* (6131), 457–460.

(29) Nolte, C.; Mayer, P.; Straub, B. F. Isolation of a Copper(I) Triazolide: A "Click" Intermediate. *Angew. Chem., Int. Ed.* **2007**, *46* (12), 2101–2103.

(30) Berg, R.; Straub, B. F. Advancements in the Mechanistic Understanding of the Copper-Catalyzed Azide-Alkyne Cycloaddition. *Beilstein J. Org. Chem.* **2013**, *9*, 2715–2750.

(31) Kolb, H.; Finn, M.; Sharpless, K. B. Click Chemistry: Diverse Chemical Function From a Few Good Reactions. *Angew. Chem., Int. Ed.* **2001**, *40* (11), 2004–2021.

(32) Ganz, D.; Harijan, D.; Wagenknecht, H.-A. Labelling of DNA and RNA in the Cellular Environment by Means of Bioorthogonal Cycloaddition Chemistry. *RSC chem. biol.* **2020**, *1* (3), 86–97.

(33) McKay, C. S.; Finn, M. G. Click Chemistry in Complex Mixtures: Bioorthogonal Bioconjugation. *Chem. Biol.* **2014**, *21* (9), 1075–1101.

(34) Meldal, M.; Diness, F. Recent Fascinating Aspects of the CuAAC Click Reaction. *Trends Chem.* **2020**, *2* (6), 569–584.

(35) Agrahari, A. K.; Bose, P.; Jaiswal, M. K.; Rajkhowa, S.; Singh, A. S.; Hotha, S.; Mishra, N.; Tiwari, V. K. Cu(I)-Catalyzed Click Chemistry in Glycoscience and Their Diverse Applications. *Chem Rev* **2021**, *121* (13), 7638–7956.

(36) Kolb, H. C.; Finn, M. G.; Sharpless, K. B. Click Chemistry: Diverse Chemical Function from a Few Good Reactions. *Angew. Chem., Int. Ed.* **2001**, *40* (11), 2004–2021.

(37) Chen, S.-Y.; Liu, S.-T.; Lin, W.-R.; Lin, C.-K.; Huang, S.-M. The Mechanisms Underlying the Cytotoxic Effects of Copper Via Differentiated Embryonic Chondrocyte Gene 1. *Int. J. Mol. Sci.* **2019**, *20* (20).

(38) Li, L.; Zhang, Z. Development and Applications of the Copper-Catalyzed Azide-Alkyne Cycloaddition (CuAAC) as a Bioorthogonal Reaction. *Molecules*. 2016, p 1393.

(39) Chan, T. R.; Hilgraf, R.; Sharpless, K. B.; Fokin, V. V. Polytriazoles as Copper(I)-Stabilizing Ligands in Catalysis. *Org. Lett.* **2004**, *6* (17), 2853–2855.

(40) Soriano Del Amo, D.; Wang, W.; Jiang, H.; Besanceney, C.; Yan, A.; Levy, M.; Liu, Y.; Marlow, F. L.; Wu, P. Biocompatible Copper(I) Catalysts for in Vivo Imaging of Glycans. *J. Am. Chem. Soc.* **2010**, *132* (47), 16893–16899.

(41) Besanceney-Webler, C.; Jiang, H.; Zheng, T.; Feng, L.; Soriano Del Amo, D.; Wang, W.; Klivansky, L. M.; Marlow, F. L.; Liu, Y.; Wu, P. Raising the Efficacy of

Bioorthogonal Click Reactions for Bioconjugation: A Comparative Study. *Angew. Chem., Int. Ed.* **2011**, *50* (35), 8051–8056.

(42) Brotherton, W. S.; Michaels, H. A.; Tyler Simmons, J.; Clark, R. J.; Dalai, N. S.; Zhu, L. Apparent Copper(II)-Accelerated Azide - Alkyne Cycloaddition. *Org. Lett.* **2009**, *11* (21), 4954–4957.

(43) Kuang, G.-C.; Guha, P. M.; Brotherton, W. S.; Simmons, J. T.; Stankee, L. A.; Nguyen, B. T.; Clark, R. J.; Zhu, L. Experimental Investigation on the Mechanism of Chelation-Assisted, Copper(II) Acetate-Accelerated Azide-Alkyne Cycloaddition NIH Public Access. *J. Am. Chem. Soc.* **2011**, *133* (35), 13984–14001.

(44) Kislukhin, A. A.; Hong, V. P.; Breitenkamp, K. E.; Finn, M. G. Relative Performance of Alkynes in Copper-Catalyzed Azide-Alkyne Cycloaddition. *Bioconjug. Chem.* **2013**, *24* (4), 684–689.

(45) Kwon, M.; Jang, Y.; Yoon, S.; Yang, D.; Jeon, H. B. Unusual Cu(I)-Catalyzed 1,3-Dipolar Cycloaddition of Acetylenic Amides: Formation of Bistriazoles. *Tetrahedron Lett.* **2012**, *53* (13), 1606–1609.

(46) Sloboda, D.; Weber, C. C.; Bakis, E. A Kinetics Study of Copper-Catalysed Click Reactions in Ionic Liquids. *Org. Biomol. Chem.* **2023**, *21* (39), 7984–7993.

(47) Presolski, S. I.; Hong, V.; Cho, S.-H.; Finn, M. G. Tailored Ligand Acceleration of the Cu-Catalyzed Azide-Alkyne Cycloaddition Reaction: Practical and Mechanistic Implications. *J. Am. Chem. Soc* **2010**, *132* (41), 14570–14576.

(48) Neumann, S.; Biewend, M.; Rana, S.; Binder, W. H. The CuAAC: Principles, Homogeneous and Heterogeneous Catalysts, and Novel Developments and Applications. *Macromol. Rapid Commun.* **2020**, *41* (1).

(49) Yang, L.; McRae, R.; Henary, M. M.; Patel, R.; Lai, B.; Vogt, S.; Fahrni, C. J. Imaging of the Intracellular Topography of Copper with a Fluorescent Sensor and by Synchrotron X-Ray Fluorescence Microscopy. *Proc. Natl. Acad. Sci. U. S. A.* **2005**, *102* (32), 11179–11184.

(50) Kennedy, D. C.; McKay, C. S.; Legault, M. C. B.; Danielson, D. C.; Blake, J. A.; Pegoraro, A. F.; Stolow, A.; Mester, Z.; Pezacki, J. P. Cellular Consequences of Copper Complexes Used to Catalyze Bioorthogonal Click Reactions. *J. Am. Chem. Soc.* **2011**, *133* (44), 17993–18001.

(51) Dizdaroglu, M.; Jaruga, P. Mechanisms of Free Radical-Induced Damage to DNA. *Free Radic. Res.* **2012**, *46* (4), 382–419.

(52) Abel, G. R.; Calabrese, Z. A.; Ayco, J.; Hein, J. E.; Ye, T. Measuring and Suppressing the Oxidative Damage to DNA during Cu(I)-Catalyzed Azide-Alkyne Cycloaddition. *Bioconjug. Chem.* **2016**, *27* (3), 698–704.

(53) Li, S.; Cai, H.; He, J.; Chen, H.; Lam, S.; Cai, T.; Zhu, Z.; Bark, S. J.; Cai, C. Extent of the Oxidative Side Reactions to Peptides and Proteins During the CuAAC Reaction. *Bioconjug. Chem.* **2016**, *27* (10), 2315–2322.

(54) José, A.; Oliveira De Almeida, P.; César, J.; Lúcio De Oliveira, P.; Virgolino Da, L.; Pontes, S.; Frederico De Souza Júnior, J.; Amanda, T.; Gonçalves, F.; Dantas, S. H.; Silva De Almeida Feitosa, M.; Oliveira Silva, A.; Almeida De Medeiros, I. ROS: Basic Concepts, Sources, Cellular Signaling, and Its Implications in Aging Pathways. *Oxidative Medicine and Cellular Longetivity* **2022**, *2022*, 1–23.

(55) Agard, N. J.; Baskin, J. M.; Prescher, J. A.; Lo, A.; Bertozzi, C. R. A Comparative Study of Bioorthogonal Reactions with Azides. *ACS Chem. Biol.* **2006**, *1* (10), 644–648.

(56) Baskin, J. M.; Prescher, J. A.; Laughlin, S. T.; Agard, N. J.; Chang, P. V; Miller, I. A.; Lo, A.; Codelli, J. A.; Bertozzi, C. R. Copper-Free Click Chemistry for Dynamic in Vivo Imaging. *Proc. Natl. Acad. Sci. U. S. A.* **2007**, *104* (43), 16793–16767.

(57) Ning, X.; Guo, J.; Wolfert, M. A.; Boons, G.-J. Live-Cell Imaging Visualizing Metabolically Labeled Glycoconjugates of Living Cells by Copper-Free and Fast Huisgen Cycloadditions. *Angew. Chem., Int. Ed.* **2008**, *47* (12), 2253–2255.

(58) Debets, M. F.; Van Berkel, S. S.; Schoffelen, S.; Rutjes, F. P. J. T.; Van Hest, J. C. M.; Van Delft, F. L. Aza-Dibenzocyclooctynes for Fast and Efficient Enzyme PEGylation via Copper-Free (3+2) Cycloaddition. *Chem. Commun.* **2010**, *46* (1), 97–99.

(59) Jewett, J. C.; Sletten, E. M.; Bertozzi, C. R. Rapid Cu-Free Click Chemistry with Readily Synthesized Biarylazacyclooctynones. *J. Am. Chem. Soc.* **2010**, *132* (11), 3688–3690.

(60) Dommerholt, J.; Schmidt, S.; Temming, R.; Hendriks, L. J. A.; Rutjes, F. P. J. T.; Van Hest, J. C. M.; Lefeber, D. J.; Friedl, P.; Van Delft, F. L. Readily Accessible Bicyclononynes for Bioorthogonal Labeling and Three-Dimensional Imaging of Living Cells. *Angew. Chem., Int. Ed.* **2010**, *49* (49), 9422–9425.

(61) Davis, D. L.; Price, E. K.; Aderibigbe, S. O.; Larkin, M. X. H.; Barlow, E. D.; Chen, R.; Ford, L. C.; Gray, Z. T.; Gren, S. H.; Jin, Y.; Keddington, K. S.; Kent, A. D.; Kim, D.; Lewis, A.; Marrouche, R. S.; O'Dair, M. K.; Powell, D. R.; Scadden, M. H. C.; Session, C. B.; Tao, J.; Trieu, J.; Whiteford, K. N.; Yuan, Z.; Yun, G.; Zhu, J.;

Heemstra, J. M. Effect of Buffer Conditions and Organic Cosolvents on the Rate of Strain-Promoted Azide-Alkyne Cycloaddition. *J. Org. Chem.* **2016**, *81* (15), 6816–6819.

(62) Chang, P. V.; Prescher, J. A.; Sletten, E. M.; Baskin, J. M.; Miller, I. A.; Agard, N. J.; Lo, A.; Bertozzi, C. R. Copper-Free Click Chemistry in Living Animals. *Proc. Natl. Acad. Sci. U. S. A.* **2010**, *107* (5), 1821–1826.

(63) He, Y.; Liu, L.; Cheng, L. A Short Review of Research Progress on the Synthesis Approaches of Aza-Dibenzocyclooctyne Derivatives. *Molecules* **2023**, *28* (9).

(64) Gröst, C.; Berg, T. PYRROC: The First Functionalized Cycloalkyne That Facilitates Isomer-Free Generation of Organic Molecules by SPAAC. *Org. Biomol. Chem* **2015**, *13* (13), 3866–3870.

(65) Svatunek, D.; Houszka, N.; Hamlin, T. A.; Bickelhaupt, F. M.; Mikula, H. Chemoselectivity of Tertiary Azides in Strain-Promoted Alkyne-Azide Cycloadditions. *Chem* **2019**, *25* (3), 754.

(66) Devaraj, N. K.; Weissleder, R.; Hilderbrand, S. A. Tetrazine-Based Cycloadditions: Application to Pretargeted Live Cell Imaging. *Bioconjug. Chem.* **2008**, *19* (12), 2297–2299.

(67) Deb, T.; Tu, J.; Franzini, R. M. Mechanisms and Substituent Effects of Metal-Free Bioorthogonal Reactions. *Chem. Rev.* **2021**, *121* (12), 6850–6914.

(68) Sauer, J. 1,2,4,5-Tetrazines. *Comprehensive Heterocyclic Chemistry II: A Review of the Literature 1982-1995* **1996**, *6*, 901–955.

(69) David Row, R.; Prescher, J. A. Constructing New Bioorthogonal Reagents and Reactions. *Acc. Chem. Res.* **2018**, *51* (5), 1073–1081.

(70) Karver, M. R.; Weissleder, R.; Hilderbrand, S. A. Synthesis and Evaluation of a Series of 1,2,4,5-Tetrazines for Bioorthogonal Conjugation. *Bioconjug. Chem.* **2011**, *22* (11), 2263–2270.

(71) Lang, K.; Davis, L.; Torres-Kolbus, J.; Chou, C.; Deiters, A.; Chin, J. W. Genetically Encoded Norbornene Directs Site-Specific Cellular Protein Labelling via a Rapid Bioorthogonal Reaction. *Nat. Chem.* **2012**, *4* (4), 298.

(72) Liu, F.; Liang, Y.; Houk, K. N. Theoretical Elucidation of the Origins of Substituent and Strain Effects on the Rates of Diels−Alder Reactions of 1,2,4,5-Tetrazines. *J. Am. Chem. Soc* **2014**, *15*, 41.

(73) Svatunek, D.; Wilkovitsch, M.; Hartmann, L.; Houk, K. N.; Mikula, H. Uncovering the Key Role of Distortion in Bioorthogonal Tetrazine Tools That Defy the Reactivity/Stability Trade-Off. *J. Am. Chem. Soc.* **2022**, *2022*, 8171–8177.

(74) Versteegen, R. M.; Rossin, R.; ten Hoeve, W.; Janssen, H. M.; Robillard, M. S. Click to Release: Instantaneous Doxorubicin Elimination upon Tetrazine Ligation. *Angew. Chem., Int. Ed.* **2013**, *52* (52), 14112–14116.

(75) Carlson, J. C. T.; Mikula, H.; Weissleder, R. Unraveling Tetrazine-Triggered Bioorthogonal Elimination Enables Chemical Tools for Ultrafast Release and Universal Cleavage. *J. Am. Chem. Soc* **2018**, *140*, 3603–3612.

(76) Fan, X.; Ge, Y.; Lin, F.; Yang, Y.; Zhang, G.; Ngai, W. S. C.; Lin, Z.; Zheng, S.; Wang, J.; Zhao, J.; Li, J.; Chen, P. R. Optimized Tetrazine Derivatives for Rapid Bioorthogonal Decaging in Living Cells. *Angew. Chem., Int. Ed.* **2016**, *55* (45), 14046–14050.

(77) Handula, M.; Chen, K.-T.; Seimbille, Y.; Thomas, J.; Joseph, N.; Eremin, D. IEDDA: An Attractive Bioorthogonal Reaction for Biomedical Applications. *Molecules* **2021**, *26* (15), 4640.

(78) Ficini, J.; Krief, A. Stereochemical Control in the Hydrolysis of an Ynamine-Cyclopentenone Adduct : A Stereoselective Route to Diastereoisomeric 2-(1-Cyclopentyl 3-Oxo) Propionic Acids. *Tetrahedron Lett.* **1970**, *11* (17), 1397–1400.

(79) Burley, G. A.; Boutadla, Y.; Davies, D. L.; Singh, K. Triazoles from N-Alkynylheterocycles and Their Coordination to Iridium. *Organometallics* **2012**, *31* (3), 1112–1117.

(80) Burley, G. A.; Davies, D. L.; Griffith, G. A.; Lee, M.; Singh, K. Cu-Catalyzed N-Alkynylation of Imidazoles, Benzimidazoles, Indazoles, and Pyrazoles Using PEG as Solvent Medium. **2010**, *75* (3), 980–983.

(81) Hatit, M. Z. C.; Sadler, J. C.; McLean, L. A.; Whitehurst, B. C.; Seath, C. P.; Humphreys, L. D.; Young, R. J.; Watson, A. J. B.; Burley, G. A. Chemoselective Sequential Click Ligations Directed by Enhanced Reactivity of an Aromatic Ynamine. *Org. Lett.* **2016**, *18* (7), 1694–1697.

(82) Hatit, M. Z. C.; Seath, C. P.; Watson, A. J. B.; Burley, G. A. Strategy for Conditional Orthogonal Sequential CuAAC Reactions Using a Protected Aromatic Ynamine. *J. Org. Chem.* **2017**, *82* (10), 5461–5468.

(83) Peschke, F.; Taladriz-Sender, A.; Andrews, M. J.; Watson, A. J. B.; Burley, G. A. Glutathione Mediates Control of Dual Differential Bio-Orthogonal Labelling of Biomolecules. *Angew. Chem., Int. Ed.* **2023**, *62* (50).

(84) Yoshida, S.; Hatakeyama, Y.; Johmoto, K.; Uekusa, H.; Hosoya, T. Transient Protection of Strained Alkynes from Click Reaction via Complexation with Copper. *J. Am. Chem. Soc.* **2014**, *136* (39), 13590–13593.

(85) Yoshida, S.; Hatakeyama, Y.; Johmoto, K.; Uekusa, H.; Hosoya, T. Transient Protection of Strained Alkynes from Click Reaction via Complexation with Copper. *J. Am. Chem. Soc.* **2014**, *136* (39), 13590–13593.

(86) Seath, C. P.; Burley, G. A.; Watson, A. J. B. Determining the Origin of Rate-Independent Chemoselectivity in CuAAC Reactions: An Alkyne-Specific Shift in Rate-Determining Step. *Angew. Chem., Int. Ed.* **2017**, *56* (12), 3314–3318.

(87) Hangauer, M. J.; Bertozzi, C. R. A FRET-Based Fluorogenic Phosphine for Live Cell Imaging with the Staudinger Ligation. *Angew. Chem., Int. Ed.* **2008**, *47* (13), 2394–2397.

(88) Lemieux, G. A.; De Graffenried, C. L.; Bertozzi, C. R. A Fluorogenic Dye Activated by the Staudinger Ligation. *J. Am. Chem. Soc.* **2003**, *125* (16), 4708–4709.

(89) Wang, C. C. Y.; Seo, T. S.; Li, Z.; Ruparel, H.; Ju, J. Site-Specific Fluorescent Labeling of DNA Using Staudinger Ligaton. *Bioconjug. Chem.* **2003**, *14* (3), 697–701.

(90) Prescher, J. A.; Dube, D. H.; Bertozzi, C. R. Chemical Remodelling of Cell Surfaces in Living Animals. *Nature* **2004**, *430* (7002), 873–877.

(91) Dube, D. H.; Prescher, J. A.; Quang, C. M.; Bertozzi, C. R. Probing Mucin-Type O-Linked Glycosylation in Living Animals. *Proc. Natl. Acad. Sci. U. S. A.* **2006**, *103* (13), 4819–4824.

(92) Wang, Q.; Chan, T. R.; Hilgraf, R.; Fokin, V. V; Sharpless, K. B.; Finn, M. G. Bioconjugation by Copper(I)-Catalyzed Azide-Alkyne [3 + 2] Cycloaddition. *J. Am. Chem. Soc.* **2003**, *125* (11), 3192–3193.

(93) Shieh, P.; Hangauer, M. J.; Bertozzi, C. R. Fluorogenic Azidofluoresceins for Biological Imaging. *J. Am. Chem. Soc.* **2012**, *134* (42), 17428–17431.

(94) Shie, J. J.; Liu, Y. C.; Lee, Y. M.; Lim, C.; Fang, J. M.; Wong, C. H. An Azido-BODIPY Probe for Glycosylation: Initiation of Strong Fluorescence upon Triazole Formation. *J. Am. Chem. Soc.* **2014**, *136* (28), 9953–9961.

(95) Neugebauer, M. E.; Kissman, E. N.; Marchand, J. A.; Pelton, J. G.; Sambold, N. A.; Millar, D. C.; Chang, M. C. Y. Reaction Pathway Engineering Converts a Radical Hydroxylase into a Halogenase. *Nat. Chem. Biol.* **2022**, *18*, 171–179.

(96) Geva-Zatorsky, N.; Alvarez, D.; Hudak, J. E.; Reading, N. C.; Erturk-Hasdemir, D.; Dasgupta, S.; von Andrian, U. H.; Kasper, D. L. In Vivo Imaging and Tracking of Host–Microbiota Interactions via Metabolic Labeling of Gut Anaerobic Bacteria. *Nat. Med.* **2015**, *21* (9), 1091–1100.

(97) Wang, D.; Zhang, Y.; Kleiner, R. E. Cell-and Polymerase-Selective Metabolic Labeling of Cellular RNA with 2′-Azidocytidine. *J. Am. Chem. Soc* **2020**, *142*, 14417–14421.

(98) Teng, M.; Li, Z.; Zhou, Y.; Zhang, Z.; Miao, L.; Bai, X.; Li, Y.; Wang, S. Real-Time Monitoring of CAR-T Cell Efficiency through a Biorthogonal Cycloaddition Labeling Strategy. *Bioconjug. Chem.* **2023**, *34* (2), 443–452.

(99) Kozma, E.; Kele, P. Bioorthogonal Reactions in Bioimaging. *Top. Curr. Chem.* **2024**, *382* (7).

(100) Lang, K.; Davis, L.; Wallace, S.; Mahesh, M.; Cox, D. J.; Blackman, M. L.; Fox, J. M.; Chin, J. W. Genetic Encoding of Bicyclononynes and Trans-Cyclooctenes for Site-Specific Protein Labeling in Vitro and in Live Mammalian Cells via Rapid Fluorogenic Diels−Alder Reactions. *J. Am. Chem. Soc* **2012**, *134*.

(101) Rieder, U.; Luedtke, N. W. Alkene-Tetrazine Ligation for Imaging Cellular DNA. *Angew. Chem., Int. Ed.* **2014**, *53* (35), 9168–9172.

(102) Oliveira, B. L.; Guo, Z.; Bernardes, G. J. L. Inverse Electron Demand Diels-Alder Reactions in Chemical Biology. *Chem. Soc. Rev.* August 2017, pp 4895–4950.

(103) Rossin, R.; Verkerk, P. R.; Van Den Bosch, S. M.; Vulders, R. C. M.; Verel, I.; Lub, J.; Robillard, M. S. In Vivo Chemistry for Pretargeted Tumor Imaging in Live Mice. *Angew. Chem., Int. Ed.* **2010**, *49* (19), 3375–3378.

(104) Wolfbeis, O. S. The Click Reaction in the Luminescent Probing of Metal Ions, and Its Implications on Biolabeling Techniques. *Angew. Chem., Int. Ed.* **2007**, *46* (17), 2980–2982.

(105) Ast, S.; Kuke, S.; Rutledge, P. J.; Todd, M. H. Using Click Chemistry to Tune the Properties and the Fluorescence Response Mechanism of Structurally Similar Probes for Metal Ions. *Eur. J. Inorg. Chem.* **2015**, *2015* (1), 58–66.

(106) Clapham, D. E. Calcium Signaling. *Cell* **2007**, *131* (6), 1047–1058.

(107) Bagur, R.; Hajnóczky, G. Intracellular Ca2+ Sensing: Its Role in Calcium Homeostasis and Signaling. *Mol. Cell.* **2017**, *66* (6), 780–788.

(108) Romani, A. M. P. Cellular Magnesium Homeostasis. *Arch. Biochem. Biophys.* **2011**, *512* (1), 1–23.

(109) Becker, P. L.; Singer, J. J.; Walsh, J. V.; Fay, F. S. Regulation of Calcium Concentration in Voltage-Clamped Smooth Muscle Cells. *Science* **1989**, *244* (4901), 211–214.

(110) Pendin, D.; Norante, R.; De Nadai, A.; Gherardi, G.; Vajente, N.; Basso, E.; Kaludercic, N.; Mammucari, C.; Paradisi, C.; Pozzan, T.; Mattarei, A. A Synthetic Fluorescent Mitochondria-Targeted Sensor for Ratiometric Imaging of Calcium in Live Cells. *Angew. Chem., Int. Ed.* **2019**, *58* (29), 9917–9922.

(111) Celsi, F.; Pizzo, P.; Brini, M.; Leo, S.; Fotino, C.; Pinton, P.; Rizzuto, R. Mitochondria, Calcium and Cell Death: A Deadly Triad in Neurodegeneration. *Biochim. Biophys. Acta*. May 2009, pp 335–344.

(112) Lock, J. T.; Parker, I.; Smith, I. F. A Comparison of Fluorescent Ca2+ Indicators for Imaging Local Ca2+ Signals in Cultured Cells. *Cell Calcium* **2015**, *58* (6), 638–648.

(113) Pérez Koldenkova, V.; Nagai, T. Genetically Encoded Ca2+ Indicators: Properties and Evaluation. *Biochim. Biophys. Acta* **2013**, *1833* (7), 1787–1797.

(114) Paredes, R. M.; Etzler, J. C.; Watts, L. T.; Zheng, W.; Lechleiter, J. D. Chemical Calcium Indicators. *Methods* **2008**, *46* (3), 143–151.

(115) Tsien, R. Y. New Calcium Indicators and Buffers with High Selectivity Against Magnesium and Protons: Design, Synthesis, and Properties of Prototype Structures. *Biochemistry* **1980**, *19* (11), 2396–2404.

(116) Pethig, R.; Kuhn, M.; Payne, R.; Adler, E.; Chen, T. H.; Jaffe, L. F. On the Dissociation Constants of BAPTA-Type Calcium Buffers. *Cell Calcium* **1989**.

(117) Oheim, M.; van 't Hoff, M.; Feltz, A.; Zamaleeva, A.; Mallet, J.-M.; Collot, M. New Red-Fluorescent Calcium Indicators for Optogenetics, Photoactivation and Multi-Color Imaging. *Biochim. Biophys. Acta* **2014**, *1843* (10), 2284–2306.

(118) Liu, M.; Yu, X.; Li, M.; Liao, N.; Bi, A.; Jiang, Y.; Liu, S.; Gong, Z.; Zeng, W. Fluorescent Probes for the Detection of Magnesium Ions (Mg 2+): From Design to Application. *RSC Adv.* **2018**, *8* (23), 12573–12587.

(119) Martínez-Zaguilán, R.; Parnami, J.; Martinez, G. M. Mag-Fura-2 (Furaptra) Exhibits Both Low (MM) and High (NM) Affinity for Ca2+. *Cell. Physiol. Biochem.* **1998**, *8* (3), 158–174.

(120) Russell, J. T. Imaging Calcium Signals in Vivo: A Powerful Tool in Physiology and Pharmacology. *Br. J. Pharmacol.* **2011**, *163* (8), 1605–1625.

(121) *Fluo-3 Calcium Indicator*. ThermoFisher.

(122) *Indo-1 Calcium Indicator*. ThermoFisher.

(123) Tsien, R. Y. A Non-Disruptive Technique for Loading Calcium Buffers and Indicators into Cells. *Nature* **1981**, *290* (5806), 527–528.

(124) Csomos, A.; Kontra, B.; Jancsó, A.; Galbács, G.; Deme, R.; Kele, Z.; Rózsa, B. J.; Kovács, E.; Mucsi, Z. A Comprehensive Study of the Ca2+ Ion Binding of Fluorescently Labelled BAPTA Analogues. *Eur. J. Org. Chem.* **2021**, *2021* (37), 5248–5261.

(125) Minta, A.; Kao, J. P.; Tsien, R. Y. Fluorescent Indicators for Cytosolic Calcium Based on Rhodamine and Fluorescein Chromophores. *J. Biol. Chem.* **1989**, *264* (14), 8171–8178.

(126) Greene, L. E.; Lincoln, R.; Cosa, G. Tuning Photoinduced Electron Transfer Efficiency of Fluorogenic BODIPY- A-Tocopherol Analogues. *Photochem. Photobiol.* **2019**, *95* (1), 192–201.

(127) Deo, C.; Sheu, S.-H.; Seo, J.; Clapham, D. E.; Lavis, L. D. Isomeric Tuning Yields Bright and Targetable Red Ca 2+ Indicators. *J. Am. Chem. Soc* **2019**, *141*, 36.

(128) Kao, J. P. Y.; Harootunian, A. T.; Tsien, R. Y. Photochemically Generated Cytosolic Calcium Pulses and Their Detection by Fluo-3. *J. Biol. Chem.* **1989**, *264* (14), 8179–8184.

(129) Gee, K. R.; Brown, K. A.; Chen, W. N. U.; Bishop-Stewart, J.; Gray, D.; Johnson, I. Chemical and Physiological Characterization of Fluo-4 Ca2+-Indicator Dyes. *Cell Calcium* **2000**, *27* (2), 97–106.

(130) Jezek, P.; Hanus, J.; Semrad, C.; Garlid, K. D. Photoactivated Azido Fatty Acid Irreversibly Inhibits Anion and Proton Transport through the Mitochondrial Uncoupling Protein. *J. Biol. Chem* **1996**, *271* (11), 6199–6205.

(131) Svoboda, K.; Denk, W.; Kleinfeld, D.; Tank, D. W. In Vivo Dendritic Calcium Dynamics in Neocortical Pyramidal Neurons. *Nature* **1997**, *385* (6612), 161–165.

(132) Grynkiewicz, G.; Poenie, M.; Tsien, R. Y. A New Generation of Ca2+ Indicators with Greatly Improved Fluorescence Properties. *J. Biol. Chem.* **1985**, *260* (6), 3440–3450.

(133) Eberhard, M.; Erne, P. Calcium Binding to Fluorescent Calcium Indicators: Calcium Green, Calcium Orange and Calcium Crimson. *Biochem Biophys Res Commun* **1991**, *180* (1), 209–215.

(134) Collot, M.; Ponsot, F.; Klymchenko, A. S. Ca-NIR: A Ratiometric near-Infrared Calcium Probe Based on a Dihydroxanthene-Hemicyanine Fluorophore. *Chem. Commun.* **2017**, *53* (45), 6117–6120.

(135) Collot, M.; Wilms, C.; Mallet, J. M. Functionalizable Red Emitting Calcium Sensor Bearing a 1,4-Triazole Chelating Moiety. *RSC Adv.* **2015**, *5* (9), 6993–7000.

(136) Gaillard, S.; Yakovlev, A.; Luccardini, C.; Oheim, M.; Feltz, A.; Mallet, J. M. Synthesis and Characterization of a New Red-Emitting Ca2+ Indicator, Calcium Ruby. *Org. Lett.* **2007**, *9* (14), 2629–2632.

(137) Collot, M.; Loukou, C.; Yakovlev, A. V.; Wilms, C. D.; Li, D.; Evrard, A.; Zamaleeva, A.; Bourdieu, L.; Léger, J. F.; Ropert, N.; Eilers, J.; Oheim, M.; Feltz, A.; Mallet, J. M. Calcium Rubies: A Family of Red-Emitting Functionalizable Indicators Suitable for Two-Photon Ca2+ Imaging. *J. Am. Chem. Soc.* **2012**, *134* (36), 14923–14931.

(138) Martin, V. V.; Beierlein, M.; Morgan, J. L.; Rothe, A.; Gee, K. R. Novel Fluo-4 Analogs for Fluorescent Calcium Measurements. *Cell Calcium* **2004**, *36* (6), 509–514.

(139) Bachollet, S. P. J. T.; Pietrancosta, N.; Mallet, J.-M.; Dumat, B. Fluorogenic and Genetic Targeting of a Red-Emitting Molecular Calcium Indicator. *Chem. Commun.* **2022**, *58*, 6594.

(140) Takei, Y.; Murata, A.; Yamagishi, K.; Arai, S.; Nakamura, H.; Inoue, T.; Takeoka, S. Intracellular Click Reaction with a Fluorescent Chemical Ca2+ Indicator to Prolong Its Cytosolic Retention. *Chem. Commun.* **2013**, *49* (66), 7313.

(141) Sneyers, F.; Speelman-Rooms, F.; Verhelst, S. H. L.; Bootman, M. D.; Bultynck, G. Cellular Effects of BAPTA: Are They Only about Ca2+ Chelation? *Biochim. Biophys. Acta* **2024**, *1871* (2), 119589.

(142) Ruiz-Castillo, P.; Buchwald, S. L. Applications of Palladium-Catalyzed C-N Cross-Coupling Reactions. *Chem. Rev.* **2016**, *116* (19), 12564–12649.

(143) Biffis, A.; Centomo, P.; Del Zotto, A.; Zecca, M. Pd Metal Catalysts for Cross-Couplings and Related Reactions in the 21st Century: A Critical Review. *Chem. Rev.* **2018**, *118* (4), 2249–2295.

(144) Louie, J.; Hartwig, J. F. Palladium-Catalyzed Synthesis of Arylamines from Aryl Halides. Mechanistic Studies Lead to Coupling in the Absence of Tin Reagents. *Tetrahedron Lett.* **1995**, *36* (21), 3609–3612.

(145) Guram, A. S.; Rennels, R. A.; Buchwald, S. L. A Simple Catalytic Method for the Conversion of Aryl Bromides to Arylamines. *Angew. Chem., Int. Ed.* **1995**, *34* (12), 1348–1350.

(146) Biscoe, M. R.; Fors, B. P.; Buchwald, S. L. A New Class of Easily Activated Palladium Precatalysts for Facile C-N Cross-Coupling Reactions and the Low Temperature Oxidative Addition of Aryl Chlorides. *J. Am. Chem. Soc.* **2008**, *130* (21), 6686–6687.

(147) Fleckenstein, C. A.; Plenio, H. Sterically Demanding Trialkylphosphines for Palladium-Catalyzed Cross Coupling Reactions-Alternatives to PtBu3. *Chem. Soc. Rev.* **2010**, *39* (2), 694–711.

(148) Díez-González, S.; Marion, N.; Nolan, S. P. N-Heterocyclic Carbenes in Late Transition Metal Catalysis. *Chem. Rev.* **2009**, *109* (8), 3612–3676.

(149) Kantchev, E. A. B.; O'Brien, C. J.; Organ, M. G. Palladium Complexes of N-Heterocyclic Carbenes as Catalysts for Cross-Coupling Reactions - A Synthetic Chemist's Perspective. *Angew. Chem., Int. Ed.* **2007**, *46* (16), 2768–2813.

(150) Takale, B. S.; Kong, F.-Y.; Thakore, R. R. Recent Applications of Pd-Catalyzed Suzuki–Miyaura and Buchwald–Hartwig Couplings in Pharmaceutical Process Chemistry. *Organics* **2022**, *3* (1), 1–21.

(151) Ullmann, F.; Bielecki, J. Ueber Synthesen in Der Biphenylreihe. *Berichte der deutschen chemischen Gesellschaft* **1901**, *34* (2), 2174–2185.

(152) Hassan, J.; Sévignon, M.; Gozzi, C.; Schulz, E.; Lemaire, M. Aryl−Aryl Bond Formation One Century after the Discovery of the Ullmann Reaction. *Chem. Rev.* **2002**, *102* (5), 1359–1470.

(153) Sperotto, E.; Van Klink, G. P. M.; Van Koten, G.; De Vries, J. G. The Mechanism of the Modified Ullmann Reaction. *Dalton Trans.* **2010**, *39* (43), 10338–10351.

(154) Kiyomori, A.; Marcoux, J.-F.; Buchwald, S. L. An Efficient Copper-Catalyzed Coupling of Aryl Halides with Lmidazoles. *Tetrahedron Lett.* **1999**, *40*, 2657–2660.

(155) Ma, D. Accelerating Effect Induced by the Structure of α-Amino Acid in the Copper-Catalyzed Coupling Reaction of Aryl Halides with α-Amino Acids. Synthesis of Benzolactam-V8. *J. Am. Chem. Soc.* **1998**, *120* (48), 12459–12467.

(156) Fagan, P. J.; Hauptman, E.; Shapiro, R.; Casalnuovo, A. Using Intelligent/Random Library Screening to Design Focused Libraries for the Optimization of Homogeneous Catalysts: Ullmann Ether Formation. *J. Am. Chem. Soc.* **2000**, *122* (21), 5043–5051.

(157) Buck, E.; Song, Z. J.; Tschaen, D.; Dormer, P. G.; Volante, R. P.; Reider, P. J. Ullmann Diaryl Ether Synthesis: Rate Acceleration by 2,2,6,6-Tetramethylheptane-3,5-Dione. *Org. Lett.* **2002**, *4* (9), 1623–1626.

(158) Klapars, A.; Antilla, J. C.; Huang, X.; Buchwald, S. L. A General and Efficient Copper Catalyst for the Amidation of Aryl Halides and the N-Arylation of Nitrogen Heterocycles. *J. Am. Chem. Soc.* **2001**, *123* (31), 7727–7729.

(159) Goodbrand, H. B.; Hu, N. X. Ligand-Accelerated Catalysis of the Ullmann Condensation: Application to Hole Conducting Triarylamines. *J. Org. Chem.* **1999**, *64* (2), 670–674.

(160) Cristau, H. J.; Cellier, P. P.; Spindler, J. F.; Taillefer, M. Highly Efficient and Mild Copper-Catalyzed N- and C-Arylations with Aryl Bromides and Iodides. *Chemistry – A European Journal* **2004**, *10* (22), 5607–5622.

(161) Otto, N.; Opatz, T. Screening of Ligands for the Ullmann Synthesis of Electron-Rich Diaryl Ethers. *Beilstein J. Org. Chem.* **2012**, *8*, 1105.

(162) Zhang, H.; Cai, Q.; Ma, D. Amino Acid Promoted CuI-Catalyzed C-N Bond Formation between Aryl Halides and Amines or N-Containing Heterocycles. *J. Org. Chem.* **2005**, *70* (13), 5164–5173.

(163) Shafir, A.; Lichtor, P. A.; Buchwald, S. L. N- versus O-Arylation of Aminoalcohols: Orthogonal Selectivity in Copper-Based Catalysts. *J. Am. Chem. Soc.* **2007**, *129* (12), 3490–3491.

(164) Ouali, A.; Spindler, J. F.; Jutand, A.; Taillefer, M. Nitrogen Ligands in Copper-Catalyzed Arylation of Phenols: Structure/Activity Relationships and Applications. *Adv. Synth. Catal.* **2007**, *349* (11–12), 1906–1916.

(165) Yip, S. F.; Cheung, H. Y.; Zhou, Z.; Kwong, F. Y. Room-Temperature Copper-Catalyzed α-Arylation of Malonates. *Org. Lett.* **2007**, *9* (17), 3469–3472.

(166) Mastalir, Á.; Molnár, Á. A Novel Insight into the Ullmann Homocoupling Reactions Performed in Heterogeneous Catalytic Systems. *Molecules*. 2023, p 1769.

(167) Monnier, F.; Taillefer, M. Catalytic C-C, C-N, and C-O Ullmann-Type Coupling Reactions. *Angew. Chem., Int. Ed.* **2009**, *48* (38), 6954–6971.

(168) Sambiagio, C.; Marsden, S. P.; Blacker, A. J.; Mcgowan, P. C. Copper Catalysed Ullmann Type Chemistry: From Mechanistic Aspects to Modern Development. *Chem. Soc. Rev* **2014**, *43*, 3525.

(169) Akhtar, R.; Ameer Fawad Zahoor; Irfan, M.; Tanveer; Bokhari, H.; Atta Ul Haq. Recent Green Synthetic Approaches toward Ullmann Reaction: A Review. *Chem. Pap.* **2022**, *76*, 7275–7293.

(170) Grobler, I.; Smith, V. J.; Bhatt, P. M.; Herbert, S. A.; Barbour, L. J. Tunable Anisotropic Thermal Expansion of a Porous Zinc(II) Metal-Organic Framework. *J. Am. Chem. Soc.* **2013**, *135* (17), 6411–6414.

(171) HUANG, Z.; ZHOU, G. Benzimidazole Derivatives and Pharmaceutical Compositions and Uses Thereof, 2012.

(172) Wei, X.; Hu, X.; Yu, R.; Wan, S.; Jiang, T. Efficient Total Synthesis of Lissodendrin b, 2-Aminoimidazole Marine Alkaloids Isolated from Lissodendoryx (Acanthodoryx) Fibrosa. *Mar. Drugs* **2020**.

(173) Ueda, S.; Su, M.; Buchwald, S. L. Completely N 1-Selective Palladium-Catalyzed Arylation of Unsymmetric Imidazoles: Application to the Synthesis of Nilotinib. *J. Am. Chem. Soc.* **2012**, *134* (1), 700–706.

(174) Newton, A. C.; Bootman, M. D.; Scott, J. D. Second Messengers. *Cold Spring Harb. Perspect. Biol.* **2016**, *1* (8).

(175) Devaraj, N. K.; Weissleder, R. Biomedical Applications of Tetrazine Cycloadditions. *Acc. Chem. Res.* **2011**, *44* (9), 816–827.

(176) Otto, S.; Engberts, J. B. F. N. Hydrophobic Interactions and Chemical Reactivity. *Org. Biomol. Chem.* **2003**, *1* (16), 2809–2820.

(177) Tanford, C.; Breslow, R.; Symp ; Rideout, D. Hydrophobic Effects on Simple Organic Reactions in Water. *Acc. Chem. Res.* **1991**, *24* (6), 159–164.

(178) Narayan, S.; Muldoon, J.; Finn, M. G.; Fokin, V. V; Kolb, H. C.; Sharpless, K. B. "On Water": Unique Reactivity of Organic Compounds in Aqueous Suspension. *Angew. Chem., Int. Ed.* **2005**, *44* (21), 3275–3279.

(179) Cortes-Clerget, M.; Yu, J.; Kincaid, J. R. A.; Walde, P.; Gallou, F.; Lipshutz, B. H. Water as the Reaction Medium in Organic Chemistry: From Our Worst Enemy to Our Best Friend. *Chem. Sci.* **2021**, *12* (12), 4237–4266.

(180) Yuan, Z.; Kuang, G.-C.; Clark, R. J.; Zhu, L. Chemoselective Sequential "Click" Ligation Using Unsymmetrical Bisazides. *Org. Lett.* **2012**, *14* (10), 2590–2593.

(181) Listunov, D.; Saffon-Merceron, N.; Joly, E.; Fabing, I.; Enisson C, Y. G.; Erie Maraval, V.; Chauvin, R. Ethynylogation Approach in Pharmacophore Design: From Alkynyl- to Butadiynyl-Carbinols vs Antitumoral Cytotoxicity. *Tetrahedron* **2016**, *72* (20), 6697–6704.

(182) Jiang, M. X. W.; Rawat, M.; Wulff, W. D. Contingency and Serendipity in the Reactions of Fischer Carbene Complexes with Conjugated Triynes. *J. Am. Chem. Soc.* **2004**, *126* (19), 5970–5971.

(183) Seath, C. P.; Burley, G. A.; Watson, A. J. B. Determining the Origin of Rate-Independent Chemoselectivity in CuAAC Reactions: An Alkyne-Specific Shift in Rate-Determining Step. *Angew. Chem., Int. Ed.* **2017**, *56* (12), 3314–3318.

(184) Chen, Y. H.; Peng, K. E.; Lee, G. H.; Peng, S. M.; Chiu, C. W. Symmetrical Non-Chelating Poly-N-Heterocyclic Carbenes. *RSC Adv.* **2014**, *4* (107), 62789–62792.

(185) Zhang, X.; Liu, P.; Zhu, L. Structural Determinants of Alkyne Reactivity in Copper-Catalyzed Azide-Alkyne Cycloadditions. *Molecules* **2016**, *21* (12), 1697.

(186) Worrell, B. T.; Malik, J. A.; Fokin, V. V. Direct Evidence of a Dinuclear Copper Intermediate in Cu(I)-Catalyzed Azide-Alkyne Cycloadditions. *Science* **2013**, *340* (6131), 457–460.

(187) Zhu, L.; Brassard, C. J.; Zhang, X.; Guha, P. M.; Clark, R. J. On the Mechanism of Copper(I)-Catalyzed Azide-Alkyne Cycloaddition. *Chem. Rec.* **2016**, *16* (3), 1501–1517.

(188) Bunschoten, R. P.; Peschke, F.; Taladriz-Sender, A.; Alexander, E.; Andrews, M. J.; Kennedy, A. R.; Fazakerley, N. J.; Jones, G. C. L.; Watson, A. J. B.; Burley, G. A. Mechanistic Basis of the Cu(OAc)2 Catalyzed Azide-Ynamine (3 + 2) Cycloaddition Reaction. *J. Am. Chem. Soc.* **2024**, *146* (19), 13558–13570.

(189) Bi, X.; Miao, K.; Wei, L. Alkyne-Tagged Raman Probes for Local Environmental Sensing by Hydrogen-Deuterium Exchange. *J. Am. Chem. Soc.* **2022**, *144* (19), 8504–8514.

(190) Martínez, C. H. R.; Dardonville, C. Rapid Determination of Ionization Constants (PKa) by UV Spectroscopy Using 96-Well Microtiter Plates. *ACS Med. Chem. Lett.* **2013**, *4* (1), 142–145.

(191) Antonov, L.; Kawauchi, S.; Shirata, K. Acid Dissociation Constants of the Benzimidazole Unit in the Polybenzimidazole Chain: Configuration Effects. *Molecules* **2022**, *27* (3), 1064.

(192) Eglinton, G.; Galbraith, A. R. Macrocyclic Acetylenic Compounds. Part I. Cyclotetradeca-1 :3-Diyne and Related Compounds. *J. Chem. Soc.* **1959**, 889–896.

(193) Motiwala, H. F.; Armaly, A. M.; Cacioppo, J. G.; Coombs, T. C.; Koehn, K. R. K.; Norwood, V. M.; Aubé, J. HFIP in Organic Synthesis. *Chem. Rev.* **2022**, *122* (15), 12544–12747.

(194) Ammer, J.; Mayr, H. Solvent Nucleophilicities of Hexafluoroisopropanol/Water Mixtures. *J. Phys. Org. Chem.* **2013**, *26* (1), 59–63.

(195) Brassard, C. J.; Zhang, X.; Brewer, C. R.; Liu, P.; Clark, R. J.; Zhu, L. Cu(II)-Catalyzed Oxidative Formation of 5,5′-Bistriazoles. *J. Org. Chem.* **2016**, *81* (24), 12091–12105.

(196) Liu, P.; Brassard, C. J.; Lee, J. P.; Zhu, L. Cu II-Catalyzed Oxidative Formation of 5-Alkynyltriazoles. *Chem.: Asian J.* **2020**, *15* (3), 380–390.

(197) Zhang, J.; Chen, M.; Ren, X.; Shi, W.; Yin, T.; Luo, T.; Lan, Y.; Li, X.; Guan, L. Effect of Conjugation Length on Fluorescence Characteristics of Carbon Dots. *RSC Adv.* **2023**, *13* (40), 27714–27721.

(198) Barandov, A.; Bartelle, B. B.; Williamson, C. G.; Loucks, E. S.; Lippard, S. J.; Jasanoff, A. Sensing Intracellular Calcium Ions Using a Manganese-Based MRI Contrast Agent. *Nat. Commun.* **2019**.

(199) Dong, X.; Yang, Y.; Sun, J.; Liu, Z.; Liu, B. F. Two-Photon Excited Fluorescent Probes for Calcium Based on Internal Charge Transfer. *Chem. Commun.* **2009**, No. 26, 3883–3885.

(200) Schwarze, T.; Sprenger, T.; Riemer, J. 1,2,3-Triazol-1,4-diyl-Fluoroionophores for Zn2+, Mg2+ and Ca2+ Based on Fluorescence Intensity Enhancements in Water. *ChemistrySelect* **2020**, *5*, 12727–12735.

(201) Barandov, A.; Bartelle, B. B.; Williamson, C. G.; Loucks, E. S.; Lippard, S. J.; Jasanoff, A. Sensing Intracellular Calcium Ions Using a Manganese-Based MRI Contrast Agent. *Nat. Commun.* **2019**, *10* (1), 1–9.

(202) Komatsu, H.; Miki, T.; Citterio, D.; Kubota, T.; Shindo, Y.; Kitamura, Y.; Oka, K.; Suzuki, K. Single Molecular Multianalyte (Ca2+, Mg2+) Fluorescent Probe and Applications to Bioimaging. *J. Am. Chem. Soc.* **2005**, *127* (31), 10798–10799.

(203) Caldwell, S. T.; Cairns, A. G.; Olson, M.; Chalmers, S.; Sandison, M.; Mullen, W.; McCarron, J. G.; Hartley, R. C. Synthesis of an Azido-Tagged Low Affinity Ratiometric Calcium Sensor. *Tetrahedron* **2015**, *71* (51), 9571–9578.

(204) Kim, H. M.; Kim, B. R.; Hong, J. H.; Park, J. S.; Lee, K. J.; Cho, B. R. A Two-Photon Fluorescent Probe for Calcium Waves in Living Tissue. *Angew. Chem., Int. Ed.* **2007**.

(205) Hirabayashi, K.; Hanaoka, K.; Egawa, T.; Kobayashi, C.; Takahashi, S.; Komatsu, T.; Ueno, T.; Terai, T.; Ikegaya, Y.; Nagano, T.; Urano, Y. Synthesis of Practical Red Fluorescent Probe for Cytoplasmic Calcium Ions with Greatly Improved Cell-Membrane Permeability. *Data Br.* **2017**, *12*, 351–357.

(206) Egawa, T.; Hirabayashi, K.; Koide, Y.; Kobayashi, C.; Takahashi, N.; Mineno, T.; Terai, T.; Ueno, T.; Komatsu, T.; Ikegaya, Y.; Matsuki, N.; Nagano, T.; Hanaoka, K.

Red Fluorescent Probe for Monitoring the Dynamics of Cytoplasmic Calcium Ions. *Angew. Chem., Int. Ed.* **2013**, *52* (14), 3874–3877.

(207) Egawa, T.; Hanaoka, K.; Koide, Y.; Ujita, S.; Takahashi, N.; Ikegaya, Y.; Matsuki, N.; Terai, T.; Ueno, T.; Komatsu, T.; Nagano, T. Development of a Far-Red to near-Infrared Fluorescence Probe for Calcium Ion and Its Application to Multicolor Neuronal Imaging. *J. Am. Chem. Soc.* **2011**, *133* (36), 14157–14159.

(208) Qi, J.; Duan, X.; Cai, Y.; Jia, S.; Chen, C.; Zhao, Z.; Li, Y.; Peng, H.-Q.; Kwok, R. T. K.; Lam, J. W. Y.; Ding, D.; Tang, B. Z. Simultaneously Boosting the Conjugation, Brightness and Solubility of Organic Fluorophores by Using AIEgens. *Chem.Sci.* **2020**, *11* (32), 8438–8447.

(209) Sivakumar, K.; Xie, F.; Cash, B. M.; Long, S.; Barnhill, H. N.; Wang, Q. A Fluorogenic 1,3-Dipolar Cycloaddition Reaction of 3-Azidocoumarins and Acetylenes. *Org. Lett.* **2004**, *6* (24), 4603–4606.

(210) Meng, G.; Guo, taijie; Ma, tiancheng; Zhang, J.; Shen, Y.; Barry Sharpless, K.; Dong, J. Modular Click Chemistry Libraries for Functional Screens Using a Diazotizing Reagent. *Nature* **2019**, No. 574, 86–89.

(211) Hatit, M. Z. C.; Reichenbach, L. F.; Tobin, J. M.; Vilela, F.; Burley, G. A.; Watson, A. J. B. A Flow Platform for Degradation-Free CuAAC Bioconjugation. *Nat. Commun.* **2018**, *9* (1), 4021.

(212) Hannant, J.; Hedley, J. H.; Pate, J.; Walli, A.; Farha Al-Said, S. A.; Galindo, M. A.; Connolly, B. A.; Horrocks, B. R.; Houlton, A.; Pike, A. R. Modification of DNA-Templated Conductive Polymer Nanowires via Click Chemistry. *Chem. Commun.* **2010**, *46* (32), 5870–5872.

(213) Chen, C.; Huang, Y.; Xu, L.; Zheng, Y.; Xu, H.; Guo, Q.; Tian, C.; Li, Y.; Shi, J. Thiol-Assisted One-Pot Synthesis of Peptide/Protein C-Terminal Thioacids from Peptide/Protein Hydrazides at Neutral Conditions. *Org. Biomol. Chem.* **2014**, *12* (46), 9413–9418.

(214) Heller, K.; Ochtrop, P.; Albers, M. F.; Zauner, F. B.; Itzen, A.; Hedberg, C. Covalent Protein Labeling by Enzymatic Phosphocholination. *Angew. Chem., Int. Ed.* **2015**, *54* (35), 10327–10330.

(215) Ziegler, B. E.; McMahon, T. B. Computational Analysis of Substituent Effects and Hammett Constants for the Ionization of Gas Phase Acids. *Comput. Theor. Chem.* **2013**, *1008*, 46–51.

(216) Hammett, L. P. The Effect of Structure upon the Reactions of Organic Compounds. Benzene Derivatives. *J. Am. Chem. Soc.* **1937**, *59* (1), 96–103.

(217) Sharma, D.; Dhayalan, V.; Manikandan, C.; Dandela, R. Recent Methods for Synthesis of Coumarin Derivatives and Their New Applications. In *Strategies for the Synthesis of Heterocycles and Their Applications*; IntechOpen, 2023.

(218) Bruna-Haupt, E. F.; Perretti, M. D.; Garro, H. A.; Carrillo, R.; Machín, F.; Lorenzo-Castrillejo, I.; Gutiérrez, L.; Vega-Hissi, E. G.; Mamberto, M.; Menacho-Marquez, M.; Fernández, C. O.; García, C.; Pungitore, C. R. Synthesis of Structurally Related Coumarin Derivatives as Antiproliferative Agents. *ACS Omega* **2023**, *8* (29), 26479–26496.

(219) Medina, F. G.; Marrero, J. G.; Macías-Alonso, M.; González, M. C.; Córdova-Guerrero, I.; Teissier García, A. G.; Osegueda-Robles, S. Coumarin Heterocyclic Derivatives: Chemical Synthesis and Biological Activity. *Nat. Prod. Rep.* **2015**, *32* (10), 1472–1507.

Appendix

The appendix is available at:

https://strath-my.sharepoint.com/:f:/r/personal/emma_alexander_100_strath_ac_uk/Documents/Finalised%20Thesis/Appendix?csf=1&web=1&e=q2knFp

or as a .zip file.